

**Trace gases in Antarctic and Greenland firn and ice:
a record of carbonyl sulphide and the isotopologues
of chlorofluorocarbons**

By

Samuel J. Allin

July 2015

A thesis submitted to the School of Environmental Sciences of the University
of East Anglia, in partial fulfilment of the requirements for the degree of
Doctor of Philosophy

This copy of the thesis has been supplied on condition that anyone who consults it is understood to recognise that its copyright rests with the author and that use of any information derived there from must be in accordance with current UK Copyright Law. In addition, any quotation or extract must include full attribution.

Abstract

Through the industrial revolution of the last 250 years, trace gases have had a significant impact on the climate. Of particular relevance to this work are species which facilitate the destruction of stratospheric ozone. In this thesis, I focus on four of these species.

Understanding the release, reaction and transport pathways of the man-made chlorofluorocarbons (CFCs) could help us to mitigate their destructive effect. Previous studies have found that both source and sink processes significantly alter the isotopic composition of trace gases (e.g. N_2O and CFC-12). Measuring these changes can be used to better constrain the interaction of these gases with the atmosphere. Atmospheric histories of $\delta(^{37}\text{Cl})$ and $\delta(^{13}\text{C})$ in CFC-11, CFC-12 and CFC-113 are presented, covering the last 20 – 60 years. Air samples came from Greenland (NEEM) and Antarctic (Fletcher Promontory) polar firn, with additional samples taken from an archive of Southern Hemispheric background air (Cape Grim, Tasmania). This study extends the novel approach to measuring trace gas isotope ratios in small air volumes (200 – 600 ml), using a single-collector gas chromatography-mass spectrometry system.

Carbonyl sulphide (COS) is the principal source of sulphur in the stratosphere, where it breaks down into sulphate aerosol which catalyses the destruction of ozone. Air was extracted from Greenland (NEEM) and Antarctic (DE08, DML (BAS) and DSS) ice core samples and analysed for COS and a range of other trace gas mole fractions. The COS measurements were affected by a previously unknown post-extraction growth effect, leading to higher than expected values. This study also presents new COS measurements in firn air from NEEM and the Southern Hemisphere (EDML, Antarctica). The observed increase and subsequent decrease largely reflects changes in anthropogenic emissions during the 20th century. These measurements also indicate that regional and site-specific effects have a significant influence on the recorded atmospheric history of COS.

Publications

Work contributing to this thesis has been published in:

Allin, S. J., Laube, J. C., Witrant, E. Kaiser, J., McKenna, E., Dennis, P., Mulvaney, R., Capron, E., Martinerie, P., Röckmann, T., Blunier, T., Schwander, J., Fraser, P. J., Langenfelds, R. L., and Sturges, W. T.: Chlorine isotope composition in chlorofluorocarbons CFC-11, CFC-12 and CFC-113 in firn, stratospheric and tropospheric air, *Atmospheric Chemistry and Physics*, 15, 6867-6877, doi:10.5194/acp-15-6867-2015, 2015.

Table of Contents

Preliminary Information

List of Figures and Tables	vii
Acknowledgements	xii

Chapter 1: Scientific background

1.1 The atmosphere	2
1.1.1 Radiative forcing	2
1.1.2 Ozone	4
1.1.2.1 Ozone production	5
1.1.2.2 Ozone loss	6
1.2 The cryosphere	10
1.2.1 Firn structure and processes	10
1.2.2 Ice cores	12
1.3 Chlorofluorocarbons (CFCs)	13
1.3.1 Background	13
1.3.1.1 Atmospheric budget	14
1.3.2 Trace gas stable isotope measurements	15
1.4 Carbonyl sulphide (COS)	20
1.4.1 Background	20
1.4.2 Atmospheric budget	21
1.4.3 Measurement history	21
1.4.4 COS and the carbon cycle	26
1.5 Research objectives	28
1.5.1 An atmospheric history of the chlorine and carbon isotope composition in CFC-11, CFC-12 and CFC-113	28

1.5.2 Carbonyl sulphide (COS) in ice and firn	29
---	----

Chapter 2: Experimental methodologies

2.1 Gas chromatography-mass spectrometry	30
2.1.1 Measurement procedure	32
2.1.1.1 Instrument setup	32
2.1.1.2 Sample preparation	37
2.1.1.3 Sample analysis	39
2.1.1.4 Data processing	41
2.1.2 Isotope ratios	42
2.1.2.1 GC-MS isotope ratio analysis	43
2.2 Firn air modelling	44
2.2.1 The firn diffusion model	44
2.3 Ice core system	47
2.3.1 Sample selection	47
2.3.1.1 Ice core dating	47
2.3.2 Air extraction and measurement procedure	51
2.3.2.1 The day before a set of extractions	52
2.3.2.2 Extraction day	53
2.3.2.3 Post extraction	53
2.3.2.4 Measurements	54
2.3.3 Advantages of the CMAR extraction system	54

Chapter 3: An atmospheric history of the chlorine and carbon isotope composition in CFC-11, CFC-12 and CFC-113

3.1 Chlorine isotope composition in chlorofluorocarbons	56
CFC-11, CFC-12 and CFC-113 in firn, stratospheric and tropospheric air	

3.1.1	Research objectives	57
3.1.2	Methodology	57
3.1.3	Results and discussion	63
3.1.3.1	Tropospheric measurements	69
3.1.3.2	Transport modelling	71
3.1.3.3	A chlorine isotope history	77
3.1.4	Summary	77
3.2	Carbon isotope composition in chlorofluorocarbons CFC-11, CFC-12 and CFC-113 in firn air	78
3.2.1	Research objectives	79
3.2.2	Methodology	79
3.2.3	Results and discussion	88
3.2.3.1	Firn measurements	90
3.2.3.2	A carbon isotope history	93
3.2.3.3	Comparison with other studies	96
3.2.4	Summary	104
 Chapter 4: Carbonyl sulphide (COS) in ice and firn		
4.1	Antarctic and Greenland ice cores	106
4.1.1	Research objectives	107
4.1.2	Methodology	107
4.1.2.1	The sample cycle	107
4.1.3	Results and discussion	111
4.1.3.1	System tests	111
4.1.3.2	Standard comparisons	117
4.1.3.3	Extracted samples	118
4.1.3.4	Sources of error and corrections	121
4.1.3.5	Gases measured at CMAR	134
4.1.4	Summary	136
4.2	Northern and Southern Hemisphere firn air	137

Table of Contents

4.2.1	Research objectives	137
4.2.2	Methodology	138
4.2.3	Results and discussion	142
4.2.3.1	Northern Hemisphere results	145
4.2.3.2	Southern Hemisphere results	154
4.2.4	Summary	160
Chapter 5: Conclusions and recommendations		
5.1	An atmospheric history of the chlorine and carbon isotope composition in CFC-11, CFC-12 and CFC-113	161
5.2	Carbonyl sulphide (COS) in ice and firn	165
5.2.1	Antarctic and Greenland ice cores	166
5.2.2	Northern and Southern Hemisphere firn air	167
Abbreviations		170
References		172

List of Figures and Tables by chapter

Chapter 1: Scientific background

Figures

1	The atmospheric abundance of CO ₂ and CH ₄ over the last 800,000 years.	1
2	An example of the Earth's annual mean energy budget.	3
3	Ozone in the atmosphere.	5
4	An example of a catalytic reaction cycle which destroys ozone.	7
5	A simple illustration of flow patterns within an ice sheet.	12
6	Average annual COS mole fractions versus latitude.	23
7	COS measurements from Antarctic ice between 1550 and 1750.	25
8	An illustration of the complex interactions of the carbon cycle.	27

Tables

1	Key atmospheric characteristics of CFC-11, CFC-12 and CFC-113.	14
2	The natural abundances of the stable isotopes of carbon and chlorine.	16

Chapter 2: Experimental methodologies

Figures

1	The mass spectra of ionisation products for hexadecane and CFC-11.	36
2	Schematic diagram of the manual inlet setup for the GC-MS system.	38
3	The stability of two UEA standards over time, with respect to COS.	40
4	Example chromatograms for SF ₆ and CFC-12.	42
5	Seasonal cycles seen in various isotopes and species within an ice core.	49
6	Non sea salt SO ₄ ²⁻ peaks representing the emissions of major sulphate-rich volcanic eruptions.	50
7	A schematic diagram of the ice core extraction line in ICELAB at	51

CMAR.

8	A schematic diagram of the ice core extraction vessel.	52
---	--	----

Tables

1	An example mass spectrometer programme.	32
2	Details of the calibration scales used in this work.	40
3	The M_{gas} (g mol^{-1}) and $D_{\text{gas}}/D_{\text{CO}_2}$ values used in this study.	46

Chapter 3: An atmospheric history of the chlorine and carbon isotope composition in CFC-11, CFC-12 and CFC-113

Figures

1	An example chromatographic output used to calculate a $\delta(^{37}\text{Cl})$ value.	59
2	A static dilution series was measured for $\delta(^{37}\text{Cl})$.	60
3	Corrections were made to $\delta_{\text{T}}(^{37}\text{Cl})$ measurements using the dilution series analysis.	65
4	CFC-12 peaks with and without CO_2 removed using an Ascarite trap.	67
5	$\delta_{\text{T}}(^{37}\text{Cl})$ measurements in CFC-11, CFC-12 and CFC-113.	68
6	Mean N_2O seasonal cycles, measured on the Cape Grim air archive.	70
7	A boxplot of the $\delta_{\text{T}}(^{37}\text{Cl}, \text{CFC-12})$ from Cape Grim samples.	71
8	Rayleigh fractionation plots of CFC-11, CFC-12 and CFC-113 chlorine isotope signatures.	73
9	$\delta_{\text{T}}(^{37}\text{Cl})$ measurements, compared to model predictions.	76
10	$\delta_{\text{T}}(^{13}\text{C})$ measurements of CFC-11, CFC-12 and CFC-113 before methodological alterations.	80
11	The mass spectrometer output for several CFC-11 fragment ions.	81
12	SF_6 and CFC-12 peaks produced from different injection volumes.	85
13	Comparison between $\delta_{\text{T}}(^{37}\text{Cl})$ and $\delta_{\text{T}}(^{37}\text{Cl}^{37}\text{Cl})$ measurements in CFC-11, CFC-12 and CFC-113.	87

14	A static dilution series was measured for $\delta(^{13}\text{C})$.	89
15	$\delta_{\text{T}}(^{13}\text{C})$ measurements in CFC-11, CFC-12 and CFC-113 after methodological alterations.	91
16	$\delta_{\text{T}}(^{13}\text{C})$ measurements, compared to model predictions.	95
17	A comparison between $\delta_{\text{T}}(^{13}\text{C})$ measurements made before and after the methodological alterations.	97
18	$\delta_{\text{T}}(^{13}\text{C}, \text{CFC-12})$ measurements made by Zuiderweg et al. (2013).	99
19	A comparison between $\delta_{\text{T}}(^{13}\text{C}, \text{CFC-12})$ measurements made in this thesis and by Zuiderweg et al. (2013).	101
20	CH_3Cl and CFC-12 peaks in measurements made by Zuiderweg et al. (2013).	102

Tables

1	The mean analytical uncertainty for $\delta(^{37}\text{Cl})$ measurements using different analysis procedures.	61
2	Details of the samples used in this study.	62
3	Details of the dilution series samples.	64
4	A comparison of $\delta_{\text{T}}(^{37}\text{Cl})$ and the original $\delta_{\text{T}}(^{13}\text{C})$ measurement uncertainties.	81
5	Source and collector slit parameters.	83
6	The gravitational and diffusive correction for the $\delta_{\text{T}}(^{37}\text{Cl})$ of CFC-11 in NEEM 2009 firn air.	92
7	The analytical uncertainties achieved for $\delta_{\text{T}}(^{13}\text{C})$ measurements in CFC-11, CFC-12 and CFC-113.	98
8	The analytical uncertainties achieved in this thesis and by Zuiderweg et al. (2013).	104

Chapter 4: Carbonyl sulphide (COS) in firn and ice

Figures

1	Ice core shipping temperature record.	109
---	---------------------------------------	-----

List of Figures and Tables

2	The location of ice core drilling sites.	110
3	The SF ₆ abundance in ice core samples.	119
4	The CFC-12 abundance in ice core samples.	119
5	The COS abundance in ice core samples.	120
6	COS measurements after dried air storage.	127
7	COS measurements after wet air storage.	128
8	COS production rate versus the grater pressure.	131
9	Corrected COS measurements.	133
10	CO ₂ and $\delta(^{13}\text{C}, \text{CO}_2)$ measurements from DML (BAS) ice core samples.	135
11	Previously published COS mole fraction measurements in firn air.	139
12	Previously published COS mole fraction measurements in firn and ice core air.	140
13	The initial input time series for COS.	141
14	Initial depth profiles of COS mole fractions from EDML and NEEM firn air.	143
15	Finalised depth profiles of COS mole fractions from EDML and NEEM firn air.	144
16	COS mole fraction measurements used to infer a seasonal cycle at Summit (Greenland).	146
17	Northern Hemisphere input and output model scenarios.	148
18	Northern Hemisphere input and output model scenarios.	150
19	Northern Hemisphere output model scenarios.	151
20	Measurements of carbon monoxide mole fractions on NEEM 2008 firn air.	153
21	Southern Hemisphere input and output model scenarios.	155
22	COS mole fraction measurements used to infer a seasonal cycle at the South Pole.	156
23	Southern Hemisphere input and output model scenarios.	158

24	Southern Hemisphere output model scenarios.	159
----	---	-----

Tables

1	Details of the drilling sites discussed in this work.	108
2	Details of the types of samples analysed during system testing.	111
3	The COS measurements made as part of the preliminary tests.	113
4	The SF ₆ measurements made as part of the preliminary tests.	114
5	The CFC-12 measurements made as part of the preliminary tests.	114
6	‘Real’ test extractions from DE08 ice.	116
7	The standard comparison results from COS measurements.	117
8	The COS measurements made as part of the extraction system tests.	123
9	The SF ₆ measurements made as part of the extraction system tests.	124
10	The CFC-12 measurements made as part of the extraction system tests.	124
11	Details of the ice core samples analysed.	126
12	A best estimate of the atmospheric history of COS.	141

Chapter 5: Conclusions and recommendations

Tables

1	The $\delta(^{37}\text{Cl})$ measurements made in CFC-11, CFC-12 and CFC-113.	162
2	The overall $\delta(^{13}\text{C})$ measurement uncertainties achieved during this study.	163
3	The ‘contemporary’ $\delta(^{13}\text{C})$ measurement uncertainties achieved during this study.	164

Acknowledgements

Firstly, I'd like to thank the Natural Environment Research Council (NERC) for funding my project. I was also the recipient of a partial CASE award, provided by the British Antarctic Survey (BAS), which exposed me to a range of high quality resources (both samples and expertise). Rob Mulvaney co-supervised my project and was my main point of contact on this front. His input regarding the direction of my work was invaluable and I thank him for that.

I was lucky enough to work with several lab groups at UEA and further afield. These were highly formative experiences and I'd like to thank a few people who were instrumental in my education. A small amount of work was conducted in SIL at the beginning of my Ph.D., under the tutelage of Alina Marca-Bell and Paul Dennis. Rob supervised my first experience of working with ice in a cold room at BAS, not something I'm likely to forget! Most exotically, I spent 3 very enjoyable weeks at CMAR in Australia, working with my 'companion in the cold', Mauro Rubino (team headed by David Etheridge). Lastly, most of my experimental work was conducted in the AutoSpec lab. I am grateful to Johannes Laube and Bill Sturges, who guided me through the many frustrations and elations of working with such a highly sensitive/temperamental instrument.

A series of setbacks meant that as my project developed, I acquired new co-supervisors at an alarming rate. By my third year a supervisory meeting was quite the event, with a turnout rivalling that of a departmental seminar! I am grateful to Rob Mulvaney and Paul Dennis who were inexhaustible sources of knowledge and guidance and to Johannes Laube, whose expertise in the AutoSpec lab was absolutely vital to the success of this project.

Through all of this, as my primary supervisor, Bill Sturges was involved in every aspect of my work. He was always supportive and encouraging, allowing me to think completely freely. Thank you, Bill.

Finally to my parents, your support means everything to me and for that I thank you. I'm not sure that dedicating this thesis to you is a suitable sentiment (it's quite long), but here it is, enjoy!

Chapter 1: Scientific background

Through the industrial revolution of the last 250 years, humans have had a significant impact on our climate and it is expected that Earth's mean surface temperature will continue to rise in the coming decades. The link between climatic conditions and the composition of the atmosphere is strong, with levels of CO₂ and CH₄ higher today than at any point in the past 800,000 years (Figure 1.1). This latter information is obtained from the analysis of the air trapped in polar ice cores.

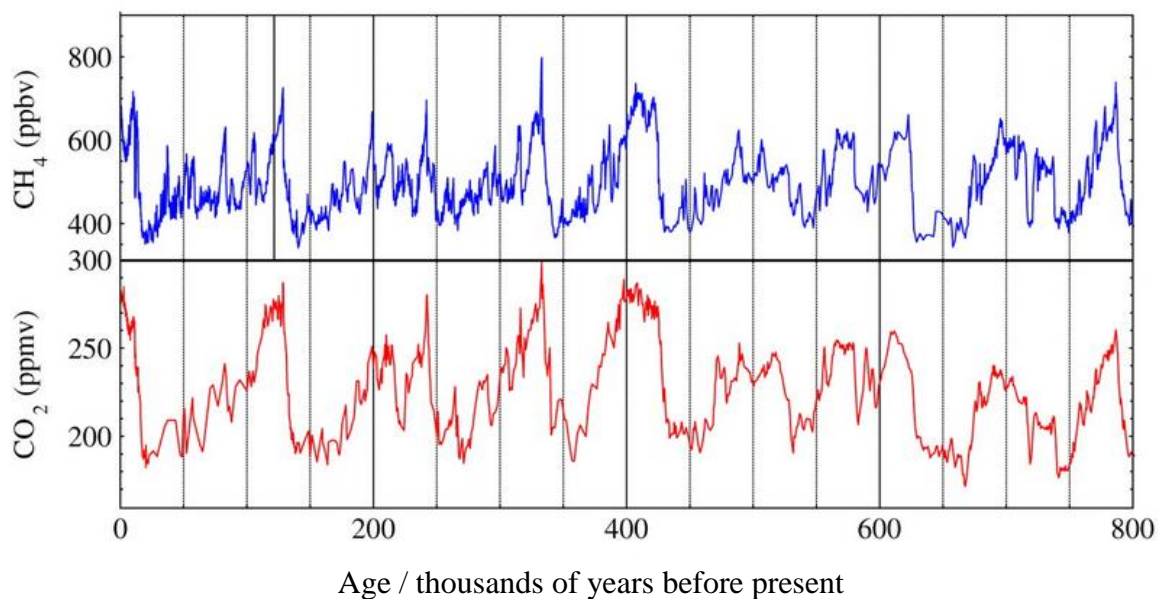


Figure 1.1. The atmospheric abundance of CO₂ (Lüthi et al., 2008) and CH₄ (Louergue et al., 2008) over the last 800,000 years, measured in air extracted from an Antarctic ice core (EPICA Community Members, 2004). Current atmospheric abundances are higher than at any point in this record and have reached approximately 400 ppmv (CO₂) and 1800 ppbv (CH₄) (Hartmann et al., 2013).

The research presented in this thesis focuses on the measurement of trace gases in atmospheric air samples. A range of species are investigated, using a variety of sample sources (including ice core and firn air samples from Greenland and Antarctica). This chapter will begin with an introduction to the spheres of the climate system most relevant to this work (the atmosphere and the cryosphere). After this, each of the species under

investigation will be discussed in the context of the climate system and the current understanding of the processes that govern them.

1.1 The atmosphere

The Earth's atmosphere is mainly composed of nitrogen (78 %) and oxygen (21 %). It also contains a plethora of 'trace gases', so-called because of their relatively low atmospheric abundances. Of these trace gases, CO₂ and CH₄ are two of the most abundant with 2011 mole fractions of 390 ppm and 1803 ppb, respectively (on the NOAA scale from Hartmann et al., 2013). Over the last few decades, improved measurement capabilities have allowed the reliable detection and characterisation of much lower abundance compounds (e.g. carbonyl sulphide, methyl halides and chlorofluorocarbons). The sources of these gases are either natural or anthropogenic (man-made) or both. For example, a significant input of COS to the atmosphere is through volcanic eruptions. On the other hand, COS is also emitted through industrial activities and chlorofluorocarbons have only been synthesised artificially.

The atmosphere can be separated into layers according to altitude-dependent variations. The layer closest to the surface is the troposphere, followed by the stratosphere, mesosphere, thermosphere and exosphere. The reaction pathways relevant to the species under investigation in this study occur in the first two layers.

The troposphere extends from the surface to an altitude of approximately 12 km, becoming colder and less dense. Vigorous mixing (mostly driven by its surface heat source), combined with the availability of water vapour, produce most of the known weather effects. This makes it the most dynamic area of the atmosphere. The tropopause marks the transition to the stratosphere, which extends vertically by approximately 40 km. Ozone absorbs some of the Sun's ultraviolet radiation, and its formation is associated with a temperature increase with altitude and much less turbulent conditions than in the troposphere.

1.1.1 Radiative forcing

The Earth's energy budget is influenced by many factors, known as 'forcings' (e.g. the Sun's output and the Earth's orbital position and atmospheric composition) (Figure 1.2). Changing the atmosphere's composition can alter the amount of radiation that is retained through the greenhouse effect, hence altering the balance of energy moving into and out of

the Earth system. In terms of their abundance, trace gases (e.g. CO_2 , CH_4 , N_2O and water vapour) are of little significance compared to the major components of the atmosphere (N_2 and O_2). However, in terms of their impact on our climate, trace gases make by far the biggest contribution. Many of these gases are referred to as ‘greenhouse gases’ because of their ability to absorb upwelling terrestrial infrared radiation. For example, the amount of CO_2 in the atmosphere has increased by approximately 40 % since the start of the industrial revolution (1750), contributing to the observed global temperature increase over the last few decades (Bindoff et al., 2013).

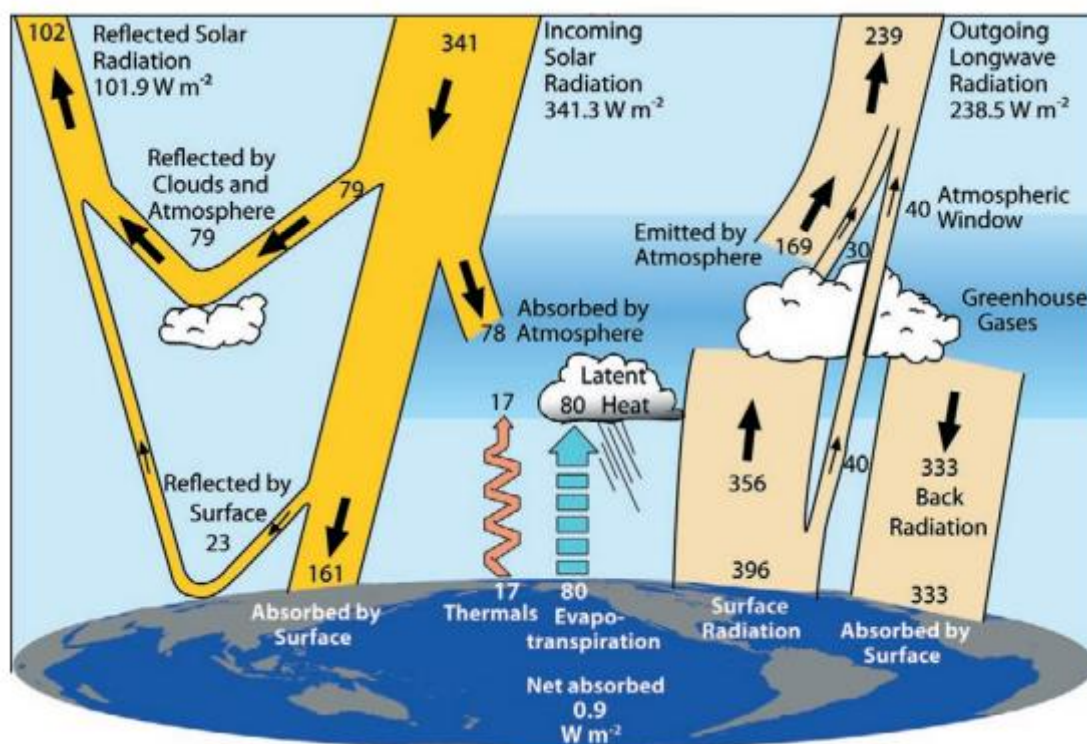


Figure 1.2. An estimate of the Earth’s annual mean energy budget between March 2000 and May 2004. The coloured sections containing arrows are sized in proportion to the magnitude of the energy flow they represent. The diagram was taken from Trenberth et al. (2009).

To assess the contribution of individual gases to the greenhouse effect, a standardised measure called the Global Warming Potential (GWP) is calculated. This factor combines

the ability of each molecule of a compound to absorb radiation over a specific time period with its atmospheric lifetime (Ramaswamy et al., 2001):

$$\text{GWP}(x) = \frac{\int_0^{\text{TH}} a_x \cdot [x(t)] dt}{\int_0^{\text{TH}} a_r \cdot [r(t)] dt} \quad (1.1)$$

In equation 1.1, TH is the time horizon over which the calculation is made, a_x is the radiative efficiency of a gas and $[x(t)]$ represents the way the abundance of a gas decreases over time. Generally, CO_2 is used as the reference gas (the denominator in equation 1.1) and is assigned the value 1 (Forster et al., 2007). In this way, GWP values are used to compare the radiative effect of different compounds. Since these values are calculated on a per molecule basis, the high atmospheric abundance of CO_2 has no effect on its GWP. Many lower abundance gases can be considered more potent based on their GWPs, even though their overall effect on the climate is less than that of CO_2 . For example, on the 100 year time horizon, SF_5CF_3 has a GWP of 17,800 (Montzka et al., 2011) and a tropospheric abundance of 0.15 pptv (Sturges et al. 2012), while CO_2 has a GWP of 1 and a tropospheric abundance of 400 ppmv (Hartmann et al., 2013).

1.1.2 Ozone

Ozone (O_3) occurs naturally in the atmosphere at abundances ranging from a few tens to hundreds of pmol mol^{-1} . It is found mostly in the stratospheric ‘ozone layer’, but there is also a significant presence near the Earth’s surface (Figure 1.3).

O_3 plays a part in both sustaining and damaging life on Earth. Tropospheric O_3 is highly reactive, destroying certain biological molecules. It reduces crop yields and can cause serious lung complaints when inhaled. On the other hand, stratospheric O_3 strongly absorbs biologically harmful UV-B radiation, preventing most of it from reaching the Earth’s surface. This makes it important to understand the processes governing its atmospheric abundance, so that we are better able to sustain it as a barrier.

O_3 production and loss mechanisms are dependent on many factors, such as latitude, season and atmospheric circulation patterns. This means that its global distribution is highly variable. Perhaps the most dramatic example of this variability was the discovery of the ozone hole over the Antarctic (Farman et al., 1985). This also made the public more aware of the damage being done by CFCs and other ozone depleting gases and served as a wakeup call for policy makers.

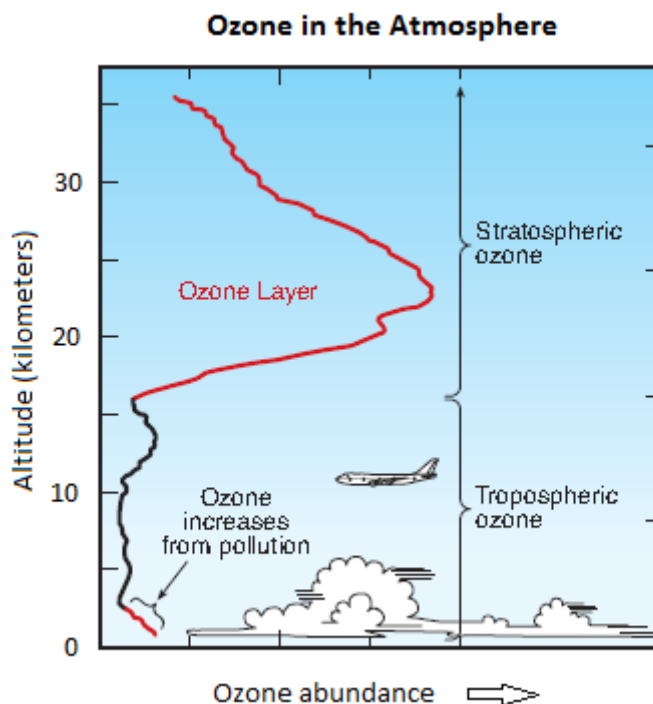
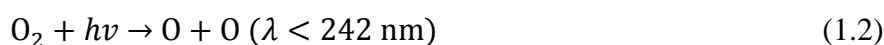


Figure 1.3. Ozone is present throughout the troposphere and stratosphere. The mid-stratosphere ‘ozone layer’ is where ozone abundance peaks. There is a second, smaller peak close to the surface, caused by anthropogenic air pollution. This schematic diagram does not convey the way ozone varies based on other factors, such as latitude and season. The diagram was taken from Fahey et al. (2010).

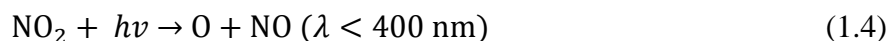
1.1.2.1 Ozone production

Ultraviolet solar radiation is integral to the production of stratospheric O_3 . The radiation splits O_2 molecules into highly reactive O atoms, which can combine with more O_2 to give O_3 . This dependence on solar radiation means that O_3 production is more prevalent in the tropics, which receive elevated levels of sunlight compared to higher latitudes. Equations 1.2 and 1.3 outline these processes (Coffey and Brasseur, 1999):



where M is a gaseous species which carries off the excess energy produced by the O₃ formation. In the atmosphere, M is typically N₂ or O₂.

Tropospheric O₃ has two main sources. The first is stratospheric O₃, transported through the tropopause. The second is from near surface chemical reactions which involve both natural and anthropogenic gases. Fossil fuel combustion is the primary source of the pollutant gases that lead to near surface O₃ production (e.g. mono-nitrogen oxides (NO_x) and hydrocarbons). For example (Liu and Ridley, 1999):



The atomic oxygen produced in this reaction can then form O₃ through equation 1.3.

1.1.2.2 Ozone loss

Equation 1.3 is one of a pair of reactions that describe the exchange of O₃ and atomic O in the stratosphere. O₃ is produced in equation 1.3 and converted back to atomic O through equation 1.5 (Coffey and Brasseur, 1999):



This mechanism forms part of the series of reactions put forward to explain the formation and destruction of the stratospheric ozone layer (Chapman, 1930). Subsequently, it has been shown that the overall atmospheric ozone abundance is overestimated by this mechanism, meaning that additional loss processes must be occurring.

Catalytic cycles have been identified which contribute significantly to the destruction of stratospheric ozone (most notably involving NO_x and species containing Cl and Br). A common catalytic cycle involving Cl will be discussed further because it is relevant to the work on CFC-11, CFC-12 and CFC-113, which all contain Cl (Chapter 3). With regards to O₃, halogens are mostly inert within their organic source gases (e.g. CFCs, CH₃Br and CH₃Cl). However, when converted to reactive species in the atmosphere, they participate in several reaction pathways which result in the destruction of O₃. For example, the photolysis of CFC-12 releases chlorine atoms (Holloway and Wayne, 2010):



Figure 1.4 illustrates an O₃ destruction cycle that occurs widely at tropical and mid-latitudes in the stratosphere. Its dominance at these latitudes is due to the higher solar radiation causing the formation of more atomic oxygen, which is required in this cycle. In

this example, the Cl atom is recycled meaning that it can go on to destroy many O₃ molecules. This preservation gives each Cl atom in the stratosphere a very high O₃ destruction potential.

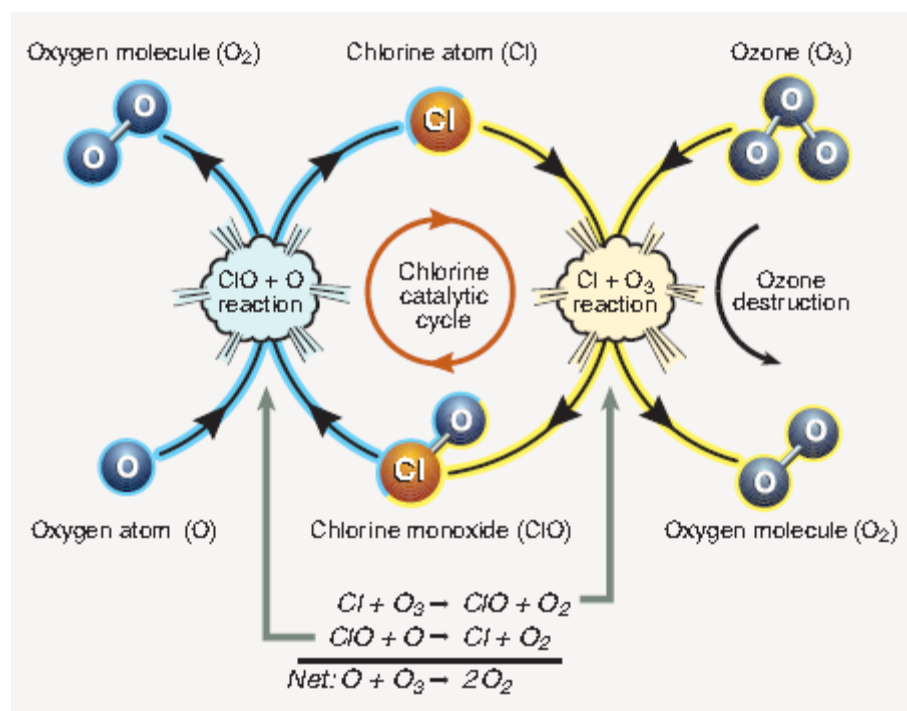


Figure 1.4. The overall reaction shown is the formation of molecular oxygen from ozone and atomic oxygen. The cycle involving Cl and ClO can be considered a catalytic one because these compounds are conserved as ozone is destroyed. The diagram was taken from Fahey et al. (2010).

The catalytic cycles involving NO_x and species containing Cl and Br are largely limited by the conversion of reactive species (e.g. Cl and ClO) into inactive forms (e.g. HCl and ClONO₂) (Coffey and Brasseur, 1999):



In these examples, HCl and ClONO₂ are termed “reservoir” species because they hold ozone destroying chemicals in an inactive form. To calculate the potential effect of ozone destroying chemicals, their total atmospheric load must be quantified, rather than just their presence as reactive species. This is because if Cl was released from one of its reservoirs, it would have the potential to destroy ozone. For example, the presence of HCl and ClONO₂ is important to the overall rate of O₃ destruction under the dynamically and chemically perturbed conditions of the polar winter (see below).

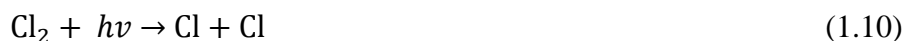
Over the last 50 years, the stratospheric conditions over the poles during winter have given rise to dramatic variations in the abundance of O₃. There are two key factors which significantly affect O₃ loss in the polar stratosphere during the winter (Holloway and Wayne, 2010):

1. Strong circumpolar winds develop in the mid-lower stratosphere above Antarctica (and the Arctic, to a lesser extent) causing what is known as the ‘polar vortex’. This acts as a barrier to horizontal transport of air, isolating the polar regions.
2. A reduction in solar radiation during this period produces low temperatures at both poles. These conditions induce the formation of polar stratospheric clouds (PSCs) which only form at temperatures below -78 °C. PSCs are particularly prevalent over Antarctica because temperatures are generally lower than over the Arctic (on average temperatures under -78 °C last for 1 – 2 months over the Arctic, compared to 5 – 6 months over the Antarctic).

The gravitational settling of PSCs which contain nitric acid causes the removal of NO_x species. This removal is termed ‘denitrification’ and results in the release of reactive species which destroy stratospheric ozone (e.g. equation 1.8). The work in this thesis relates to halogens rather than nitrogen species specifically, so denitrification will not be discussed further and subsequent examples will instead relate to chlorine. PSCs also provide a surface for the reservoir species produced in equations 1.7 and 1.8 to react on, releasing chlorine (Coffey and Brasseur, 1999):



Due to the limited available sunlight, this is followed by the slow photodissociation of Cl₂ into Cl (Coffey and Brasseur, 1999):



A small amount of this atomic chlorine will enter the reaction cycle in Figure 1.4. However, lower levels of solar radiation reduce the abundance of atomic oxygen, limiting the rate of this reaction. An alternative cycle can be used to explain the observed ozone depletion events in the polar stratosphere. In this case, ClO is formed through the reaction of Cl (from equation 1.10) with O₃ (Figure 1.4). At low temperatures, (ClO)₂ can be formed which is then photolysed to produce two chlorine atoms, leading to the destruction of O₃ (Coffey and Brasseur, 1999):



In this way, the dynamically and chemically perturbed stratospheric conditions over the poles during the winter activate large amounts of inactive ozone destroying chemicals which significantly deplete O₃ in early spring, leading to ‘ozone holes’.

Typically, naturally produced sulphur compounds (e.g. CS₂) are oxidised to SO₂ in the troposphere (Fried and Tyndall, 1999). However, the longer-lived COS is the only reduced sulphur gas which regularly reaches the stratosphere. This is due to its relatively slow reaction rate with OH, giving it a tropospheric lifetime of approximately 10 years. In the stratosphere it is either oxidised by O atoms or through photolysis (Fried and Tyndall, 1999):



Both mechanisms produce SO₂, which is further oxidised to SO₃ and H₂SO₄. Sulphate aerosol is produced when sulphuric acid condenses to form particles, which makes COS a

precursor of sulphate aerosol. These particles act in a similar way to PSCs, providing a surface for reactions to occur on. Although COS does not cause stratospheric O₃ depletion, its indirect role in the catalytic destruction process makes it a species of interest in this regard.

1.2 The cryosphere

Areas of the Earth's surface where water is found in its solid form are collectively known as the cryosphere (e.g. mountain glaciers and frozen lakes). In the case of this study, samples are taken from the ice sheets covering Antarctica and Greenland.

Polar ice deposits are formed through the gradual burial and compression of snow falling as precipitation. Air is incorporated into the ice during this burial process, meaning that samples of the paleo-atmosphere have been locked within polar ice since permanent ice sheets have covered the poles. By drilling into this ice, air can be extracted and analysed to determine the atmospheric composition hundreds of thousands of years into the past. This makes these cryospheric samples an invaluable tool in our attempts to understand the mechanisms by which the climate changes.

1.2.1 Firn structure and processes

The firn layer is the uppermost part of the polar ice sheet consisting of consolidated snow, progressively transforming into ice. The thickness of this layer varies geographically, depending on the depositional environment. Typically, the firn layer extends for 70 – 100 m, providing samples of air corresponding to approximately the last 50 – 100 years (e.g. Martinerie et al., 2009; Buizert et al., 2012). The low density and open porosity allows large air volumes to be pumped out at a selected depth, making these samples ideal for producing atmospheric histories of trace gases over the last few decades.

The convective, diffusive and lock-in zones are the three main sections of the firn column (Sowers et al., 1992; Buizert et al., 2012). They are defined according to the diffusion behaviour of gases and the physical properties of the ice at certain depths.

Convective zone

This layer consists of the least consolidated material and occupies the area closest to the surface. At most sites this zone does not extend below 12 m (Landais et al., 2006), but in

extreme environments this limit can be broken; at a site close to Vostok, with an accumulation rate approaching zero, Severinghaus et al. (2003) reported a 20 m convective zone. This zone has high porosity and is therefore well-mixed, meaning that its composition is representative of the contemporary atmosphere. Most of the air movement in this layer is driven by surface air motion ('windpumping', Colbeck, 1989) and the diffusion of gases due to temperature gradients across the convective zone (Severinghaus et al., 2001).

Diffusive zone

The weight of accumulating snow above this zone increases density and reduces porosity with depth. Gas movement in this region is dominated by molecular diffusion and gravitational settling (Sowers et al., 1992). These processes enrich heavier gases and isotopologues at the base of the firm (Craig et al., 1988; Schwander, 1989), according to the barometric equation:

$$\frac{P_z}{P_0} = e^{-\frac{mgz}{RT}} \quad (1.21)$$

where P represents the partial pressure of a species at depth z (m) and the surface ($z = 0$), m is the molecular mass of the species (kg mol^{-1}), g is the acceleration due to gravity (9.8 ms^{-2}), R is the universal gas constant ($8.314 \text{ J K}^{-1} \text{ mol}^{-1}$) and T is the temperature (K).

These processes will occur at different rates according to the position in the firm since they require open porosity, which is a depth-dependent variable. Also, the physical properties of a specific gas (e.g. molecular mass and radius) affect its movement potential. This means that the movement of a gas is dependent not only on the effective diffusivity of the firm column, but also the diffusivity characteristics of the individual species.

Lock-in zone

Sometimes referred to as the non-diffusive zone, gases are much less free to move and any motion that occurs is dominated by advection. This zone typically takes up no more than the bottom 10 m of the firm column (Schwander et al., 1993 and 1997; Battle et al., 1996; Landais et al., 2006) and is the region where most bubble close-off occurs. There is some open porosity, meaning that air can still be pumped out.

1.2.2 Ice cores

The bottom of the lock-in zone marks the firn-ice transition and is known as the close-off depth (COD). Below this point, air bubbles are no longer connected and the diffusion of gases ceases completely. This prevents air from being pumped out, necessitating the retrieval of ice samples, from which air is extracted for analysis. While firn air provides information regarding the most recent decades, ice cores preserve air from the preceding millennia. Currently, the oldest air retrieved from an ice core was drilled by the European Project for Ice Coring in Antarctica (EPICA) at the Dome C site. It extends the ice core record to approximately 800,000 years before present (e.g. EPICA Community Members, 2004; Jouzel et al., 2007; Lüthi et al., 2008).

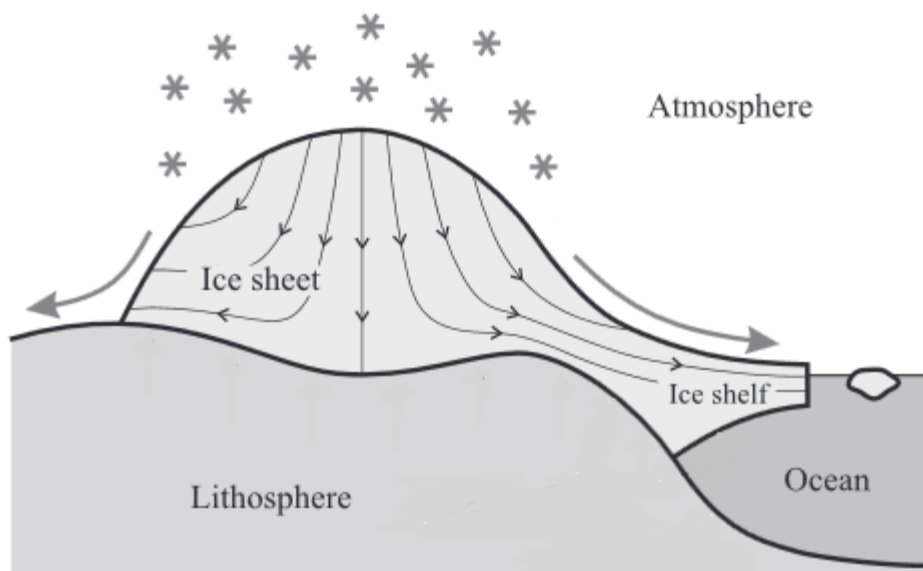


Figure 1.5. A simple illustration of flow patterns within an ice sheet. The figure was adapted from the original in Greve and Blatter (2009).

Although there has been a permanent ice sheet covering Greenland for over 2 million years (Bartoli et al., 2005) and Antarctica for approximately 14 million years (Bo et al., 2009), they are in a constant state of unrest. At the surface, material is added through precipitation and removed by ablation. Also, the ice sheet flows across the landscape under the force of gravity leading to ice shelves at the land-ocean interface, from which sections break off to

form ice bergs (Figure 1.5). This means that material deposited at a particular surface site in the past, will not necessarily be located directly beneath this spot in the present (arrows in the ice sheet in Figure 1.5 show potential paths of ice from its deposition to its eventual loss). When ice cores are dated, glaciological flow models are used to account for this motion (further details of ice core dating can be found in Section 2.3.1.1). Techniques such as radar are employed to determine sub-surface ice flow characteristics in an area. This information is used to select a site which is of adequate depth and has the least complex ice flow pattern possible. This means that drilling sites are often located at or close to a summit which typically undergoes relatively little sub-surface deformation (Figure 1.5).

Compared to a firm air sample, extracting and analysing an ice core sample is a very time consuming process. Also, sample size is significantly reduced when dealing with ice. Hundreds of litres of air can be extracted per firm sample, whereas ice is approximately 10 % air by volume, meaning that a typical 700 g sample will yield 70 ml of air. This limits the number and range of possible measurements that can be made on the air extracted from an ice core. Further details of the air extraction process can be found in Section 2.3.2.

1.3 Chlorofluorocarbons (CFCs)

Section 1.3 is based on a published paper, for which I am the lead author (Allin et al., 2015).

1.3.1 Background

CFCs are compounds containing carbon, chlorine and fluorine. They are man-made and have been used since the middle of the 20th century as refrigerants, aerosol propellants and foam blowing agents, due in part to their stability and their low flammability and toxicity. The work in this thesis refers to the three most abundant CFCs in the contemporary atmosphere (Table 1.1), which are CFC-11 (CCl_3F), CFC-12 (CCl_2F_2) and CFC-113 ($\text{CClF}_2\text{CCl}_2\text{F}$).

A direct link between CFCs and stratospheric O_3 depletion was suggested during the 1970s (e.g. Molina and Rowland, 1974). The importance of this work was publicly recognised when these authors were awarded the Nobel Prize for Chemistry in 1995, along with their collaborator, Dr. Paul Crutzen. It was not until 1985 that Farman et al. provided some of the first measurements dramatically demonstrating the environmental effect of CFCs. They presented evidence of significant O_3 losses over Antarctica (a feature now commonly

referred to as the ‘ozone hole’). As the immediacy of the threat became apparent, the international community took the effects of CFCs seriously, agreeing a plan to phase out their production and consumption under the Montreal Protocol (1987) and its subsequent amendments.

Table 1.1. Key atmospheric characteristics of CFC-11, CFC-12 and CFC-113. (a) NOAA/AGAGE mean values taken from Montzka et al. (2011) and (b) data from SPARC (2013).

	Compound		
	CFC-11	CFC-12	CFC-113
^(a) 2009 mole fraction / pmol mol ⁻¹	243	535	76
^(b) Atmospheric lifetime / years	52	102	93
^(a) Ozone Depletion Potential (ODP)	1	0.82	0.85

1.3.1.1 Atmospheric budget

Measurements performed on air from porous firn (Section 1.2.1) show that CFCs were absent from the atmosphere before the middle of the 20th century (e.g. Butler et al., 1999; Sturrock et al., 2002; Buizert et al., 2012), suggesting that they have no natural sources. CFC-11, CFC-12 and CFC-113 first appeared in the atmosphere in the 1940s – 1960s

(Sturrock et al., 2002; Martinerie et al., 2009), which coincides with the start of their widespread anthropogenic production.

CFCs are typically produced through the fluorination of chlorinated hydrocarbons. For example, equation 1.22 describes the production of CFC-11:



The main feedstock in this example (CCl_4) has been synthesised by the chlorination of CS_2 and, more recently, CH_4 . The more technically challenging use of CH_4 has been favoured over the last 50 years because it is less polluting (Rossberg et al., 2003).

Atmospheric removal occurs in the stratosphere, where sink processes are dominated by photo-dissociation (equation 1.23) and reaction with $\text{O}(^1D)$ (equation 1.24), e.g.



Cl and ClO released in these reactions catalyse the destruction of O_3 (Molina and Rowland, 1974) (Figure 1.4, Section 1.1.2.2).

1.3.2 Trace gas stable isotope measurements

By adding or subtracting neutrons from the nucleus of a chemical element, different isotopes of that element are created. For example, the nucleus of a carbon atom contains 6 protons and typically 6 neutrons, producing the most common carbon isotope (carbon-12 or ^{12}C). ^{13}C contains 7 neutrons and is the other stable isotope of carbon. Table 1.2 gives the natural abundances of the stable isotopes of carbon and chlorine, which are measured in CFCs in this thesis (Chapter 3). When these isotopes are contained within molecules, they are termed ‘isotopologues’. For example, $^{12}\text{CCl}_2\text{F}_2$ and $^{13}\text{CCl}_2\text{F}_2$ are isotopologues of CFC-12. Mass spectrometry can be used to separately measure and compare the abundance of these isotopes, producing an isotope ratio. This measured isotope ratio can then be compared to that of other samples by calculating an isotope delta (δ), expressed in per mill (‰) to represent each sample. From the above example,

$$\delta(^{13}\text{C}) = \frac{R_{\text{sample}}}{R_{\text{standard}}} - 1 \quad (1.25)$$

In equation 1.25, R represents the $^{13}\text{C}/^{12}\text{C}$ abundance ratio of a sample or standard. In this example, measurements use an internationally agreed upon ‘standard’ material called Vienna Pee Dee Belemnite (VPDB) to ensure that all measurements are comparable.

Table 1.2. The natural abundances of the stable isotopes of carbon and chlorine.

Isotope	Natural abundance / %
³⁵ Cl	76
³⁷ Cl	24
¹² C	99
¹³ C	1

In general, lighter isotopes form weaker bonds (Hoefs, 2009), meaning that compounds behave differently in physical and chemical reactions, depending on the isotopes they contain. For example, it has been found that compared to its natural abundance, ¹²C is disproportionately concentrated in biological material, partly because CO₂ containing ¹²C is preferentially used during photosynthesis (Gannes et al., 1998).

Of particular relevance to this work is the isotope dependence of reactions which destroy trace gases in the stratosphere (e.g. equations 1.23 and 1.24). Using stratospheric δ measurements, this process has been partially quantified for several species, such as N₂O (Röckmann et al., 2003; Kaiser et al., 2006) and CFC-12 (Laube et al., 2010a). These studies assume a Rayleigh-type fractionation mechanism where isotopes are partitioned by a constant factor as material is continuously removed from a reservoir (in this case, the stratosphere). By using the linear relationship in equation 1.26, this Rayleigh-type mechanism quantifies the way isotopologues of a species are partitioned during its stratospheric breakdown (defined as the apparent stratospheric isotope fractionation, ε_{app}) (Kaiser et al., 2006)

$$\ln(1 + \delta) \approx \varepsilon_{\text{app}} \ln\left(\frac{y}{y_T}\right) \quad (1.26)$$

In equation 1.26, δ represents the isotope delta measurements made on stratospheric air (e.g. $\delta(^{37}\text{Cl})$) in Laube et al., 2010a) and y and y_{T} are the stratospheric and tropospheric mole fractions, respectively.

As described above, measuring isotope ratios can provide information regarding the chemical reactions that break down a gas. In this way, isotope ratios measured in trace gases can be used to infer changes in their sources and sinks, as well as the ways in which they contribute to biogeochemical cycles (Brenninkmeijer et al., 2003; Goldstein and Shaw, 2003). Long-term studies have investigated a range of species in this way, for example, CH_4 (Etheridge et al., 1998), CO_2 (Francey et al., 1999; Rubino et al., 2013) and N_2O (Röckmann et al., 2003; Kaiser et al., 2006).

N_2O is a much studied gas with similar sinks and a comparable lifetime to CFC-12, making it relevant to the work in this thesis. Various studies have used firn and ice core samples (Sowers et al., 2002; Röckmann et al., 2003; Bernard et al., 2006; Ishijima et al., 2007), as well as direct atmospheric samples (Yoshida and Toyoda, 2000; Kaiser et al., 2006) to investigate large scale N_2O isotope and abundance changes. Source inputs depleted in ^{15}N and ^{18}O are thought to have caused the concurrent tropospheric N_2O abundance increase and $\delta(^{15}\text{N})$ and $\delta(^{18}\text{O})$ decrease over the last century, while sink processes enrich stratospheric N_2O in heavy isotopes (Röckmann et al., 2003). The heavier isotopes of nitrogen and oxygen form stronger bonds, requiring more energy to break them (as determined empirically in the activation energy term of the Arrhenius equation). This means that heavier N_2O isotopologues are less likely to dissociate in stratospheric sink reactions and are broken down more slowly, leading to the observed enrichment. Subsequently, Kaiser et al. (2006) found that this stratospheric enrichment increases with altitude and as the sampling point moves towards the equator. These effects can be explained by a variety of factors, such as changes in mixing regimes at high altitudes and the effect of the dynamically isolated and reduced sunlight environment of the polar vortex (Kaiser et al., 2006). Firn air studies are limited in their temporal resolution because diffusion processes smooth inter-annual and seasonal variations. Direct atmospheric air samples have been used to study these shorter scale changes (Nevison et al., 2005; Röckmann and Levin, 2005; Nevison et al., 2011; Park et al., 2012). Nevison et al. (2007) found that a May minimum in N_2O mole fractions at Cape Grim was replicated in CFC-11 and CFC-12 data. Since these three compounds share a stratospheric sink, it was thought that the seasonal movement of stratospheric air to the surface was a more likely explanation for this effect than a change in local sources or sinks. Subsequently, Nevison

et al. (2011) presented strong empirical evidence that the observed seasonal cycle in N₂O mole fractions at Northern Hemisphere sites is influenced by stratospheric air, as previously suggested (Nevison et al. 2005). For example, Nevison et al. (2011) found that the observed N₂O minimum was deeper in years when the lowest stratospheric temperatures were higher than average. A mechanism has not been put forward which fully explains this stratospheric influence. However, it is likely that the break-up of the polar vortex in late spring allows polar tropospheric air (which has been influenced by the stratosphere through Brewer-Dobson circulation) to be transported to lower latitudes (Nevison et al., 2011). Park et al. (2012) found that the N₂O mole fraction minimum at Cape Grim approximately coincides with a maximum in $\delta(^{15}\text{N}, \text{N}_2\text{O})$ and $\delta(^{18}\text{O}, \text{N}_2\text{O})$. This finding supports the conclusions of Nevison et al. (2005 and 2011) since stratospheric air becomes enriched in $\delta(^{15}\text{N}, \text{N}_2\text{O})$ and $\delta(^{18}\text{O}, \text{N}_2\text{O})$ as N₂O is removed. The tropospheric seasonality observed in isotope and mole fraction measurements has not been fully explained, but the seasonal movement of N₂O-depleted air with a correspondingly enriched isotopic composition from the stratosphere to the surface seems likely to be a significant contributory factor.

In contrast to N₂O, the much lower abundance CFCs are poorly characterised because very few studies have investigated their isotope ratios. Redeker et al. (2007) measured tropospheric $\delta(^{13}\text{C})$ values for 37 hydrocarbons and halocarbons, including CFC-11, CFC-12 and CFC-113, over the course of a year. In these three compounds, they found no diurnal or seasonal trends outside their analytical uncertainties. Zuiderweg et al. (2012) measured the stable carbon isotope fractionation of CFC-12 and CFC-11 by conducting UV photolysis experiments at stratospherically relevant temperatures. They found a fractionation (ϵ) of -55.3 ‰ for CFC-12, compared to -23.0 ‰ for CFC-11 (at 233 K). Zuiderweg et al. (2013) reported a large ¹³C depletion of CFC-12 measured on Greenland firn air, suggesting that a highly ¹³C-depleted reservoir has undergone significant enrichment (up to 80 ‰) from 1950 to 2009. This $\delta(^{13}\text{C})$ change is largely inferred from a single measurement at 1970, meaning that the veracity of these conclusions hinges on the reliability of this measurement. Several potential issues have been found relating to the measurements presented by Zuiderweg et al. (2013) and are discussed in Section 3.2.3.3.

The only chlorine isotope ratio study of atmospheric CFCs measured the $\delta(^{37}\text{Cl})$ of CFC-12 in the tropical stratosphere (Laube et al., 2010a). Enrichment with altitude, to a maximum of 27 ‰ relative to the tropospheric value, was attributed to sink reactions (equations 1.23 and 1.24) occurring more readily with the lighter isotopologue (as seen for N₂O). The

apparent stratospheric isotope fractionation (equation 1.26) was calculated to be $(-12.1 \pm 1.7) \%$. Laube et al. (2010a) highlighted the large effect of sink reactions on the isotopic composition of CFC-12 in the stratosphere. They did not attempt to link this effect to tropospheric signals, which would allow source isotopic characterisation. It is expected that this stratospheric effect should, in the long-term, lead to a relative ^{37}Cl -enrichment of tropospheric CFC-12 with respect to the average source isotope ratio through stratosphere-troposphere air exchange, similar to observations made on other gases, such as CH_4 (McCarthy et al., 2001), H_2 (Batenburg et al., 2012) and N_2O (Röckmann et al., 2003).

As shown by the extensive work done on N_2O (discussed above), the isotopic characterisation of trace gases can improve our understanding of their reaction and transport pathways as well as their sources. In this thesis, measurements of $\delta(^{37}\text{Cl})$ and $\delta(^{13}\text{C})$ in CFC-11, CFC-12 and CFC-113 in tropospheric samples are made as a step towards the isotopic characterisation of these gases. Below are three examples of the advances that could be made based on isotopic studies of these gases:

1. Equations 1.23 and 1.24 show the dominant stratospheric loss processes for CFCs. It could be that these reactions cause different fractionation effects. Measurements of $\delta(^{37}\text{Cl})$ in CFCs in the stratosphere (e.g. Laube et al., 2010a) and laboratory studies which isolate the effect of a single reaction (e.g. Zuiderweg et al., 2012) are informative in this regard. They could be used to quantify the lifetime of CFCs through individual reactions and calculate the relative contribution of each to CFC destruction. These measurements could also reveal spatial and temporal variations in these factors, as seen for N_2O (e.g. Kaiser et al., 2006).
2. Nevison et al. (2005) noted a similarity in the seasonal cycles of N_2O , CFC-11 and CFC-12 mole fractions at Cape Grim. It seems reasonable to expect that $\delta(^{37}\text{Cl})$ and $\delta(^{13}\text{C})$ in CFCs will exhibit comparable seasonality effects as seen in $\delta(^{15}\text{N}, \text{N}_2\text{O})$ and $\delta(^{18}\text{O}, \text{N}_2\text{O})$ (Park et al., 2012). This would provide further evidence for the influence of large-scale circulation patterns, as suggested previously (Nevison et al., 2005 and 2011; Park et al., 2012).
3. Zuiderweg et al. (2013) describe how industrial advances in the 20th century altered the manufacturing processes used to produce CFCs. The most significant change occurred in the production of the main feedstock (CCl_4). In the last 50 years it has been synthesised through the chlorination of CH_4 , whereas CS_2 had previously been used in this way. If this change caused an alteration in the emissions $\delta(^{37}\text{Cl})$ or

$\delta(^{13}\text{C})$, a change in the atmospheric isotope delta could be produced (e.g. Zuiderweg et al., 2013). Whether this change was detectable or not would depend on its magnitude and timing. Earlier emissions of these gases represent a larger proportion of the total atmospheric load, meaning that atmospheric isotope measurements are increasingly sensitive to source changes the closer they are to the point of first release.

Since CFC-11 and CFC-113 are destroyed through the same stratospheric processes as CFC-12, it is reasonable to expect that they will also exhibit sink reaction isotope dependencies. This study builds on the work of Laube et al. (2010a) to better characterise the source and sink reactions which affect the three most abundant CFCs.

More work has been done to investigate the carbon isotopes of CFCs, leading to the discovery of several isotope dependencies. However, question marks remain regarding the reliability of some of these challenging measurements. This study intends to revisit the measurements made by Zuiderweg et al. (2013) and expand the knowledge base to a long-term investigation of CFC-11, CFC-12 and CFC-113 in the troposphere.

1.4 Carbonyl sulphide (COS)

1.4.1 Background

Carbonyl sulphide (COS) has been identified as the most abundant sulphur-containing trace gas in the atmosphere (Montzka et al., 2011). Its role as a precursor for stratospheric sulphate aerosols (Section 1.1.2.2), which catalyse the destruction of O_3 (Andreae and Crutzen, 1997), makes it an important gas to characterise more fully.

The global warming potential (GWP) of COS is 27 times higher than CO_2 on the 100 year time horizon (Brühl et al., 2012). In opposition to this effect, sulphate aerosol formed from COS act to cool the planet by reflecting solar radiation away from the Earth's surface. Brühl et al. (2012) have calculated that these two effects approximately cancel each other out. Therefore, while COS is important in stratospheric O_3 destruction, it is not recognised as a net contributor to global warming in its capacity as a greenhouse gas (GHG).

1.4.2 Atmospheric budget

Several studies have investigated the COS budget (Khalil and Rasmussen, 1984; Chin and Davis, 1993; Kettle et al., 2002; Watts, 2000; Montzka et al., 2007). This has proved a challenge because it is a highly complex system, with various terrestrial, oceanic and atmospheric processes contributing to the production and removal of atmospheric COS.

The oxidation of carbon disulphide (CS_2) in the atmosphere is thought to be the main source of COS (Watts, 2000). As well as its natural presence, CS_2 is emitted during the production of viscose-rayon (an artificial fibre). This process began in Europe in 1910 and is still operational today, although production shifted to Asia by the early 1990s (source: Fiber Economics Bureau, Inc.). As well as an anthropogenic influence through the viscose-rayon industry, domestic stoves and heating systems have been cited as direct sources of COS (Mu et al., 2002). COS is also the atmospheric oxidation product of dimethyl sulphide (DMS), an oceanic phytoplankton emission (Barnes et al., 1994). Other natural sources of COS include the oceans, biomass burning, volcanoes, wetlands and anoxic soils (Aydin et al., 2008).

By far the largest COS sink is uptake by vegetation during photosynthesis (this link will be discussed further in Section 1.4.4). Other sinks include the oceans, soils, reaction with OH and stratospheric photolysis. These sinks give COS a tropospheric lifetime of 2 – 4 years (Montzka et al., 2007; Suntharalingham et al., 2008).

The oceans are both a COS source and sink, depending on the season (Wilhelm et al., 1977; DeBruyn et al., 1995; Weiss et al., 1995; Ulshofer et al., 1995, 1996). Out-gassing peaks during the summer/autumn (Ulshofer et al., 1996) and at the point of maximum daylight (Zepp and Andreae, 1994) due to various production mechanisms. It is thought that the oceans act as a global net source over an average annual cycle (Watts, 2000).

1.4.3 Measurement history

COS was first measured in the atmosphere approximately 40 years ago (Hanst et al., 1975; Sandalls and Penkett, 1977). Since then, Bandy et al. (1992) have presented a Northern Hemisphere time series over the period 1977 – 1991. They made more than 1000 aircraft- and ground-based measurements with a mean mole fraction of $512 \text{ pmol mol}^{-1}$. However, a standard deviation of $119 \text{ pmol mol}^{-1}$ made it difficult to draw conclusions regarding either annual or seasonal variations in this period. Bingemer et al. (1990) had similar variability

issues, only allowing the authors to tentatively suggest an anthropogenic source, based on a strong correlation with CO and CH₄.

Other direct atmospheric studies have focused on specific air environments. Kourtidis et al. (1995) used balloons to measure vertical profiles in the Arctic vortex. They show a steep decline in COS above the tropopause, as would be expected. Marine air has been investigated in an attempt to understand the COS budget (Thornton et al., 1996) and quantify its air-sea flux (Xu et al., 2001). Urban air presents an interesting study environment because of the proximate anthropogenic influence along with the natural background level. Mu et al. (2002 and 2004) measured generally elevated values in Beijing City as well as a diurnal cycle with high values at night (attributed to increased thermal convection during the day).

Several short-term COS studies have successfully quantified its large seasonal cycle. For example, the Global Monitoring Division of the Earth System Research Laboratory (ESRL), at the National Oceanic and Atmospheric Administration (NOAA), has made high time resolution COS measurements since 2000 at 11 Northern and Southern Hemisphere sites (these data are published at <http://www.esrl.noaa.gov/gmd/hats/gases/OCS.html>). Montzka et al. (2007) found the highest annual average mole fractions at the equator, with reduced abundances at higher latitudes in both hemispheres. The terrestrial vegetation sink is more prevalent in the Northern Hemisphere (NH) because land masses are concentrated there, leading to a COS minimum in the late NH summer. Conversely, the Southern Hemisphere (SH) COS cycle is dominated by the oceanic source, which produces a maximum in the Austral summer (February). Due to the dominance of a sink in the NH and a source in the SH, there is a mean inter-hemispheric gradient of approximately 3 % towards the SH (Montzka et al., 2007; Figure 1.6).

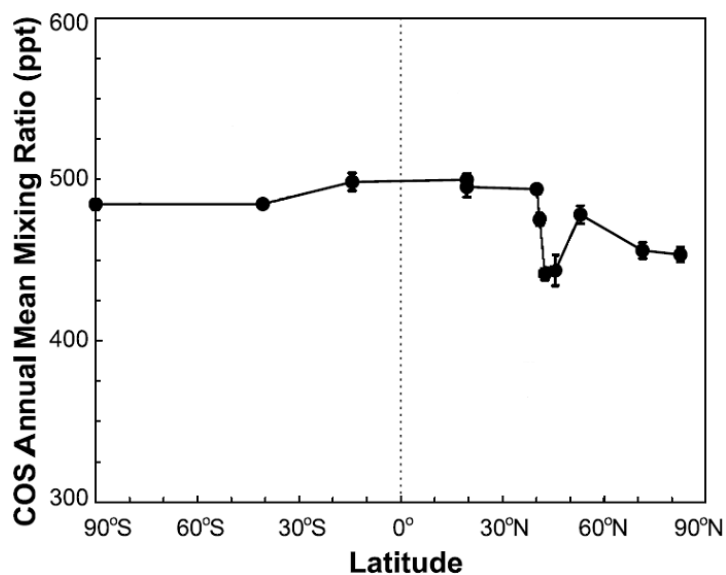


Figure 1.6. The NOAA average annual COS mole fractions from up to 5 years of ground-based data, plotted against each station's latitude. The figure was adapted from Montzka et al. (2007).

The analysis of firm air samples extended the measurement history to earlier in the twentieth century. This was first achieved by Sturges et al. (2001) when they analysed air extracted from firm at Devon Island (Canada), Dronning Maud Land and Dome Concordia (both Antarctica). A physical transport model was used to consider possible historical changes (a full inversion to actual trends was not possible at this time). At the Antarctic sites, they found lower COS in the early 20th century and the Devon Island record revealed a possible NH decline in recent years of $8 \pm 5\%$.

Montzka et al. (2004) reported a pre-1980s rise in the SH, before a fall of 60 – 90 pmol mol⁻¹ to ambient levels of 480 – 490 pmol mol⁻¹. A firm diffusion model was used to calculate the increasing trend to the 1980s and the subsequent decline was inferred largely from surface measurements made between 2000 and 2002 (from NOAA ground-based stations). The firm measurements at depths shallower than 40 m do not wholly agree with this decline between the 1980s and 2000. Montzka et al. (2004) suggest that rapid diffusion in the shallow firm has caused abrupt changes in atmospheric abundance to be smoothed, meaning that model-derived peak mole fractions are higher than those measured in the firm.

Data from other sources support a decrease since the 1980s, although there is some disagreement regarding its magnitude. For example, Rinsland et al. (2002 and 2008) found a small but statistically significant long-term NH free tropospheric COS change between 1978 and 2002 of -0.25 ± 0.04 %/year, from solar absorption spectra.

Most recently, the twelve NOAA ground-based stations have provided a continuous record of COS abundance from early in the 21st century to the present day (<http://www.esrl.noaa.gov/gmd/hats/gases/OCS.html>). These measurements show significant variation over this period due to the presence of strong seasonal cycles. However, based on these measurements, average annual tropospheric mole fractions have not changed significantly in the 21st century.

Aydin et al. (2002) found no evidence of COS loss in ice cores and suggested that a long-term record of COS mole fractions could be measured. Aydin et al. (2007) found good agreement between Northern and Southern Hemisphere ice core records, concluding that the observed signals reflect real paleo-atmospheric variations. Subsequently, two studies have found evidence of contamination processes that would affect the COS record (Aydin et al., 2010 and 2014). Aydin et al. (2010) measured CFC-12 (an anthropogenic gas with a high contemporary abundance) in firn and ice from three sites. As expected, CFC-12 decreased to zero at the base of the firn and was not present in ice core samples significantly below the deepest firn sample. However, ice core samples at the firn-ice transition showed elevated levels. A post-coring entrapment process was used to explain this observation. It is possible that some pores remain open at this depth, allowing modern air to be included as the core is recovered. Following this, Aydin et al. (2014) investigated the effect of water on measured COS values from ice core samples. They reported that hydrolysis of COS occurs within the ice core, leading to a progressive loss as the sample age increases. Thompson et al. (1935) first described the hydrolysis of COS in aqueous solution and subsequent studies have used reaction kinetic experiments to make COS hydrolysis lifetime estimates (Elliot et al., 1989; Assonov et al., 2005). Aydin et al. (2014) infer a lifetime of ~10000 years at -30 °C (a typical mean surface temperature at their Antarctic drilling sites). Warmer sites exhibit the fastest hydrolysis rates, leading to the largest correction at a given age. Aydin et al. calculated that there was a loss of ~100 pmol mol⁻¹ 3000 years before present at the warmest site (Siple Dome C). Loss rates were calculated to be approximately half this at colder locations.

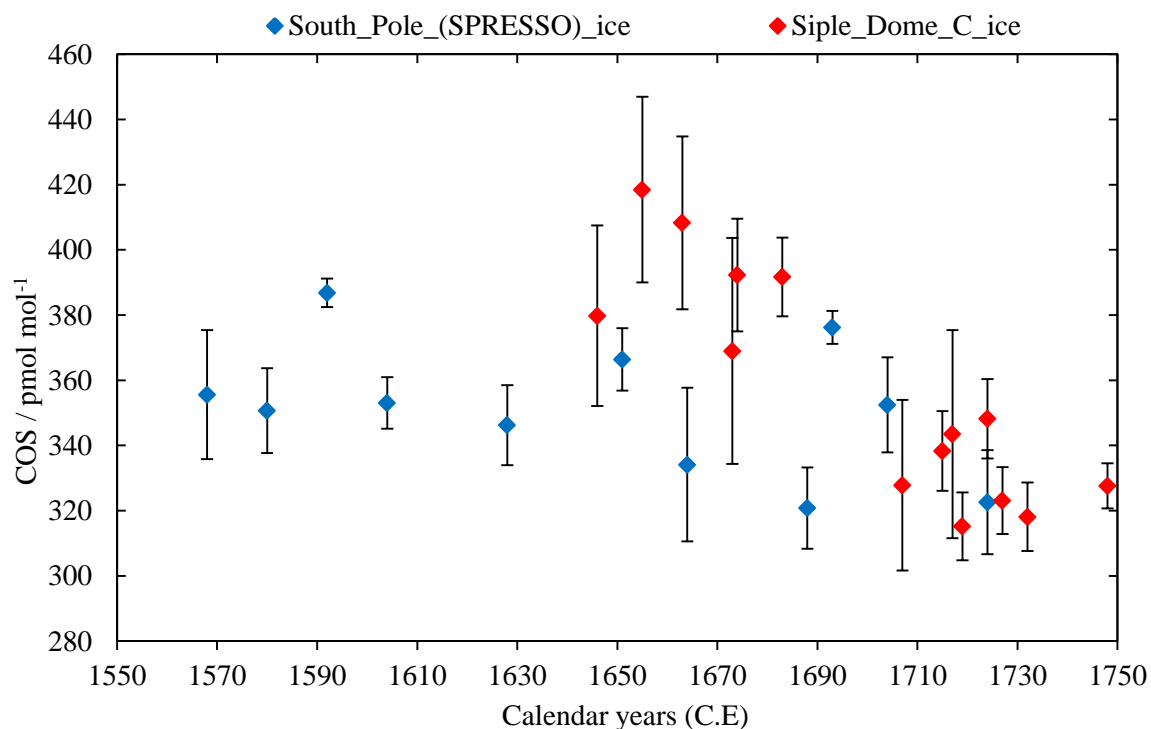


Figure 1.7. COS measurements from South Pole SPRESSO (blue diamonds) and Siple Dome C (red diamonds) ice between 1550 and 1750. 1σ error bars are shown. The figure was adapted from Aydin et al. (2008).

The Saltzman/Aydin Research Group at the University of California, Irvine has published a series of studies regarding pre-industrial atmospheric COS in air extracted from ice cores (Aydin et al., 2002, 2008 and 2014; Montzka et al., 2004). 11 ice core samples with air ages ranging from 1616 to 1694 AD were analysed for COS mole fractions (Aydin et al., 2002). A mean value of (373 ± 37) pmol mol⁻¹ was reported, which is approximately 25 % lower than contemporary levels. Data from Montzka et al. (2004) agree with this 17th century level, as well as extending the record to establish a pre-industrial level of just under 350 pmol mol⁻¹ between 1700 and 1900. Following this, Aydin et al. (2008) presented data from the SPRESSO ice core (South Pole), covering the last 2000 years. This work suggests that COS levels were relatively stable at slightly below 350 pmol mol⁻¹ over the last 2000 years. These data (Aydin et al., 2008) do not show elevated COS levels during the 1600s, contradicting the measurements from the Siple Dome C core (Montzka et al., 2004; Figure 1.7). The slightly elevated levels during the 1600s from Siple Dome C ice

(Montzka et al., 2004) represent the only significant change in the natural COS budget over the last 2000 years. However, these elevated Siple Dome C measurements have larger uncertainties than the South Pole measurements made over the same period (Aydin et al., 2008; Figure 1.7). There are mean 1σ uncertainties of 23.0 and 11.8 pmol mol⁻¹ from Siple Dome C and South Pole ice, respectively (between 1600 and 1700). The reason for this difference in uncertainties is not known, although it does cast some doubt on the robustness of the measurements made by Montzka et al., 2004.

A longer-term study measured COS in ice from several Antarctic ice cores (Byrd, Siple Dome, South Pole, Taylor Dome and WAIS Divide), covering various age ranges, up to almost 8000 years before present (Aydin et al., 2014). After accounting for the observed COS losses due to hydrolysis, the authors report a slow COS increase which started approximately 5000 years ago. They suggest that a decline in the net terrestrial primary productivity during this period is the most likely cause. Further details of this link can be found in Section 1.4.4.

A significant amount of work has been done on SH firn and ice (particularly by the Saltzman/Aydin group), but there is very little long-term NH data. The Devon Island record presented by Sturges et al. (2001) is the only NH record that extends pre-1978 (judging by the CFC-12 mole fractions used as an age normaliser). The NH firn air measurements presented in this thesis (Chapter 4) provide a new constraint on the atmospheric history of COS in the NH during the 20th century.

1.4.4 COS and the carbon cycle

The carbon cycle describes the ways in which carbon is exchanged between the atmosphere, hydrosphere, biosphere and lithosphere (Figure 1.8). Understanding these exchange processes helps to create a global carbon budget, which is a way of describing where all of the carbon on Earth is (Williams and Follows, 2011). Perhaps the most dynamic parts of this system are the atmosphere, biosphere and hydrosphere, which play host to a wide variety of reactions. Public awareness of the atmospheric component of the carbon budget is high, because of the well documented anthropogenic rise of CO₂ levels and the harm this could cause. Other reservoirs are less well understood in the public forum, for example, the role of vegetation in this system (Sarmiento and Gruber, 2002).

As described in Section 1.4.2, uptake by vegetation is the dominant COS sink. Many studies have attempted to understand this terrestrial uptake process (e.g Kluczewski et al., 1985; Goldan et al., 1988; Protoschill-Krebs and Kesselmeier, 1992; Protoschill-Krebs et al., 1996; Sandoval-Soto et al., 2005; Seibt et al., 2010; Stimler et al., 2010). It has been found that COS follows the same path as CO₂ through leaf stomata, before being consumed by photosynthetic enzymes (particularly carbonic anhydrase). At this point COS is destroyed, whereas CO₂ is subsequently released from the plant during respiration. This means that, subject to certain conditions (listed below), COS can be used as a proxy for terrestrial Gross Primary Production (GPP). GPP is a measure of the amount of chemical energy an ecosystem produces in a given time. This makes it a suitable variable to constrain when attempting to determine the state of the paleo-climate. This information can then be used to make predictions regarding future climatic conditions.

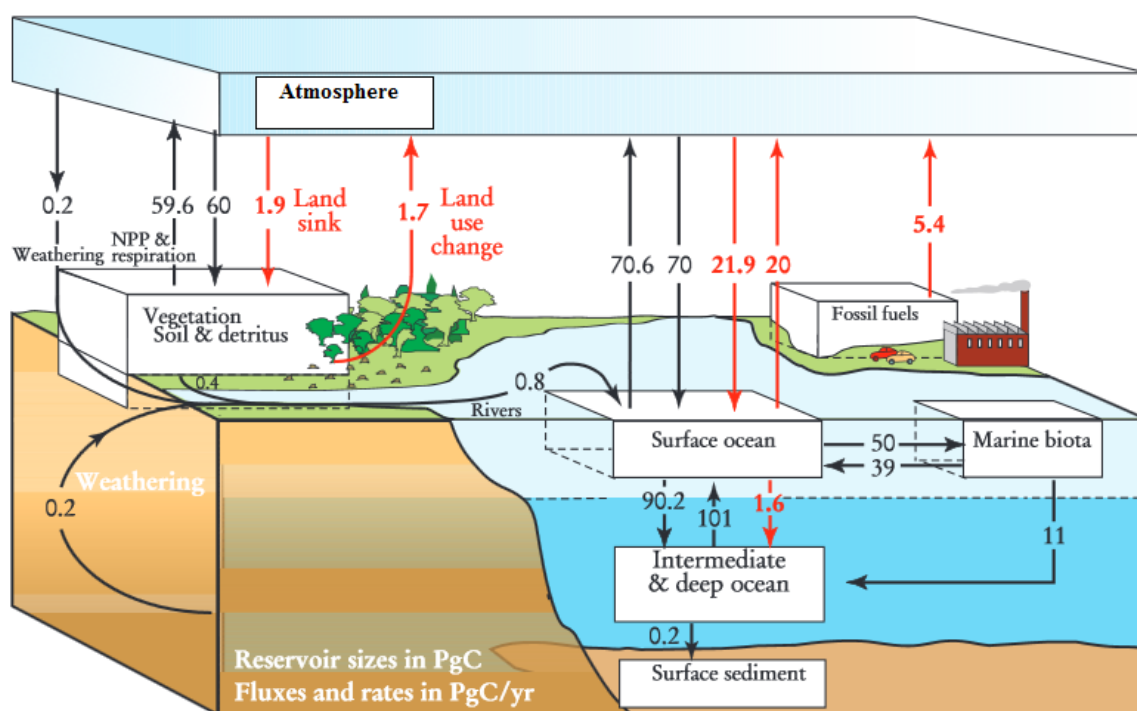


Figure 1.8. An illustration of the complex interactions of the carbon cycle. The average anthropogenic (red) and natural (black) fluxes during the 1980s are represented by arrows (in petagrams of carbon per year). The figure was taken from Sarmiento and Gruber (2002).

The link between COS and the global carbon cycle has developed rapidly in recent years (e.g. Campbell et al., 2008; Suntharalingam et al., 2008; Blonquist et al., 2011; Berry et al., 2013). Blonquist et al. (2011) provide a comprehensive summary of the current evidence. Four assumptions are made in order to use COS as a proxy for GPP:

1. An identical diffusion pathway into the leaf is used by COS and CO₂.
2. Once inside the leaf, there is no subsequent COS release.
3. COS and CO₂ act entirely independently.
4. The diffusion of COS into leaves is the only interaction between COS and the ecosystem.

Assumptions 1 and 3 have been widely supported by leaf and canopy scale gas exchange studies (e.g. Xu et al., 2002; Stimler et al., 2010). However, nocturnal emissions have been recorded from a spruce forest tower site meaning that further work is required to fully satisfy the second and fourth conditions (Xu et al., 2002).

In general, the overwhelmingly positive outcome of these gas exchange studies supports the use of COS as a proxy for GPP (Blonquist et al., 2011). However, the isolated examples of environments which violate the requirements should be investigated further to determine their overall significance.

1.5 Research objectives

This section outlines the broad research objectives of this work and how they relate to the field of atmospheric science in general. Chapters 3 and 4 will provide details regarding the expected scientific outcomes specific to the work presented in each chapter.

1.5.1 An atmospheric history of the chlorine and carbon isotope composition of CFC-11, CFC-12 and CFC-113

Isotopic characterisation is an essential tool in understanding the atmospheric history of a trace gas. For example, source inputs depleted in ¹⁵N and ¹⁸O are thought to have caused the concurrent tropospheric N₂O abundance increase and $\delta(^{15}\text{N})$ and $\delta(^{18}\text{O})$ decrease over the last century (Röckmann et al., 2003).

- This study aims to produce a tropospheric chlorine and carbon isotope history of CFC-11, CFC-12 and CFC-113 as a step towards the construction of their global

isotope budgets. This work is vital in order to better understand the way these gases interact with the climate system.

- The use of a single-collector GC-MS instrument to measure trace gas isotope ratios is a relatively new advance in this field. This study aims to expand the range of fragment ions available for effective analysis by developing methodological improvements to enhance measurement precision.

1.5.2 Carbonyl sulphide (COS) in ice and firn

Further characterisation of the atmospheric history of COS and its link to the global carbon cycle would improve our understanding of the way our climate has changed in the past, potentially leading to better climate change predictions.

- This study aims to make high precision COS, CO₂ and $\delta(^{13}\text{C}, \text{CO}_2)$ measurements on ice core samples from the last 1000 years to confirm or refute the discussed link between COS and the global carbon cycle.
- Uncertainty remains over the global atmospheric history of COS during the 20th century. A new set of Northern and Southern Hemisphere firn air measurements will improve our understanding of COS mole fraction changes during this period.

Chapter 2: Experimental methodologies

This chapter provides a general overview of the techniques used to perform this trace gas work. Methods developed for specific periods of analysis will be discussed in the relevant results chapters (3 and 4).

2.1 Gas Chromatography-Mass Spectrometry

In the last two decades, coupled gas chromatography-mass spectrometry (GC-MS) systems have become more widespread and are particularly useful in the analysis of multiple compounds in air samples. The high sensitivity of these systems has opened up the possibility of detecting gases at very low abundances. For example, Laube et al. (2014) measured HCFC-133a in archived air samples to a minimum abundance of approximately $0.02 \text{ pmol mol}^{-1}$.

The measurements discussed in this thesis were performed using an Agilent 6890 GC, coupled to a VG/Waters “AutoSpec” EBE tri-sector mass spectrometer. This system was designed to make high precision measurements of pmol mol^{-1} level gases in small air samples. Details of previous work conducted using this system can be found in Laube et al. (2010b), Sturges et al. (2012) and Allin et al. (2015). A detailed description of GC-MS techniques can be found in Skoog et al. (2004) and Williams (2006). A general overview of gas chromatography and mass spectrometry is given below and a more detailed description of the instrument used in this work can be found in Section 2.1.1.

Gas Chromatography

Gas chromatography allows the separation of compounds according to their partitioning on a ‘stationary phase’, when transported across it by a ‘mobile phase’. In this case, the ‘stationary phase’ is a porous layer on a capillary column and the ‘mobile phase’ is helium gas, flowing constantly through the system. It is important to regulate the temperature of the column so that the elution of compounds is predictable. In this work, the column was housed in a programmable Agilent GC oven. This control allows specific compounds to be observed at pre-determined points during an analysis (see Section 2.1.1 for more details).

Mass Spectrometry

Once eluted from the column, compounds are transported into the ionisation source of the mass spectrometer. A heated filament produces a beam of electrons which bombard the sample gas molecules and produce molecular and fragment ions. For example, this process produces the molecular ion of CFC-11 (CCl_3F):



As discussed in Section 2.1.1.1, the CCl_2F^+ fragment is typically used to measure CFC-11. This ion results from further fragmentation of the radical cation formed in equation 2.1 and can be produced through the loss of a Cl atom:



The AutoSpec instrument used in this work is a tri-sector mass spectrometer, meaning that these ions pass through two electric sectors, one on either side of the magnetic sector. The electric sectors improve sensitivity through de-magnifying optics and reduce background noise through the removal of metastable ions. The magnetic sector deflects the ions according to their mass to charge ratio (m/z) towards the detector. The flight path within the mass spectrometer must be kept under vacuum using scroll and diffusion pumps. This prevents air molecules from interacting with the in-flight sample ions. The presence of air molecules would disrupt the sample detection by reacting with the ions or simply by deflecting them.

The AutoSpec uses an off-axis ion detector which further reduces the background noise level by preventing neutral ions from striking the detector. A dual conversion dynode configuration releases electrons as sample ions strike its surface. These electrons then impact a phosphor screen which emits photons. Lastly, a photomultiplier tube converts these photons into an electronically detectable signal. This is achieved through the ‘photoelectric effect’ (where photons impact a surface releasing electrons) and ‘secondary emission’ of electrons (where an electron strikes the surface of an electrode releasing several electrons). Section 2.1.1.4 describes how this signal is viewed and interpreted.

2.1.1 Measurement procedure

2.1.1.1 Instrument setup

Waters® provide the software package ‘MassLynx’ as an interface between the instrument and user; it controls all aspects of the instrument setup.

The MS was operated at a mass resolution of 1000 in EI-SIR (Electron Impact-Selected Ion Recording) mode. The SIR programme is split into functions which define set time periods after a sample has been injected into the GC-MS system. Based on the elution times of specific compounds, mass to charge ratios (m/z) are included in each function, which correspond to known source ionisation products of these species (e.g. Table 2.1).

Table 2.1. An example of a programme used for measurements made in Selected Ion Recording mode on a 49 m GS-GasPro porous layer open tubular column. Empirical formulae are given and the monitored ions include the most abundant isotopes, unless otherwise stated.

Function	Start time / mins	End time / mins	Compound	Monitored m/z	Major ion
1	5.5	7.4	C ₂ F ₄	99.9936	C ₂ F ₄ ⁺
			SF ₆	126.9641	SF ₅ ⁺
			C ₁₆ H ₃₄ (lock mass)	113.1330	C ₈ H ₁₈ ⁺
2	7.4	9.2	CH ₂ F ₂	51.0046	CH ₂ F ₂ ⁺
				52.0125	CHF ₂ ⁺
			COS	59.9670	COS ⁺
				60.9664	CO ³³ S ⁺
				61.9628	CO ³⁴ S ⁺
C ₁₆ H ₃₄ (lock mass)	57.0704	C ₄ H ₉ ⁺			
3	9.2	10.4	C ₂ ClF ₅ (CFC-115)	84.9657	CClF ₂ ⁺
				86.9627	C ³⁷ ClF ₂ ⁺
			C ₁₆ H ₃₄ (lock mass)	99.1174	C ₇ H ₁₅ ⁺

Table 2.1.

4	10.4	11.2	CCl ₂ F ₂ (CFC-12)	100.9361	CCl ₂ F ⁺
				101.9395	¹³ CCl ₂ F ⁺
				102.9332	C ³⁵ Cl ³⁷ ClF ⁺
			C ₁₆ H ₃₄ (lock mass)	99.1174	C ₇ H ₁₅ ⁺
5	11.2	11.95	CH ₃ Cl	49.9923	CH ₃ Cl ⁺
				50.9957	¹³ CH ₃ Cl ⁺
				51.9894	CH ₃ ³⁷ Cl ⁺
			CH ₂ FCF ₃ (HFC-134a)	68.9952	CF ₃ ⁺
			C ₁₆ H ₃₄ (lock mass)	99.1174	C ₇ H ₁₅ ⁺
6	11.95	12.8	CS ₂	75.9441	CS ₂ ⁺
				77.9399	CS ³⁴ S ⁺
			C ₁₆ H ₃₄ (lock mass)	71.0861	C ₅ H ₁₁ ⁺
7	12.8	13.3	CH ₃ Br	93.9418	CH ₃ Br ⁺
				94.9452	CH ₂ ⁸¹ Br ⁺
				95.9398	CH ₃ ⁸¹ Br ⁺
			C ₁₆ H ₃₄ (lock mass)	99.1174	C ₇ H ₁₅ ⁺
8	13.3	14.1	CCl ₃ F (CFC-11)	100.9361	CCl ₂ F ⁺
				101.9395	¹³ CCl ₂ F ⁺
				102.9332	CCl ³⁷ ClF ⁺
			C ₁₆ H ₃₄ (lock mass)	99.1174	C ₇ H ₁₅ ⁺
9	14.1	15.3	C ₂ H ₅ Cl	64.0080	C ₂ H ₅ Cl ⁺
				66.0050	C ₂ H ₅ ³⁷ Cl ⁺
			CH ₂ Cl ₂	85.9504	CH ₂ Cl ³⁷ Cl ⁺
				87.9475	CH ₂ ³⁷ Cl ₂ ⁺
			C ₁₆ H ₃₄ (lock mass)	85.1017	C ₆ H ₁₃ ⁺

Table 2.1.

10	15.3	16.3	$C_2Cl_3F_3$ (CFC-113)	100.9361	CCl_2F^+
				101.9395	$^{13}CCl_2F^+$
				102.9332	$CCl^{37}ClF^+$
			$C_{16}H_{34}$ (lock mass)	99.1174	$C_7H_{15}^+$
11	16.3	17.2	$CHCl_3$	82.9455	$CHCl_2^+$
				84.9426	$CHCl^{37}Cl^+$
			CCl_4	116.9066	CCl_3^+
			CH_2ClBr	129.9008	$CH_2^{81}BrCl^+$
			$C_{16}H_{34}$ (lock mass)	99.1174	$C_7H_{15}^+$
12	17.2	17.85	C_2HCl_3	129.9144	$C_2HCl_3^+$
				133.9085	$C_2HCl^{37}Cl_2^+$
			C_2H_5I	156.9514	$C_2H_5I^+$
			$C_{16}H_{34}$ (lock mass)	141.1643	$C_{10}H_{21}^+$
13	17.85	18.3	$CHCl_2Br$	82.9455	$CHCl_2^+$
				84.9426	$CHCl^{37}Cl^+$
			CH_2Br_2	92.9340	$CH_2^{79}Br^+$
				94.9319	$CH_2^{81}Br^+$
			CH_3CCl_3	96.9612	$CH_3CCl_3^+$
		$C_{16}H_{34}$ (lock mass)	85.1017	$C_6H_{13}^+$	
14	18.3	18.75	C_3H_7Br	121.9731	$C_3H_7Br^+$
				123.9711	$C_3H_7^{81}Br^+$
			$C_{16}H_{34}$ (lock mass)	113.1130	$C_8H_{18}^+$
15	18.75	19.5	$(CH_2Cl)_2$	61.9923	$C_2H_3Cl^+$
				63.9894	$C_2H_3^{37}Cl^+$
			C_2Cl_4	93.9377	$C_2Cl_2^+$
				95.9348	$C_2Cl^{37}Cl^+$
			$C_{16}H_{34}$ (lock mass)	71.0861	$C_5H_{11}^+$

Table 2.1.

16	19.5	20.6	CHClBr ₂	126.8950	CHClBr ⁺
				128.8930	CHCl ⁸¹ Br ⁺
			C ₁₆ H ₃₄ (lock mass)	127.1486	C ₉ H ₁₉ ⁺
17	20.6	25	C ₂ H ₄ Br ₂	106.9496	C ₂ H ₄ Br ⁺
			CHBr ₃	170.8445	CHBr ₂ ⁺
				172.8425	CHBr ⁸¹ Br ⁺
			C ₁₆ H ₃₄ (lock mass)	141.1643	C ₁₀ H ₂₁ ⁺

Each species is fragmented into a wide range of ionisation products. This means that several fragments of the same species can be measured in a single acquisition, allowing the investigation of multiple isotopologues (e.g. three ions represent three isotopologues of CFC-11 in function 8, Table 2.1). Figure 2.1 shows the mass spectra of the reference gas (hexadecane) and CFC-11. Each peak in Figure 2.1 represents a fragment ion of the parent molecule, with a unique mass to charge ratio (m/z). Given the extensive list of ionisation products which could be measured, a decision needed to be made regarding which fragment ions were included in the mass spectrometer programme (Table 2.1). This decision was made based on two factors:

1. The size of the peaks. Both the target species (e.g. CFC-11) and the reference gas (hexadecane) must provide peaks which are large enough to be detected, but not so large that the detector will become saturated and prevent a robust measurement.
2. The proximity of the peaks. In terms of their m/z values, the target species and reference peaks must be as close to each other as possible. Typically, the largest detectable m/z value in a function is 1.5 times the smallest detectable m/z value.

In the case of CFC-11, the CCl₂F⁺ ion is used (m/z 101) because it is the most abundant fragment ion and there are several close-by hexadecane peaks (m/z 85, 99 and 113) which can be used in the tuning and mass calibration process (Figure 2.1).

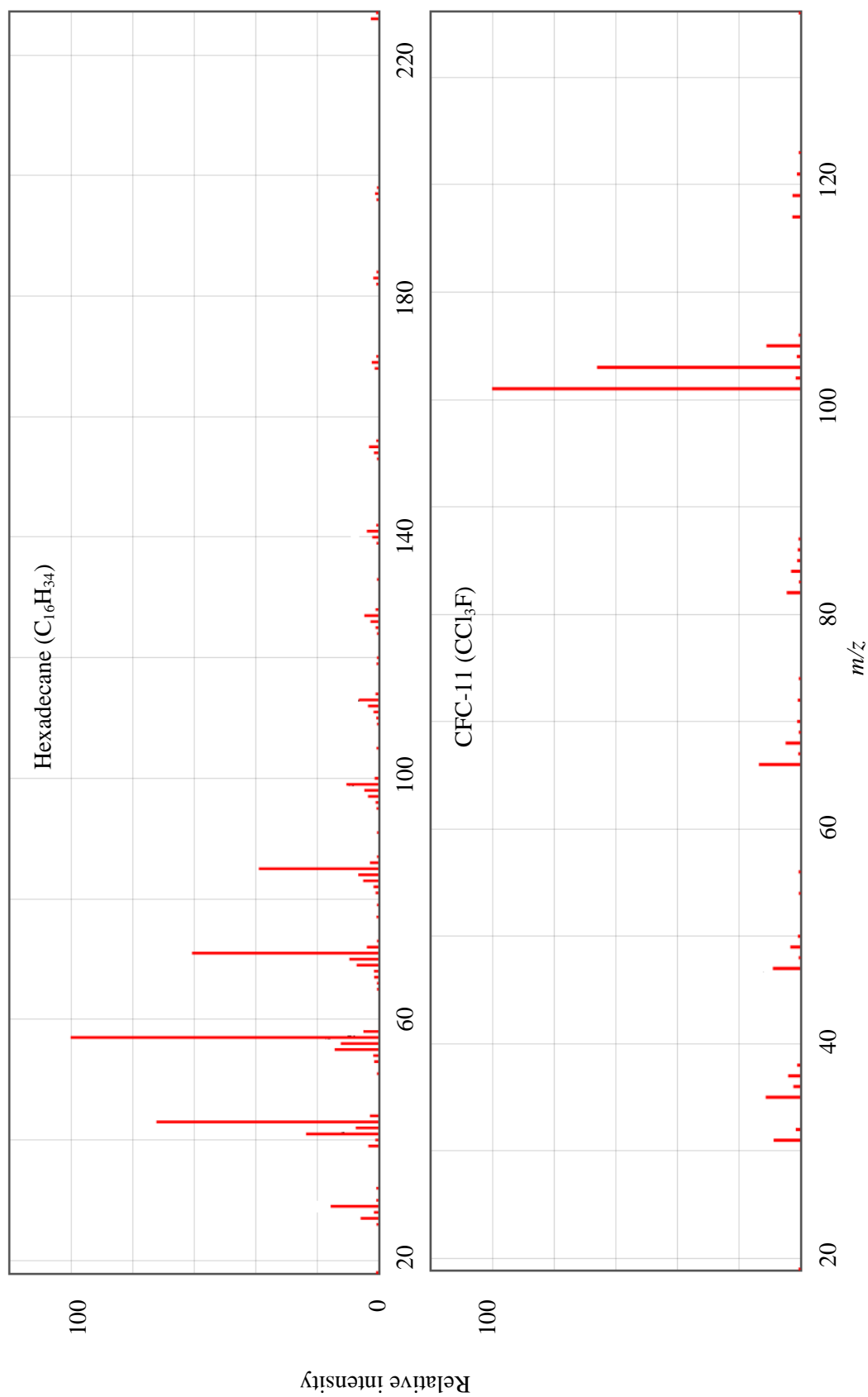


Figure 2.1. The mass spectra of ionisation products for hexadecane (C₁₆H₃₄) and CFC-11 (CCl₃F). The most abundant fragment ions are found at m/z 57 (C₄H₉⁺) and m/z 101 (CCl₂F⁺) for hexadecane and CFC-11, respectively. The spectra were taken from the NIST online database: <http://webbook.nist.gov/chemistry/name-ser.html>.

To optimise the instrument's performance, a daily process of tuning and mass calibration was necessary. Before any measurements were made, the ion repeller and focusing lenses were adjusted whilst observing a reference gas peak to produce a large, symmetric peak. This reference gas is contained in a glass vessel which is attached to a movable stainless steel tube, directly linked to the ion source. The flow rate is controlled using a valve and by adjusting the distance between the hexadecane and the ion source to achieve a constant flow at the desired level. The mass calibration process ensures that the m/z values of the various hexadecane fragment ions are correctly identified. This is particularly important for the hexadecane m/z value included in each function (known as the lock mass). The accelerating voltage jumps between masses in an appropriate range, matching peaks with known hexadecane fragment ions. This procedure allows small peak position changes to be tracked and corrected for, meaning that the masses corresponding to species of interest are reliably detected.

2.1.1.2 Sample preparation

A glass tube containing magnesium perchlorate ($\text{Mg}(\text{ClO}_4)_2$) was included in the inlet system (Figure 2.2). Due to its hygroscopic nature, it was used to dry all air before being introduced to the GC-MS system. A short $1/16^{\text{th}}$ inch outside diameter stainless steel pre-concentration loop, packed with Heysep D (80/100 mesh), was cooled to $-78\text{ }^\circ\text{C}$ by immersion in a dry ice/ethanol mixture. Approximately 200 ml of the dried sample was passed through the loop, trapping the species of interest. A reference volume and a Baratron pressure sensor were used to measure the actual volume of air used. The loop was then opened to the carrier gas (research grade helium) which flows into the GC oven at a constant 2 ml/min. By removing the dry ice/ethanol mixture and immediately replacing it with hot water ($\sim 95\text{ }^\circ\text{C}$), the trapped gases were released. Figure 2.2 shows a schematic diagram of the inlet system.

The GC oven contains a GS-GasPro column (length 49 m, ID 0.32 mm) which was cooled to a start temperature of $-10\text{ }^\circ\text{C}$. After 2 minutes, the temperature was ramped up by $10\text{ }^\circ\text{C}/\text{min}$ to hold at a final temperature of $200\text{ }^\circ\text{C}$, thereby producing a set of elution times for the pre-concentrated compounds.

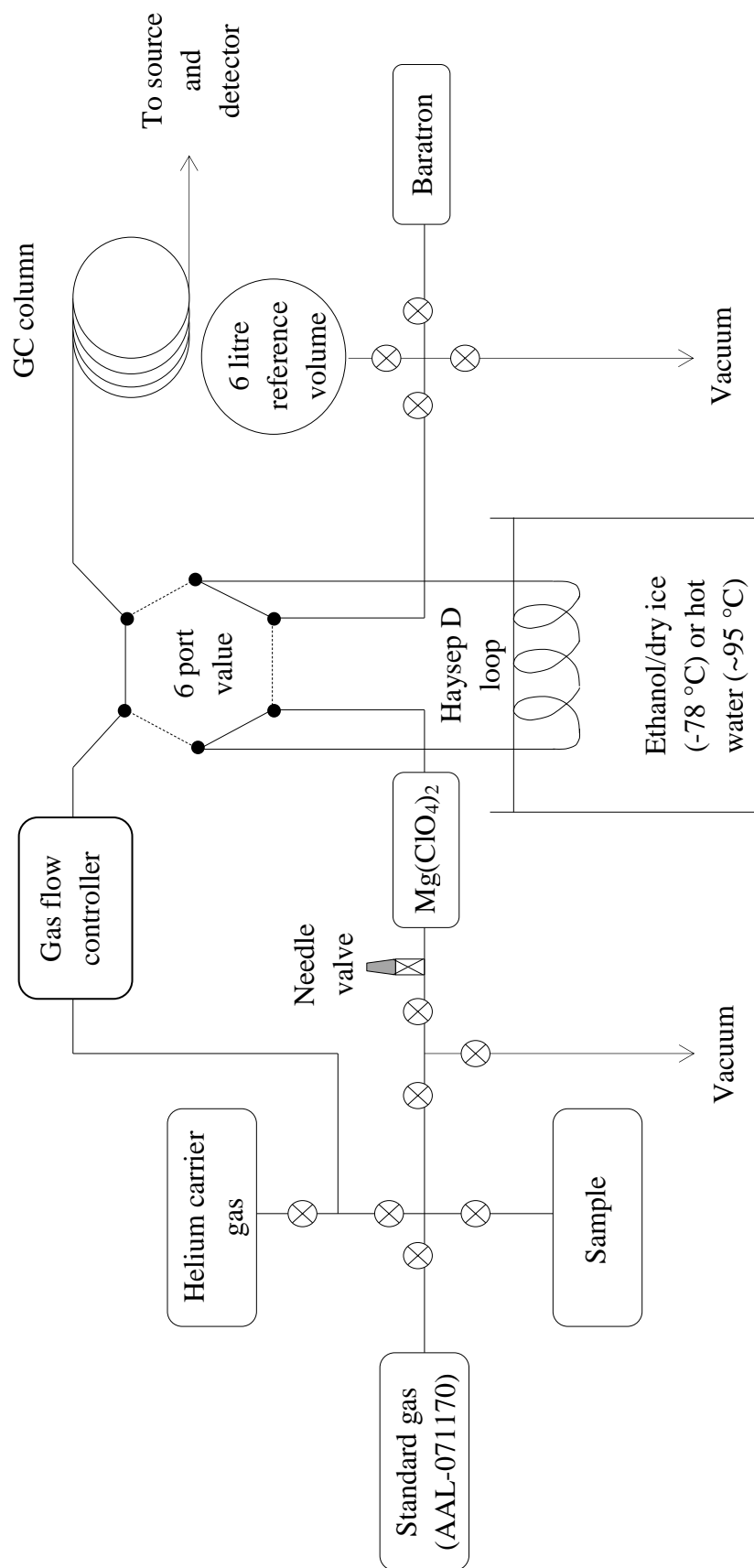


Figure 2.2. Schematic diagram of the manual inlet setup for the GC-MS system. A cross contained within a circle represents a valve.

2.1.1.3 Sample analysis

It is preferable for the system 'blank' to be quantified on each analysis day. This means that, rather than an air sample, an aliquot of the helium carrier gas is passed through the inlet system and injected into the GC-MS for analysis. A peak detected in a blank run constitutes the zero point and is subtracted from all other runs on that day. As well as this, the daily blank run is a useful diagnostic tool, for example, a higher than expected blank level is often the first sign of a leak in the system.

It is necessary to begin the day with at least two standard runs, to allow the instrument to settle. Once a stable peak is achieved, samples are typically analysed twice in succession with standards bracketing the two runs. In this way, several samples can be analysed each day (typically three). After the instrument has stabilised, standard runs are used to track instrumental drift; bracketing samples with standards enable this drift to be corrected for during data processing (details in Section 2.1.1.4).

The same standard (AAL-071170) was used for all of the work presented in this thesis. It was collected by the National Oceanic and Atmospheric Administration (NOAA) at Niwot Ridge, Colorado in 2006. It is a real air sample, contained in a pressurised Aculife-treated aluminium cylinder. The NOAA Climate Monitoring and Diagnostics Laboratory (CMDL) analysed the sample for a range of trace gases, including all of the gases discussed in this work. This means that the mole fractions reported in this thesis are consistent with NOAA calibration scales. The root calibration scale has been updated several times using standard inter-comparisons, which track the ratio of one standard to another with respect to individual compounds. Details of the calibration scales and mole fraction values used in this thesis can be found in Table 2.2. Figure 2.3 shows how the COS content of two UEA standards has varied over time, with respect to each other.

Table 2.2. Details of the calibration scales used to assign mole fraction values to six compounds in the AAL-071170 standard air. 1σ analytical uncertainties are also included.

Compound	Scale	Scale year	AAL-071170 mole fraction / pmol mol^{-1}	1σ uncertainty / pmol mol^{-1}
SF_6	NOAA	2006	5.89	0.08
CFC-11	NOAA	1993	249.61	2.25
CFC-12	NOAA	2008	539.89	2.35
CFC-113	NOAA	2002	79.15	0.55
CH_3CCl_3	NOAA	2003	18.65	0.81
COS	NOAA	2004	666.23	5.18

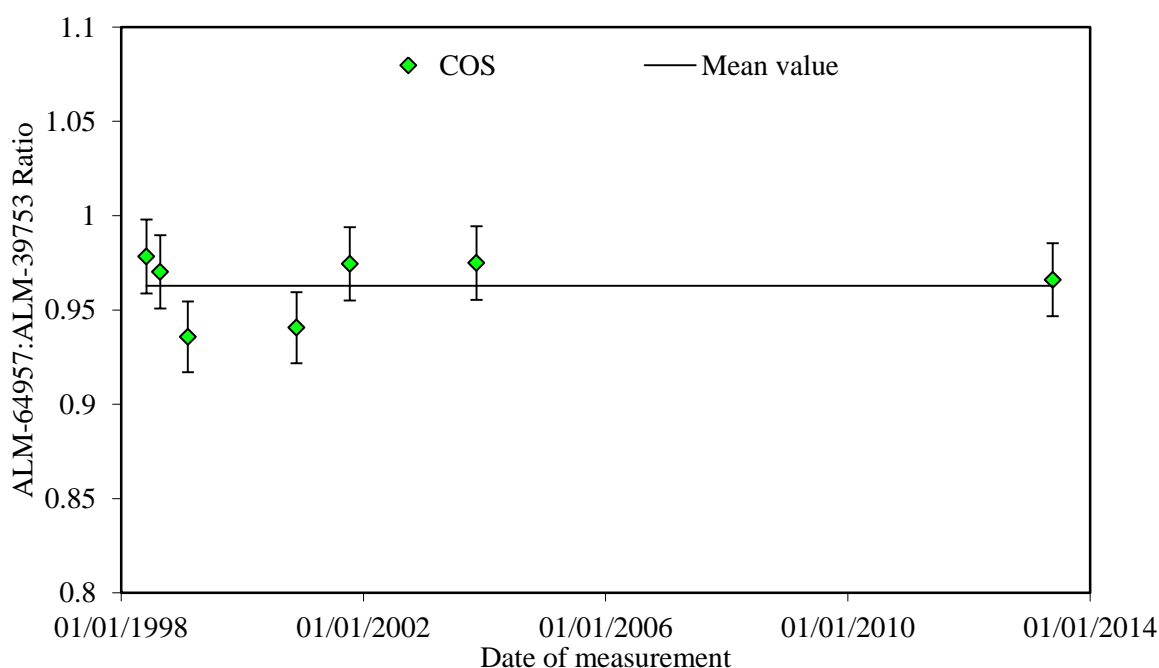


Figure 2.3. An example of the results from standard inter-comparisons, which are used to assess the stability of COS and other species of interest within pressurised laboratory standards over long time periods. Measurements of COS in two laboratory standards (ALM-64957 and ALM-39753) between 1998 and 2013 are shown here as a ratio. Analytical uncertainties are not readily available for these measurements, so reasonable uncertainties are included for each point (2 %). Typically the GC-MS used in this thesis achieves between 1 and 4 % 1σ uncertainties. The consistency shown is excellent, with no apparent drift over time between the two standards. This comparison was used as an example because of its exceptional length.

2.1.1.4 Data processing

As well as controlling the instrument setup (Section 2.1.1.1), MassLynx facilitates peak integrations and outputs the raw data necessary for all other data processing steps.

A sample peak area of a compound (e.g. SF₆) is compared to an equivalent peak from the laboratory standard (AAL-071170), after each area is normalised according to the exact air volume injected. This sample to standard ratio is then multiplied by the known mole fraction of SF₆ in the standard, producing a sample SF₆ mole fraction value. Figure 2.4 shows example peak outputs.

As mentioned in Section 2.1.1.3, the instrument is not entirely consistent between runs; there is a small amount of drift in the detector response during an analysis day. This means that comparing temporally distant sample and standard peaks introduces a bias in the resulting sample mole fraction. To minimise this effect, instrumental drift was tracked in the standard. To calculate a mole fraction, the sample was compared to a combination of its surrounding standards. Each standard is weighted according to its temporal proximity to the sample. Based on this weighting, a combined standard value is used to calculate the standard to sample ratio.

The 1σ total analytical uncertainty of a measurement is calculated by combining the sample standard deviation (SD) and the daily standard SD, using equation 2.3:

$$\text{Total uncertainty} = \sqrt{SD_{\text{sample}}^2 + SD_{\text{standard}}^2} \quad (2.3)$$

In most cases, equation 2.3 is sufficient. However, where a repeat analysis of the sample has not been made, the SD of a sample measured under similar instrument conditions is used to substitute into equation 2.3. In practice, this means that the substituting sample must have been analysed within a few days of the single repeat sample. A further requirement is that the substituting sample must contain similar levels of the species being measured because there is a general deterioration in the measurement precision achieved as mole fractions decrease. In the absence of a suitable substitute sample, the daily standard SD is doubled to produce an estimate of the total measurement uncertainty.

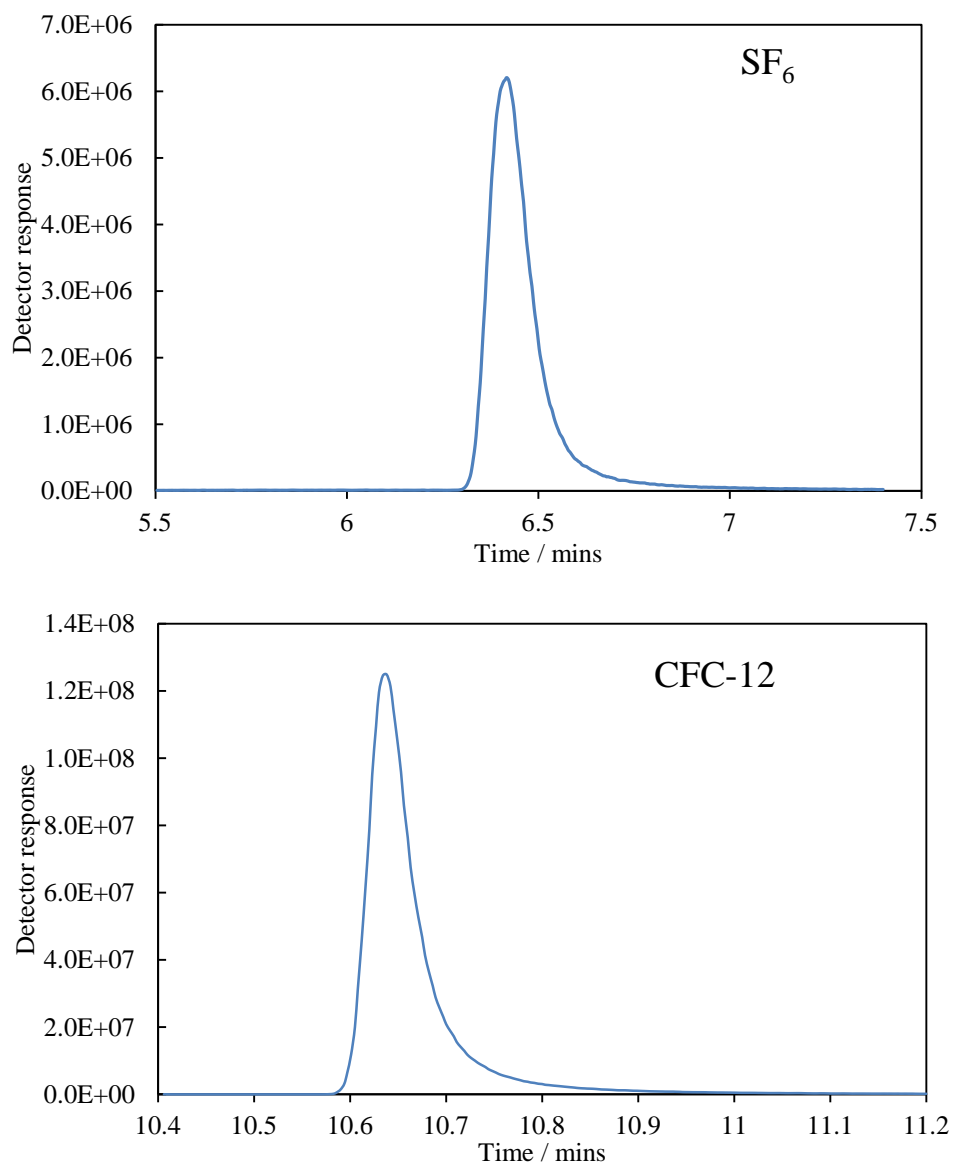


Figure 2.4. Example chromatograms for SF₆ and CFC-12 which have standard (AAL-071170) mole fractions of 5.9 and 539.9 pmol mol⁻¹, respectively. The peaks shown represent the fragment ions ³²SF₅⁺ (*m/z* 126.96) and ¹²C(³⁵Cl₂)F⁺ (*m/z* 100.94).

2.1.2 Isotope ratios

Isotope Ratio Mass Spectrometry (IRMS) has been used for many years to measure the isotope ratios within a species. These instruments typically collect individual fragment ions in separate detectors, by exploiting differences in their *m/z* values, which affect their

degree of deflection in a magnetic field. In each detector, a hit count is converted to a current, which is then amplified before being displayed. By comparing the responses of individual detectors, an isotope ratio can be obtained.

Although excellent precision can be achieved using IRMS, it is not always suitable for multiple trace gas isotope ratio analysis. Also, samples collected from air archives generally have small volumes (e.g. ice cores), making them unsuitable for IRMS analysis which typically requires many litres to get a large enough signal from low abundance gases (pmol mol^{-1} level).

2.1.2.1 GC-MS isotope ratio analysis

An alternative method for measuring isotope ratios in trace gases has been recently developed (e.g. Laube et al., 2010a) which uses a GC-MS system to overcome some of the inherent drawbacks to IRMS outlined above. This section provides a brief introduction to the potential advantages of using a GC-MS instrument to measure isotope ratios. Specific details of these methods can be found in Chapter 3, which is partially based on Allin et al. (2015).

The GC-MS measurement procedure detailed in Section 2.1.1 is mostly unchanged when attempting to quantify isotope ratios, rather than mole fractions. Multiple m/z values are included in each function, corresponding to fragments of a species with different isotopic compositions (e.g. Table 2.1). The multi-detector array of IRMS systems means that information on each isotope is collected simultaneously. This is not possible in a single-detector GC-MS system which cycles through the defined m/z values of a function, producing slightly offset peaks for all fragments. This is not a significant issue because the offset is very small (typically 80 ms).

A major advantage of the GC-MS system is its high sensitivity. Compared to IRMS, smaller sample sizes can be used and less abundant species can be investigated, broadening the potential scope of isotope ratio studies. Also, the GC separation of species allows an unmodified air sample to be introduced to the system. Therefore, isotope analysis of multiple species is possible in a single measurement, making this technique highly efficient in terms of the temporal and sample volume requirements.

2.2 Firm air modelling

Measurements of gases in firn air are initially reported versus depth, rather than as time series. Modelling techniques are used to perform the essential normalising step of converting firn depths to air ages, enabling comparisons between multiple data sets. As described in Section 1.2.1, the firn layer is a heterogeneous and highly dynamic environment, meaning that the process of assigning an air age to a given depth is not a simple one. The diverse depositional environments of different drilling sites and the inconsistent behaviour of various species within the firn preclude the use of a single air age versus depth scale. Instead, each site and each species must be modelled to arrive at individual time series.

A firn diffusion model is used to simulate the movement of gases in the firn layer at a given site. This characterises the effective diffusivity of the site and allows mole fraction versus depth profiles to be used to reconstruct the atmosphere's composition over time.

2.2.1 The firn diffusion model

The Centre National de la Recherche Scientifique – Laboratoire de Glaciologie et Géophysique de l'Environnement (CNRS-LGGE) developed the model used in this thesis. An overview of the model is given below and a detailed description can be found in Rommelaere et al. (1997).

Using environmental factors and site characteristics (e.g. close-off depth, convective layer depth, site temperature and site accumulation rate) as well as the physical properties of the gas being modelled (e.g. molecular diffusivity and molecular mass), the transport rate of the gas can be determined. This model incorporates similar physical properties to previous studies (Schwander et al., 1993; Trudinger et al., 1997), although Rommelaere et al. (1997) also accounted for the downward air flux created by the process of air trapping at the firn-ice transition. These models all assume that the diffusivity profile of a site is in a steady state, the corollary being that external factors such as the climate have not changed over the study period.

A site-specific tuning procedure is performed using a range of trace gases. A diffusivity profile is produced using the known atmospheric history of a gas (e.g. CO₂), before optimising the fit to the measured firn air values (Buizert et al., 2012; Witrant et al., 2012). By optimising the fit of several gases, a better estimate of the firn diffusivity profile can be obtained (Buizert et al., 2012). It should be noted that the process of defining the effective

diffusivity of a site cannot account for heterogeneities in the firn, such as melt layers (Martinerie et al., 2009). Buizert et al. (2012) outline a multi-gas method which systematically analyses the inherent uncertainties and minimises them by monitoring a root mean square deviation value. The gases used as tuning species by Buizert et al. (2012) to model the 2008 drilling campaign at the NEEM site in Greenland were CO₂, CH₄, SF₆, CFC-11, CFC-12, CFC-113, HFC-134a, CH₃CCl₃, $\Delta^{14}\text{CO}_2$ and $\delta^{15}\text{N}$. Gases are chosen as tuning species based on two main criteria:

1. Gases with distinct atmospheric histories are used to provide variety in the time series that the model is exposed to. For example, CO₂ increases steadily during the 20th century whereas CH₃CCl₃ increased rapidly until the early 1990s before declining sharply. Constraining the model using both of these species improves its capacity to accurately characterise a variety of additional species.
2. A gas that has increased or decreased steeply in abundance during the 20th century provides a better temporal constraint in the tuning process. This is because the change in abundance over a given time period is greater than for a species which has increased or decreased more gradually. For example, CO₂ and CH₄ increased rapidly during the 20th century and continue on this trajectory to the present day.

This multi-gas approach has several advantages over using the reduced list of compounds previously included (often only CO₂ and CH₄). By including more gases, a wider range of atmospheric histories and transport behaviours are incorporated. This means that the movement of gases in the firn is characterised more completely. Consequently, the scope of the model's output will be broadened. Finally, a significant underlying difficulty in this modelling process is that a diffusivity profile is always mathematically underdetermined. This means that a large number of solutions fit the data, rather than a single result (Rommelaere et al., 1997). Including more species in the tuning process allows the diffusivity profile to be constrained more strongly, making the result less underdetermined (Buizert et al., 2012).

Once a site's diffusivity profile has been defined, the transport of any gas through the firn can be modelled by inputting its molecular mass (M_{gas}) and diffusion coefficient (D_{gas}). The diffusion coefficient is scaled relative to CO₂, meaning that a $D_{\text{gas}}/D_{\text{CO}_2}$ value is used for each species. Together, M_{gas} and $D_{\text{gas}}/D_{\text{CO}_2}$ values can be used to define the diffusion speed of a gas in firn. Table 2.3 lists these values for the species modelled in this thesis. D_{gas} values are calculated using equation 2.4 (Chen and Othmer, 1962):

$$D_{\text{gas}} = \frac{0.43 \left(\frac{T}{100}\right)^{1.81} \left(\frac{1}{M_1} + \frac{1}{M_2}\right)^{0.5}}{P \left(\frac{T_{c1} T_{c2}}{10000}\right)^{0.1405} \left[\left(\frac{V_{c1}}{100}\right)^{0.4} \left(\frac{V_{c2}}{100}\right)^{0.4}\right]^2} \quad (2.4)$$

In equation 2.4, subscripts of “1” and “2” are used to identify quantities relating to air and a specific gas, respectively. T is the ambient temperature and T_C is the critical temperature (both in K). M is the molar mass (g mol^{-1}) and V_C is the critical volume ($\text{cm}^3 \text{mol}^{-1}$).

Table 2.3. The molar mass (M_{gas}) and diffusivity relative to CO_2 ($D_{\text{gas}}/D_{\text{CO}_2}$) are given for various compounds. D_{gas} values were calculated using the methodology outlined in Chen and Othmer (1962).

Compound	M_{gas} (g mol^{-1})	$D_{\text{gas}}/D_{\text{CO}_2}$
SF_6	146.06	0.621
CFC-11	137.37	0.575
CFC-12	120.90	0.618
CFC-113	187.38	0.495
CH_3CCl_3	133.40	0.537
COS	60.08	0.785

In Chapter 4 of this thesis (Section 4.2), I have used the model framework described above to produce firm air profiles of carbonyl sulphide (COS). An inverse version of the diffusivity model described above was used to reconstruct the atmospheric history of chlorine isotopes in CFC-11, CFC-12 and CFC-113, using measurements of $\delta(^{37}\text{Cl})$ in firm air and the known past atmospheric changes in their mole fractions (Section 3.1). These inverse methods are not described here because the work was conducted by Dr. Patricia Martinerie at LGGE (details can be found in Allin et al., 2015).

2.3 Ice core system

The methods described in this section relate to work conducted in the Ice Core Extraction Laboratory (ICELAB) at the Commonwealth Scientific and Industrial Research Organisation (CSIRO) Marine and Atmospheric Research (CMAR) in Australia. Below is an overview of the “cheese grater” dry extraction system used; a more complete description can be found in Etheridge et al. (1988 and 1996) and Rubino et al. (2013).

2.3.1 Sample selection

The most important consideration when selecting an ice core sample is the age of the trapped gas. For a study to capture a time period of interest and to enable the temporal analysis of ice core measurements, an accurate depth versus age relationship for the ice core must be established (Section 2.3.1.1). Once a section with an appropriate air age range has been identified, several criteria are used to choose the specific piece of ice that will be sampled from within this section. These criteria relate to the quality of the ice; sections that have been damaged during drilling and transportation or through in-situ degradation are avoided (e.g. visible cracks or complete fractures). These features could interfere with the measurements if the damage has facilitated the ingress of modern air. This means that a single, unblemished piece is selected whenever possible.

2.3.1.1 Ice core dating

Typically, an ice core is dated using a range of techniques. Shallow cores (covering approximately the last 1000 years) are easier to date than deep cores, just as high accumulation sites can be dated more accurately than low accumulation sites. This is because a given time period will be represented by a larger range of depths in young ice or at a site where precipitation is high. Under these conditions, the resolution of measurements is greater, meaning that the site can be better characterised.

Shallow cores can often be dated by observing seasonal cycles through various chemical analyses (e.g. Mulvaney et al., 2002; Hofstede et al., 2004). Figure 2.5 shows the results of some of these measurements and highlights the seasonal cycles within them. $\delta(^{18}\text{O})$ and δD in water act as a partial proxy for temperature, leading to a summer peak and winter trough (Figure 2.5). Also, species which are produced indirectly by phytoplankton display strong seasonality (e.g. non sea salt sulphate, nss SO_4^{2-} , and methane sulphonate, MSA^-).

Electrical conductivity measurements are largely dependent on the acidity of the ice, meaning that the presence of compounds which are deposited as acids (e.g. SO_4^{2-}) can be used to discern seasonal cycles. The Electrical Conductivity Method (ECM) and dielectric profiling (DEP) are commonly used for this purpose (e.g. Mulvaney et al., 2002).

After an initial depth versus age relationship is produced through annual layer counting as outlined above, verification from an independent method is required. Reference horizons can be used in this capacity, particularly through the identification of known volcanic eruptions in the ice record. Figure 2.6 shows the effect of some major eruptions on the sulphate content of the ice. Some of the larger eruptions can be seen globally (e.g. Tambora, Indonesia in 1815), whereas others have only a local influence (e.g. Laki in Iceland produces strong signals in Greenland, but not in Antarctica).

These measurements can be compared to glaciological model outputs, providing an additional constraint on the depth versus age relationship. This type of model takes into account the near-surface accumulation rate (obtained through layer counting), a known density profile and a Nye thinning model (which factors in thinning due to lateral flow at the bedrock; Nye, 1963). Although slightly simplistic (a constant accumulation rate over the study period is assumed), this method is useful as a check of previous dating efforts.

Finally, radioactivity peaks in 1954 and 1963 (caused by intense nuclear weapons testing) can be used to constrain the recent accumulation rate. The nuclear weapons debris can be clearly seen by measuring beta particles (a by-product of certain types of radioactive decay).

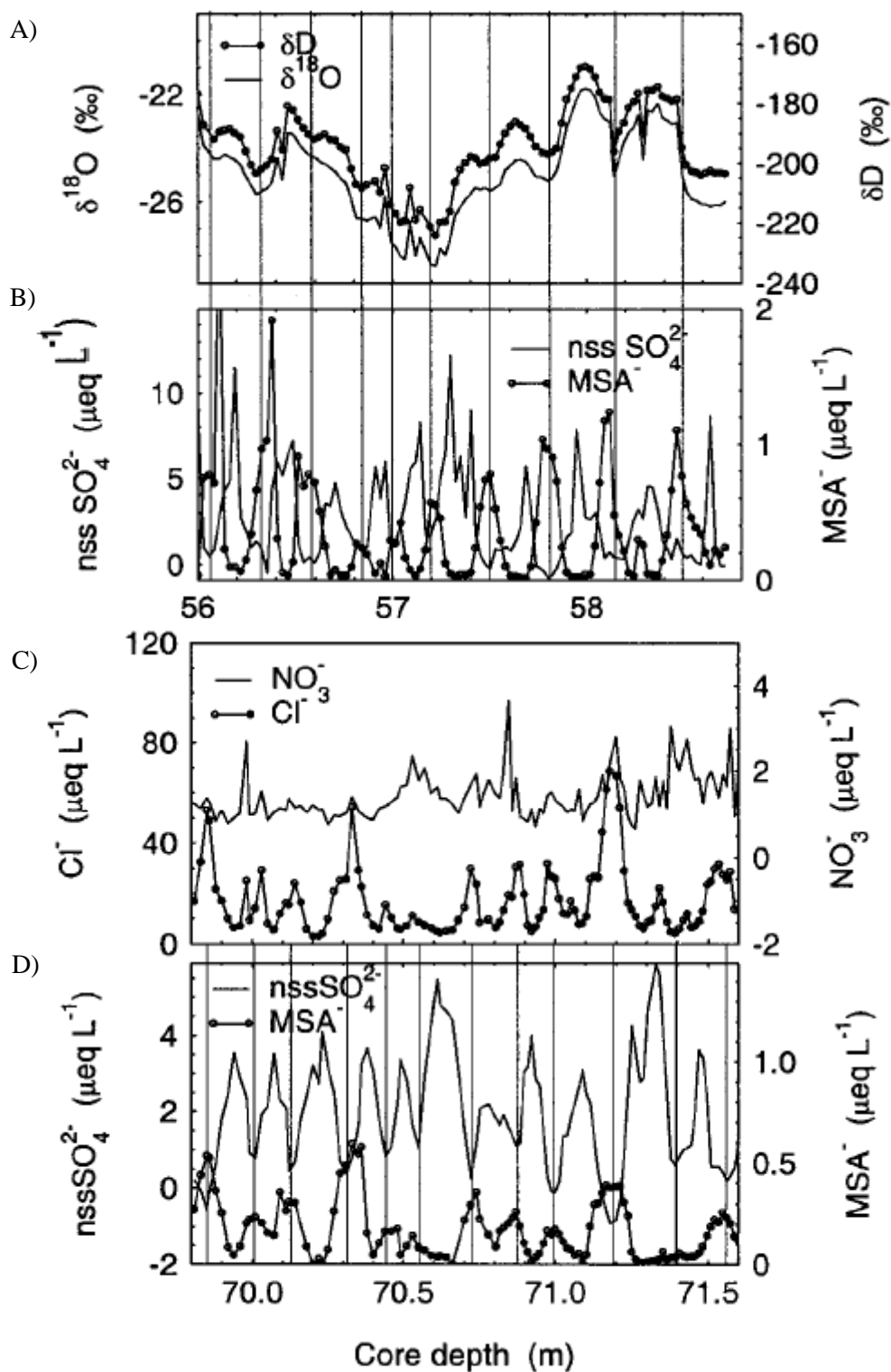


Figure 2.5. Seasonal cycles seen in various isotopes and species, with vertical lines representing the annual layers at Berkner Island. Above (56.0 – 58.8 m): A) stable isotopes of water ($\delta^{18}\text{O}$) and δD); B) non sea salt sulphate (nss SO_4^{2-}) and methanesulphonate (MSA^-). Below (69.8 – 71.6 m): C) chloride (Cl^-) and nitrate (NO_3^-); D) nss SO_4^{2-} and MSA^- . All figures are taken from Mulvaney et al. (2002).

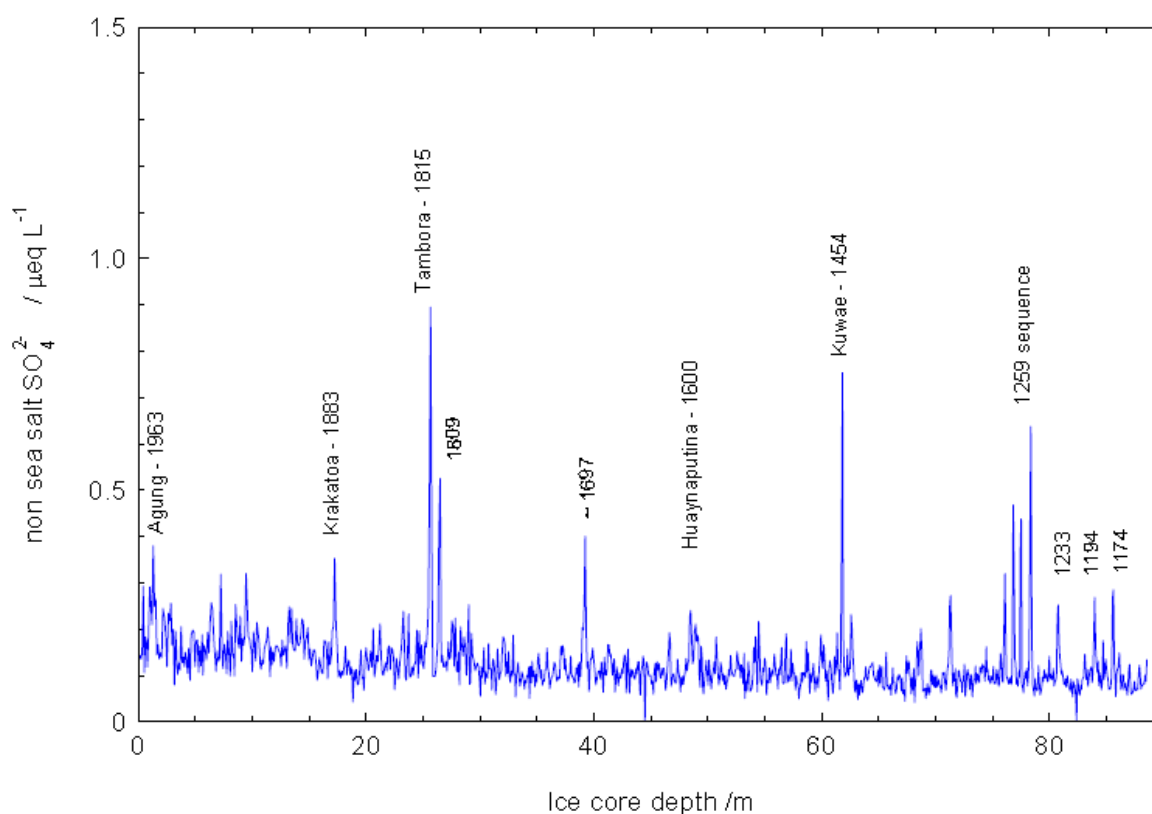


Figure 2.6. The nss SO₄²⁻ peaks in the British Antarctic Survey’s Dronning Maud Land ice core record, representing the emissions of major sulphate-rich volcanic eruptions. These characteristic peaks help to date shallow ice cores, refining existing estimates from annual layer counting (Figure 2.5). This figure was provided through personal communication with Dr. Robert Mulvaney of the British Antarctic Survey.

Additional complications arise when dating deep cores:

- Glaciological models are less able to deal with the thinning process at great depth, eventually producing infinitesimally thin layers.
- Deep cores traverse periods of significant climatic change which can significantly alter the accumulation rate (e.g. glacial transitions).
- Volcanic eruptions are less well constrained further back in time, making it more difficult to use them as reference horizons.

- With increasing depth it becomes more difficult and eventually impossible to achieve the required measurement resolution for effective seasonal cycle identification.

In this study, all of the samples were retrieved from shallow cores, avoiding these difficulties.

2.3.2 Air extraction and measurement procedure

Figures 2.7 and 2.8 are schematic diagrams which show aspects of the ice core extraction system.

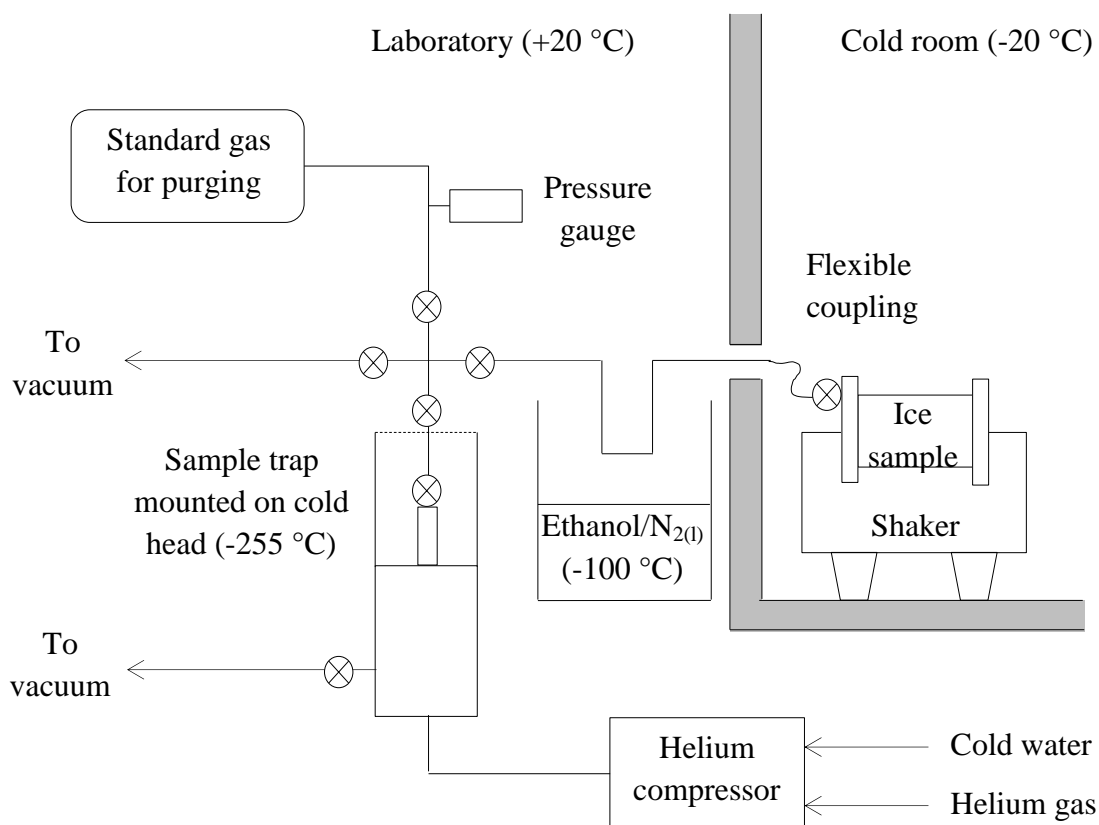


Figure 2.7. A schematic diagram of the ice core extraction line in ICELAB at CMAR. A cross contained within a circle represents a valve. The figure was modified from the original diagram which was provided through personal communication with Dr. Mauro Rubino of the Commonwealth Scientific and Industrial Research Organisation.

2.3.2.1 The day before a set of extractions

Core sections of appropriate ages were identified and samples between 0.7 and 1.5 kg were cut using a band saw (work carried out in the cold room at $-20\text{ }^{\circ}\text{C}$). The outer 5 – 20 mm of the core was removed because the risk of contamination to exterior surfaces is high (e.g. through partial melting or contact with foreign materials). This process left samples of approximately 0.5 – 1.2 kg, which were sealed in polyethylene bags and cooled to $-80\text{ }^{\circ}\text{C}$ for 24 hours. This cooling makes the ice more brittle, promoting a higher grating efficiency and resulting in a higher air recovery percentage (typically 80 %). Also, at $-80\text{ }^{\circ}\text{C}$ the sample is less vulnerable to state changes, which would increase the chances of contamination.

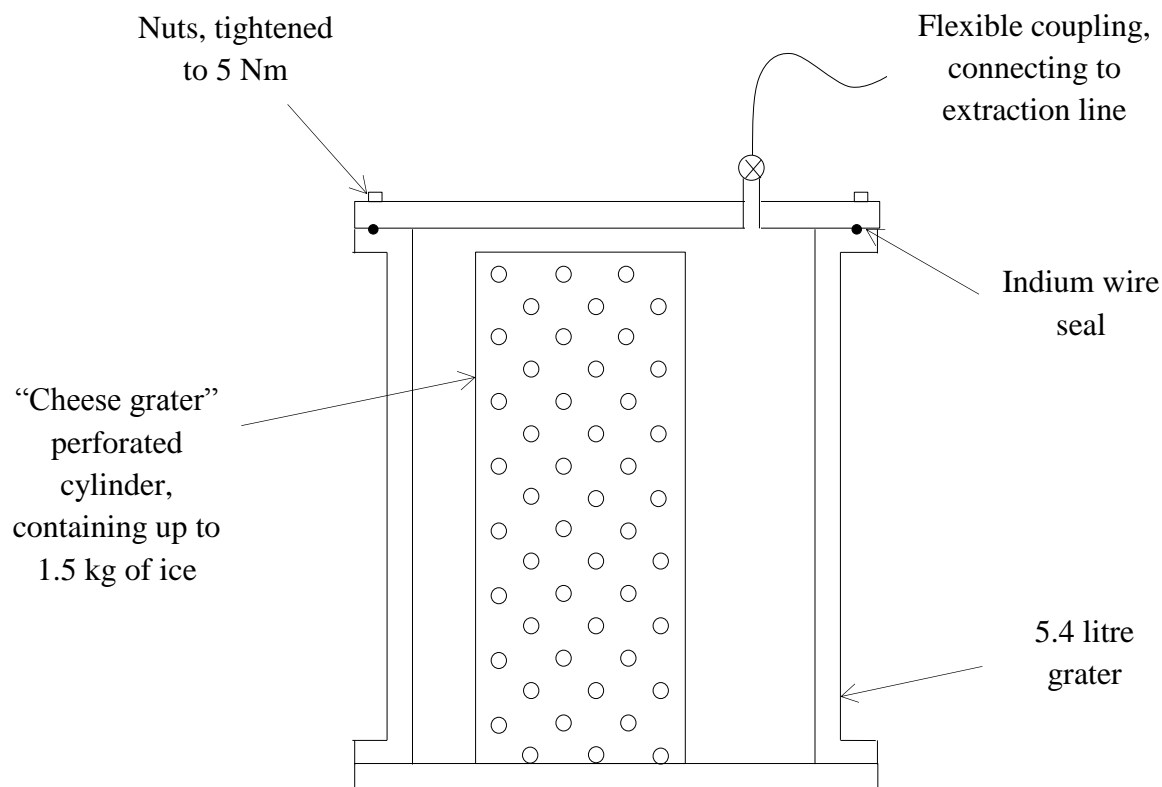


Figure 2.8. A schematic diagram of the ice core extraction vessel, including the “cheese grater” component. A cross contained within a circle represents a valve. The figure was modified from the original diagram in Etheridge et al. (1988).

2.3.2.2 Extraction day

The helium compressor (which drives the cryostat) was turned on several hours before the first extraction to allow time for it to cool. The extraction line and the ‘cold head jacket’ were then evacuated. (The ‘cold head’ is the part of the cryostat that reaches the lowest temperature and is where a ‘trap’ is positioned to collect the sample. The ‘jacket’ is the space surrounding the cold head and must be under vacuum to facilitate cooling. The traps have electro-polished stainless steel internal surfaces and Stellite (a cobalt-based alloy) stem tips.)

The first sample was sealed inside the grater vessel using indium wire and a series of nuts, tightened to 5 Nm (Figure 2.8). The sample was then attached to the extraction line and the whole system was opened to an array of pumps. Vacuum was maintained through a roughing pump for 5 minutes before the system was backfilled with clean air and evacuated twice. (Backfilling the whole system with clean air flushes the line and ensures that the grater is not sealed by the partial vacuum created during cryogenic trapping.) Finally, a turbo pump was engaged and the vessel was evacuated for at least 10 minutes (the pressure must be $<10^{-4}$ Torr). At this point, the grater vessel was sealed and removed from the extraction line. An ethanol/N_{2(l)} mixture at approximately -100 °C was put in place, acting as a water trap (Figure 2.7). The sample was shaken vigorously for 10 minutes and re-attached to the extraction line. When the cold head had reached -255 °C, the pumps were sealed off and the trap opened to the sample vessel. Complete cryogenic trapping took approximately 1 minute. The trap was sealed, removed from the cold head and partially immersed in tap water, gradually warming it to room temperature. (Pressure sensors are continually monitored to ensure adequate vacuum is achieved, complete trapping takes place and that the system is leak tight.)

Samples of approximately 50 – 90 ml were collected through this method, which were then analysed using the steps outlined in Section 2.3.2.4.

2.3.2.3 Post extraction

The system was evacuated after each extraction, while using a heat gun to evaporate the water trapped by the ethanol/N_{2(l)} mixture. Additionally, the next sample trap was inserted to begin cooling in the cryostat, and compressed air was used to clear the grater vessel of ice chip debris.

At the end of the day (typically after four extractions), the system was more thoroughly purged, preparing it for the next set of extractions. Firstly, the highly malleable indium wire seal was replaced because leaks quickly develop as the wire is flattened during the sealing process. Secondly, the grater vessel was more thoroughly cleaned, ensuring that all ice chip debris was removed. Also, the vessel was disassembled, rinsed with deionised water, baked at 120 °C and steam cleaned with deionised water-saturated air at 120 °C.

2.3.2.4 Measurements

Within an hour, the trapped sample was analysed on several Gas Chromatography (GC) instruments, which measure mole fractions of CO₂, CH₄, CO and N₂O. After this, the remaining air was analysed for $\delta(^{13}\text{C})$ and $\delta(^{18}\text{O})$ of CO₂ on an IRMS (MAT252, Finnigan). Approximately 30 ml and 40 ml aliquots of air were used for the CMAR mole fraction and isotope measurements, respectively. These measurements were performed by Dr. Mauro Rubino at CMAR.

The complete set of analyses was performed only when sufficient air was available. The trace gas and isotope analysis at CMAR had to leave at least 15 ml of air for trace gas analysis at UEA. As detailed in Chapter 4, the main aim of this work was to obtain measurements of COS, CO₂ and $\delta(^{13}\text{C}, \text{CO}_2)$ in each sample, in order to investigate the link between COS and Gross Primary Production (GPP, Section 1.4.4). This means that only CO₂ and $\delta(^{13}\text{C}, \text{CO}_2)$ measurements were made at CMAR, unless there was more than ~80 ml available. The trace gas analysis at UEA was conducted according to practices laid out in Section 2.1. Although COS was the primary target species in the UEA analysis, the MS programme used for firn air samples (Table 2.1) remained largely unchanged. This continuity was retained because naturally produced species such as CH₃Cl and CH₃Br have pre-industrial background levels, making measurements of these compounds in pre-industrial air potentially scientifically valuable. Also, species with no natural sources act as sample integrity checks. For example, the presence of SF₆ or CFC-12 in these samples could be an indication that the sample has been contaminated by modern air.

2.3.3 Advantages of the CMAR system

In general, bubbles occluded in ice cores provide a highly valuable archive of the atmospheric history of trace gases. This ice core resource is unique because air is preserved for thousands of years without alteration, allowing direct measurements to be made,

removing the need for proxies. The species of interest in this study contribute to ozone depletion and/or are significant greenhouse gases (GHG), making their characterisation important from an environmental perspective.

The system developed at CMAR was designed to process large samples (Etheridge et al. 1988). With a grater vessel that can accommodate up to 1.5 kg of ice, the system has a very large maximum sample yield (approximately 125 ml). In this air volume, less abundant species are more likely to be above analysis detection limits, increasing the array of measurements that can be made. The measurement output is also increased because the large sample size means that analyses can be made using multiple instruments. Finally, sample size often limits the measurement precision that can be achieved. The exceptional size of the samples generated leads to a more precise characterisation of the measured compounds.

Chapter 3: An atmospheric history of the chlorine and carbon isotope composition in CFC-11, CFC-12 and CFC-113

Background information on CFCs and the way they deplete stratospheric ozone can be found in Sections 1.1.2.2 and 1.3. The atmospheric histories of CFC-11, CFC-12 and CFC-113 are well characterised; however, the processes that govern their production and destruction are less well understood. This means that our understanding of their longevity and hence their ozone destruction potential (ODP) is compromised.

This chapter aims to better characterise CFC-11, CFC-12 and CFC-113 by constraining their tropospheric chlorine and carbon isotope histories. This is an important step in the construction of a global isotope budget for these gases, which is an invaluable tool in understanding their atmospheric cycling. Subscripts of “T” and “S” are used in this chapter to indicate tropospheric and stratospheric measurements, respectively.

3.1 Chlorine isotope composition in chlorofluorocarbons CFC-11, CFC-12 and CFC-113 in firn, stratospheric and tropospheric air

Section 3.1 is based on a published paper, for which I am the lead author:

Allin, S. J., Laube, J. C., Witrant, E., Kaiser, J., McKenna, E., Dennis, P., Mulvaney, R., Capron, E., Martinerie, P., Röckmann, T., Blunier, T., Schwander, J., Fraser, P. J., Langenfelds, R. L., and Sturges, W. T.: Chlorine isotope composition in chlorofluorocarbons CFC-11, CFC-12 and CFC-113 in firn, stratospheric and tropospheric air, *Atmospheric Chemistry and Physics*, 15, 6867-6877, doi:10.5194/acp-15-6867-2015, 2015.

To date, the only study to investigate the $\delta(^{37}\text{Cl})$ of CFCs measured the stratospheric fractionation of CFC-12 (Laube et al., 2010a). The continued isotopic characterisation of these gases could help to identify individual sources and better quantify the contribution of

different sink reactions. This could lead to better lifetime estimates and hence better ozone recovery predictions. Since CFC-11 and CFC-113 are destroyed in the same way as CFC-12, it is reasonable to expect that they may be susceptible to the same isotope dependencies and therefore warrant the same examinations (Section 1.3). This section describes the novel measurements made to better characterise the $\delta(^{37}\text{Cl})$ of CFC-11, CFC-12 and CFC-113 in the atmosphere.

3.1.1 Research objectives

- The GC-MS “AutoSpec” instrument at UEA has been used once before to make trace gas isotope ratio measurements (Laube et al., 2010a). This study will extend this work to two additional gases (CFC-11 and CFC-113) and new areas of the atmosphere.
- Produce the first tropospheric chlorine isotope history of CFC-11, CFC-12 and CFC-113, from $\delta_{\text{T}}(^{37}\text{Cl})$ measurements.
- Compare these measurements to modelled expectations, based on the current understanding of CFC production, breakdown and transport processes.
- Evaluate the observed long-term tropospheric chlorine isotope changes in these gases in terms of source and sink processes to better constrain their atmospheric isotope budgets.

3.1.2 Methodology

Section 2.1.2.1 provides a brief overview of the potential benefits of using a GC-MS instrument to measure isotope ratios in trace gases. The specific methods used for calculating $\delta(^{37}\text{Cl}, \text{CFCs})$ values are outlined below.

As defined in Section 1.3.2, an isotope delta (δ), expressed in per mill (‰), is used to denote the relative $^{37}\text{Cl}/^{35}\text{Cl}$ ratio difference of CFCs in sample air with respect to a standard

$$\delta(^{37}\text{Cl}) = \frac{R_{\text{sample}}}{R_{\text{standard}}} - 1 \quad (3.1)$$

where R represents the $^{37}\text{Cl}/^{35}\text{Cl}$ abundance ratio of a sample or standard. There is no internationally recognised isotope standard for these measurements. For this reason, all delta values are relative to a laboratory standard (AAL-071170). This is a background air

sample collected in 2006 at Niwot Ridge, Colorado, by the National Oceanic and Atmospheric Administration (NOAA).

The isotopologue ratios of the CCl_2F^+ fragment are considered, rather than directly measuring Cl^+ ions. This is because the CCl_2F^+ fragment provides larger peaks than fragmented Cl^+ ions, leading to better measurement precision (see Section 2.1.1.1 for full details). To accurately determine δ , it is important that the calculated R value introduces as little uncertainty as possible (equation 3.1). Three methods for determining R values were tested:

1. The ‘plot method’. Figure 3.1 shows how the linear regression slope of the $\text{C}^{35}\text{Cl}^{37}\text{ClF}^+$ against the $\text{C}^{35}\text{Cl}_2\text{F}^+$ ion current over the duration of a peak is used to derive R .
2. The ‘Gaussian fit method’ was developed at the University of Frankfurt (Laube, 2008) and the work was performed by Dr. Johannes Laube. This method follows similar steps to the ‘plot method’, although a Gaussian distributed peak is fitted to the data before a linear regression slope is plotted.
3. The ‘peak areas method’. As described in Section 2.1.1.4, the integrated peak area of fragment ions are typically used to infer species mole fractions. In this case, the ratio between the integrated peak areas of two fragment ions derived from a single species produce an R value.

A static dilution series (details in ‘*Determination of non-linearities*’, Section 3.1.3) was analysed on three occasions between July and October 2013, using the three data processing steps outlines above. This dilution series contains a wide range of mole fractions (Table 3.3 in Section 3.1.3) which is representative of the range found in the samples analysed in this chapter. Figure 3.2 shows that each method produced consistent results in all three species. Based on this, it was decided that the method which induced the smallest analytical uncertainties would be adopted. Overall, the ‘Plot method’ (number 1 from above) gave the smallest uncertainties (Table 3.1) and was used for all sample analysis in this chapter. Drift corrections and error calculations were made using the method described in Section 2.1.1.4.

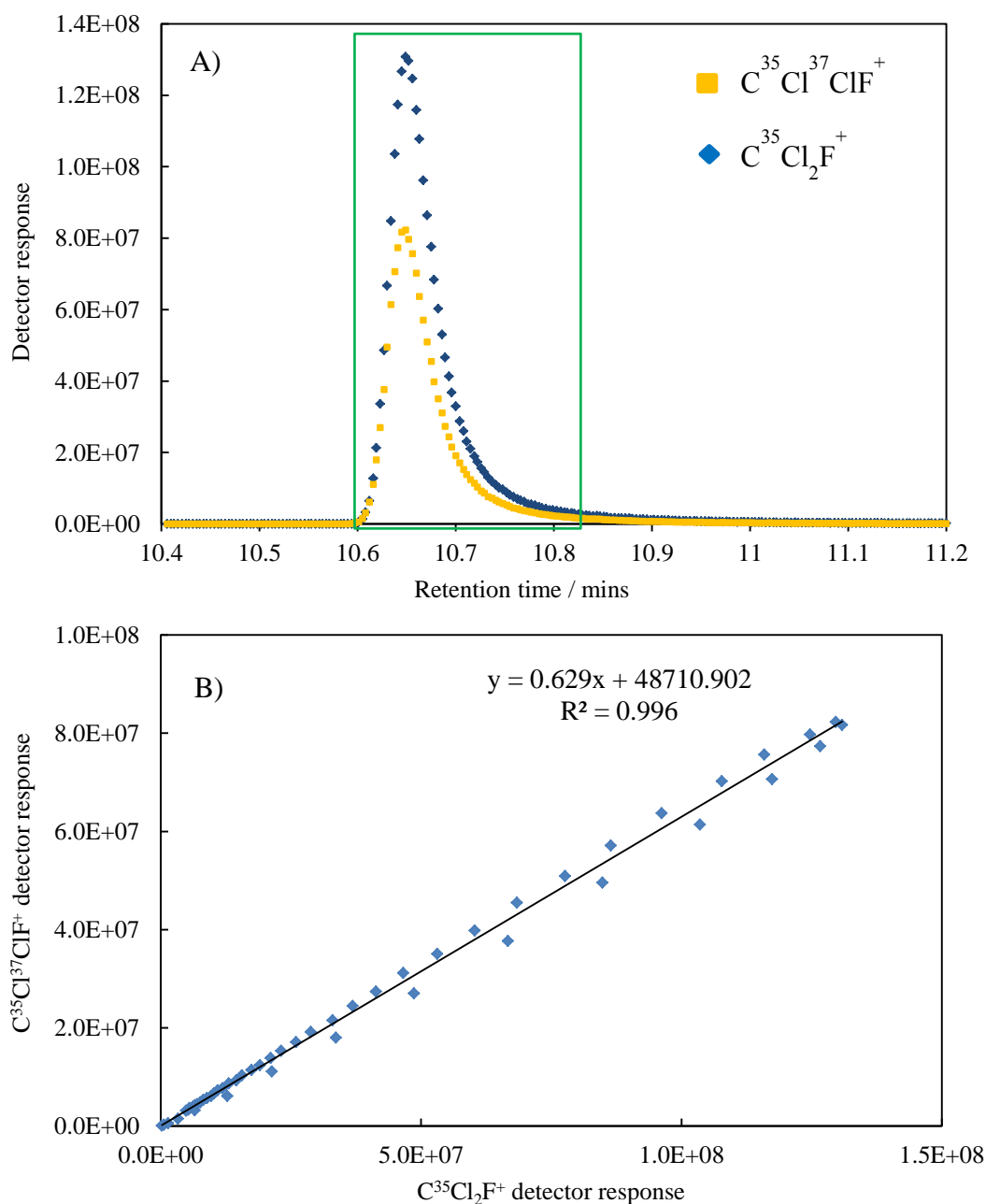


Figure 3.1. A) An example chromatographic output used to calculate a $\delta(^{37}Cl)$ value. B) The peaks are isolated (outline in green in A) and the absolute detector response values are plotted against each other. The gradient of the resulting trend line is the ratio of $C^{35}Cl^{37}ClF^+$ to $C^{35}Cl_2F^+$ in a given sample or standard. This ratio is used to calculate a delta value. All data shown are from CFC-12.

Figure 3.2 (next page). A static dilution series (see ‘*Determination of non-linearities*’, Section 3.1.3) was measured for $\delta(^{37}Cl)$, plotted against the integrated peak area of the CCl_2F^+ fragment ion (m/z 101). Three different methods were used to determine the ratio between the $C^{35}Cl^{37}ClF^+$ (m/z 103) and $C^{35}Cl_2F^+$ (m/z 101) fragment ions and to calculate $\delta(^{37}Cl)$ values (equation 3.1). The analytical uncertainties in these measurements are summarised in Table 3.1. All delta values are relative to an air sample collected at Niwot Ridge in 2006 (AAL-071170).

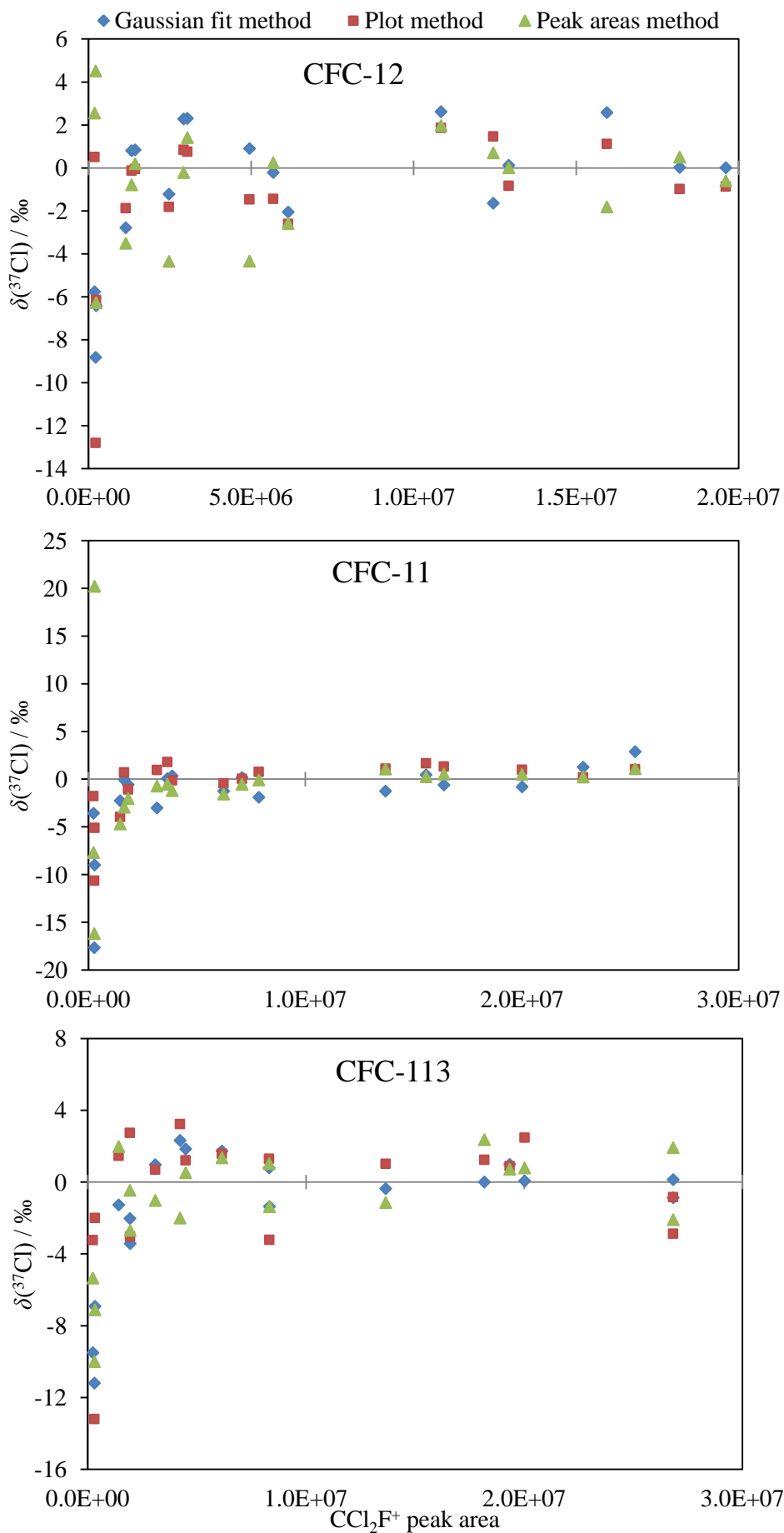


Table 3.1. Three different methods were used to calculate $\delta(^{37}\text{Cl})$ values from the analysis of a static dilution series (see ‘*Determination of non-linearities*’, Section 3.1.3). The mean analytical uncertainty is stated for each compound, through each method.

Method	Mean $\delta(^{37}\text{Cl})$ measurement uncertainty / ‰		
	CFC-11	CFC-12	CFC-113
Gaussian fit	3.7	3.8	3.9
Plot	2.0	3.7	3.1
Peak areas	4.6	3.9	2.8

No chromatographic interferences were found for these ions at the retention times corresponding to CFC-11 and CFC-12. However, CFC-113a has grown to a current atmospheric abundance of $\sim 0.5 \text{ pmol mol}^{-1}$ since its emergence in the 1960s (Laube et al., 2014) and partially co-elutes with CFC-113. CFC-113a ($\text{Cl}_3\text{C-CF}_3$) is an isomer of CFC-113 ($\text{Cl}_2\text{FC-CClF}_2$) and it was detected above the surrounding noise in one sample. This peak was manually excluded by beginning the linear regression slope after the CFC-113a peak, before calculating a delta value using equation 3.1. Within 1σ , this value is the same as the original delta value calculated (without removing the CFC-113a interference). Based on this, it was assumed that a correction was not necessary.

Poor quality measurements were defined as a measurement with a standard deviation (from repeat analyses) of more than three times the average standard deviation of the R_{standard} values during an analysis period. A new analysis period was deemed to have begun when a change was made to the GC-MS system which would significantly alter its performance (e.g. replacing the source filament). Typically, an analysis period would last a few weeks to months. Less than 1 % of the measurements were rejected as poor quality. Measurements were also rejected if there was uncertainty regarding the integrity of the sample; small system leaks can be identified through the analysis of other trace compounds

(e.g. sulphur hexafluoride, SF₆). 2 % were excluded due to a suspected loss of sample integrity.

Table 3.2 gives details of the samples used in this study. Firn air was sampled during the North Greenland Eemian Ice Drilling field campaign (NEEM Community Members, 2013) and from the Fletcher Promontory ice core site in Antarctica (Mulvaney et al., 2014). In each case, ice core drills progressively penetrated the firn column, stopping every few meters to allow the firn air to be recovered. The firn air extraction technique (Schwander et al., 1993) uses a bladder inflated at the bottom of the borehole to seal off ambient air from above. Gas pumps draw sample air from the firn surrounding the lowest level of the borehole, compressing the air into sample flasks at the surface. Additional samples were sourced from an archive of Southern Hemispheric background air (Cape Grim, Tasmania).

Table 3.2. Details of the samples used in this study.

Sample type	Sampling location	Sampling dates	Approx. air age	Further details
Free tropospheric air	Cape Grim, Tasmania	1978 – 2010	1978 – 2010	Sampling procedure previously reported (e.g Langenfelds et al., 1996)
Firn air	Fletcher Promontory, Antarctica	January 2012	1970 – 2012	Drilling and firn air pumping operations conducted by the British Antarctic Survey
Firn air	North Greenland	July 2009	1950 – 2009	Drilling and firn air pumping operations during the NEEM field campaign

Dr. Patricia Martinerie and Dr. Emmanuel Witrant used a model of gas transport in firn was used to obtain air ages for the firn air measurements. The migration of gases from the atmosphere through firn is largely controlled by diffusional and gravitational effects. In

this way, less diffusive gases move through the firn more slowly than more diffusive gases and heavier gases and isotopologues are enriched at depth relative to lighter gases and isotopologues. Consequently, there is no unique “age-of-air” at a given depth in the firn, rather an age distribution is calculated for a specific gas or isotopologue. Also, a gas can undergo significant isotope fractionation during its movement through the firn. A model of gas transport in firn must therefore include both diffusive transport and gravitational separation to reconstruct changes in atmospheric abundances and isotope ratios over time. The physical basis of the model is fully described in Witrant et al. (2012) and outlined in Section 2.2.1. The model was further refined to provide a more rigorous treatment of isotopes based on a forward firn model written in terms of delta values (Witrant and Martinerie, 2013). As described in Section 2.2.1, several species with well-known atmospheric histories are used to produce an holistic description of the diffusive behaviour of gases. These gases are referred to as ‘tuning species’ and include SF₆, HFC-134a, CFC-11, CFC-12, CFC-113 and CH₃CCl₃. Using the “AutoSpec” instrument, I performed the analysis of Fletcher Promontory and NEEM 2009 firn air to obtain mole fraction histories for these ‘tuning species’.

Thermal diffusion was not incorporated into the model, despite an observed gradient of 2 to 3 °C in the firn column at NEEM (due to recent local warming in Northwest Greenland; Carr et al., 2013). This is because, although the thermal diffusion effect on the CFC mole fractions is of the order of 0.2 %, the effect on the measured $\delta_T(^{37}\text{Cl})$ is estimated to be less than 0.02 ‰ (Leuenberger and Lang, 2002), since the measured isotopologues have similar masses.

3.1.3 Results and discussion

Determination of non-linearities

Using the AutoSpec instrument, Laube et al. (2010a) verified that their isotope ratio measurements were not biased by the response behaviour of the analytical system. The tests performed by these authors were designed to assess the response behaviour of this system when measuring CFC-12 to a minimum of 77 pmol mol⁻¹. The measurements presented in this thesis also include CFC-11 and CFC-113 and cover a wider range of sample mole fractions, meaning that a more extensive effort was necessary to remove the possibility of a bias.

An air sample collected at Niwot Ridge in 2009 (SX-0706077) was diluted with nitrogen and collected in three litre Silco-treated stainless steel containers. Pressure sensors were used to estimate the dilution factors and produce a static dilution series with a range of mole fraction values (Table 3.3). These samples were analysed to determine whether the measured isotope ratio of a sample is dependent on its mole fraction (i.e. whether a change in chromatographic peak size alters the measured isotope delta).

Table 3.3. An air sample collected at Niwot Ridge in 2009 (SX-0706077) was diluted with nitrogen. Three litre Silco-treated stainless steel containers were used to hold the diluted air (sample IDs beginning with ‘K’). Mole fractions for CFC-11, CFC-12 and CFC-113 were measured using the most abundant fragment ion (m/z 101). 1σ standard deviations are given.

Sample ID	Measured mole fraction / pmol mol ⁻¹		
	CFC-11	CFC-12	CFC-113
SX-0706077	245.1 ± 3.6	540.0 ± 3.4	78.1 ± 0.2
K1579	164.9 ± 2.4	363.4 ± 0.7	52.7 ± 0.1
K1578	75.9 ± 0.7	167.0 ± 0.8	24.1 ± 0.1
K1583	38.5 ± 0.3	84.1 ± 0.4	12.2 ± 0.1
K1569	17.7 ± 0.2	38.8 ± 0.1	5.6 ± 0.02
K1575	2.9 ± 0.02	6.6 ± 0.1	0.9 ± 0.01
K1576	0	0.1	0

Figure 3.3 (next page). Dilution series measured for $\delta(^{37}\text{Cl})$, plotted against the integrated peak area of the $\text{C}^{35}\text{Cl}^{37}\text{ClF}^+$ fragment ion (m/z 103). 1σ standard deviation error bars are shown. Insets highlight the firm air measurements that fall within the depleted region of the dilution series analysis (red highlighted regions on the left). Regression lines are used to correct the firm sample measurements, based on the observed non-linear responses in the dilution series. Unaffected samples are not displayed. All delta values are relative to an air sample collected at Niwot Ridge in 2006 (AAL-071170).

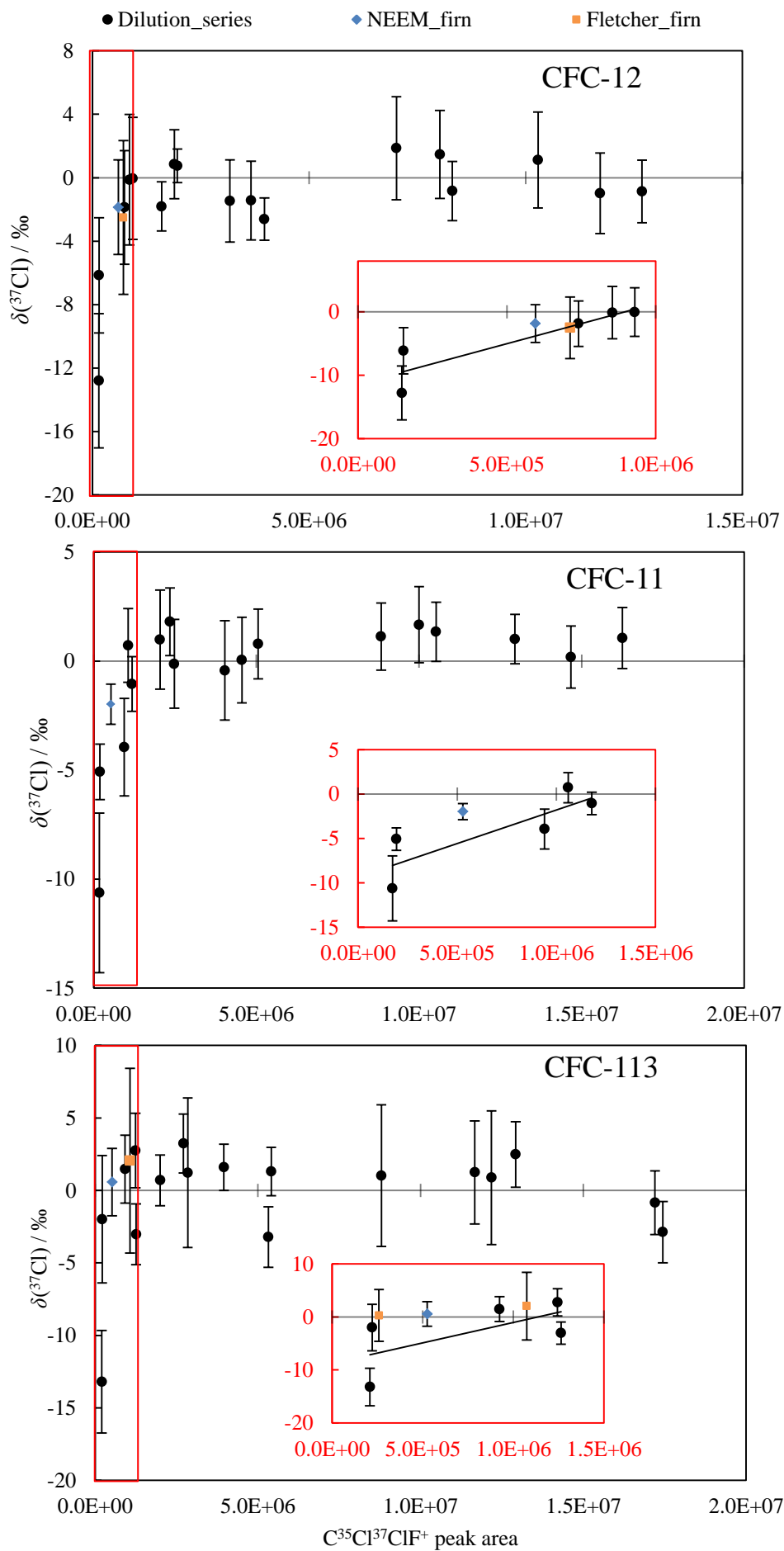


Figure 3.3 shows that delta values derived from the smallest peak areas exhibit erroneously low $\delta_T(^{37}\text{Cl})$ values for all three species, which requires a correction. 99 % of the samples analysed have peak areas in the region where the dilution series showed no bias. However, a total of 1 (CFC-11), 2 (CFC-12) and 2 (CFC-113) $\delta_T(^{37}\text{Cl})$ measurements were corrected, based on the results from the smallest peaks in the dilution series analysis (Figure 3.3 insets). A regression line was used to track the depletion in the smallest dilution series peaks. This line was then used to correct the firm measurements, based on their peak areas. An additional uncertainty was applied to each corrected measurement based on the uncertainty in the regression line. This uncertainty was factored such that the size of the additional error applied to a measurement is directly related to the size of the correction required.

The dilution series analysis shows an isotope delta bias which is limited to the lowest abundance samples; most samples display no bias. The unaffected samples cover a large range of mole fractions and were analysed using a variety of air volumes. Any systematic effect should be shown in these data. The absence of an effect suggests that the GC, MS and inlet systems do not affect isotope deltas. It is likely that the bias shown in small peaks is introduced during data processing, rather than during the measurement acquisition.

Further quality assurance considerations

CO_2 gradually elutes from the column during a run and can sometimes cause peak distortion because of its much higher concentration (particularly in early eluting compounds). Sample K1569 (Table 3.3) was analysed for $\delta(^{13}\text{C})$ with and without removing CO_2 using an Ascarite trap. ($\delta(^{13}\text{C})$ rather than $\delta(^{37}\text{Cl})$ measurements were used for this quality assurance test because it was performed after the period of $\delta(^{13}\text{C})$ analysis described in Section 3.2). For all compounds, delta values agreed within 1σ analytical uncertainties when analysed with and without the Ascarite trap. CFC-12 elutes earlier than CFC-11 and CFC-113 meaning that it is most susceptible to distortion by CO_2 . Figure 3.4 shows CFC-12 peaks produced with and without the CO_2 removed. The small differences in peak size and shape are likely to be caused by slight variations in the injected volume and other procedural variations. No systematic distortion is evident, suggesting that the effect of CO_2 is not significant.

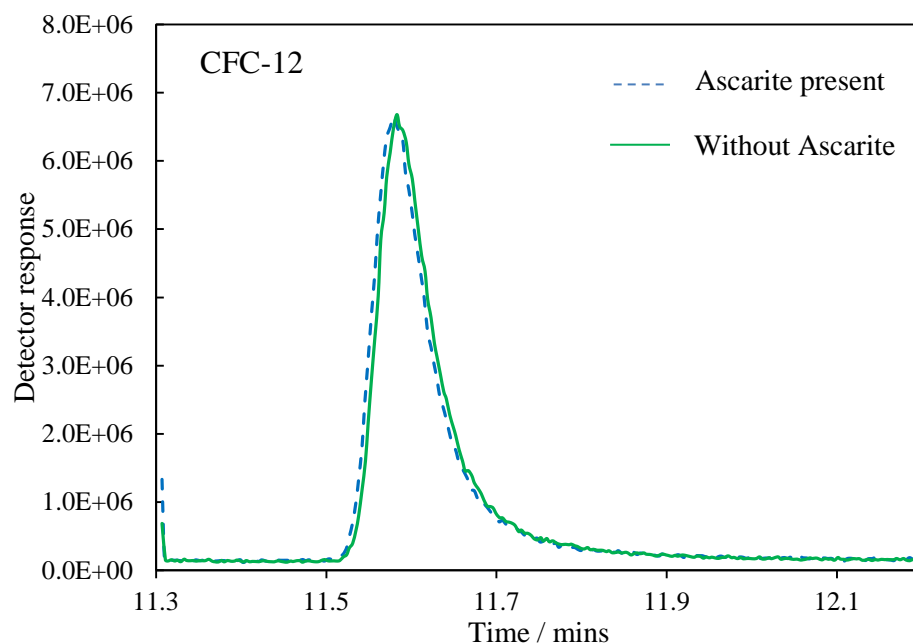
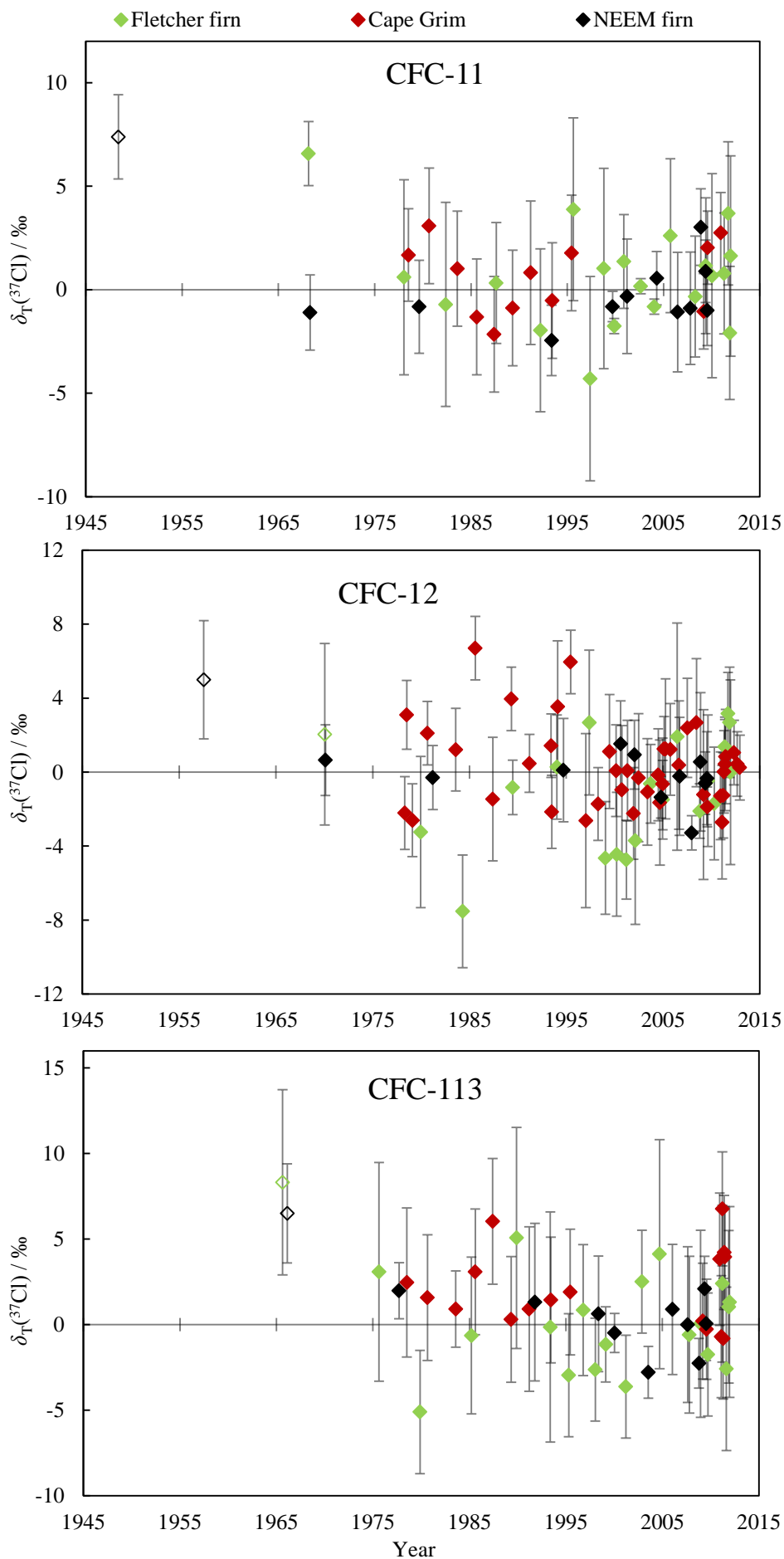


Figure 3.4. Smoothed data showing two CFC-12 peaks from the dilution series sample K1569 (Table 3.3). In two of the analyses, an Ascarite trap was added to the inlet system to remove CO₂ from the air samples (the dashed blue line represents one of these). The remaining analyses were performed without an Ascarite trap (the green line represents one of these). The repeat analyses were indistinguishable from those presented and are not included. In all cases the peaks from the ¹²C³⁷Cl₂F⁺ fragment are presented.

Figure 3.5 (next page). $\delta_T(^{37}\text{Cl})$ measurements in CFC-11, CFC-12 and CFC-113. Black diamonds (NEEM firn air), green diamonds (Fletcher Promontory firn air) and red diamonds (Cape Grim air archive) represent the tropospheric chlorine isotope history of CFC-11, CFC-12 and CFC-113. The average repeatability for individual samples was ± 2.7 ‰ (CFC-11), ± 2.7 ‰ (CFC-12) and ± 3.8 ‰ (CFC-113). 1σ standard deviation error bars are shown. Open symbols indicate that the measurement was subject to a small correction, based on the dilution series analysis (see ‘*Determination of non-linearities*’, Section 3.1.3). All delta values are relative to an air sample collected at Niwot Ridge in 2006 (AAL-071170).



3.1.3.1 Tropospheric measurements

Samples from the Cape Grim air archive (Tasmania, 1978 – 2010) and firn air samples from NEEM (Greenland) and Fletcher Promontory (Antarctica) have been analysed for the $\delta_T(^{37}\text{Cl})$ of CFC-11, CFC-12 and CFC-113. A total of 44 (CFC-11), 74 (CFC-12) and 48 (CFC-113) $\delta_T(^{37}\text{Cl})$ measurements are presented, approximately covering the last 60, 50 and 45 years, respectively (Figure 3.5).

In general, there is good agreement between the Cape Grim and firn air measurements. This agreement is in line with expectations from these well-mixed gases. In all three species, the measurements remain around the line of zero fractionation for almost the entire record (within their uncertainties). The oldest air samples in all species show a slight positive offset from zero. These samples are discussed in Section 3.1.3.3.

Seasonality

Firn air samples represent spatially and temporally averaged values, whereas each Cape Grim sample is representative of the Southern Hemisphere on a particular day. This means that Cape Grim samples have the potential to reveal short-term variations, such as seasonal cycles and spatial variations.

Redeker et al. (2007) found annual variations in all three CFCs, with higher $\delta_T(^{13}\text{C})$ values in the summer. However, these changes were within analytical uncertainties. Park et al. (2012) observed seasonality in $\delta(^{15}\text{N}, \text{N}_2\text{O})$ and $\delta(^{18}\text{O}, \text{N}_2\text{O})$ at Cape Grim between 1940 and 2005. The largest effect was seen in the $\delta(^{15}\text{N})$ of the central position nitrogen atom, which displayed a maximum seasonal offset of just under 1 ‰. Park et al. (2012) found that peak delta values (May-July) overlap with the period of minimum N_2O mole fractions (April-May) (Figure 3.6). They suggested that this approximate synchronicity is partially caused by an increase in transport of N_2O -depleted and ^{15}N - and ^{18}O -enriched stratospheric air to the surface. Given the parallels between N_2O and CFC-12 (similar sinks and comparable lifetimes), similar seasonal effects may be expected in CFC-12. The stronger stratospheric fractionation seen in N_2O (e.g. Kaiser et al., 2006) would suggest that the magnitude of seasonality in CFC-12 should be smaller than N_2O (likely a maximum seasonal offset of less than 0.5 ‰). Figure 3.7 shows a CFC-12 seasonality analysis of the Cape Grim data compiled in this thesis. Measurements are grouped into three-month sections, corresponding to the maximum ('peak') and minimum ('trough') periods of N_2O delta values from Park et al. (2012), as well as the intervening ('transition') periods.

Although the level of atmospheric variability is high, maximum and minimum delta values approximately correspond to ‘peak’ and ‘trough’ periods respectively. A study similar in scope to Park et al. (2012) would be needed to quantitatively assess this effect, although the magnitude of the expected seasonality is unlikely to be detectable at the current level of precision. The available CFC-11 and CFC-113 data were insufficient to extend this analysis to all three compounds.

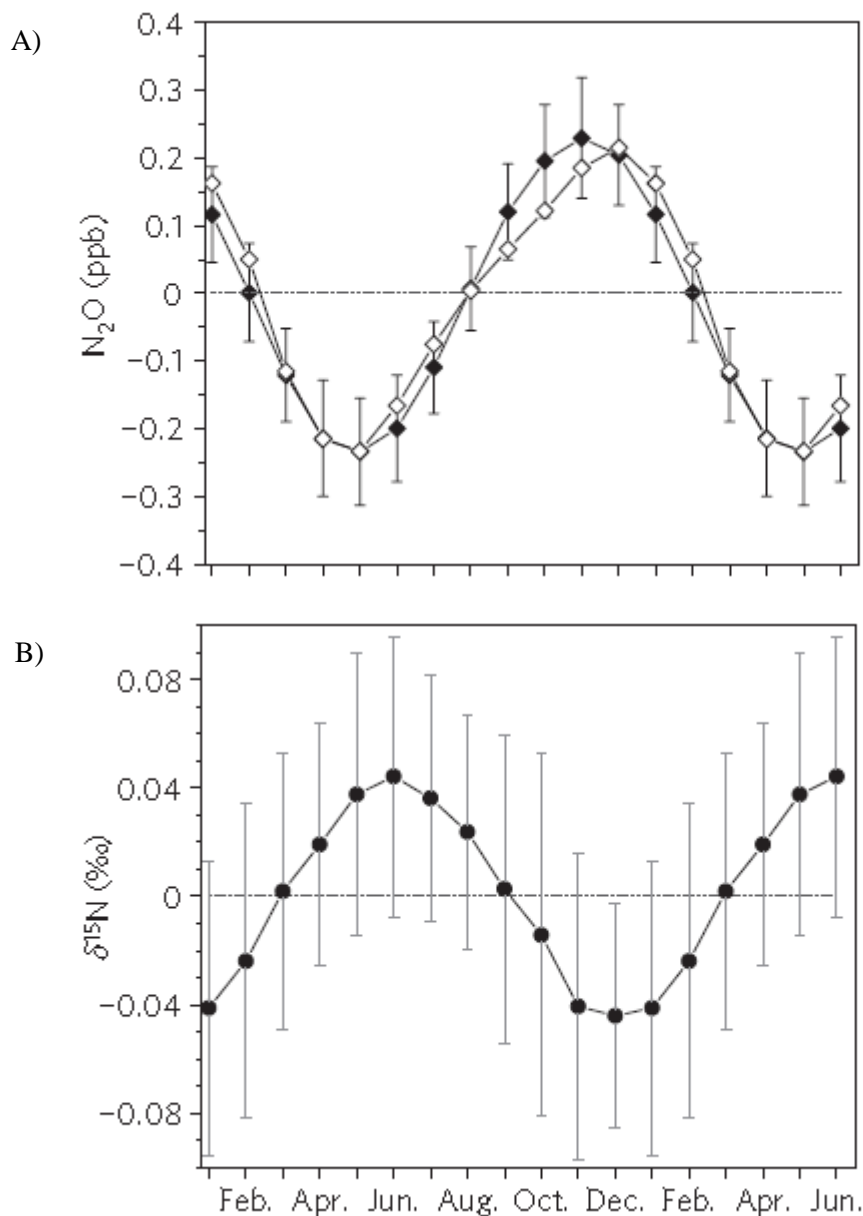


Figure 3.6. The mean N₂O seasonal cycles, measured on the Cape Grim archive between 1978 and 2005. A) N₂O mole fractions were measured by Nevison et al. (2005) (white diamonds) and Park et al. (2012) (black diamonds). B) δ(¹⁵N) values are given in ‰ (versus air-N₂). The figures were taken from Park et al. (2012).

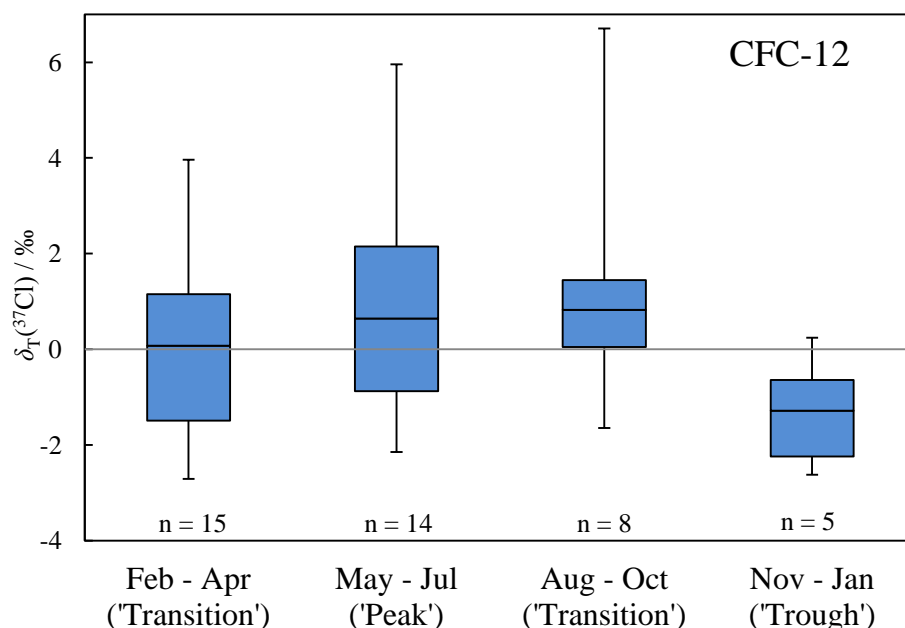


Figure 3.7. A boxplot of the $\delta_T(^{37}\text{Cl})$, CFC-12) from Cape Grim samples. The year is split into three-month sections, with the maximum value, upper quartile, median, lower quartile and minimum value displayed in each. The ‘Peak’, ‘Trough’ and ‘Transition’ periods were identified from a seasonality analysis of $\delta(^{15}\text{N}, \text{N}_2\text{O})$ (Figure 3.6, Park et al., 2012) and correspond to observed maximum, minimum and in-between periods. The sample count in each section is given on the plot. All delta values are relative to an air sample collected at Niwot Ridge in 2006 (AAL-071170).

3.1.3.2 Transport modelling

Since air is exchanged between the stratosphere and the troposphere, both source (troposphere) and sink (stratosphere) processes will affect tropospheric measurements of these gases. The CFCs discussed in this work are destroyed in the stratosphere through similar processes to N_2O . These sink reactions have been shown to enrich the heavy isotopes of N_2O and CFC-12, leading to increasing $\delta_s(^{15}\text{N})$, $\delta_s(^{18}\text{O})$ and $\delta_s(^{37}\text{Cl})$ with altitude (Kaiser et al., 2006; Laube et al., 2010a). If CFC-11 and CFC-113 are affected in the same way, the $\delta_T(^{37}\text{Cl})$ of all three CFCs should have increased as a result.

Stratospheric measurements

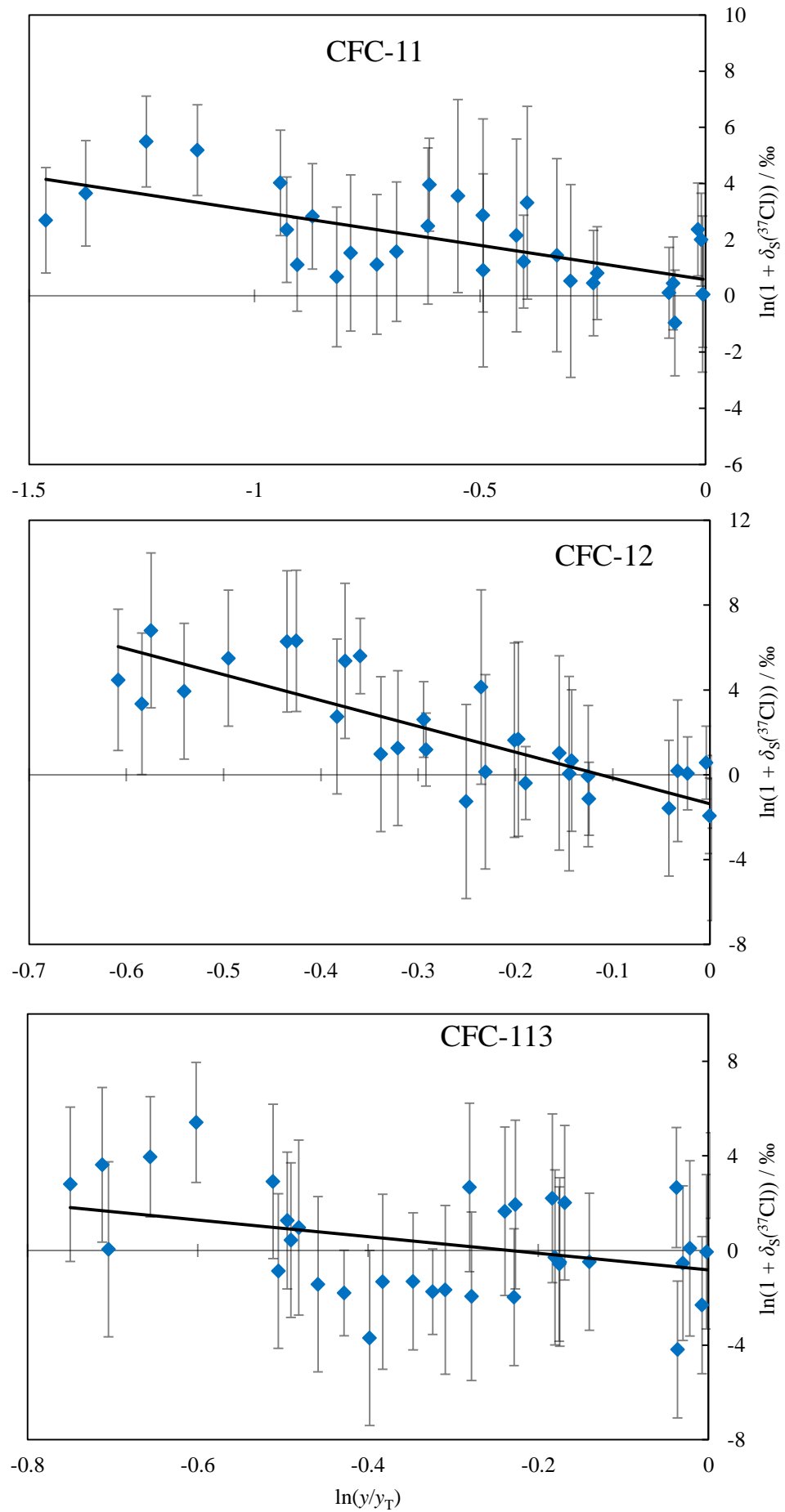
In order to determine whether the CFC sink reactions are isotope dependent, stratospheric samples were collected and analysed for $\delta_S(^{37}\text{Cl})$. Mid-latitude (48.1 – 53.4 °N) stratospheric air was collected on an M55 Geophysica research aircraft in 2009, as part of the European Union's FP7 project RECONCILE (von Hobe et al., 2013).

Dr. Johannes Laube performed the laboratory work from 2009-2010 and Eimear McKenna performed the initial data processing as part of her Master's project (McKenna, 2011). My contribution was an appraisal of the initial data processing, as well as completing the final steps (e.g. error calculations).

Using equation 1.25 (Chapter 1), a statistical “bootstrap” analysis technique was used to determine ε_{app} values and their uncertainties (Volk et al., 1997). In this technique, a data pool is created by describing each sample with three values (the measured delta value and this value $\pm 1\sigma$). The “bootstrap” tool draws 500 random samplings from the complete stratospheric data pool (including the possibility of drawing the same value repeatedly) to produce an overall ε_{app} value and a robust associated uncertainty range. Anomalous stratospheric samples were omitted using an iterative least squares method. Any sample more than two times the standard error of the $\ln(1 + \delta)$ estimate away from the linear regression of the Rayleigh fractionation plot was removed. This process was repeated until all data points fell within two times the standard error of the $\ln(1 + \delta)$ estimate, reducing the ε_{app} standard error in all cases.

After this outlier correction, a total of 31 (CFC-11), 33 (CFC-12) and 36 (CFC-113) measurements remained. Negative apparent isotope fractionations (ε_{app}) have been calculated for all three species (Figure 3.8). This indicates that the heavier isotopologue is broken down more slowly by sink reactions, causing the observed enrichment in ^{37}Cl .

Figure 3.8 (next page). Rayleigh fractionation plots of CFC-11, CFC-12 and CFC-113 chlorine isotope signatures, derived from mid-latitude stratospheric samples. Trend lines correspond to apparent fractionations (ε_{app}) of -2.4 ± 0.5 ‰ (CFC-11), -12.2 ± 1.6 ‰ (CFC-12) and -3.5 ± 1.5 ‰ (CFC-113). The standard error of the gradient is quoted for ε_{app} values. The average repeatability for individual samples was ± 2.3 ‰ (CFC-11), ± 3.2 ‰ (CFC-12) and ± 3.2 ‰ (CFC-113). 1σ standard deviation error bars are shown.



Model predictions

A modelling study was undertaken to calculate how the $\delta_T(^{37}\text{Cl})$ in CFC-11, CFC-12 and CFC-113 is expected to have changed over time, given the current understanding of transport and sink processes. These predictions can then be compared to the measured $\delta_T(^{37}\text{Cl})$ values (Figure 3.5). This will allow these measurements to be interpreted in terms of the isotope delta of emissions for each species. The modelling work described below follows Kaiser (2002) and Röckmann et al. (2003) and was performed by Prof. Jan Kaiser at UEA.

To perform this work, the model atmosphere was split into two parts: the troposphere and the stratosphere. It was assumed that the CFCs only break down in the stratosphere and that the isotopic effect of this process is fully described by the ϵ_{app} values calculated in Figure 3.8. These mid-latitude ϵ_{app} values were used in the absence of globally representative values. Also, estimates of the stratosphere-troposphere exchange were made based on the differing definitions of the tropopause by Holton (1990) and Appenzeller et al. (1996). These studies used the 100 mbar and the 380 K isentrope, respectively. These factors were used to solve mass balance equations for the troposphere and stratosphere. By performing these calculations for both isotopologues, the difference can be used to reconstruct the expected $\delta_T(^{37}\text{Cl})$ changes in CFC-11, CFC-12 and CFC-113. Since measurements of $\delta(^{37}\text{Cl})$ in source materials have not been made, it was assumed that no changes have occurred for the purposes of this model. The validity of this assumption was tested by comparing the model predictions to $\delta_T(^{37}\text{Cl})$ measurements (Figure 3.9) and is discussed in Section 3.1.3.3. Full methodological details of the modelling can be found in Allin et al. (2015).

Figure 3.9 shows how the $\delta_T(^{37}\text{Cl})$ of these three compounds would have changed over time, assuming no source variations. From their first release until the present-day, the $\delta_T(^{37}\text{Cl})$ of CFC-11, CFC-12 and CFC-113 are predicted to have increased by 1, 3 and 1 ‰, respectively. Maximum rates of increase are predicted to have occurred since 1990, which coincide with the sharp reduction in CFC emissions due to the introduction of legislation phasing out their production and consumption (Montzka et al., 2011). A drop in the anthropogenic input means that the existing atmospheric pool will become increasingly enriched, as demonstrated by the predicted acceleration of the $\delta_T(^{37}\text{Cl})$ increase after 1990. After 2010, mole fraction measurements are not available. Instead, the A1 scenario predictions in Daniel et al. (2011) are used to project $\delta_T(^{37}\text{Cl})$ changes into the middle of the 21st century. The A1 scenario predicts continued reductions in CFC emissions, leading

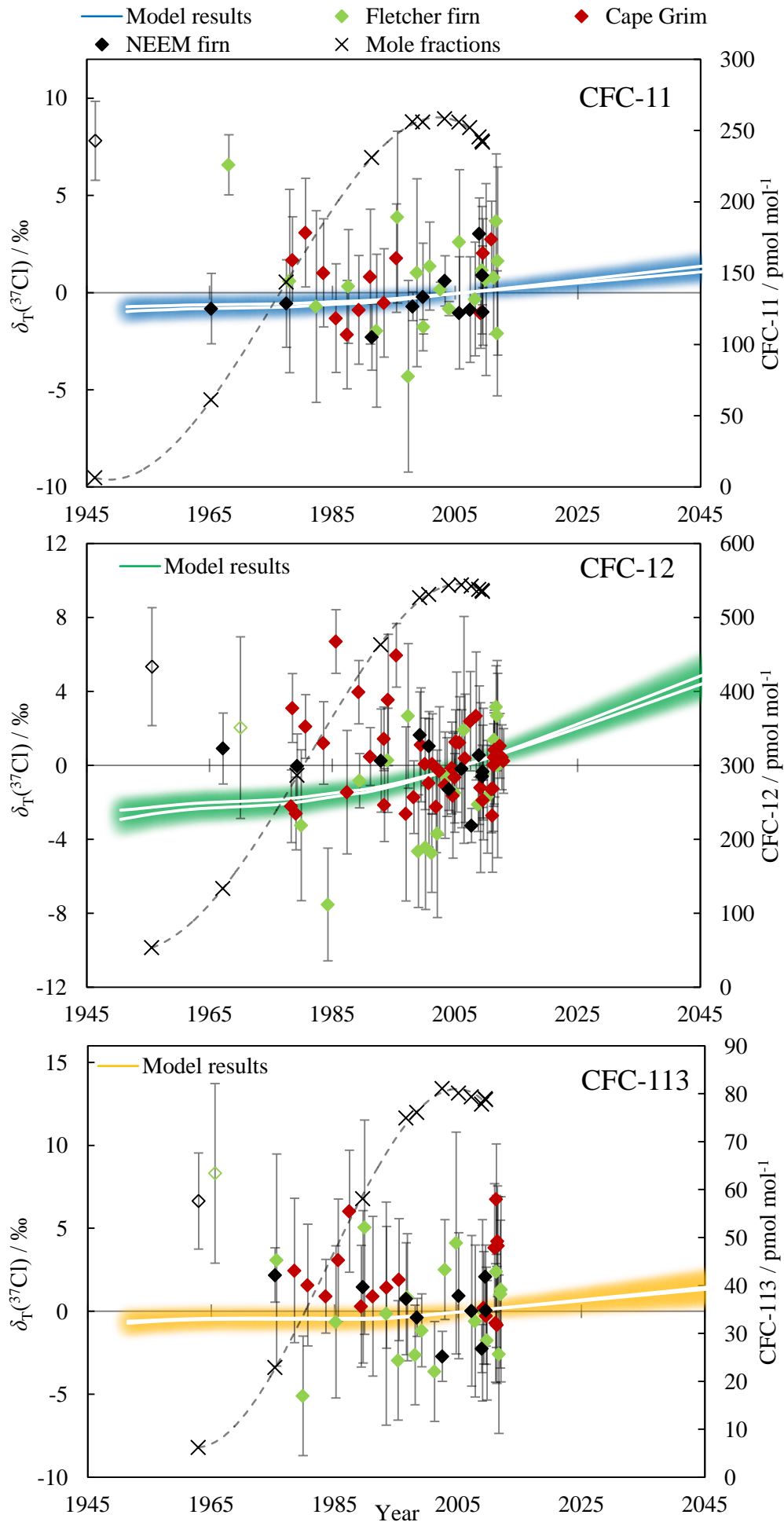
to further $\delta_T(^{37}\text{Cl})$ increases. From their first release until 2050, the $\delta_T(^{37}\text{Cl})$ of CFC-11, CFC-12 and CFC-113 are predicted to increase by 2, 7 and 2 ‰, respectively.

The areas of shading in Figure 3.9 represent the uncertainty envelopes. Approximately equal contributions to the uncertainty arise from:

1. The differing interfaces for stratosphere-troposphere exchange used by Holton (1990) and Appenzeller et al. (1996).
2. The 1σ uncertainty in ε_{app} values (from Figure 3.8).
3. The range of ‘most likely’ stratospheric CFC lifetime values from SPARC (2013).

Figure 3.9 (next page). $\delta_T(^{37}\text{Cl})$ measurements, compared to model predictions and measured mole fractions (black dashed lines). Black diamonds (NEEM firn air), green diamonds (Fletcher Promontory firn air) and red diamonds (Cape Grim air archive) represent the tropospheric chlorine isotope history of CFC-11, CFC-12 and CFC-113. White trend lines represent model estimates of the temporal evolution of $\delta_T(^{37}\text{Cl})$. Two lines are displayed per species, one for each stratosphere-troposphere exchange flux estimate (Holton, 1990; Appenzeller et al., 1996). Blue (CFC-11), green (CFC-12) and orange (CFC-113) shading indicates the model uncertainty envelopes. These uncertainties are described in the text. Open symbols indicate that the measurement was subject to a small correction, based on the dilution series analysis (see ‘*Determination of non-linearities*’, Section 3.1.3). All delta values are relative to an air sample collected at Niwot Ridge in 2006 (AAL-071170) and the model output has been adjusted so that it passes through 0 ‰ in 2006 to reflect this normalisation.

Isotope composition in atmospheric CFC-11, CFC-12 and CFC-113



3.1.3.3 A chlorine isotope history

From 1970 to the present-day, the modelled changes can be accounted for, within the analytical uncertainties of the $\delta_T(^{37}\text{Cl})$ measurements (Figure 3.9). For these three CFCs, the measured $\delta_T(^{37}\text{Cl})$ values are consistent with an isotopically constant source signature, but the measurement uncertainty is too high to preclude the possibility that it has changed over time. Despite the noted parallels in atmospheric chemical behaviour between CFC-12 and N_2O , their atmospheric isotope histories differ because N_2O has been present in the atmosphere for at least 800,000 years longer than CFC-12 (Spahni et al., 2005; Schilt et al., 2010). When anthropogenic emissions began, atmospheric N_2O isotope deltas were perturbed from a near steady-state source-sink system, whereas the industrial release of CFC-12 was not preceded by any atmospheric burden. This has caused $\delta(^{15}\text{N}, \text{N}_2\text{O})$ and $\delta(^{18}\text{O}, \text{N}_2\text{O})$ to decrease over the last century (Röckmann et al., 2003), while $\delta_T(^{37}\text{Cl}, \text{CFC-12})$ is predicted to have increased slightly (Figure 3.9).

Before 1970, there are 2 (CFC-11), 1 (CFC-12) and 2 (CFC-113) measurements 5 – 10 ‰ higher than expected, which could represent source $\delta(^{37}\text{Cl})$ changes. Emissions of these gases earlier in the record represent a larger proportion of their total atmospheric load, making the measurements more sensitive to potential source $\delta(^{37}\text{Cl})$ changes at this time. As the oldest samples, these five measurements contain the lowest CFC mole fractions, producing higher than average analytical uncertainties. Also, a small correction was applied to four of them, introducing an additional error (see ‘*Determination of non-linearities*’, Section 3.1.1). The limited number and precision of these measurements make it premature at this stage to report a source $\delta(^{37}\text{Cl})$ change in these gases.

3.1.4 Summary

- CFC-11, CFC-12 and CFC-113 are isotopically enriched in the stratosphere by destruction processes.
- This measured stratospheric isotope dependence and an assumed constant source $\delta(^{37}\text{Cl})$ were used to reconstruct the expected long-term changes in their tropospheric chlorine isotope signatures (using stratosphere-troposphere exchange flux estimates).
- Samples from the Cape Grim air archive (Tasmania, 1978 – 2010) and firn air samples from NEEM (Greenland) and Fletcher Promontory (Antarctica) have been

used to infer an atmospheric history of chlorine isotopes in CFC-11, CFC-12 and CFC-113.

- These measurements approximately cover the last 60 (CFC-11), 50 (CFC-12) and 45 (CFC-113) years and represent the first measurements of the $\delta_T(^{37}\text{Cl})$ in all three species.
- The predicted trends are small due to their long atmospheric lifetimes and can largely be accounted for in the tropospheric measurements. Significant improvements in measurement precision may make identification of the predicted 21st century increases in $\delta_T(^{37}\text{Cl})$ detectable, at least in the case of CFC-12.
- Across all species, five pre-1970 $\delta_T(^{37}\text{Cl})$ values are higher than predicted. Source $\delta(^{37}\text{Cl})$ changes could explain these offsets, but at present the available data are too limited in number and precision to confirm this.

3.2 Carbon isotope composition in chlorofluorocarbons CFC-11, CFC-12 and CFC-113 in firm air

The UEA-based studies of CFC isotopes are unique in their use of small samples (a few hundred ml) and a single-collector GC-MS system (Laube et al., 2010a; Allin et al., 2015; this thesis). Previously, several studies investigated the $\delta(^{13}\text{C})$ of some CFCs using large samples (tens to hundreds of litres) and various IRMS systems. No seasonal or diurnal cycles outside of analytical uncertainties were found by Redeker et al. (2007) in their measurements of the $\delta_T(^{13}\text{C})$, CFC-12). Zuiderweg et al. (2012) reported strong isotope dependence during the laboratory UV photolysis of CFC-11 and CFC-12, simulating the most prevalent stratospheric sink reaction. This suggests that the $\delta_S(^{13}\text{C})$ of these gases would reveal a similar isotope dependence. Finally, Zuiderweg et al. (2013) reported a large CFC-12 carbon isotope enrichment from the 1950s to the present-day, based on firm air measurements.

This section aims to describe the novel measurements made using the “AutoSpec” instrument to build on these studies and better characterise the $\delta_T(^{13}\text{C})$ of CFC-11, CFC-12 and CFC-113.

3.2.1 Research objectives

- Develop a method for making $\delta(^{13}\text{C})$ measurements in CFCs, using the GC-MS “AutoSpec” instrument.
- Produce a tropospheric carbon isotope history of CFC-11, CFC-12 and CFC-113, from $\delta_{\text{T}}(^{13}\text{C})$ measurements.
- Compare these measurements to modelled expectations, based on the current understanding of CFC breakdown and transport.
- Evaluate the observed long-term tropospheric carbon isotope changes in terms of the source and sink processes of the three most abundant CFCs.
- Confirm or refute the measurements made by Zuiderweg et al. (2013) of $\delta_{\text{T}}(^{13}\text{C})$, CFC-12) in NEEM firn air.

3.2.2 Methodology

For this work, significant adjustments were made to the methodology outlined in Section 3.1.2. The same basic instrumentation was used, but significant changes were made to the experiment setup to optimise the measurement conditions.

Before introducing these methodological alterations, $\delta_{\text{T}}(^{13}\text{C})$ measurements were made using the same instrument setup as for the $\delta_{\text{T}}(^{37}\text{Cl})$ measurements (Figure 3.10). Isotope deltas were calculated using equation 3.2, where R represents the $^{13}\text{C}/^{12}\text{C}$ abundance ratio of a standard or sample (from the $^{13}\text{CCl}_2\text{F}^+ / ^{12}\text{CCl}_2\text{F}^+$ ratio):

$$\delta(^{13}\text{C}) = \frac{R_{\text{sample}}}{R_{\text{standard}}} - 1 \quad (3.2)$$

The analytical precision achieved in these $\delta_{\text{T}}(^{13}\text{C})$ measurements was poor compared to the $\delta_{\text{T}}(^{37}\text{Cl})$ analysis (Table 3.4). Due to the naturally lower abundance of the ^{13}C isotope compared to ^{37}Cl (Table 1.2, Chapter 1), the $^{13}\text{C}^{35}\text{Cl}_2\text{F}^+$ peak is much smaller than the $^{12}\text{C}^{35}\text{Cl}^{37}\text{ClF}^+$ peak (Figure 3.11). A further discussion of these “original” results (Figure 3.10) is presented in Section 3.2.3.3 as a comparison to the new measurements made through the methodological improvements detailed below.

Figure 3.10 (next page). $\delta_{\text{T}}(^{13}\text{C})$ measurements in CFC-11, CFC-12 and CFC-113, using the original methodology. SF_6 is used as an age normaliser because firn model derived air ages are not available for all data. All delta values are relative to an air sample collected at Niwot Ridge in 2006 (AAL-071170).

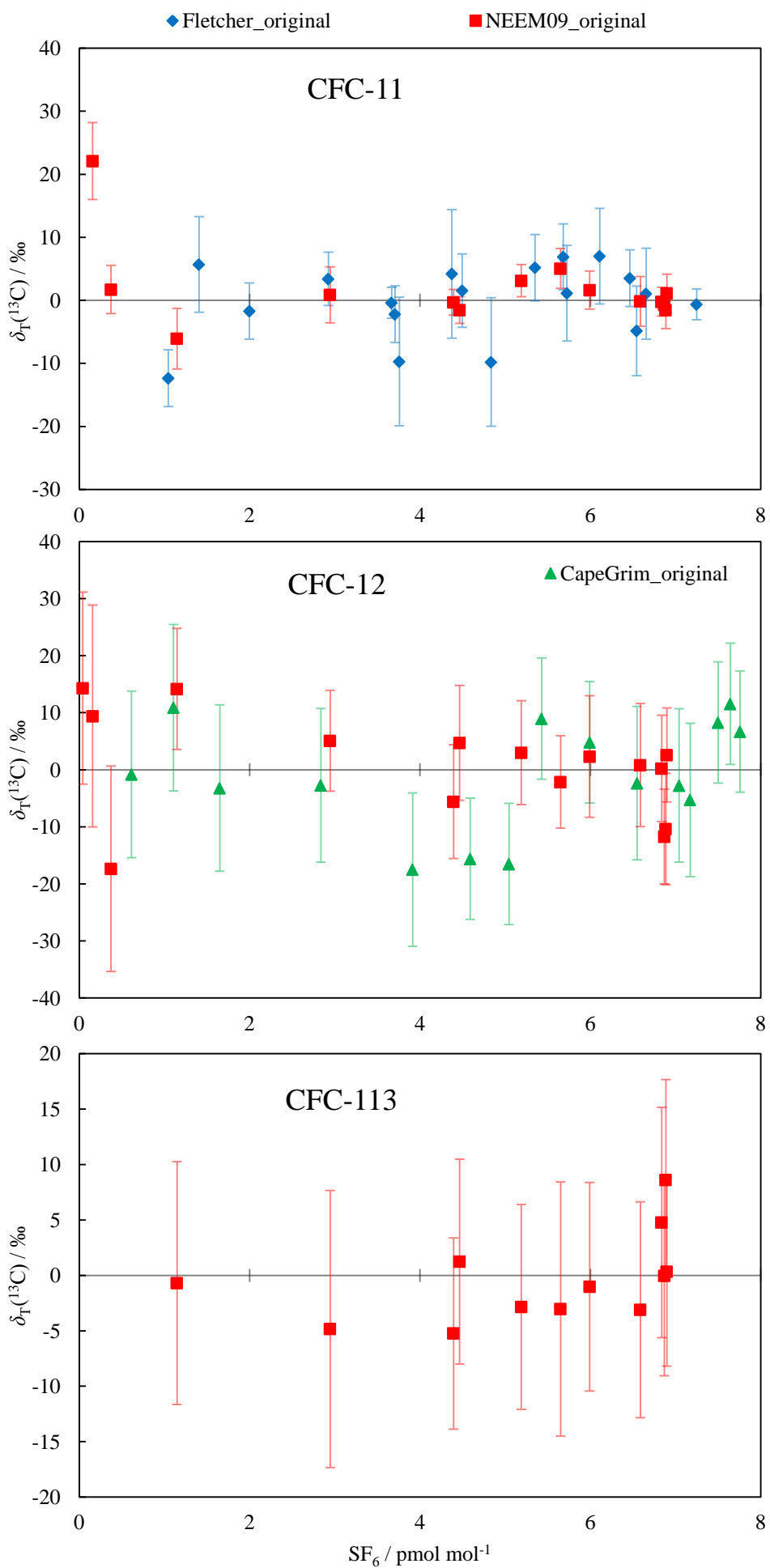


Table 3.4. The mean analytical uncertainty in $\delta_T(^{37}\text{Cl})$ (Section 3.1) and the original $\delta_T(^{13}\text{C})$ measurements. The uncertainties are mean values from all species and all tropospheric samples.

Measurement type	Mean analytical uncertainty / ‰	Number of samples
$\delta_T(^{37}\text{Cl})$	3	175
$\delta_T(^{13}\text{C})$	8	76

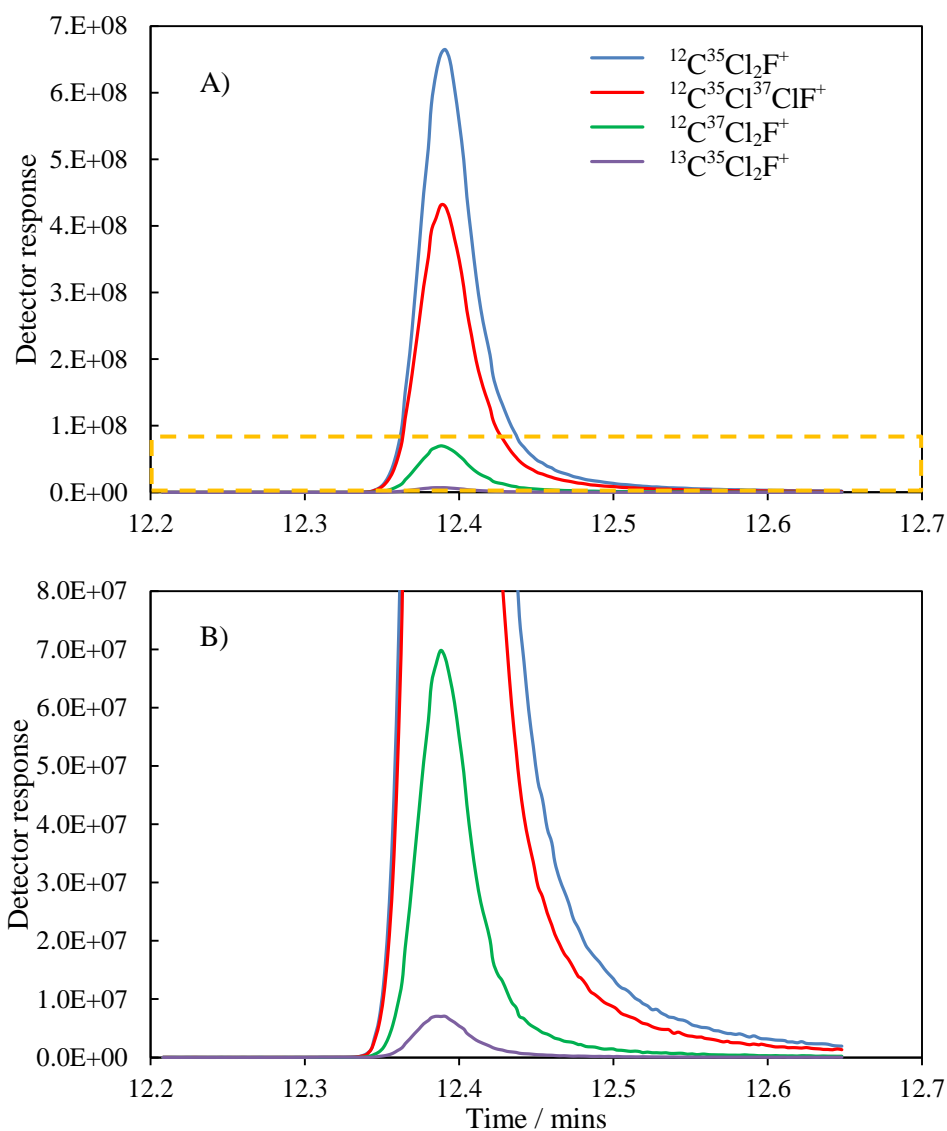


Figure 3.11. A) The mass spectrometer output produced by the most common CFC-11 fragment ion (CCl_2F^+). The fragment containing ^{13}C is the least abundant, followed by the fragment containing two ^{37}Cl atoms. B) As in A, but with adjusted axes to highlight the two smallest peaks. The orange dotted box in A indicates the axes values in B.

Methodological alterations were attempted in order to reduce this adverse effect of the precision of delta values calculated using the smallest peaks. An improvement of this kind would allow the $\delta(^{13}\text{C})$ of CFC-11, CFC-12 and CFC-113 to be better constrained. These adjustments were approached in two ways:

1. Increase the size of chromatographic peaks.
2. Increase the number of points on these peaks.

It was thought that these changes would reduce the uncertainty in calculated delta values by more accurately constraining the regression lines which give R values. The specific adjustments made to achieve these improvements are detailed below and Section 3.2.3 displays and discusses the results obtained using this new method.

Instrument setup

As described in Section 2.1.1.1, several fragment ions are included in each function (Table 2.1). These ions correspond to fragments of one or several species, as well as a reference 'lock mass' (from hexadecane which flows continuously into the ion source, see Section 2.1.1.1). This allows multiple species with similar elution times to be measured in a single acquisition. In a given function, this single-collector instrument must continuously cycle between the selected m/z values. This means that over a given time period, reducing the number of m/z values in a function decreases its cycle time and therefore increases the number of cycles completed. For these measurements, a reduced number of fragment ions were included in the functions corresponding to CFC-11, CFC-12 and CFC-113. After these adjustments they contained two CFC fragment ions and one lock mass. This led to an increase in the number of points used to plot the regression lines that produce R values (equation 3.1).

Table 3.5 details the changes made to the source and collector slit parameters. These slits define the width of the ion beam in the Y plane as it enters the first electrostatic analyser (source slit) and leaves the second electrostatic analyser (collector slit). Each parameter was adjusted to maximise the sensitivity of the instrument by monitoring a hexadecane (reference) peak.

Table 3.5. Source and collector slit parameters. The numbers represent the various adjustable parts of the slits and are given as a percentage of their maximum width. The “normal” operational parameters correspond to the conditions used for multi-species mole fractions analysis. The “ $\delta_T(^{13}\text{C})$ analysis” values quoted here are not fixed, they represent the optimum values at the time of tuning. The instrument performance determines these values for a given analysis period. In the same way, “normal” operational parameters can also change.

“Normal” operational parameters			$\delta_T(^{13}\text{C})$ analysis	
Source			Source	
	91.60	47.40	91.60	74.60
	66.80	20.80	66.80	20.80
Collector			Collector	
	51.00	54.00	64.60	56.60
	41.80	46.60	41.80	46.60
Source Slit:	100		Source Slit:	100
Collector Slit:	70		Collector Slit:	93.12

In the mass spectrometer functions containing CFC-11, CFC-12 and CFC-113, the detector voltage was increased from 375 to 400 V to amplify the peaks. However, the CCl_2F^+ fragment produced by CFC-11 gives a larger peak than CFC-12 and CFC-113, meaning that a detector voltage of 400 V will often cause the more abundant CFC-11 isotopologue peaks to saturate the detector. Reducing the detector voltage to 375 V in the CFC-11 function was often necessary. The detector voltage and slit width changes increased the amplitude of the peaks and the length of the regression lines used to calculate R values (Figure 3.1 and equations 3.1 and 3.2).

During a period of typical usage (which measures the mole fractions of many species), a mass resolution of approximately 1000 is achieved. While the adjustments made to the

detector voltage and slit widths increased the instrument's sensitivity, the mass resolution was reduced to approximately 500, making the measurements more vulnerable to interferences. CFC-113a partially co-elutes with CFC-113, although no CFC-113a peaks can be seen above the background noise in these $\delta_T(^{13}\text{C})$ measurements. There are no known interferences for CFC-11 and CFC-12 on any of the measured isotopologue fragments. This suggests that these measurements are free of interferences.

Section 2.1.1.1 describes the daily task of tuning and mass calibration. Ordinarily, the instrument is tuned using the C_4H_9^+ hexadecane fragment (m/z 57) because this produces the largest peak. The increased sensitivity due to the adjustments described above mean that the C_4H_9^+ peak saturates the detector. The lower abundance $\text{C}_7\text{H}_{15}^+$ fragment (m/z 99) is used instead.

Before commencing measurements, it is also important to check that the reference gas fragments used in the mass calibration of each function are not saturating the detector. Detector saturation is most likely to occur in CFC-11, CFC-12 and CFC-113 because it is necessary to approach the upper limit of peak sizes in these functions. The lock mass (m/z 99, $\text{C}_7\text{H}_{15}^+$) along with the masses immediately above (m/z 113, $\text{C}_8\text{H}_{18}^+$) and below (m/z 85, $\text{C}_6\text{H}_{13}^+$) are used in the calibration process. The mass calibration will be ineffective if any of these peaks reach saturation.

Sample preparation

200 ml samples were used during the $\delta(^{37}\text{Cl})$ analysis. In the inlet system, this corresponds to a Baratron pressure reading of 30 Torr (Section 2.1.1.2) and is a typical injection amount for this instrument. By injecting a larger sample, the peak sizes were increased. The pressure range of the Baratron limited the sample size to approximately 600 ml (90 Torr). Ordinarily, the release of CO_2 from the column has no effect on peak shapes. However, analysing more than 500 ml causes significant distortion of early eluting peaks (e.g. SF_6), although later peaks (including CFC-11, CFC-12 and CFC-113) were not affected (Figure 3.12).

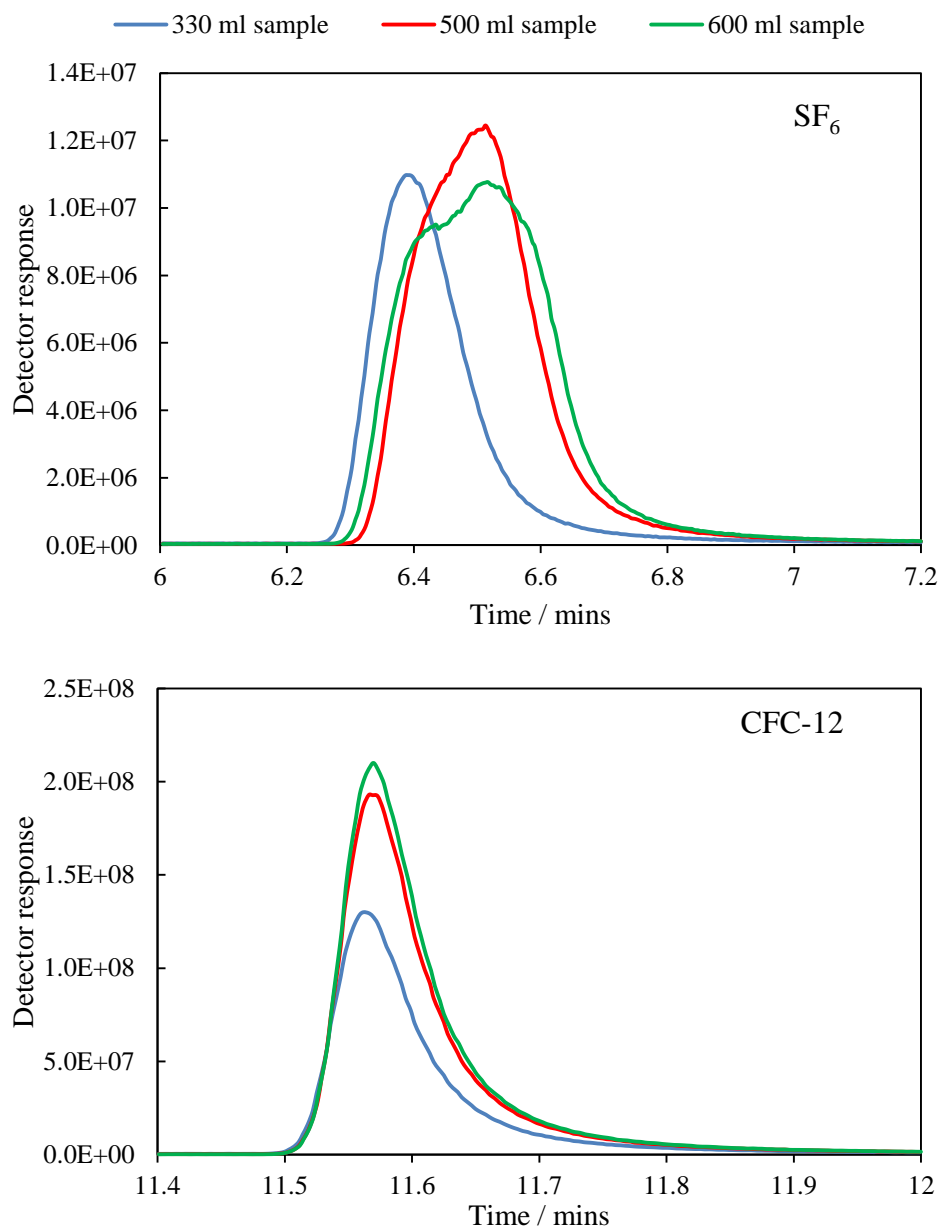


Figure 3.12. Smoothed data showing the SF₆ and CFC-12 peaks produced from different injection volumes. SF₆ displays peak distortion caused by the release of CO₂ from the column. Later eluting peaks were unaffected (e.g. CFC-12).

Data processing

Before the optimisation process detailed above, the $^{12}\text{C}^{35}\text{Cl}_2\text{F}^+$ fragment (m/z 101) produced a peak close to the upper limit of the measurement range in all three species. The adjustments to the instrument setup and sample preparation procedure outlined above increased the peak sizes. Consequently, the $^{12}\text{C}^{35}\text{Cl}_2\text{F}^+$ peak is unusable because it saturates

the detector. This means that $\delta(^{13}\text{C})$ values cannot be calculated from the $^{13}\text{CCl}_2\text{F}^+ / ^{12}\text{CCl}_2\text{F}^+$ ratio (equation 3.2).

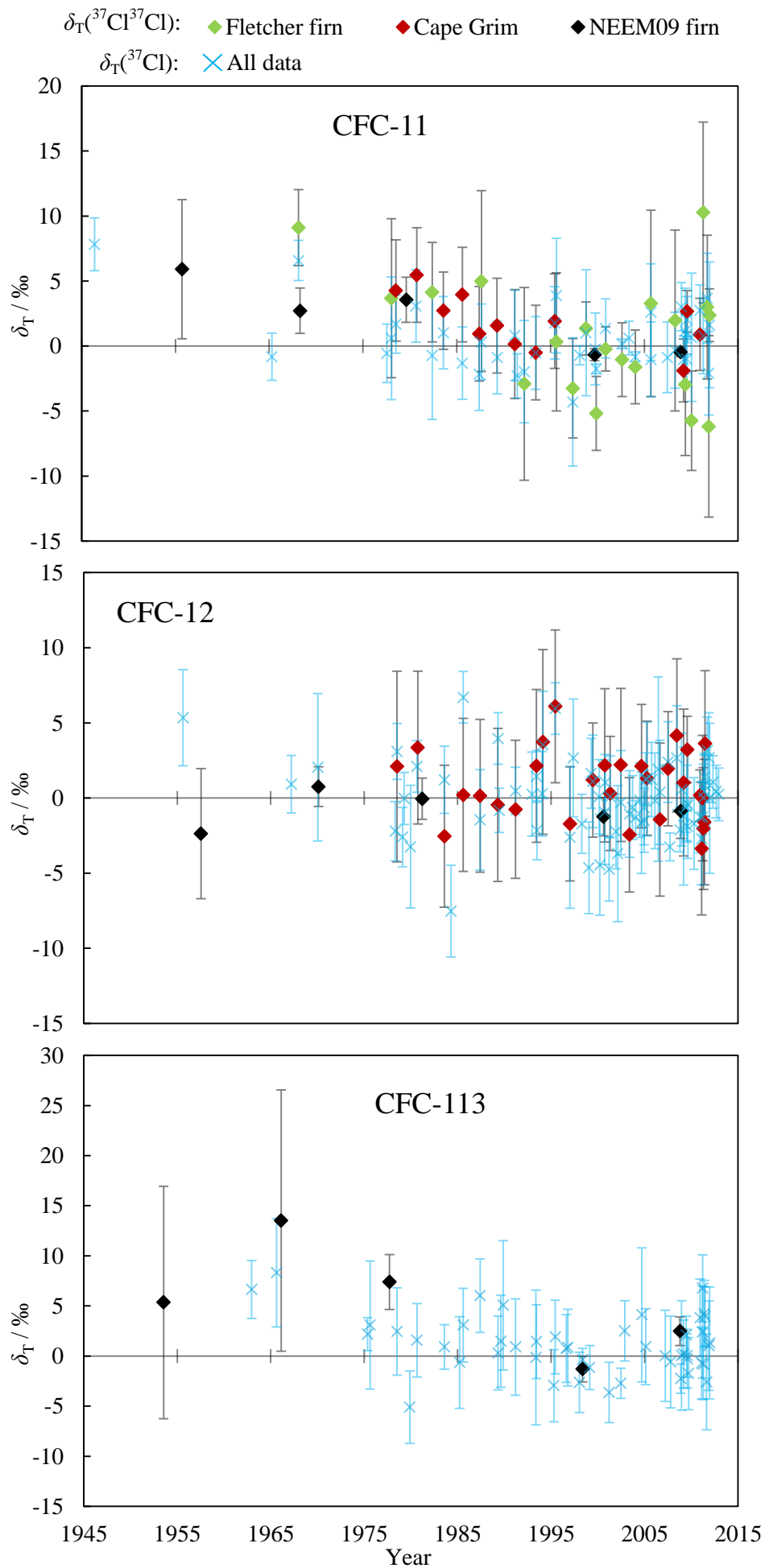
Section 3.1 shows that relative to AAL-071170 (an air sample collected in 2006), the $\delta_{\text{T}}(^{37}\text{Cl})$ of these gases is 0 ‰, within analytical uncertainties (at least since 1970). These values were obtained by comparing the ratio of $^{12}\text{C}^{35}\text{Cl}^{37}\text{ClF}^+$ to $^{12}\text{C}^{35}\text{Cl}_2\text{F}^+$. A $\delta_{\text{T}}(^{37}\text{Cl})$ value of 0 ‰ is produced when the $^{12}\text{C}^{35}\text{Cl}^{37}\text{ClF}^+$ fragment changes concurrently with the $^{12}\text{C}^{35}\text{Cl}_2\text{F}^+$ fragment. $\delta_{\text{T}}(^{37}\text{Cl}^{37}\text{Cl})$ values derived from the ratio of $^{12}\text{C}^{37}\text{Cl}_2\text{F}^+$ to $^{12}\text{C}^{35}\text{Cl}_2\text{F}^+$, should follow the direction of the $\delta_{\text{T}}(^{37}\text{Cl})$ signal, but at twice the magnitude (due to the presence of two ^{37}Cl atoms). Equation 3.3 was used to calculate $\delta_{\text{T}}(^{37}\text{Cl}^{37}\text{Cl})$, expressed in ‰:

$$\delta(^{37}\text{Cl}^{37}\text{Cl}) = \frac{R_{\text{sample}}}{R_{\text{standard}}} - 1 \quad (3.3)$$

where R represents the $^{37}\text{Cl}^{37}\text{Cl} / ^{35}\text{Cl}^{35}\text{Cl}$ abundance ratio of a standard or sample. In common with all delta values presented in this thesis, there is no internationally recognised isotope standard. For this reason, all isotope deltas are calculated relative to an air sample collected at Niwot Ridge, Colorado, by the National Oceanic and Atmospheric Administration (NOAA) in 2006 (AAL-071170).

Measurements of $\delta_{\text{T}}(^{37}\text{Cl}^{37}\text{Cl})$ were made on 5 NEEM 2009 firn samples in all species, 20 Fletcher firn samples (CFC-11) and 12 (CFC-11) and 29 (CFC-12) Cape Grim samples. These data agree well with $\delta_{\text{T}}(^{37}\text{Cl})$ values (Figure 3.13). This means that the $^{12}\text{C}^{35}\text{Cl}^{37}\text{ClF}^+$ and $^{12}\text{C}^{37}\text{Cl}_2\text{F}^+$ fragments both change concurrently with the $^{12}\text{C}^{35}\text{Cl}_2\text{F}^+$ fragment peak (at least since 1970). As a result, the smaller $^{12}\text{C}^{37}\text{Cl}_2\text{F}^+$ peak can be used instead of the $^{12}\text{C}^{35}\text{Cl}_2\text{F}^+$ peak in calculations of $\delta_{\text{T}}(^{13}\text{C})$. This means that $\delta_{\text{T}}(^{13}\text{C})$ values can be calculated using the optimisations outline above (without saturating the detector).

Figure 3.13 (next page). Comparison between all available $\delta_{\text{T}}(^{37}\text{Cl})$ (blue crosses) and $\delta_{\text{T}}(^{37}\text{Cl}^{37}\text{Cl})$ (green, red and black diamonds) measurements in CFC-11, CFC-12 and CFC-113. 1σ standard deviation error bars are shown. All delta values are relative to an air sample collected at Niwot Ridge in 2006 (AAL-071170).



To quantify any instrument bias in these measurements, the dilution series detailed in Table 3.3 was also analysed for $\delta(^{37}\text{Cl}^{37}\text{Cl})$. Similar to $\delta(^{37}\text{Cl})$ (see Section 3.1.3.1), the smallest peak areas displayed erroneously low delta values. However, all of the samples have peak areas in the region where the dilution series showed no bias, meaning that the $\delta_{\text{T}}(^{37}\text{Cl}^{37}\text{Cl})$ measurements do not require any corrections.

Equation 3.2 was used to calculate the relative $^{13}\text{C}/^{12}\text{C}$ ratio difference of CFCs in sample air with respect to a standard. As discussed above, the R value in this case was derived from the ratio between $^{13}\text{C}^{35}\text{Cl}_2\text{F}^+$ and $^{12}\text{C}^{37}\text{Cl}_2\text{F}^+$ (rather than the $^{13}\text{CCl}_2\text{F}^+ / ^{12}\text{CCl}_2\text{F}^+$ ratio). There is no internationally recognised isotope standard for these measurements, so the same 2006 NOAA air sample was used as the reference material (AAL-071170).

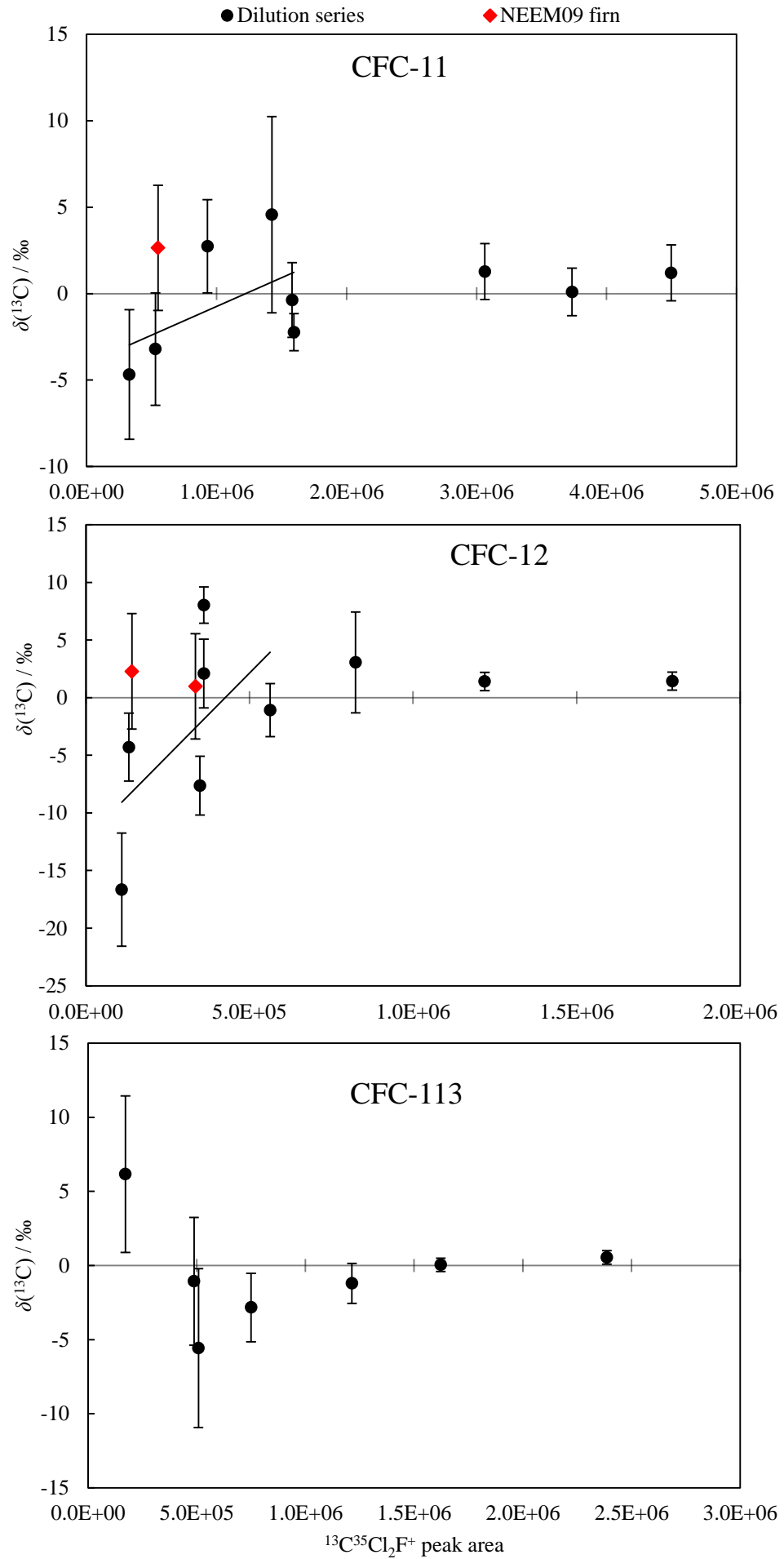
3.2.3 Results and discussion

Determination of non-linearities

The GC-MS AutoSpec instrument has been previously tested to characterise any biases in chlorine isotope ratio measurements (Laube et al., 2010a; Allin et al., 2015). This section details the first $\delta(^{13}\text{C})$ measurements attempted using this instrument. As described in Section 3.1, a static dilution series was analysed to assess the response behaviour of the analytical system. The static dilution series used in Section 3.1.3.1 (Table 3.3) were analysed for $\delta(^{13}\text{C})$ in CFC-11, CFC-12 and CFC-113.

Figure 3.14 shows that delta values derived from the smallest peak areas exhibit larger than average uncertainties and erroneously low $\delta(^{13}\text{C})$ values for CFC-11 and CFC-12. In general, the smallest CFC-113 peaks also follow the pattern of progressive depletion. However, the smallest CFC-113 peak produces an enriched delta value. This discrepancy produces a greater level of uncertainty in the response behaviour of the instrument to small CFC-113 peaks. For this reason, corrections were not attempted for CFC-113, leaving a less extensive $\delta_{\text{T}}(^{13}\text{C}, \text{CFC-113})$ record compared to CFC-11 and CFC-12.

Figure 3.14 (next page). Dilution series measured for $\delta(^{13}\text{C})$, plotted against the integrated peak area of the $^{13}\text{C}^{35}\text{Cl}_2\text{F}^+$ fragment ion (m/z 102). 1σ standard deviation error bars are shown. Included are the firm air measurements that fall within the depleted region of the dilution series analysis (red diamonds). Linear regression lines are used to adjust the firm samples, based on the observed dilution series depletion. Unaffected samples are not displayed. All delta values are relative to an air sample collected at Niwot Ridge in 2006 (AAL-071170).



More than 90 % of the samples analysed have peak areas in the region where the dilution series showed no bias in isotope deltas. However, a total of 1 (CFC-11) and 2 (CFC-12) $\delta_T(^{13}\text{C})$ measurements were corrected based on the quantified instrument bias and 3 CFC-113 measurements were discarded (due to the discrepancy in the smallest CFC-113 peaks, as outlined above). The corrections and additional uncertainty calculations were made using the method outlined in Section 3.1.3.

3.2.3.1 Firn measurements

Firn air samples from NEEM (Greenland), collected during the 2008 and 2009 field campaigns have been analysed for the $\delta_T(^{13}\text{C})$ of CFC-11, CFC-12 and CFC-113. A total of 20 (CFC-11), 21 (CFC-12) and 18 (CFC-113) $\delta_T(^{13}\text{C})$ measurements are presented, approximately covering the last 55, 50 and 20 years, respectively (Figure 3.15). Based on the dilution series analysis (see ‘*Determination of non-linearities*’, Section 3.2.3), 1 (CFC-11) and 2 (CFC-12) NEEM 2009 samples required a correction. Additionally, the uncertainty in the dilution series analysis at low CFC-113 abundances was too high to determine a robust correction factor. For this reason, the 3 deepest CFC-113 measurements were rejected.

Figure 3.15 (next page). $\delta_T(^{13}\text{C})$ measurements in CFC-11, CFC-12 and CFC-113. Black diamonds (NEEM 2009 firn air) and blue diamonds (NEEM 2008 firn air) represent the tropospheric carbon isotope history of CFC-11, CFC-12 and CFC-113. The average repeatability for individual samples was ± 2.0 ‰ (CFC-11), ± 3.8 ‰ (CFC-12) and ± 2.0 ‰ (CFC-113). 1σ standard deviation error bars are shown. Open symbols indicate that the measurement was subject to a small correction, based on the dilution series analysis (see ‘*Determination of non-linearities*’, Section 3.2.3). All delta values are relative to an air sample collected at Niwot Ridge in 2006 (AAL-071170).

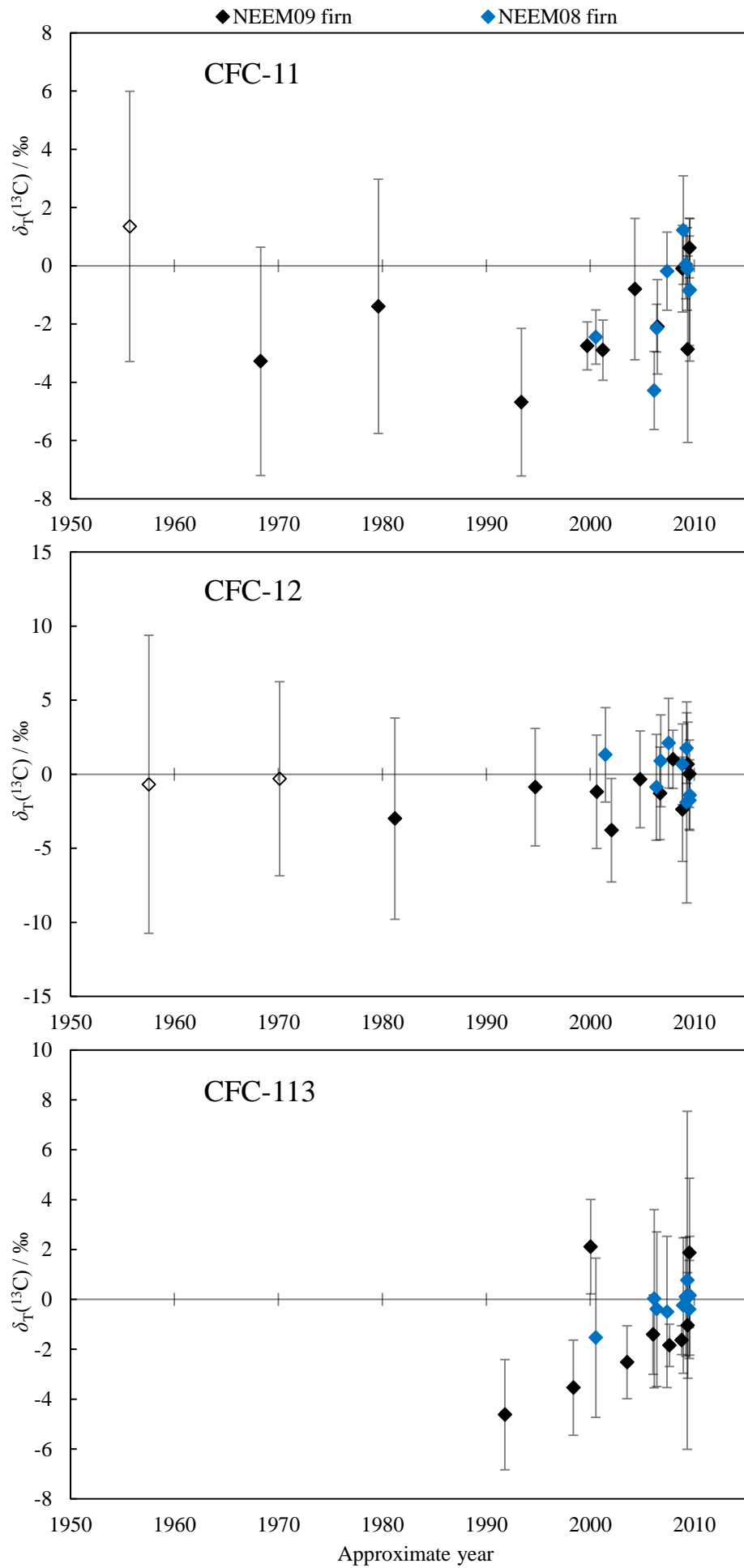


Table 3.6. The gravitational and diffusive correction for the $\delta_T(^{37}\text{Cl})$ of CFC-11 in NEEM 2009 firn air, calculated by Dr. Patricia Martinerie using the LGGE firn diffusion model. These values are used to calculate the approximate correction required for the $\delta_T(^{13}\text{C})$ values. As described in the text, the $\delta_T(^{37}\text{Cl})$ correction at each depth was multiplied by -1.5 to give an approximate $\delta_T(^{13}\text{C})$ correction value.

Depth / m	CFC-11 gravitational and diffusive fractionation corrections / ‰	
	$\delta_T(^{37}\text{Cl})$	$\delta_T(^{13}\text{C})$
0	0	0
10.5	0.103	-0.1545
20.4	0.248	-0.372
30.2	0.414	-0.621
39.23	0.498	-0.747
50.7	0.627	-0.9405
60.3	0.67	-1.005
62.02	0.641	-0.9615
63.8	0.362	-0.543
66.8	0.497	-0.7455
69.4	1.674	-2.511
71.9	3.048	-4.572

Section 3.1.2 details the methods used to infer air ages in firn samples. Due to time constraints, a model of gas transport in firn could not be used to obtain age of air estimates for the measurements in Figure 3.15. However, since the gas concentration gradients in the $\delta_T(^{37}\text{Cl})$ measurements are the same as the $\delta_T(^{13}\text{C})$ measurements, diffusional mixing is likely to be similar. Based on this assumption, the $\delta_T(^{37}\text{Cl})$ air ages have been used in the plots of $\delta_T(^{13}\text{C})$ and are referred to as ‘approximate ages’. Similarly, an approximate gravitational and diffusive correction was applied to these new data, based on the

correction calculated using the firm model for $\delta_T(^{37}\text{Cl})$ measurements. $\delta_T(^{13}\text{C})$ values are calculated based on the ratio between $^{13}\text{C}^{35}\text{Cl}_2\text{F}^+$ and $^{12}\text{C}^{37}\text{Cl}_2\text{F}^+$ (m/z 102 and 105), whereas $\delta_T(^{37}\text{Cl})$ values are calculated based on the ratio between $^{12}\text{C}^{35}\text{Cl}^{37}\text{ClF}^+$ and $^{12}\text{C}^{35}\text{Cl}_2\text{F}^+$ (m/z 103 and 101). Hence, the $\delta_T(^{13}\text{C})$ correction was assumed to be 1.5 times larger than the $\delta_T(^{37}\text{Cl})$ correction, and in the opposite direction (Table 3.6). This is a crude method, however the corrections are generally small (a mean value of 0.73 ‰ across all species), meaning that using a firm diffusion model to calculate accurate values would not have significantly altered the measurement values and would not change their interpretation.

3.2.3.2 A carbon isotope history

Laboratory UV photolysis measurements

Section 3.1.3.2 describes how $\delta_S(^{37}\text{Cl})$ measurements were used to infer the chlorine isotope dependence of processes that destroy CFC-11, CFC-12 and CFC-113 in the stratosphere. The measured dependence is caused by the preferential inclusion of lighter isotopologues in sink reactions (dominated by UV photolysis), causing the observed enrichment in ^{37}Cl . Measurements of $\delta_S(^{13}\text{C})$ are not available at this time. However, the carbon isotope dependence of CFC-11 and CFC-12 as they are photolysed by UV light has been investigated in a laboratory study (Zuiderweg et al., 2012).

Zuiderweg et al. (2012) quantified the isotope dependence of carbon in CFC-11 and CFC-12 during their photolysis by UV light. At atmospherically relevant temperatures, they found carbon isotope fractionations of (-23.8 ± 0.9) to (-17.7 ± 0.4) ‰ for CFC-11 and (-66.2 ± 3.1) to (-51.0 ± 2.9) ‰ for CFC-12. UV photolysis is the dominant loss process of CFC-11 and CFC-12 in the stratosphere meaning that these values can be used to approximate the carbon isotope dependence of these gases in stratospheric sink reactions. There has been no such study of CFC-113, meaning that a model output cannot be produced for this species.

Model predictions

As described in Section 3.1.3.2 and Allin et al. (2015), the current understanding of transport and sink processes can be used in a modelling study to predict how the $\delta_T(^{13}\text{C})$ of CFC-11 and CFC-12 would have evolved over time. By comparing these predictions with measured values, the measurements can be interpreted in terms of the isotope delta of

emissions for each species (Figure 3.16). Since ε_{app} values are not available, the measurements made by Zuiderweg et al. (2012) can be used alongside stratosphere-troposphere exchange flux estimates to make these predictions. Again, Prof. Jan Kaiser performed the modelling work presented in this section.

Figure 3.16 shows how the $\delta_{\text{T}}(^{13}\text{C})$ of CFC-11 and CFC-12 would have changed over time, assuming no source carbon isotope variations. From their first release until the present-day, CFC-11 and CFC-12 $\delta_{\text{T}}(^{13}\text{C})$ values are predicted to have increased by 4 and 5 ‰, respectively. As with $\delta_{\text{T}}(^{37}\text{Cl})$, maximum rates of increase are predicted to have occurred since 1990, coinciding with the introduction of legislation phasing out CFC production and consumption (Montzka et al., 2011). The predicted rise in the $\delta_{\text{T}}(^{13}\text{C})$ of these gases is caused by the enriching effect of isotope dependent stratospheric sink reactions. After 2009, mole fraction measurements are not available. Instead, the A1 scenario predictions in Daniel et al. (2011) are used to project $\delta_{\text{T}}(^{13}\text{C})$ changes into the middle of the 21st century. The A1 scenario predicts continued reductions in CFC emissions, leading to further $\delta_{\text{T}}(^{13}\text{C})$ increases as the remaining atmospheric pool becomes increasingly enriched. From their first release until 2050, CFC-11 and CFC-12 $\delta_{\text{T}}(^{13}\text{C})$ values are predicted to increase by 11 and 18 ‰, respectively. These values are larger than the predicted $\delta_{\text{T}}(^{37}\text{Cl})$ increases for CFC-11 and CFC-12 over the same period (2 and 8 ‰, respectively). This is due to the higher isotope dependence of carbon compared to chlorine in sink reactions, inferred from $\delta_{\text{S}}(^{37}\text{Cl})$ measurements (Figure 3.8) and measurements presented in Zuiderweg et al. (2012).

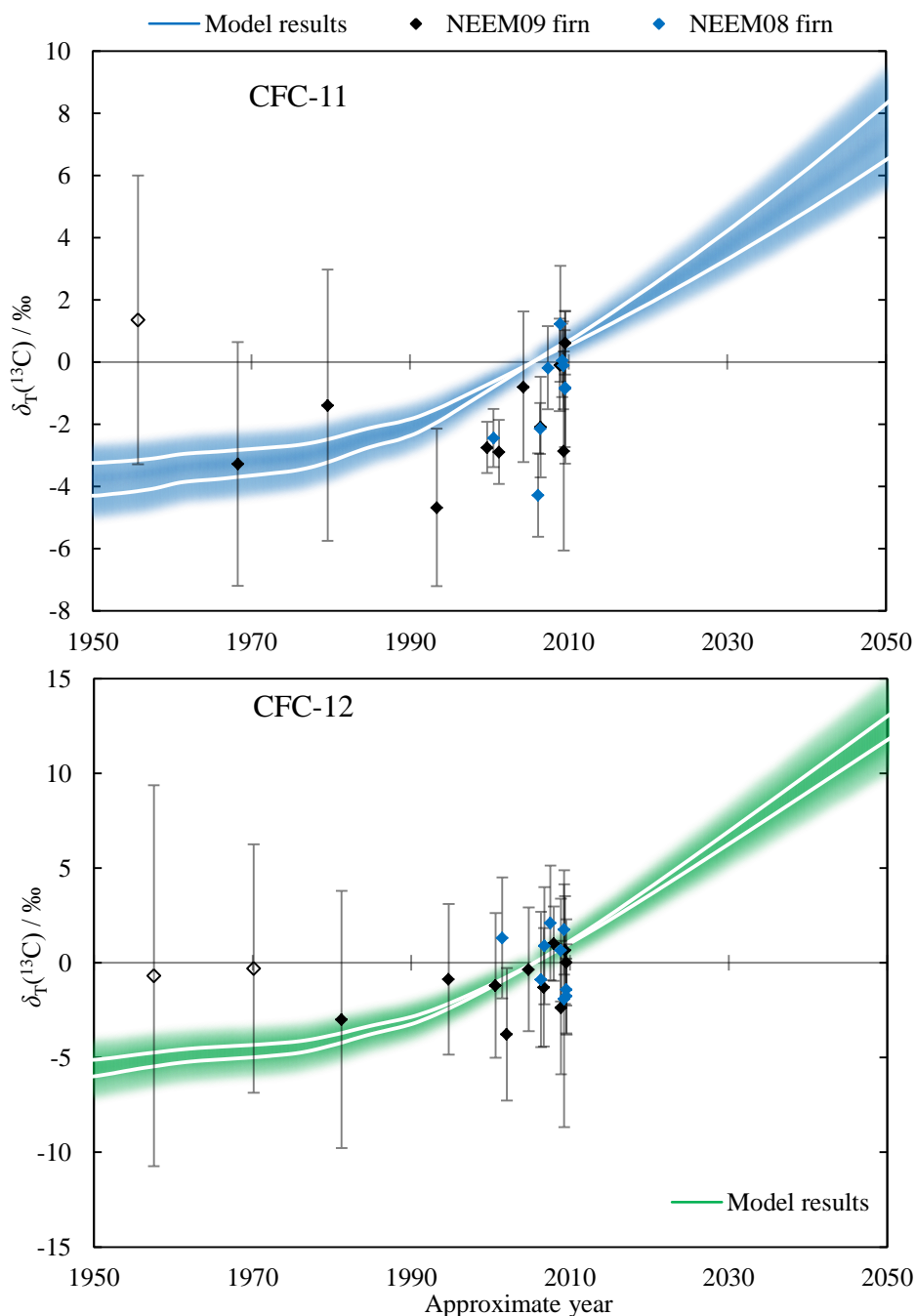


Figure 3.16. $\delta_T(^{13}\text{C})$ measurements, compared to model predictions. The measurements are unchanged from Figure 3.15: black diamonds (NEEM 2009 firn air) and blue diamonds (NEEM 2008 firn air) represent the tropospheric carbon isotope history of CFC-11 and CFC-12. White trend lines represent model estimates of the temporal evolution of $\delta_T(^{13}\text{C})$. Two lines are displayed per species, one for each stratosphere-troposphere exchange flux estimate (Holton, 1990; Appenzeller et al., 1996). Blue (CFC-11) and green (CFC-12) shading indicates the model uncertainty envelopes. These uncertainties are based on two independent sources of error: 1) the 1σ uncertainty in UV photolysis $\delta(^{13}\text{C})$ values; 2) the range of ‘most likely’ lifetime values from SPARC (2013). All delta values are relative to an air sample collected at Niwot Ridge in 2006 (AAL-071170) and the model output has been adjusted so that it passes through 0 ‰ at 2006.

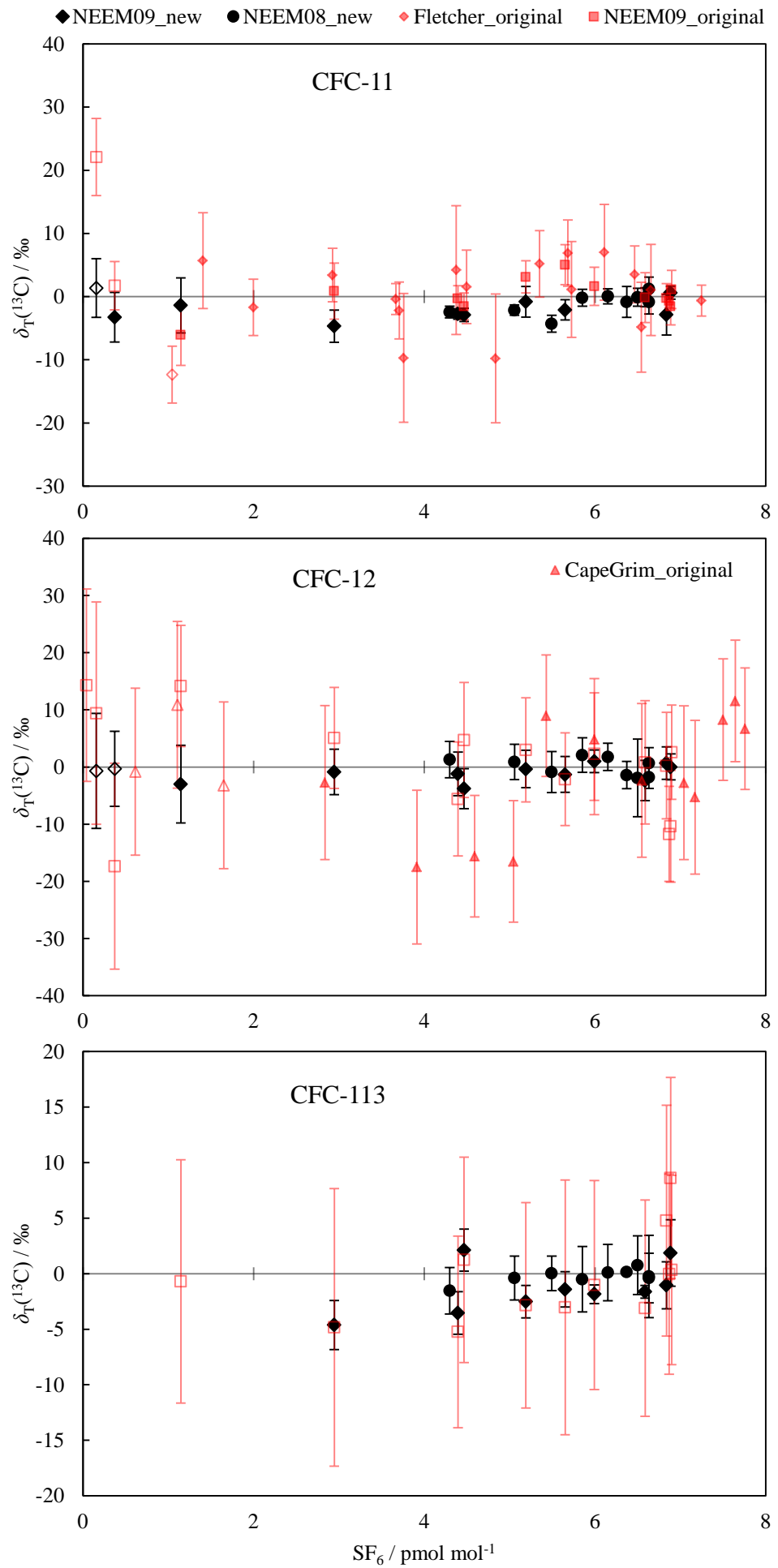
The areas of shading in Figure 3.16 represent the uncertainty envelopes. The same factors contribute to this uncertainty as described in Section 3.1.3.2. Within analytical uncertainties, there is good agreement between the firm measurements and modelled $\delta_T(^{13}\text{C})$ changes (Figure 3.16). This means that for CFC-11 and CFC-12, an isotopically constant source signature is consistent with the observations, based on the current understanding of transport and destruction processes. Between 1999 and 2009, there are 6 $\delta_T(^{13}\text{C}, \text{CFC-11})$ measurements slightly lower than expected, which could indicate that changes to source or sink processes have occurred. However, the $\delta_T(^{13}\text{C})$ model output is derived from a laboratory study using higher than atmospheric concentrations (Zuiderweg et al., 2012), rather than stratospheric measurements. Only one sink reaction has been included in the model calculations, meaning that the errors assigned to the model output are likely to be underestimates. Also, the other 10 measurements in this period agree with expected values. It seems likely that the observed disagreement does not indicate a source or sink change, but can be attributed to natural variability and a slightly underestimated model uncertainty envelope.

3.2.3.3 Comparison with other studies

Methodological improvements

As discussed in Section 3.2.2, $\delta_T(^{13}\text{C})$ measurements were initially made using the low abundance $^{13}\text{C}^{35}\text{Cl}_2\text{F}^+$ fragment ion. Figure 3.17 shows how the original results compare to the measurements displayed in Figures 3.15 and 3.16 (using the methodological improvements detailed in Section 3.2.2). A total of 56 samples were analysed using the original method, of which 33 were also measured after the methodological improvements were implemented. Very good agreement is shown, with 30 of these producing $\delta_T(^{13}\text{C})$ values that are indistinguishable, within 1σ analytical uncertainties.

Figure 3.17 (next page). $\delta_T(^{13}\text{C})$ measurements in CFC-11, CFC-12 and CFC-113. Results using the original methodology (red symbols) are compared to results obtained using the new methodology (black symbols), as described in Section 3.2.2. SF_6 is used as an age normaliser because firm model derived air ages are not available for all data. An open symbol indicates that the measurement was subject to a small correction, based on the dilution series analysis (see ‘*Determination of non-linearities*’, Section 3.2.3.1). All delta values are relative to an air sample collected at Niwot Ridge in 2006 (AAL-071170).



There is a significant improvement in measurement precision from the original to the new analyses (Table 3.7). For a given species, the overall mean analytical uncertainty of each method cannot be compared because only a subset of samples were re-analysed using the new method. Samples with low mole fractions produce $\delta_T(^{13}\text{C})$ values with larger uncertainties than those at contemporary levels. To remove a bias due to variations in sample distribution, samples are grouped based on their age before comparing analytical uncertainties (Table 3.7). In ‘modern’ air (1995 – 2010), the mean 1σ analytical uncertainty has been reduced by 67 % (CFC-11), 71 % (CFC-12) and 79 % (CFC-113).

Table 3.7. A comparison between the analytical uncertainties of $\delta_T(^{13}\text{C})$ measurements in CFC-11, CFC-12 and CFC-113. The data are separated according to their air age (either pre-1995 or between 1995 and 2010).

Age range	Mean 1σ analytical uncertainty / ‰					
	CFC-11		CFC-12		CFC-113	
	Original method	New method	Original method	New method	Original method	New method
1995 - 2010	4.8	1.6	10.6	3.1	9.5	2.0
Pre-1995	4.8	3.7	14.5	6.8	11.7	-

Previous $\delta_T(^{13}\text{C})$, CFC-12) firm air measurements

Zuiderweg et al. (2013) measured significant ^{13}C enrichment in CFC-12 from NEEM 2009 firm air (Figure 3.18) and cite changes in production processes as the most likely cause. However, as they concede, there is no direct evidence that the reported manufacturing methodology changes had any effect on the isotope signature of CFC-12.

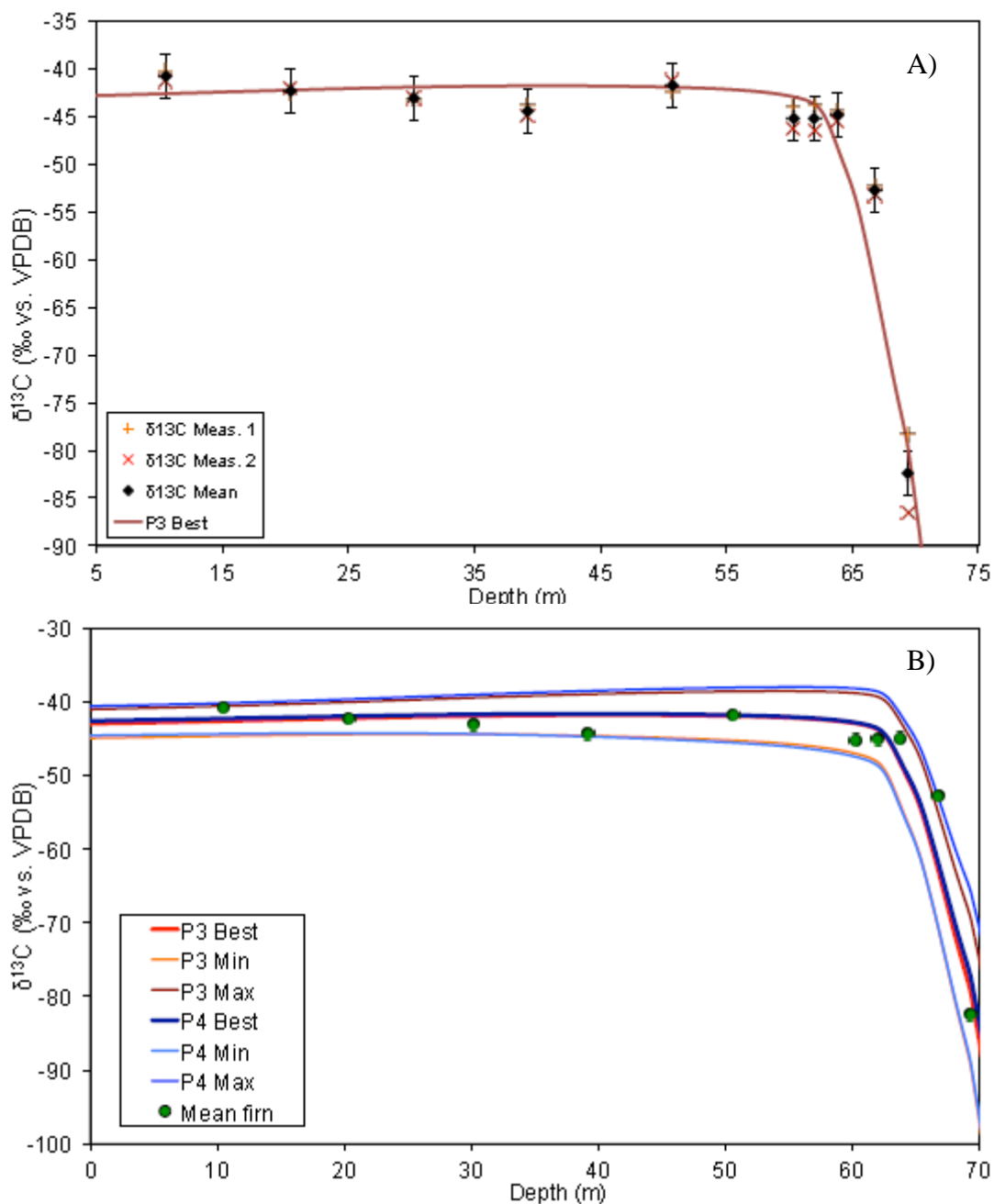


Figure 3.18. A) Depth profile of $\delta_T(^{13}\text{C}, \text{CFC-12})$ measurements (black diamonds) from NEEM 2009 firn air and a best estimate scenario from a firn model (red curve). B) The firn measurements from A (green circles) are plotted alongside best estimate forward models (red and blue curves). Maximum and minimum uncertainty estimates are shown. Both figures were taken from Zuiderweg et al. (2013).

Figure 3.19 compares the measurements of Zuiderweg et al. (2013) to the results produced in this thesis. Two factors should be noted regarding the way the data from Zuiderweg et al. (2013) has been treated and presented:

1. Zuiderweg et al. (2013) combusted CFC-12 to CO₂ for IRMS analysis, using the methodology detailed in Zuiderweg et al. (2011). This means that these authors are able to quote their $\delta_T(^{13}\text{C})$ measurements on the international ¹³C standard scale (VPDB). In this study, $\delta_T(^{13}\text{C})$ values were obtained by directly measuring fragment ions, for which there is no recognised international standard. In order to plot the data on the same axes, the measurements made by Zuiderweg et al. (2013) were adjusted to ensure that the measurements made on modern air agreed with those of this study. Since the best precision was achieved in the measurements on modern air (due to higher mole fractions), it is likely that the two studies will agree here. It should be noted that a bias between the two analytical systems cannot be ruled out at this stage (a series of measurements are currently being undertaken to determine whether the data sets are consistent).
2. Zuiderweg et al. (2013) calculated the 98 % confidence interval of the measurements at each depth and the mean of these values was then applied to all measurements (shown by the error bars in Figure 3.18A). It is unclear why this approach was taken, but perhaps the authors were assuming that the measurement uncertainty did not vary based on the sample's CFC-12 mole fraction. It is clear from the data presented in Zuiderweg et al. (2013) that this is not the case, since the oldest samples exhibit significantly worse than mean precision. In this way, most samples (those containing CFC-12 at close to contemporary levels) have slightly overestimated uncertainties and the samples at greatest depths have significantly underestimated uncertainties (particularly the sample at 69.4 m). In Figure 3.19, 1σ uncertainties were applied to each measurement, based on the repeated measurement values only.

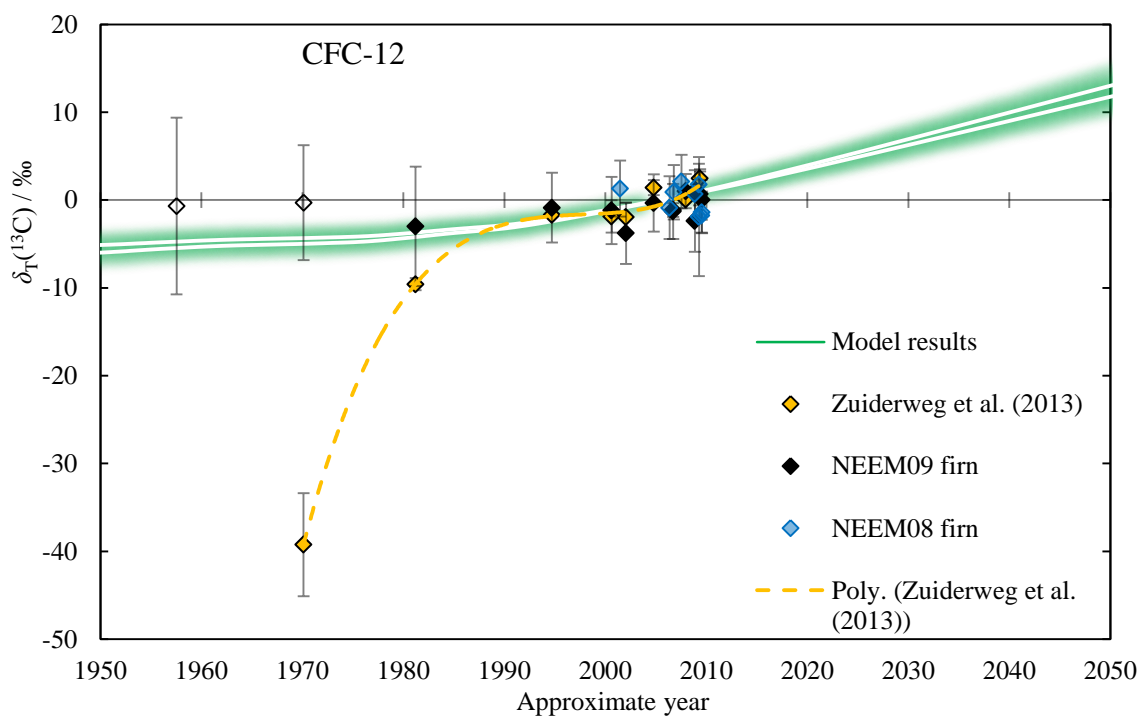


Figure 3.19. $\delta_T(^{13}\text{C})$ measurements on NEEM firm air collected in 2008 (blue diamonds) and 2009 (black diamonds) are presented. These measurements are compared to model predictions, as presented in Figure 3.16. $\delta_T(^{13}\text{C})$ measurements made by Zuiderweg et al. (2013) on NEEM 2009 firm air are also included (orange diamonds, black outline). The orange dashed line is a polynomial trend line, fitted to these data. Correct errors are not available for the Zuiderweg et al. (2013) measurements. Instead, partial 1σ analytical uncertainties are applied (discussed in the main text).

The NEEM 2009 firm air measurements made as part of this thesis can be directly compared to the measurements made by Zuiderweg et al. (2013) because the same samples were analysed in each case (Figure 3.19). As well as repeating the Zuiderweg et al. (2013) measurements, this study analysed a greater range of the available samples (e.g. the measurement at 1957). Within analytical uncertainties, this study finds no offset from zero between 1957 and 2009. Before 1981, measurements in this study disagree significantly with the large $\delta_T(^{13}\text{C})$ change reported by Zuiderweg et al. (2013) (Figures 3.18B and 3.19).

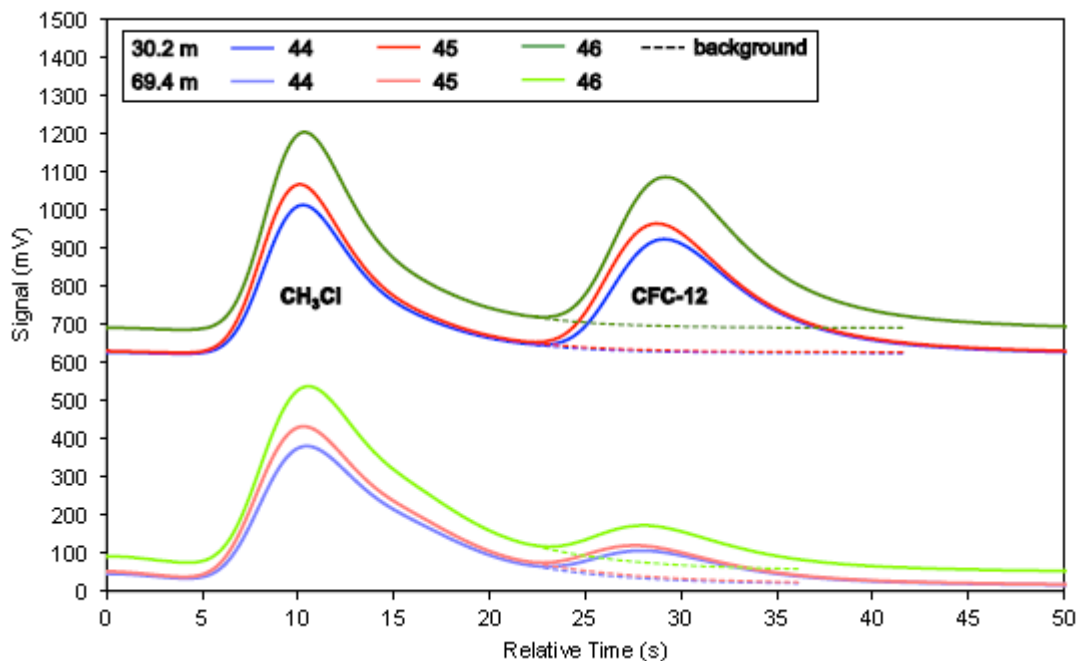


Figure 3.20. The chromatographic output from two NEEM firn samples have been manually offset for readability: 30.2 m (upper) and 69.4 m (lower). The proximity of CH₃Cl and CFC-12 peaks is displayed. The figure is taken from Zuiderweg et al. (2013).

Given the significant disagreement between the conclusions of this study and those of Zuiderweg et al. (2013), it is likely that one or both of the data sets are erroneous. The measurements presented in this thesis are not reported relative to an international isotope standard, whereas Zuiderweg et al. (2013) are able to report absolute $\delta(^{13}\text{C})$ values against VPDB. It is possible that the relationship between the measurements in this thesis and the VPDB scale is not linear (as mentioned previously, quantifying this relationship is an important task that is still outstanding). Additionally, two potential sources of error have been identified in the analytical system and data processing steps used by Zuiderweg et al. (2013):

1. It seems that a constant uncertainty was erroneously applied to all measurements (as discussed earlier in this section). Consequently, the magnitude of the model uncertainty envelope in the early part of the record is significantly underestimated.

2. The methyl chloride (CH_3Cl) and CFC-12 peaks partially co-elute on the column used by Zuiderweg et al. (2013) (Figure 3.20). This interference will affect the shape of the CFC-12 peak and hence the delta value calculated. This effect will be particularly significant in the oldest samples which have the smallest CFC-12 peaks. A dilution series was analysed by Zuiderweg et al. (2013) which confirmed the linearity of their system for a large range of CFC-12 peaks (including the peaks produced by their oldest sample). In these dilutions, the CH_3Cl peak was reduced by the same factor as CFC-12. However, in the deepest firm samples presented, the CH_3Cl peak is proportionally much larger than that of CFC-12 (CH_3Cl levels remain relatively constant into the middle of the 20th century, whereas CFC-12 levels decline sharply). This means that the linearity tests do not fully simulate effects in the firm samples.

The proposed effect of the CH_3Cl peak (as stated above) is qualitatively supported by an appraisal of the analytical uncertainties achieved in this thesis, compared to Zuiderweg et al. (2013) (Table 3.8). In this thesis, the analytical uncertainties are relatively uniform across all samples, with a slight increase in the three deepest samples (66.8, 69.4 and 71.9 m, which contain the lowest mole fractions). The analytical uncertainties achieved by Zuiderweg et al. (2013) follow a similar pattern, although the increase in uncertainty in their deepest sample (69.4 m) is much more pronounced. This greater than expected increased uncertainty could be caused by the observed interference from the CH_3Cl peak as CFC-12 mole fractions decrease.

Table 3.8. A comparison between the analytical uncertainties achieved in this thesis and by Zuiderweg et al. (2013) from measurements of $\delta_T(^{13}\text{C})$, CFC-12) on NEEM 2009 firn air. Correct errors are not available for the Zuiderweg et al. (2013) measurements. Instead, partial 1σ analytical uncertainties are applied (discussed in the main text).

Depth / m	CFC-12 mole fraction / pmol mol ⁻¹	$\delta_T(^{13}\text{C})$ uncertainty from this thesis / ‰	Partial $\delta_T(^{13}\text{C})$ uncertainties from Zuiderweg et al. (2013) / ‰
0	534.0	2.3	
10.5	536.8	2.8	0.8
20.4	537.9	3.5	0.4
30.2	542.3	2.0	0.1
39.2	544.1	3.1	0.8
50.7	543.3	3.3	0.8
60.3	531.2	3.5	1.6
62.0	526.7	3.8	1.8
63.8	463.2	4.0	0.7
66.8	286.5	6.8	0.7
69.4	133.5	6.6	5.9
71.9	53.6	10.1	

3.2.4 Summary

- The carbon isotope dependence of the photolysis sink reaction in CFC-11 and CFC-12 (Zuiderweg et al., 2012) and an assumed constant source $\delta(^{13}\text{C})$ value were used to reconstruct the expected long-term changes in their tropospheric carbon isotope signatures.
- Firn air samples from NEEM (Greenland) have been used to infer an atmospheric history of carbon isotopes in CFC-11, CFC-12 and CFC-113, covering the last 55,

50 and 20 years, respectively. These include the first measurements of $\delta_T(^{13}\text{C})$ in CFC-11 and CFC-113.

- The predicted $\delta_T(^{13}\text{C})$ trends in CFC-11 and CFC-12 are small due to the long atmospheric lifetimes of the species and can largely be accounted for in the tropospheric measurements. Based on this, these new measurements do not support a large change in the emissions carbon isotope composition of CFC-11 or CFC-12. Without information regarding the carbon isotope dependence of CFC-113 sink reactions and further measurements to extend the CFC-113 time series, it is impossible to infer the emissions carbon isotope history of this species.
- These measurements were made following a successful methodological development process. The 1σ analytical uncertainty for $\delta_T(^{13}\text{C})$ measurements of modern samples (1995 – 2010) was improved by 67 % (CFC-11), 71 % (CFC-12) and 79 % (CFC-113).
- These measurements represent a significant advancement in the approach used to measure $\delta(^{13}\text{C})$ in trace gases (pmol mol^{-1} level) in a few hundred millilitres of air. Previous studies have required tens to hundreds of litres of air to achieve this. These techniques can now be used to extend this pool of isotopic information to new sample sources and new gases. For example, the $\delta(^{13}\text{C})$ analysis of CFC-11, CFC-12 and CFC-113 in stratospheric samples would better constrain their global isotope budgets.
- The conclusions of this study regarding the carbon isotope history of CFC-12 differ significantly from those of Zuiderweg et al. (2013). Potential sources of error in the previously published measurements have been highlighted.

Chapter 4: Carbonyl sulphide (COS) in ice and firn

This chapter focuses on measurements of carbonyl sulphide (COS) in firn and ice core air. COS is currently the most abundant sulphur-containing trace gas in the atmosphere, at approximately $500 \text{ pmol mol}^{-1}$. It acts as a precursor for stratospheric sulphate aerosols, which facilitate the destruction of ozone. COS has a large number of natural and anthropogenic sources and sinks, making its budget difficult to constrain. Since the 1970s, studies have attempted to characterise it over seasonal to centennial timescales. More detail can be found in Section 1.4.

4.1 Antarctic and Greenland ice cores

Measurements of COS in air from ice cores have revealed a relatively consistent level of approximately $350 \text{ pmol mol}^{-1}$ over the last 2000 years of the pre-industrial era (Aydin et al., 2002 and 2008; Montzka et al., 2004). The only significant deviation from this natural background level appears to have been during the 1600s, when the atmospheric abundance is reported to have increased to a maximum of approximately $375 \text{ pmol mol}^{-1}$ (Aydin et al., 2008). This finding was the main motivation for the work presented in this section. By producing a continuous, high precision record over this period, this study aimed to confirm or refute this positive excursion. Further details can be found in Section 1.4.3.

Separate studies have measured a decrease in CO_2 which coincides with this COS increase (Etheridge et al., 1996; Siegenthaler et al., 2005; MacFarling Meure et al., 2006; Frank et al., 2010; Mitchell et al., 2011; Ahn et al., 2012). As discussed in Section 1.4.4, it has been suggested that measurements of natural COS levels can be used to track terrestrial Gross Primary Production (GPP), due to the link between the uptake of CO_2 and COS by terrestrial vegetation (e.g. Blonquist et al., 2011). By also measuring CO_2 and $\delta(^{13}\text{C}, \text{CO}_2)$ in the extracted ice core air, this thesis aims to provide the first record of COS and CO_2 from a single ice core and using only one sample for each set of measurements. Additionally, the $\delta(^{13}\text{C}, \text{CO}_2)$ measurements should indicate whether COS mole fractions can be used as a proxy for terrestrial GPP (providing information regarding the state of the carbon cycle during this period).

4.1.1 Research objectives

- Extract air from Antarctic ice cores with gas ages between 1089 and 1953 AD at the CSIRO Marine and Atmospheric Research (CMAR) laboratories.
- From each extraction, COS will be measured at UEA and CO₂ and $\delta(^{13}\text{C}, \text{CO}_2)$ at CMAR, providing a high precision, continuous record.
- From this, the reported peak in COS during the 1600s could be verified or refuted and the link between COS and the carbon cycle in this period will be investigated.

4.1.2 Methodology

Chapter 2 provides details regarding the methodological approach used in this work. Section 2.1 describes the trace gas analysis system at UEA and Section 2.3 describes the ice core extraction system at CMAR.

The GC-MS inlet system (Figure 2.1, Chapter 2) was modified to allow the analysis of samples received from CMAR. An extra piece was added which could join, through a clamp and an aluminium O-ring, to the CMAR sample. This addition was made, rather than modifying the existing system, because firn samples were also being analysed during this measurement period. These firn samples required the original inlet set-up and changing between systems was not feasible. The attachment was positioned after the Mg(ClO₄)₂ water trap, making the instrument vulnerable to the effects of wet samples (e.g. chromatographic distortions). To mitigate these effects, water vapour in the CMAR samples was frozen out by immersion of the sample traps in ethanol, cooled to -25 °C in the laboratory freezer room. A temperature of -25 °C was used to ensure that as much water was prevented from entering the GC oven as possible, without removing species of interest.

4.1.2.1 The sample cycle

A variety of ice core samples were used in this work mostly sourced in Antarctica, with supplementary samples provided by the North Greenland Eemian Ice Drilling Project (NEEM) (Table 4.1). Samples from the British Antarctic Survey (BAS) core at Dronning Maud Land (DML) and from NEEM were selected, cut and packed at BAS in Cambridge (UK). Their air ages ranged from 1089 – 1953 AD, with the highest concentration of samples in the 1600s (the method for determining air ages is outlined in Section 2.3.1.1).

Freezer containers were used to transport these samples from the UK to Australia because soluble gases such as CO₂ are vulnerable to contamination effects from partial melting. The samples were shipped in a box with ‘vacuum insulation panels’ and surrounded by ‘-23 °C eutectic gel packs’ which acted as further insulation. A temperature logger was also included in the shipment which recorded a value every 20 minutes, providing a temperature history of the samples during transit. Figure 4.1 shows that the temperature increased steadily over the 6 day transit from -25 to -10 °C.

Table 4.1. The samples used in this study came from several drilling sites: NEEM (Rasmussen et al., 2013), DML (Hofstede et al., 2004), DE08 (Etheridge et al., 1992) and DSS (Rubino et al., 2013). The surface elevation at DSS is not specified, but is similar to the DE08 site.

Site (drill date)	Location	Surface elevation / m	Accumulation rate / kg m ⁻² yr ⁻¹	Total core depth / m	Number of samples analysed
NEEM (2008-2010)	77°27' N, 51°04' W	2479	202	2540	7
DML (BAS) (1998)	77°02' S, 10°30' W	2176	71	121.7	17
DE08 (1987)	66°43' S, 113°12' E	1250	1160	234	4
DSS (1988-1993)	66°46' S, 112°48' E	-	600	772	2

This BAS/UEA ice was supplemented with samples from the DE08 (Law Dome east) and DSS (Law Dome south-southwest) cores, drilled by CSIRO (Table 4.1; Figure 4.2). This thesis will refer to the Dronning Maud Land ice samples as ‘DML (BAS)’, to distinguish them from the much deeper EPICA DML drilling project at the same site.

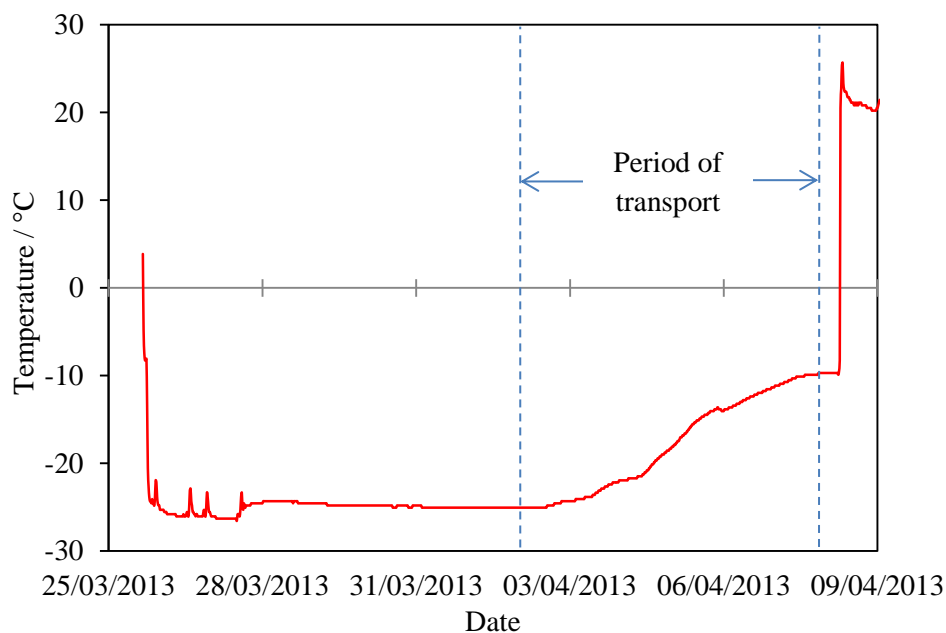


Figure 4.1. A record of the internal temperature of the shipping container used to transport ice from the UK to Australia.

At CMAR, an analysis cycle was adopted to extract and measure the air in the most efficient way possible. Several factors limited the effectiveness of this system. The major issue was that the trace gas measurements took place in the UK (because an AutoSpec instrument was not available at CMAR). This meant that for a given sample trap there was a minimum period of about two weeks between consecutive extractions. Further limitations regarding the number of extractions per day (4 – 5), and the number of sample traps available (10), allowed for a maximum measurement output of 5 per week. As well as this, the sample size limited the number of measurements possible, so maximising ice volume was crucial.

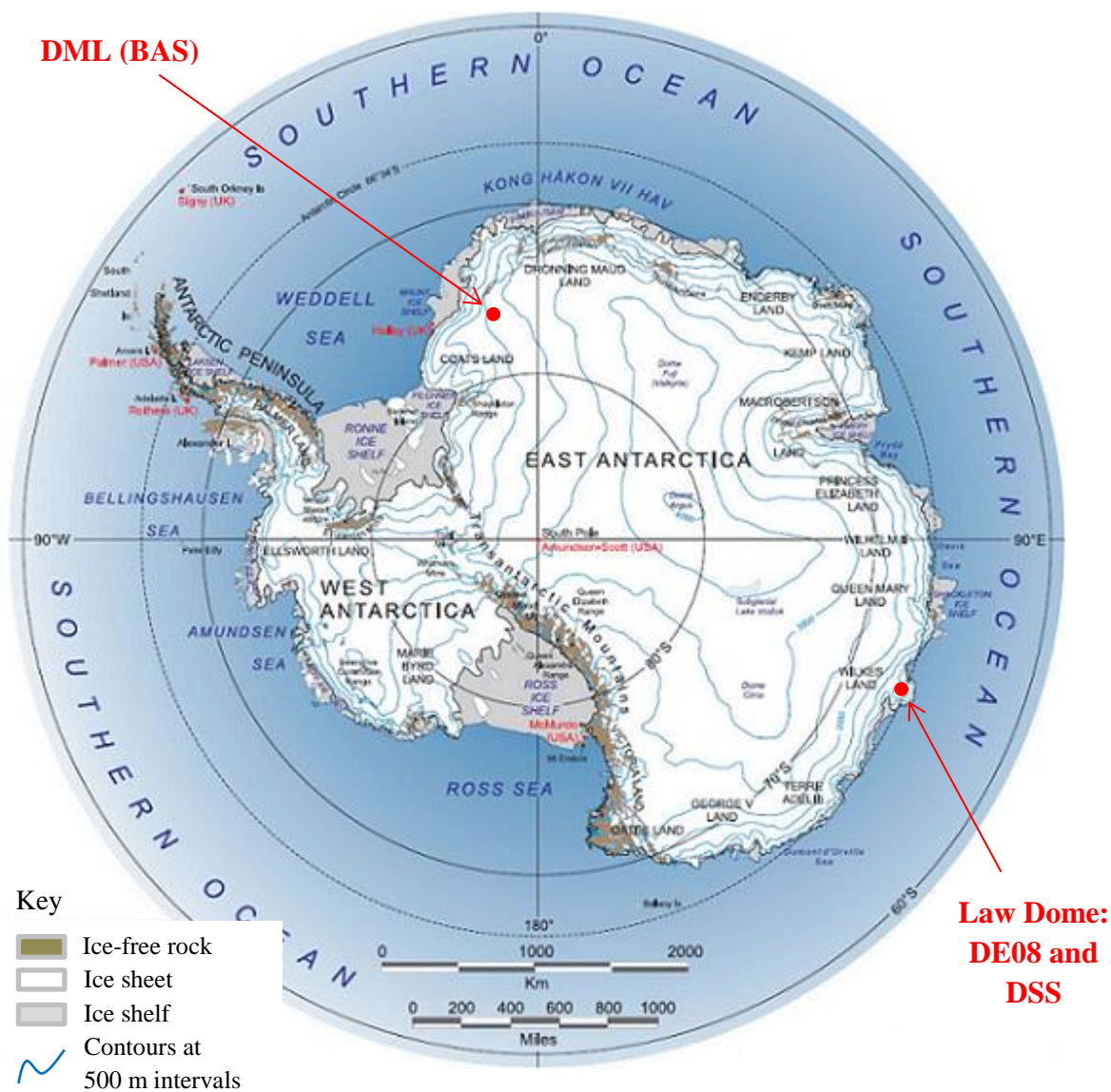


Figure 4.2. The images are taken from the NEEM ice core drilling project (right) and the Landsat Image Mosaic of Antarctica (LIMA) Project (above). The locations of several research stations and drilling sites are shown, including the sites from which our samples originated (NEEM, DML (BAS), DE08 and DSS).

4.1.3 Results and discussion

4.1.3.1 System tests

Before extractions began, a series of tests were conducted to assess the system's suitability to the planned measurement regime. These tests are detailed in Table 4.2 and discussed in this section.

Table 4.2. Details of the types of samples analysed during the period of system testing, before performing the planned air extractions from ice cores at CMAR.

Test type	Description
Mock extractions	These tests follow the extraction procedure detailed in Section 2.3.2 (Chapter 2), with only slight adjustments. For example, if the ice is not to be grated, the grater vessel is attached to the shaker and left for 10 minutes, without being shaken. For the purposes of these tests, either bubble-free ice (BFI: grated or ungrated) or no ice was used to replace the ice sample. By injecting gas (typically firm air) into the grater vessel immediately before shaking, a 'real' extraction is simulated most closely.
"No gas" blanks	"No gas" blanks were produced in the same way as mock extraction samples, with the air injection step omitted. BFI was again used in these tests, grated or ungrated. As detailed in Section 2.1.1.3 (Chapter 2), the UEA system blank is quantified almost daily. These "no gas" tests were valuable because they allowed the CMAR system blank to be quantified. At UEA, research grade helium was used to flush the CMAR sample traps, forcing any gas present into the GC-MS for analysis.
Ice core samples	A small number of 'real' ice core samples were selected for extraction and analysis during this period. Samples were selected using the following criteria: 1) 20 th century samples were selected in an attempt to overlap with and compare to firm air data; 2) samples of similar air ages were selected to give a measure of the extraction and analysis procedure repeatability.

Typically, pressure sensors are used to assess the integrity of an extraction line. For example, a significant leak can be recognised if a pump is not achieving a low enough vacuum, or if the pressure of a space under static vacuum rises. When measuring pre-industrial air from ice cores, an additional means of making this kind of assessment is available. As described previously, the GC-MS AutoSpec instrument at UEA makes high precision measurements of a wide range of trace level compounds. This means that if an air sample from the 1600s contains anthropogenic compounds that did not exist until the 20th century (e.g. SF₆), it must have been contaminated by modern air. Whilst pressure sensors are generally the best way to identify leaks in an extraction system, the sample could already be contaminated (e.g. through deformation processes in the ice or during drilling and transportation). This range of potential issues makes the measurement of anthropogenic gases a valuable quality assurance step.

“No gas” blanks were used to test the integrity of the CMAR system (Table 4.2). It was found that the CMAR system does not add significantly to the UEA COS blank (UANs 601373 and 601377, Table 4.3). As well as this, SF₆ measurements in firn air during mock extractions showed excellent agreement, again suggesting that the samples are not contaminated by the CMAR system (UANs 601366 – 601369 and 601374 - 601376, Table 4.4). In these mock extractions the agreement shown is less good for COS, with mole fractions slightly above those of previous measurements (UANs 601366 – 601369 and 601374 - 601376, Table 4.3). Due to the small sample size and lack of repeats in ice core measurements, significantly worse precision is expected compared to firn air measurements. For example, Aydin et al. (2008) present an average 1σ uncertainty of ± 15 pmol mol⁻¹ in ice core air and ± 4.3 pmol mol⁻¹ in firn air. Considering this, if uncertainties of ± 15 pmol mol⁻¹ were included for the test values, 5 out of 7 tests would agree within 1σ .

It was suspected that COS concentrations in the UEA laboratory standard had drifted since the original firn sample analysis in 2009. This seemed like a reasonable assumption given the excellent blank test results, and the fact that all of the mock extractions produced measurements higher than expected (rather than a more irregular distribution). This meant that, by taking into account the assumed calibration offset, all values were likely to agree, within 1σ uncertainties.

Table 4.3. A summary of the COS measurements made during the system tests conducted before the ice extraction period began. The unique analysis number (UAN) is given to identify each test (these numbers are used in the main text). Lines are highlighted according to the gas used in each test (firn air samples from the NEEEM 2008 field campaign). In “no gas” blanks, the ‘COS mole fraction’ is the UEA system blank on the day of analysis, which is compared to the ‘COS mole fraction measured in test’. Uncertainties are not shown when a measured value is obtained from a single analysis only.

Purpose of tests	UAN	Mass of ice / g	Number of pieces	Grated?	Sample ID of gas used for test	COS mole fraction / pmol mol ⁻¹	1 σ uncertainty / pmol mol ⁻¹	COS mole fraction measured in test / pmol mol ⁻¹	Difference / pmol mol ⁻¹
	601366	0	0	No ice	SC1242	543	14	557	14
	601367	0	0	No ice	SC1241	486	9	505	19
	601368	0	0	No ice	SC1159	559	16	571	12
Testing before ice extraction period	601369	129	1	Ungrated	SC1166	635	13	697	63
	601373	0	0	No ice	“No gas”	1.5	-	0.6	-0.9
	601374	0	0	No ice	SC1166	635	13	647	12
	601375	91	1	Ungrated	SC1166	635	13	662	27
	601376	91	1	Grated	SC1166	635	13	719	84
	601377	145	1	Grated	“No gas”	0.3	-	1.6	1.3

Table 4.4. A summary of the SF₆ measurements made during the system tests conducted as quality assurance during the period of system testing. The unique analysis number (UAN) and highlighting are used as described in Table 4.3. A description of the “no gas” blanks and details regarding the ice used in these tests are described in Table 4.2. UANs 601366 – 601369 were conducted using Kel-F stem tips and UANs 601373 – 601377 with Stellite stem tips. Uncertainties are not shown when a measured value is obtained from a single analysis only.

UAN	Sample ID of gas used for test	SF ₆ mole fraction / pmol mol ⁻¹	1σ uncertainty / pmol mol ⁻¹	SF ₆ mole fraction measured in test / pmol mol ⁻¹	Difference / pmol mol ⁻¹
601366	SC1242	4.5	0.07	4.4	-0.06
601367	SC1241	0.1	0.00	0.1	0.00
601368	SC1159	0.3	0.00	0.3	-0.02
601369	SC1166	4.0	0.04	4.1	0.03
601373	"No gas"	0.0	-	0.0	0.00
601374	SC1166	4.0	0.04	4.0	-0.03
601375	SC1166	4.0	0.04	4.0	0.01
601376	SC1166	4.0	0.04	4.1	0.05
601377	"No gas"	0.0	-	0.0	0.00

Table 4.5. A summary of the CFC-12 measurements made during the system tests conducted as quality assurance during the period of system testing. As described in the caption for Table 4.4.

UAN	Sample ID of gas used for test	CFC-12 mole fraction / pmol mol ⁻¹	1σ uncertainty / pmol mol ⁻¹	CFC-12 mole fraction measured in test / pmol mol ⁻¹	Difference / pmol mol ⁻¹
601366	SC1242	536	3	546	9
601367	SC1241	47	1	71	24
601368	SC1159	110	1	137	26
601369	SC1166	520	7	544	24
601373	"No gas"	0	-	0	0
601374	SC1166	520	7	518	-2
601375	SC1166	520	7	517	-3
601376	SC1166	520	7	521	1
601377	"No gas"	0	-	0	0

In addition to SF₆, CFCs were used as leak indicators since they are entirely anthropogenic in origin. Elevated levels of these compounds would indicate that modern air has contaminated the ice core air during the sample collection, transport or extraction. CFC-12 has previously been used in this capacity (Aydin et al., 2007). CFC-11, CFC-12 and CFC-113 were measured during testing and found to be highly variable and, in general, significantly above expected levels. Given the strong evidence for a leak-tight system (“no gas” tests), it was unlikely that entrainment of laboratory air was the cause, suggesting that an internal source existed. The most obvious potential sources were the traps’ stem tips, which contain Kel-F (a chlorofluoropolymer). It is normal practice at UEA to use only stainless steel components in extraction lines leading to trace gas analysis. However, testing at CMAR has shown that stainless steel seals can produce CH₄, which is a target species in their system. Copper tips would not release CFCs, but they have a tendency to degrade with time which does not allow the fine adjustments necessary to control the flow into instruments at CMAR. Stellite (a cobalt-based alloy) was identified as having the best potential for these measurements and was used to replace the Kel-F stem tips. After changing to Stellite stem tips, the test samples showed good agreement with measured CFC-12 levels (UANs 601374 – 601376, Table 4.5), although CFC-11 and CFC-113 remained elevated. (Information used to determine the best replacement material was obtained through personal communication with Dr. David Etheridge, Dr. Mauro Rubino and Prof. Bill Sturges.)

Aydin et al. (2007) found that measuring CFC-12 in each ice core sample was sufficient to identify modern air contamination. Since the CMAR-UEA system showed good results for both SF₆ and CFC-12, it was decided that together, these species would be adequate to act in this capacity. The elevated levels of CFC-11 and CFC-113 meant that they could not be used alongside SF₆ and CFC-12, but this was not considered a limitation. The source of this excess CFC-11 and CFC-113 is currently unknown and time constraints prevented further investigations.

A suite of measurements were made at CMAR immediately following an extraction. Depending on the amount of air available, CO₂, δ(¹³C, CO₂), CH₄, CO and N₂O were measured. CO₂ and CH₄ were always measured and since their atmospheric abundances have increased dramatically over the past century, these measurements act as a further test of sample quality. Elevated levels of these gases indicate ingress of modern air, as in the cases of CFC-12 and SF₆.

Table 4.6. ‘Real’ test extractions from DE08 ice. Samples were cut from a single bag of ice, to ensure any pre-extraction processes affected both identically. Adjacent samples were cut to give the same air ages.

Depth / m	Air age / years AD	COS / pmol mol ⁻¹
180.50 – 180.69	1886	404
180.69 – 180.89	1886	398

Table 4.6 gives details of the two ‘real’ extractions performed during the testing period. These samples were cut from adjacent pieces of ice in a single bag, giving the same air age and ensuring that any drilling, storage and transport effects were consistent. In this way, these samples provided a measure of extraction accuracy and precision. The consistency shown is excellent, giving confidence in the system. A comparison between these values and previous measurements (Aydin et al., 2008) show the same positive offset seen in the mock extractions which was again put down to a COS drift in the UEA laboratory standard.

The low levels of contamination shown in “no gas” blanks were well within acceptable limits and the excellent reproducibility of SF₆ and CFC-12 values in mock extractions suggested that contamination from small leaks was not a factor. It was thought that a COS calibration offset was the cause of the slightly high COS values measured in the mock extractions. An inter-comparison of standards at UEA was planned to quantify the drift and make the necessary adjustments to absolute values. Overall, the tests suggested that good COS measurements could be made using this system.

4.1.3.2 Standard comparisons

The comparison of various UEA standards took place at the same time as the extracted samples were being analysed. This meant that the comparison results were not fully compiled until after the majority of the extractions had taken place.

The working standard (AAL-071170) was compared to two other standards (ALM-39753 and SX-0706077), all of which had been calibrated for their COS content at NOAA and had been previously measured in a similar exercise (May 2010). The ability to make a historical comparison is vital when assessing whether a drift has occurred.

Within 1σ analytical uncertainties, complete agreement was found between AAL-071170, ALM-39753 and SX-0706077 (Table 4.7). As described in Section 2.1, mole fractions in pmol mol^{-1} are obtained by measuring the ratio between two air samples and multiplying that number by a known factor (i.e. the mole fraction of one of the air samples) to give the mole fraction in the other sample. Since the ‘known factor’ is the mole fraction in AAL-071170, it is possible that the COS content of all three of these standards have simply drifted by the same factor, making their absolute values falsely consistent. This is unlikely to be the case here because SX-0706077 is contained in an electro-polished stainless steel cylinder, whereas both AAL-071170 and ALM-39753 are contained in an Aculife-treated aluminium cylinder. The variation in container type makes a synchronous drift unlikely.

This means that the agreement shown in Table 4.7 can be accepted in absolute as well as relative terms, indicating that the COS content of the working standard has not drifted. Therefore, the positive offset between measurements and expectations (e.g. Section 4.1.3.1) must have been caused by a different effect. At this point, it was unclear what the additional factor was. Section 4.1.3.4 explores this question in detail.

Table 4.7. The standard comparison results from COS measurements. All measurements were made relative to AAL-071170.

Standard ID	Measured COS (May 2010) / pmol mol^{-1}	Measured COS (April 2013) / pmol mol^{-1}
ALM-039753	497.1 ± 8.7	487.8 ± 6.2
SX-0706077	551.0 ± 9.7	548.7 ± 2.8

4.1.3.3 Extracted samples

Throughout the extraction period, testing continued in a quality assurance capacity (details of test types in Section 4.1.3.1). The results of this testing are presented below and discussed further in Section 4.1.3.4.

Quality assurance

As discussed in Section 4.1.3.1, the measurement of anthropogenic gases provided an assessment of sample and extraction integrity. In general, these results confirmed that the samples were free of contamination (Figures 4.3 and 4.4). This means that the ice was in good condition at the point of extraction and that the extraction-transport-analysis cycle did not compromise it. However, Figures 4.3 and 4.4 highlight some samples that have elevated levels of these gases, indicating the presence of modern air. Below the depth at which firn samples can be collected, air occluded in ice has been found to exhibit some open porosity, leading to ingress of younger air (Aydin et al., 2010). Aydin et al. (2007) measured non-zero levels of CFC-12 in some ice core samples from well below the firn-ice transition, but found that other trace species were not affected in a significant way. An adequate explanation for this inter-species variation is not provided. In this study, COS results from samples with elevated levels of either SF₆ or CFC-12 (or both) will be highlighted, but not discarded.

The measurements at CMAR were compared to spline curves fitted to existing records (Trudinger et al., 1999 and Rubino et al., 2013). In general, the samples that exhibit abnormal CO₂ and CH₄ results (CMAR measurements) also gave poor SF₆ and CFC-12 results (UEA measurements). All of the NEEM samples and two DML (BAS) samples were high in CO₂ (DML 6 and DML 9; sample details are compiled in Table 4.11, page 126). With the exception of two of the NEEM samples (NEEM 6 and NEEM 7, Table 4.11), these same extractions gave either high SF₆ values, high CFC-12 values, or both (Figures 4.3 and 4.4). Again, samples identified as suspect based on their CO₂ and CH₄ levels will be highlighted, but not discarded.

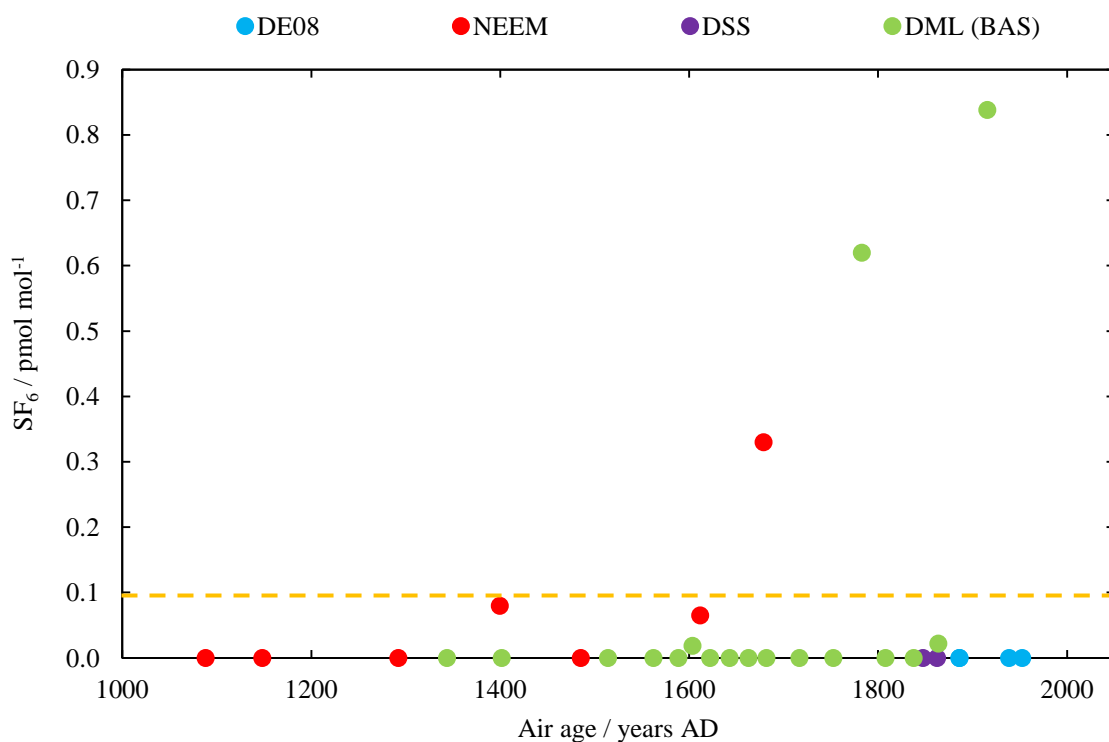


Figure 4.3. The measured SF₆ abundance in extracted ice samples. An orange dashed line is drawn at 0.1 pmol mol⁻¹ which is ~1.8 % of modern values (corresponding to the CFC-12 value used by Aydin et al. (2007) to indicate the potential ingress of modern air). Samples above this line are identified in subsequent plots using open symbols.

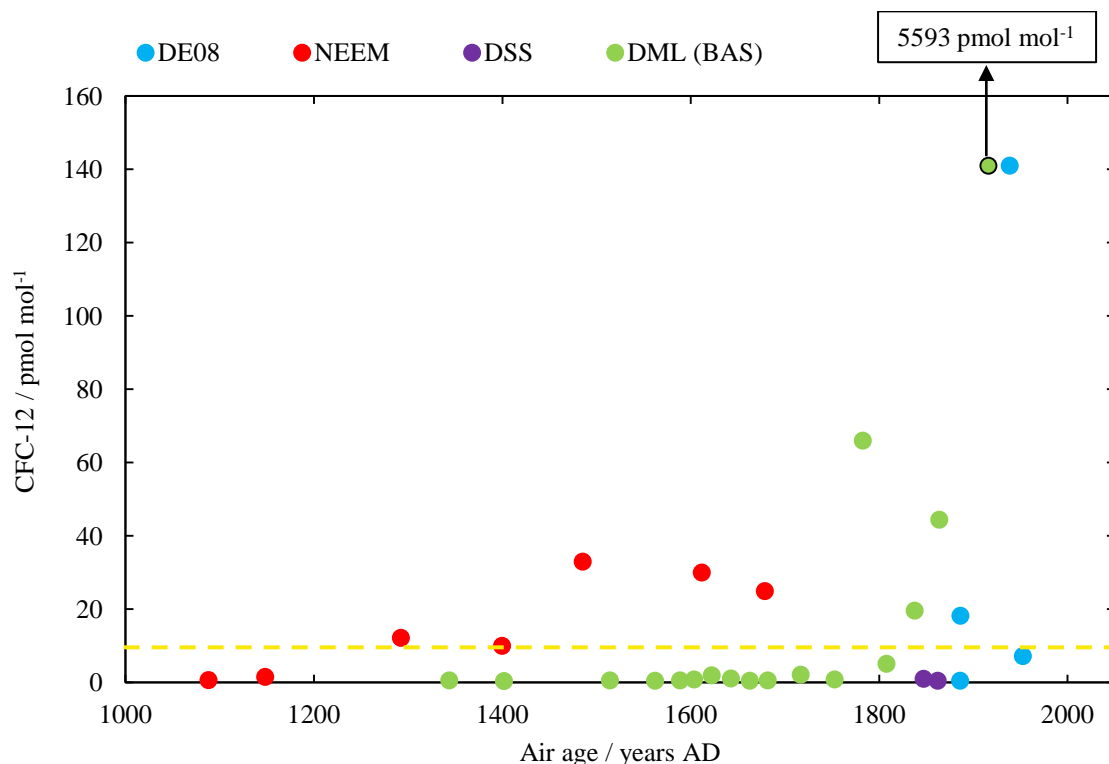


Figure 4.4. The measured CFC-12 abundance in extracted samples. An orange dashed line is drawn at 10 pmol mol⁻¹ which is the level used by Aydin et al. (2007) to indicate the potential ingress of modern air. Samples above this line are identified in subsequent plots using open symbols.

COS results

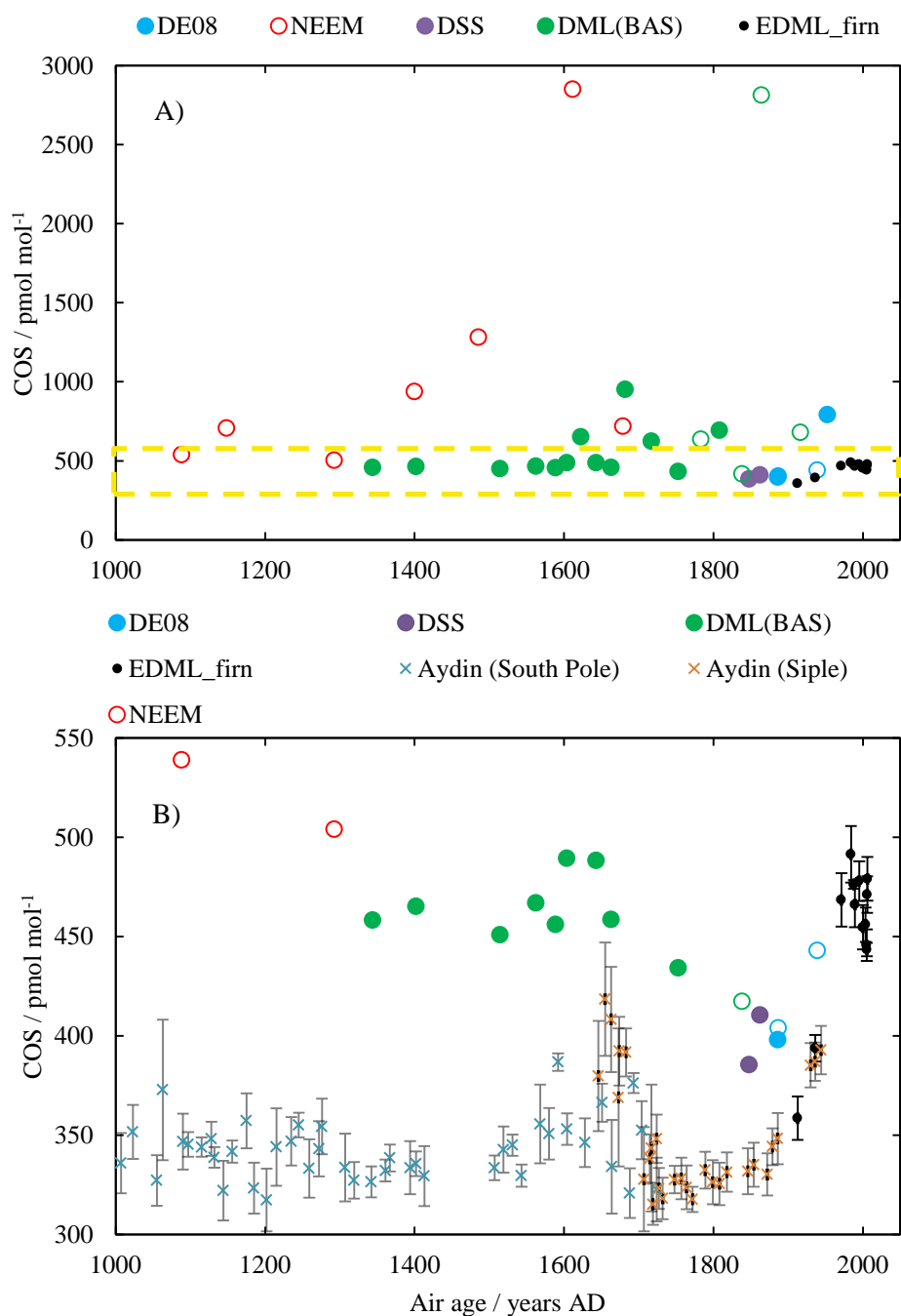


Figure 4.5. A) The measured COS abundance in extracted samples. B) As in A, but with adjusted axes to compare the lowest measurements made at UEA to ice core data from Aydin et al. (2008) and firn air measurements made at UEA (see Section 4.2). The orange dotted box in A indicates the axes values in B. In both, open symbols indicate that the sample is suspect based on CO₂, CH₄, SF₆ or CFC-12 measurements. Uncertainties are not shown when points represent single analyses only.

The first set of extractions were of NEEM ice core air and gave COS mole fractions much higher than expected, based on the results of previous studies (e.g. Aydin et al., 2008). All of the NEEM samples were measured above $500 \text{ pmol mol}^{-1}$ (approximate contemporary levels) and two were measured above 1 nmol mol^{-1} (Figure 4.5). Even taking into account the suspected calibration offset, these values are all higher than expected.

Measurements of COS in DML (BAS) ice core air show a pattern similar to NEEM measurements: values are generally higher than expected and there are also some extremely high values (Figure 4.5). All DML (BAS) samples had COS levels above $400 \text{ pmol mol}^{-1}$ (approximately 25 % higher than expected). As well as this, of the 17 samples, 7 were measured above ambient levels and 1 was above 2 nmol mol^{-1} . This level of variation was not expected.

Finally, a small number of DSS and DE08 samples were analysed. Only one sample contains COS above contemporary levels and no samples were measured in the nmol mol^{-1} range (Figure 4.5A). However, as seen in the NEEM and DML (BAS) measurements, these Antarctic samples contain higher COS than previous studies have reported (Figure 4.5B).

The measurements displayed in Figure 4.5 are consistently higher than expected, with a very large range of values. Since there has been no standard drift (Section 4.1.3.2) to account for the observed positive offset, it seems likely that an additional systematic factor is causing the apparent production of COS during extraction and/or transport (Section 4.1.3.4).

4.1.3.4 Sources of error and corrections

During the extraction period, it became apparent that several previously unidentified factors were affecting the measured COS levels. This section details the attempts made to characterise these factors and correct the results.

Quality assurance tests

Tables 4.8, 4.9 and 4.10 show the mole fractions measured in mock extractions performed during the extraction period of COS, SF_6 and CFC-12, respectively. One of these tests was

included with each set of samples (typically 3 – 4 extractions), in an attempt to quantify daily variations in the CMAR system.

Apart from one SF₆ value (UAN 601458), SF₆ and CFC-12 show good agreement with the original UEA measurements, suggesting that the system remains leak-tight (Tables 4.9 and 4.10). Contrary to this, COS is elevated to a greater degree than it was during testing. Several mock extractions contain COS mole fractions significantly above peak known levels, meaning that ingress of air cannot account for the measured values (Table 4.8). Since the COS content of the standard air has not drifted (Section 4.1.3.2), the observed offset is likely due to a systematic production of COS. This effect seems to have significantly worsened since the system was tested (Section 4.1.3.1).

Two “no gas” blanks were measured during the NEEM extractions, both yielding poor results for COS and CFC-12 (Tables 4.8 and 4.10). A sample trap at high pressure is unlikely to be compromised by a small leak because the prevailing movement of air will be outwards. This is not the case in “no gas” blank tests, where the trap is at significantly sub-atmospheric pressure. A good “no gas” test result provides information (i.e. that the trap and extraction line are leak-tight), whereas the cause of a poor result is very difficult to trace. Although “no gas” blanks initially gave excellent results, it was decided that these tests were unreliable in this situation and should be discontinued.

Table 4.8. A summary of the COS measurements made during the system tests conducted as quality assurance during the ice extraction period. The unique analysis number (UAN) and highlighting are used as described in Table 4.3. A description of the “no gas” blanks and details regarding the ice used in these tests are also described in Table 4.3. Uncertainties are not shown when a measured value is obtained from a single analysis only.

Purpose of tests	UAN	Mass of ice / g	Number of pieces	Grated?	Sample ID of gas used for test	COS mole fraction / pmol mol ⁻¹	1 σ uncertainty / pmol mol ⁻¹	COS mole fraction measured in test / pmol mol ⁻¹	Difference / pmol mol ⁻¹
	601396	49	1	Grated	SC1166	635	13	721	86
	601401	0	0	No ice	“No gas”	2.2	-	33	30
	601402	0	0	No ice	“No gas”	1.4	-	334	332
Quality assurance during ice extraction period	601406	445	1	Ungrated	SC1242	543	14	538	-5
	601415	489	1	Ungrated	SC1242	543	14	532	-11
	601424	81	1	Grated	SC1242	543	14	658	115
	601435	478	2	Grated	SC1242	543	14	531	-12
	601445	80	1	Ungrated	SC1095	555	8	579	24
	601458	440	1	Grated	SC1095	555	8	956	401

Tables 4.9. A summary of the SF₆ measurements made during the system tests conducted as quality assurance during the ice extraction period. The unique analysis number (UAN) and highlighting are used as described in Table 4.3. A description of the “no gas” blanks and details regarding the ice used in these tests are described in Table 4.2. Uncertainties are not shown when a measured value is obtained from a single analysis only.

UAN	Sample ID of gas used for test	SF ₆ mole fraction / pmol mol ⁻¹	1σ uncertainty / pmol mol ⁻¹	SF ₆ mole fraction measured in test / pmol mol ⁻¹	Difference / pmol mol ⁻¹
601396	SC1166	4.0	0.04	4.1	0.05
601401	"No gas"	0.0	-	0.1	0.07
601402	"No gas"	0.0	-	0.1	0.09
601406	SC1242	4.5	0.07	4.5	-0.01
601415	SC1242	4.5	0.07	4.5	-0.03
601424	SC1242	4.5	0.07	4.5	-0.05
601435	SC1242	4.5	0.07	4.4	-0.06
601445	SC1095	6.7	0.10	6.5	-0.16
601458	SC1095	6.7	0.10	5.7	-1.00

Table 4.10. A summary of the CFC-12 measurements made during the system tests conducted as quality assurance during the ice extraction period. As described in the caption for Table 4.9.

UAN	Sample ID of gas used for test	CFC-12 mole fraction / pmol mol ⁻¹	1σ uncertainty / pmol mol ⁻¹	CFC-12 mole fraction measured in test / pmol mol ⁻¹	Difference / pmol mol ⁻¹
601396	SC1166	520	7	511	-9
601401	"No gas"	0	-	65	65
601402	"No gas"	0	-	22	22
601406	SC1242	536	3	534	-2
601415	SC1242	536	3	533	-3
601424	SC1242	536	3	530	-6
601435	SC1242	536	3	534	-2
601445	SC1095	540	3	544	4
601458	SC1095	540	3	540	-1

COS measurements

During their analysis at UEA, it was observed that, in general, a large amount of water was included in the NEEM sample air. Characteristic chromatographic interferences of a wet sample were seen (deformation of the CFC-113 peak and all those following it). Also, after the sample had been entirely flushed out of the system, residual water vapour was present in the GC column for at least an hour after analysis. The GC oven was baked at 230 °C and the flow rate increased to 3 ml/min until the water level returned to normal. This showed that the water traps in the CMAR and UEA systems were not removing all of the water. Multiple sections of ice were grouped to create each NEEM ice sample because the available samples were typically thinner than from other ice cores. This means that, compared to the two samples extracted during testing (DE08 469 and DE08 471, Table 4.11), the surface area to volume ratio of the NEEM samples was much higher and they would have experienced a faster increase in temperature when moving from the -80 °C chest freezer to the -20 °C cold room. Consequently, the NEEM samples would have exhibited a higher sublimation rate. Additionally, the CH₃CCl₃ values measured at the UEA were highly variable, but generally lower than expected during testing. This is not a species of interest, except that as an anthropogenic gas it has the potential to act as another test of sample integrity. It was thought that the CMAR water trap was freezing out some of the CH₃CCl₃, leading to the variable and low values. For this reason, the trap temperature was increased to approximately -50 °C from -100 °C (Table 4.11). A -50 °C water trap has been successfully used by Dr. David Worton at UEA to remove water from ice core air extractions, suggesting that this temperature should be effective (information gained through personal communication with Prof. Bill Sturges). However, in this case it seems that the temperature increase reduced the trap's effectiveness, allowing large amounts of water to be included with the NEEM samples.

The CMAR trap was adjusted back to -100 °C for the extraction of DML (BAS), DSS and DE08 samples. These Antarctic samples were larger than those taken from NEEM, giving them a lower surface area to volume ratio and hence a lower sublimation rate. The chromatographic interferences due to the presence of water vapour noted during the analysis of NEEM samples were not seen again, suggesting that the Antarctic samples yielded drier air. However, all samples are elevated in COS to some degree, meaning that the production of COS persisted, even in the absence of excess water.

Table 4.11. Details of the ice core samples analysed. The UAN is the ‘unique analysis number’ given to each extraction at CMAR which is used for identification. Air age, water trap temperature, ice mass, measured COS mole fraction and the number of ice pieces in each sample are given.

UAN	Sample ID	Air age [AD]	CMAR water trap temperature / °C	Ice mass / g	Number of pieces	COS / pmol mol ⁻¹
601370	DE08 469	1886	-103	1285	1	404
601397	DE08 471	1886	-96	1283	1	398
601398	DE08 472	1953	-100	1132	1	793
601399	DE08 473	1939	-93	1264	1	443
601400	NEEM 1	1679	-98	698	7	719
601403	NEEM 3	1486	-50	943	7	1283
601404	NEEM 4	1400	-58	932	8	938
601405	NEEM 2	1612	-46	679	5	2851
601407	NEEM 5	1293	-98	742	8	504
601408	NEEM 6	1149	-97	723	9	707
601409	NEEM 7	1089	-96	740	6	539
601416	DML 1	1563	-93	733	2	467
601417	DML 2	1402	-87	726	2	465
601418	DML 3	1344	-90	782	4	458
601425	DML 4	1864	-90	663	3	2813
601426	DML 5	1682	-88	702	3	953
601427	DML 6	1783	-94	627	3	637
601432	DML 9	1916	-105	690	3	681
601433	DML 7	1838	-104	674	3	417
601434	DML 8	1515	-100	764	3	451
601442	DML 10	1808	-102	673	3	694
601443	DML 11	1753	-103	627	3	434
601444	DML 12	1717	-103	711	4	624
601455	DML 20	1663	-114	810	4	458
601456	DML 21	1589	-111	740	3	456
601457	DML 22	1623	-122	652	3	653
601460	DML 23	1643	-108	603	2	488
601461	DML 24	1604	-105	635	2	489
601459	DSS 31	1848	-109	950	2	385
601462	DSS 32	1863	-106	614	2	411

Storage tests

A series of storage tests were performed, in an attempt to quantify the systematic COS production. The objectives of these tests were:

- To confirm whether COS is being produced in the sample traps.
- To characterise this production in terms of variations due to sample moisture content and the differences between traps.

Dried air (a UEA laboratory standard, AAL-071170) was stored for up to 12 days in the sample traps. The air was then analysed on the AutoSpec and a comparison made with known trace gas levels in AAL-071170. Additionally, air collected on the RRS James Clark Ross research ship (JCR121) was stored and analysed in the same way. This air was collected at the ocean-atmosphere interface, meaning that its water saturation level was very high. In this way, the growth of COS was quantified in both a dry and wet sample.

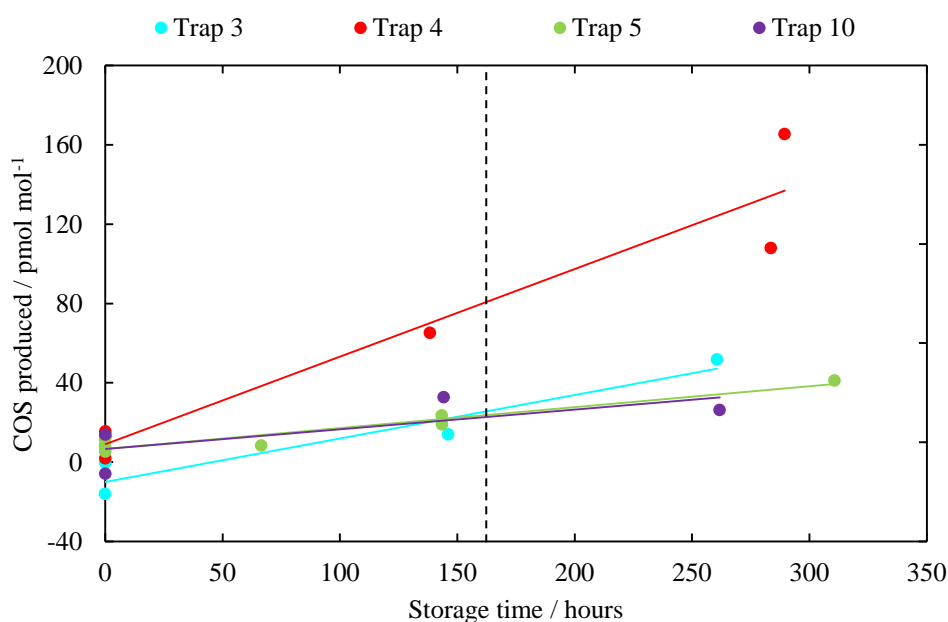


Figure 4.6. COS measurements in dried air storage tests, using a UEA laboratory standard (AAL-071170). Only selected traps are shown, although maximum and minimum values across all traps are represented. The vertical dashed line indicates the average time between CMAR extraction and UEA analysis (just under 7 days). Uncertainties are not shown because points represent single analyses only.

Figure 4.6 shows the linear COS increase associated with dry air storage in four of the sample traps. All traps exhibited COS production, but their individual rates of increase are highly variable. A COS increase of between 20 and 80 pmol mol^{-1} is expected when a dried sample is stored for just under 7 days (the average transport time between CMAR and UEA; dashed line, Figure 4.6).

Figure 4.7 shows how the same traps react to the storage of wet air. Again, all traps exhibited production and a large amount of variation is shown between traps. Over a similar period of storage the observed COS increases are much larger in wet air. This suggests that the presence of water does contribute to COS production in these sample traps.

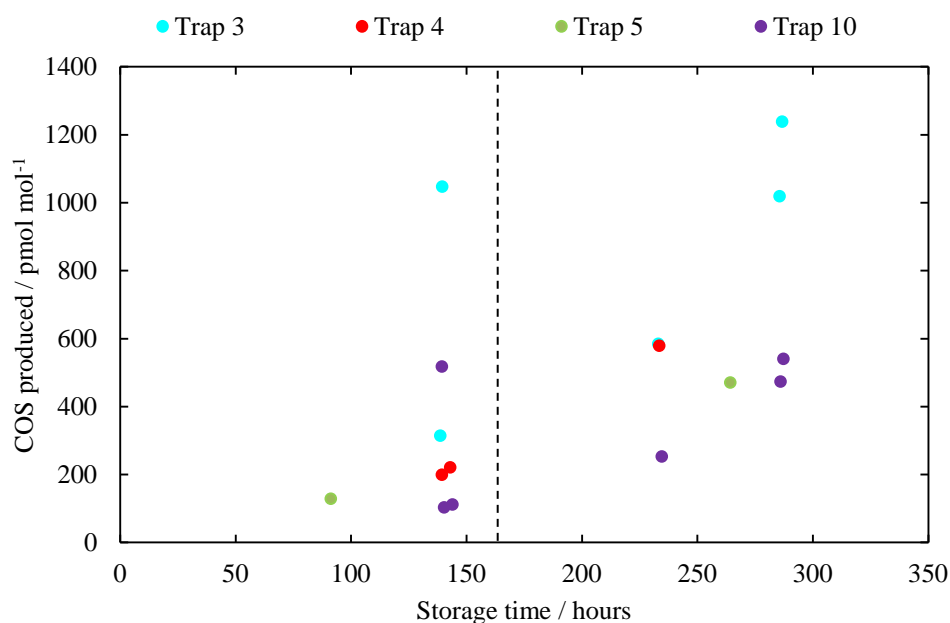


Figure 4.7. Wet air storage using a sample collected at the ocean-atmosphere interface from the RRS James Clark Ross (JCR121). Only selected traps are shown, although maximum and minimum values across all traps are represented. The vertical dashed line indicates the average time between CMAR extraction and UEA analysis (just under 7 days). Uncertainties are not shown because points represent single analyses only.

Analytical uncertainties have not been calculated because the limited amount of air available prevented repeat measurements. However, where separate storage periods of a similar length have been used, some measure of uncertainty can be established for individual traps. Using this method, some traps show good precision (e.g. dry air in trap 5 and wet air in trap 4), whereas others show poor precision (e.g. dry air in trap 4 and wet air in trap 3).

This study does not attempt to constrain a reaction mechanism to explain the observed in-situ COS production. However, the elements necessary to make up COS are all readily available. Oxygen is present in air and carbon and sulphur are contained in stainless steel (sulphur is sometimes added to stainless steel to aid the welding process, e.g. Fihey and Simoneau, 1982). Assuming that the production occurs through an interaction with the stainless steel surface, welds and other areas with large surface areas could increase the production rate. For example, Stedman et al. (1984) found that COS is produced through the oxidative decomposition of pyrite (FeS_2) in the presence of organic matter and water. This mechanism could be used to qualitatively explain the higher COS production in Northern Hemisphere samples. As inferred earlier in this section (under ‘*COS measurements*’), significantly more water was collected along with the NEEM sample air, compared to the Antarctic samples.

It is possible that the sample trap surface does not play a role in the observed COS production, although given the unique COS production behaviour of each trap, it is likely that the trap surface plays a significant role.

The results of these tests can be summarised:

- Both dried and wet air stored in these traps is subject to COS production.
- Each trap displays unique COS production behaviour.
- Wet air exhibits a much higher rate of COS production than dried air.

Limitations in the experimental design make more quantitative information difficult to produce. The amount of water present in the dried and wet air is not known. This means that a quantitative relationship between COS production and sample water content for each trap cannot be calculated. However, constraining this relationship would not enable corrections to be made to the ice core measurements because the water content of each ice core sample is not known and cannot be calculated retrospectively. Even if the storage tests

were performed on air of known water content, they could not be used to make wholesale corrections.

Factors affecting sample water content

Based on the assumption that the presence of water in the sample traps is the predominant cause of the observed COS production, three major variables have been identified which determine the amount of water present in each trap and the effect this will have on COS:

1. The surface area to volume ratio of the ice sample

This variable incorporates factors such as the initial ice mass, the number and shape of ice pieces and the presence of contaminants. A lower initial ice mass, a larger number of ice pieces and a lower concentration of contaminants will lead to a higher surface area to volume ratio and hence a faster sublimation rate.

2. The trap used

The storage tests showed significant differences in the behaviour of individual traps (Figures 4.6 and 4.7).

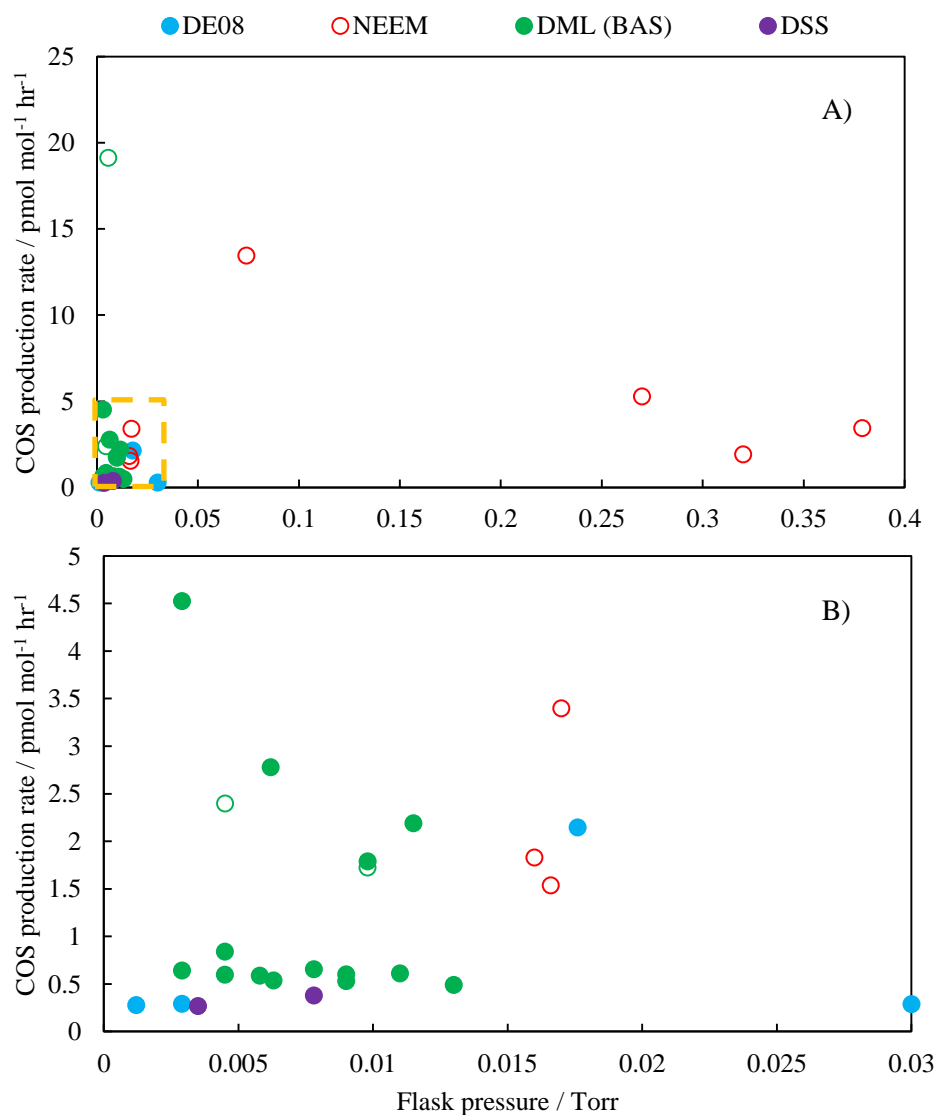
3. The extraction history of the trap

The extraction system and the sample traps have specific usage histories. Although the system was flushed with dried air and evacuated after each use, the amount of residual water after each measurement is unknown.

The above is not an exhaustive list; inconsistent results (e.g. some of the variability seen during storage tests, Figure 4.7) indicate that other factors are involved.

In an attempt to quantify the amount of water vapour contained in each ice core air sample, the link between the observed COS production rate and the extraction line pressure was investigated. After the ice sample has been sealed inside the grater vessel for 2 minutes, a pressure reading is taken. A small increase in pressure is expected (due to the release of water vapour from the sample surface), and a large increase is indicative of a leak in the grater. In a completely leak-tight system, the observed pressure increase could be used as a measure of the sublimation rate. NEEM extractions show significantly higher pressure readings than Antarctic samples, qualitatively supporting their high rates of COS production (Figure 4.8). However, overall there is a weak relationship between this pressure reading and the COS production rate (Figure 4.8). This poor fit is likely due to a number of factors (e.g. small leaks will diminish the accuracy of the reading). Also, at the

point of measurement, the sample is yet to be crushed which is the period of most rapid sublimation. This means that the extraction line pressure cannot be reliably used to estimate the amount of water vapour contained in each ice core air sample.



Corrected COS data

A simple means of fully accounting for the observed COS production does not exist. As a sensitivity study, an attempt was made to partially correct the data by accounting for the growth of COS in dried air (Figure 4.7). The time between extraction and COS analysis was used in conjunction with the observed growth rate in dried air to make ‘dried air corrections’. These corrected values are shown in Figure 4.9.

As described previously, analytical uncertainties are not available because there was insufficient air for repeat measurements. However, using the AutoSpec instrument, analysis of COS in firn air has achieved a mean 1σ analytical uncertainty of $\pm 8 \text{ pmol mol}^{-1}$. This level of precision relates to samples with a mean abundance of $500 \text{ pmol mol}^{-1}$ and no sample at less than $360 \text{ pmol mol}^{-1}$. Based on this, it was thought that the UEA analytical system would achieve similar precision to previous studies (e.g. Aydin et al., 2008). Given the additional uncertainty associated with the correction process, it seems reasonable to assume that the ice core measurements presented in this thesis have significantly larger uncertainties than the $\pm 15 \text{ pmol mol}^{-1}$ achieved by Aydin et al. (2008).

The corrected data (Figure 4.9B) are compared to previously published measurements (Aydin et al., 2008). All data points have been individually corrected, according to the trap used and their transport time. This downward shift improves the comparability to existing data sets, although a discrepancy remains in almost all points. The first measurements were made on the three DE08 samples with air ages in the late 19th and early 20th centuries. These extractions were performed during the system tests and the corrected values agree with Aydin’s data. This agreement suggests that, at this time, the system had not been contaminated by excess water. Extractions were then performed on NEEM, DML (BAS) and finally DSS samples. In general, the DML values are higher than expected, even after correction. This suggests that residual water from the wet NEEM extractions has contaminated the system and that dry air corrections are not sufficient to account for the COS growth. The DSS samples were extracted last, at which point some of the water from NEEM extractions may have dissipated, but it is difficult to draw conclusions from these data because a consistent pattern is absent.

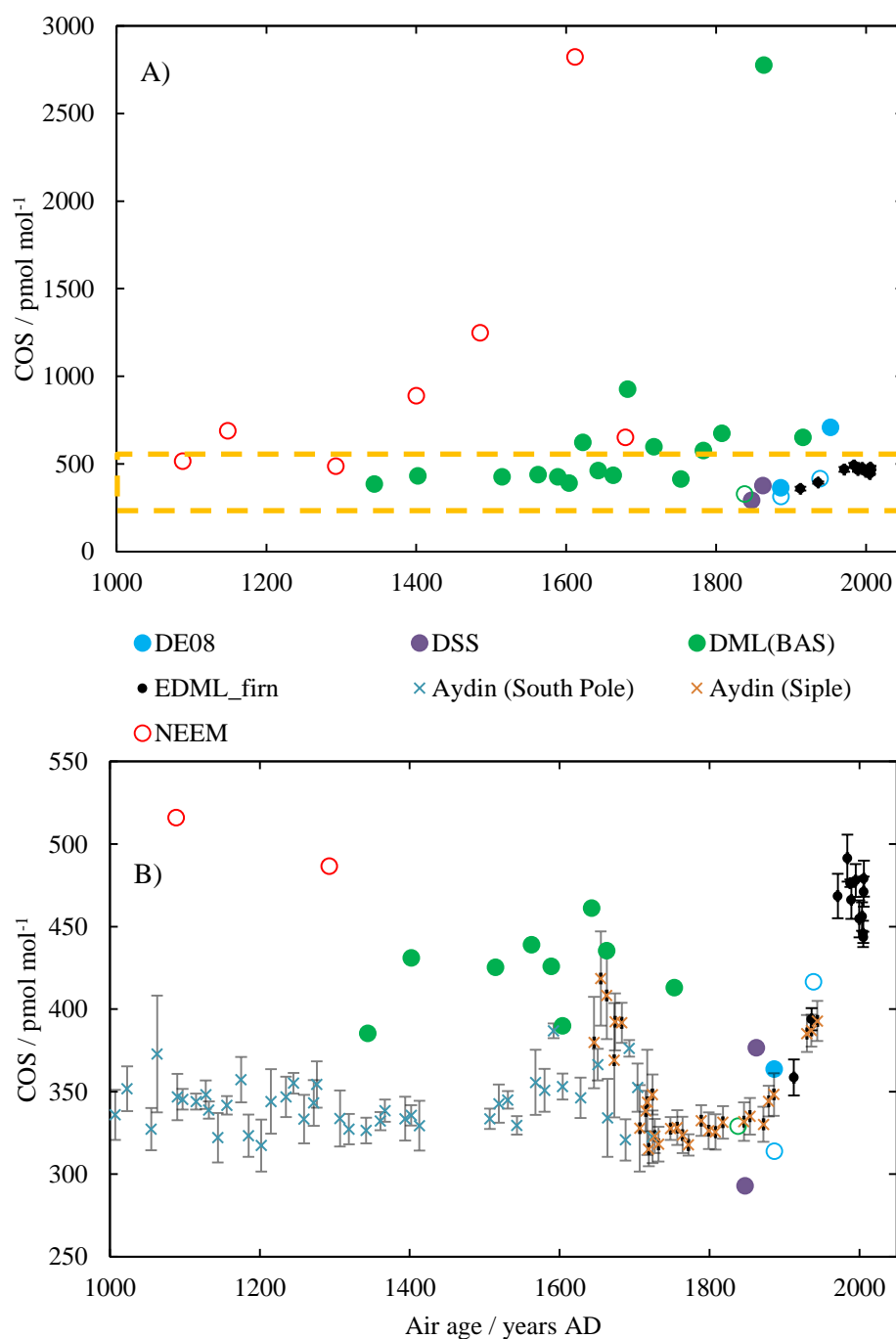


Figure 4.9. A) The corrected COS abundance measurements based on the COS production rates observed in individual traps using dried air. B) As in A, but with adjusted axes to compare the lowest measurements made at UEA to ice core data from Aydin et al. (2008) and firn air measurements made at UEA (see Section 4.2). The orange dashed box in A indicates the axes values in B. In both, open symbols indicate that the sample is suspect based on CO₂, CH₄, SF₆ or CFC-12 measurements. Uncertainties are not shown when points represent single analyses only.

At the lowest COS concentrations, the corrected measurements (Figure 4.9B) show greater variability than the uncorrected values (Figure 4.5B). The variability shown in Figure 4.9B is unlikely to be natural variation and could represent the additional uncertainty introduced by the correction.

It seems likely that the excess water released from the previously extracted NEEM ice samples was the main cause of the poor DML measurements. The agreement between corrected DE08 samples and previously published data suggest that the system was reasonably dry before the NEEM extractions were performed. After this, corrections became less effective due to the presence of water.

4.1.3.5 Gases measured at CMAR

Before being sent to UEA for trace gas analysis, the extracted air was analysed at CMAR for CO₂, CH₄ and CO (within 1 hour) and $\delta(^{13}\text{C}, \text{CO}_2)$ (within 12 hours). CMAR measurements of this sort have been previously reported (e.g. Etheridge et al., 1996; Francey et al., 1999; MacFarling Meure et al., 2006; Rubino et al., 2013). These high precision CO₂ and $\delta(^{13}\text{C}, \text{CO}_2)$ measurements have helped to constrain the global carbon cycle in modelling studies covering the last 2000 years (e.g. Trudinger et al., 1999 and 2005).

The DML (BAS) samples provided for this study were used to increase the CO₂ and $\delta(^{13}\text{C}, \text{CO}_2)$ measurement density in the 16th and 17th centuries to better constrain the $\delta(^{13}\text{C})$ increase and CO₂ decrease during this period (Figure 4.10). Rubino et al. (in preparation) report a 0.14 ‰ increase in $\delta(^{13}\text{C})$ and a 7 ppm decrease in CO₂ between 1502 and 1592 from these new records. A Kalman Filter Double Deconvolution Model (KFDD, Trudinger et al., 2002a and 2002b) was then used to determine the relative contributions of the terrestrial biosphere and the ocean to the observed changes in CO₂ and $\delta(^{13}\text{C})$. The terrestrial biosphere was found to be the main contributor in this case. Since respiration is more sensitive to temperature changes than photosynthesis (Trudinger et al., 1999), Rubino et al. (in preparation) argue that a decrease in global photosynthetic activity and respiration (due to a temperature decrease) is the most likely cause of the reported CO₂ and $\delta(^{13}\text{C})$ changes. This conclusion is supported by their use of a COS budget to test the effect of a 1 °C temperature decrease on the atmospheric abundance of COS (based on fluxes published by Berry et al., 2013). These authors found that this temperature change would have increased COS by 18 pmol mol⁻¹, which can qualitatively explain the positive COS excursion reported by Aydin et al. (2008) during the 1600s. This means that the CO₂

decrease and the $\delta(^{13}\text{C})$ and COS increases at this time can be qualitatively explained by a temperature-induced decrease in GPP and respiration.

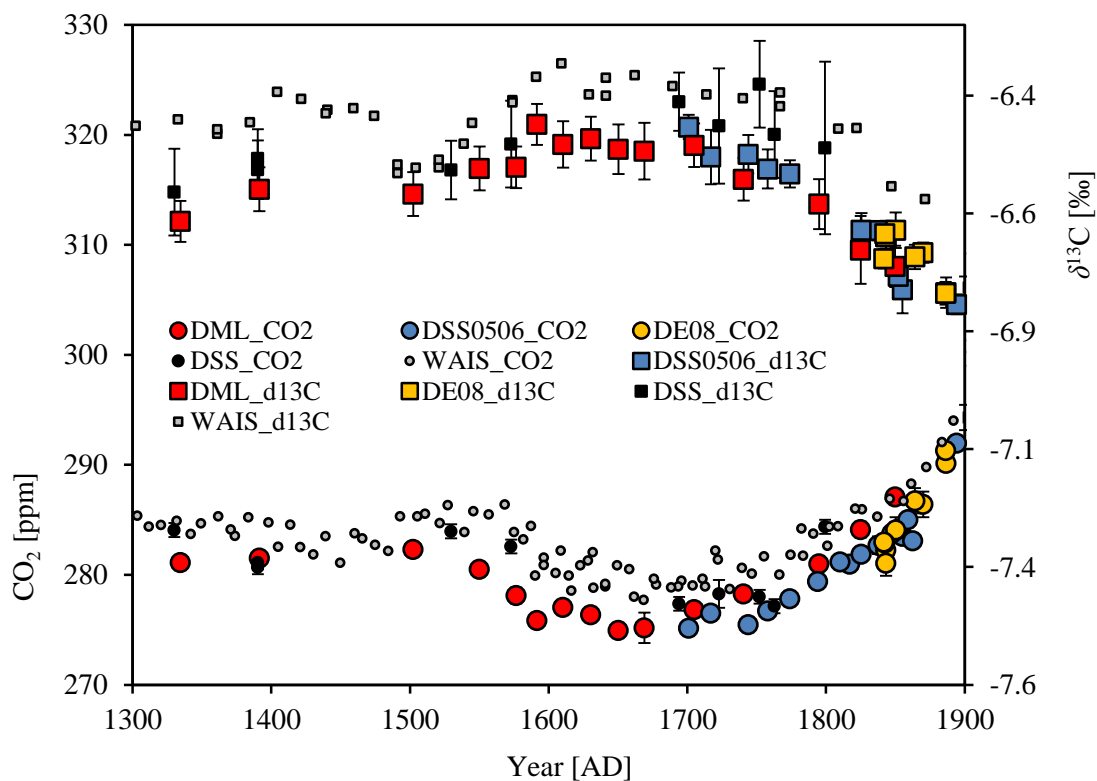


Figure 4.10. A record of CO_2 mole fractions and $\delta(^{13}\text{C}, \text{CO}_2)$ from various Antarctic ice cores (see legend). Error bars give an estimate of the 1σ analytical uncertainties (see Rubino et al., 2013 for details of the calculation). The mean errors were $0.5 \mu\text{mol mol}^{-1}$ and 0.05‰ . The figure was adapted from Rubino et al. (in preparation).

The high quality of these CO_2 and $\delta(^{13}\text{C}, \text{CO}_2)$ measurements provide evidence that the difficulties encountered in this project were confined to COS; other species were unaffected. From this, it can be deduced that the DML (BAS) ice core samples and the air extraction system were of high quality, with no sign of leaks in the extraction system. This assessment supports the view that the artificial COS growth occurred entirely post-

extraction and was related to the interior surface of the air sample traps, rather than the drilling and storage procedure.

4.1.4 Summary

- The CMAR laboratories in Australia were used to extract air from Northern and Southern Hemisphere ice core samples (NEEM, DE08, DML (BAS) and DSS). These samples were analysed for CO₂ and $\delta(^{13}\text{C}, \text{CO}_2)$ at CMAR and a range of trace gases at UEA (including COS). The results from a total of 30 samples have been presented in this thesis.
- The high quality CO₂, $\delta(^{13}\text{C}, \text{CO}_2)$, SF₆ and CFC-12 measurements show that the DML (BAS) ice core was not contaminated by ingress of modern air during its drilling, transport, storage, extraction and analysis.
- The AutoSpec instrument described in this thesis was used to measure COS (at an abundance of a few hundred pmol mol⁻¹), using a small amount of extracted air (approximately 30 ml).
- It is likely that COS was produced in the sample traps, post-extraction. Storage tests confirmed that the growth rate varies from trap to trap, likely due to small differences in their interior surfaces. The presence of water provoked a range of growth rates in the traps as well as a generally accelerated increase.
- The COS mole fraction measurements were corrected based on the partially characterised COS production and show no substantial trends over the last 1000 years, in broad agreement with previously published values (Aydin et al., 2008).
- The reported rise in COS abundance during the 1600s (Aydin et al., 2008) cannot be supported or refuted by these new data due to the post-extraction growth of COS. A large number of factors have been identified which contribute to this effect, not all of which can be quantified. The full scope of this issue could not be adequately constrained, meaning that wholesale corrections were not possible.

4.2 Northern and Southern Hemisphere firn air

Very few studies have measured COS in firn air; question marks remain regarding its global atmospheric history and inter-hemispheric differences. This uncertainty is particularly apparent in the Northern Hemisphere (NH), for which Sturges et al. (2001) provide the only long-term study. Some recent work (e.g. Aydin et al., 2002 and 2008; Montzka et al., 2004) has suggested that COS levels increased from pre-industrial levels to peak in the 1980s, before decreasing to present-day levels. Uncertainty remains regarding the rate of decline from peak levels as well as the magnitude and timing of the COS peak. Given the role of COS in stratospheric ozone destruction, it is important to understand its atmospheric chemistry in order to support ozone recovery predictions. More detail can be found in Section 1.4.

The original EDML and NEEM firn air analyses were performed at UEA by Dr. Francis Mani and Dr. Chris Hogan, respectively. These samples were collected at the EDML (EPICA European Project for Ice Coring in Antarctica/Dronning Maud Land) and NEEM (North Greenland Eemian Ice Drilling) sites. I reanalysed 25 of these firn samples as well as carrying out the modelling work presented in this section. The reanalysis was done for two reasons:

1. To verify the integrity of the samples. COS is potentially unstable during storage (e.g. the growth effect seen in Section 4.1). By reanalysing these samples, any COS degradation can be identified.
2. To ensure that all COS measurements are quoted using a single calibration scale. Where samples have not degraded, agreement between old and new measurements would demonstrate that the two sets of analysis are consistent with each other. Also, this would confirm that all measurements correspond to the NOAA (2004) calibration scale which is used to define the COS content of the working laboratory standard (AAL-071170).

4.2.1 Research objectives

1. Reanalyse a set of Northern and Southern Hemisphere firn air samples for COS and other trace gases, to ensure a consistent calibration scale and verify the integrity of the samples.

2. Use a firn diffusion model developed at the Laboratoire de Glaciologie et Géophysique de l'Environnement (LGGE), to infer new long-term Northern and Southern Hemisphere COS atmospheric histories from these firn air measurements.
3. Use these time series to better constrain spatial variations in COS mole fractions.

4.2.2 Methodology

Section 2.1 describes the trace gas analysis system at UEA which was used to perform the reanalyses. Similar methods were used in the original measurement period (descriptions can be found in Mani, 2010 and Hogan, 2013). Section 2.2 describes the model used in this work.

Previously published atmospheric time series were compiled to produce a best estimate of the atmospheric history of COS (Figures 4.11 and 4.12). The way these data were combined is outlined in Table 4.12. Since the inter-hemispheric ratio of COS has only been determined in recent years (with the inclusion of anthropogenic emissions), COS mole fractions measured in Antarctic ice cores were used as a global average up to the early 1900s. After this, various firn air studies were used until the late 20th century. Finally, ground-based stations run by NOAA were used to constrain the trends in the early 21st century. The NOAA stations at Summit (Greenland) and the South Pole were selected because they closely represent the environmental conditions at the firn air sites used in this thesis. There are trends in the high temporal resolution NOAA data, but the mole fractions change by $< 1 \text{ pmol mol}^{-1} \text{ yr}^{-1}$, so a flat trend was assumed at the mean value for the first 15 years of the 21st century. Using these time series as the input to the firn diffusion model (Figure 4.13), site-specific depth profiles were produced. This allowed a comparison to be made between the previously published data and the new data presented in this thesis. Throughout Section 4.2 various atmospheric time series (model ‘input scenarios’) will be used to produce mole fraction depth profiles (model ‘output scenarios’).

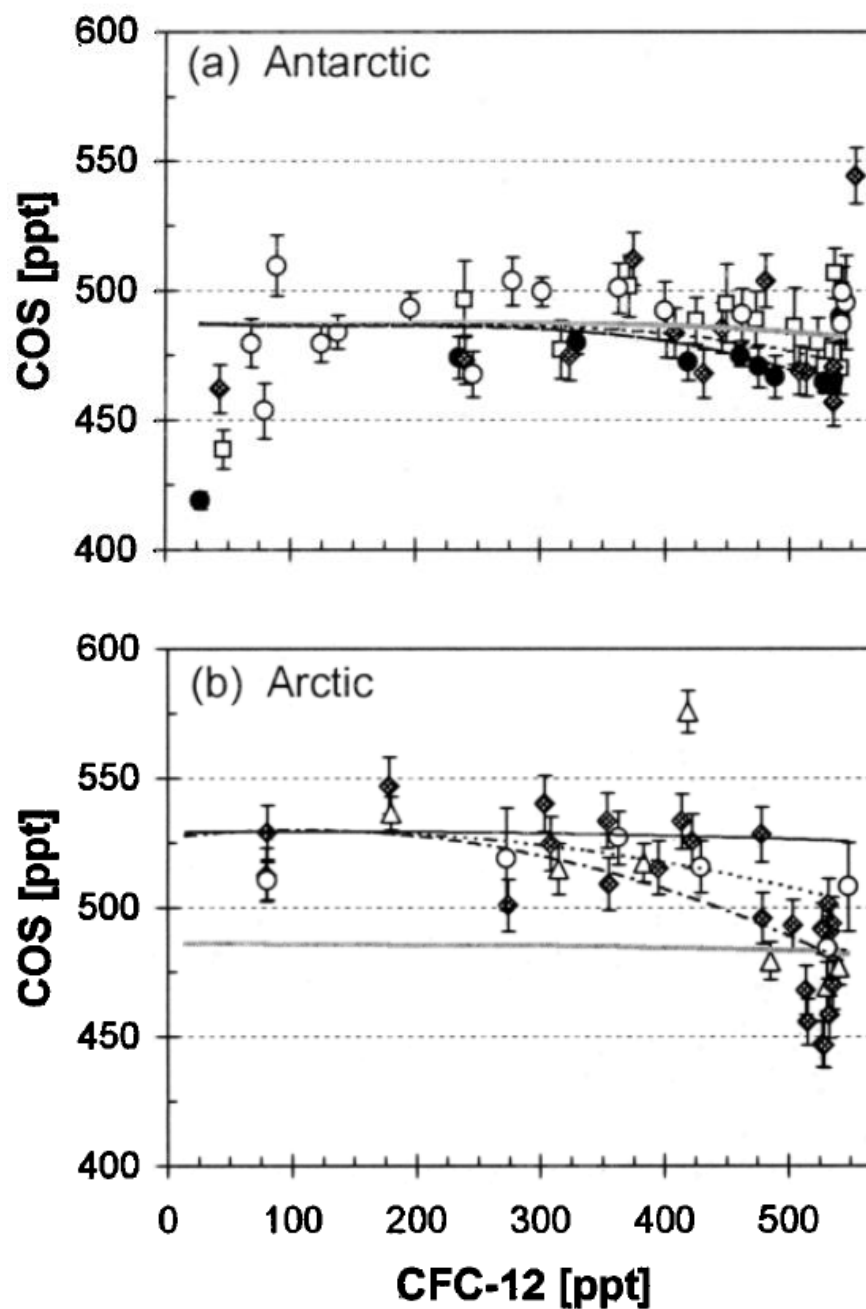


Figure 4.11. Previously published COS mole fraction measurements in firn air. COS is plotted against CFC-12 (as an age normaliser) in firn air from (a) DML and Dome C in Antarctica and (b) Devon Island in the Arctic. Lines indicate various atmospheric trend scenarios. Symbols identify flask types and sampling locations. Filled (Dome C) and open (DML) circles represent samples collected in SilcoCans, with some DML samples also collected in MPI flasks (open squares) and NCAR flasks (shaded diamonds). Devon Island samples were collected in Stabilizer flasks (open triangles) as well as SilcoCans and NCAR flasks (symbols as above). The figures were taken from Sturges et al. (2001).

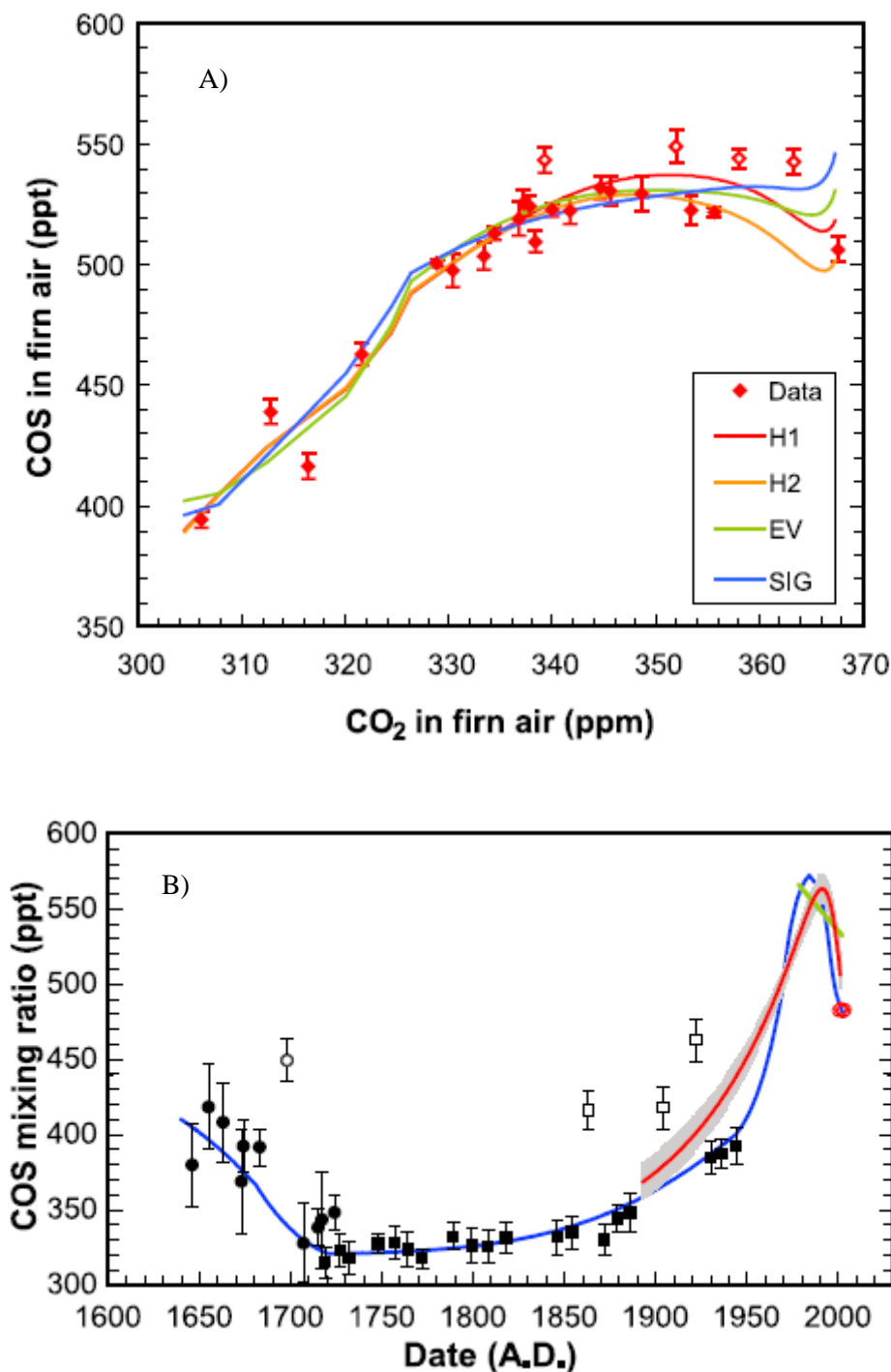


Figure 4.12. Previously published COS mole fraction measurements in firn and ice core air. A) COS is plotted against CO₂ (as an age normaliser) in South Pole firn air, approximately representing the period from 1940 – 2000. The solid lines represent various optimised model relationships. B) Black symbols indicate COS measurements on Siple Dome (Antarctica) ice core air. The red line is the inferred atmospheric history based on the measurements in A. An open symbol indicates an anomalous measurement. The figures were taken from Montzka et al. (2004).

Table 4.12. Based on previously published data, a best estimate of the atmospheric history of COS has been temporally constrained. The source of each constraint is given alongside the relevant data. Data from the NOAA ground-based station data can be found at: ftp://ftp.cmdl.noaa.gov/hats/carbonyl%20sulfide/OCS_GCMS_flask.txt.

Time constraint	Northern Hemisphere	Southern Hemisphere
1800s	325 pmol mol ⁻¹ (Antarctic ice core air in Aydin et al., 2008 used as a global average)	325 pmol mol ⁻¹ (Antarctic ice core air in Aydin et al., 2008 used as a global average)
Early 1900s	385 pmol mol ⁻¹ (firn and ice core air in Montzka et al., 2004)	385 pmol mol ⁻¹ (firn and ice core air in Montzka et al., 2004)
Mid-1980s	525 pmol mol ⁻¹ (firn air in Sturges et al. (2001), CFC-12 values provide approximate air ages)	525 pmol mol ⁻¹ (firn air in Montzka et al. (2004), CO ₂ values provide approximate air ages)
Early 2000s and seasonality	476 pmol mol ⁻¹ (2004 - 2014 average taken from the NOAA ground-based station at Summit, Greenland)	490 pmol mol ⁻¹ (2000 - 2014 average taken from the NOAA ground-based station at the South Pole)

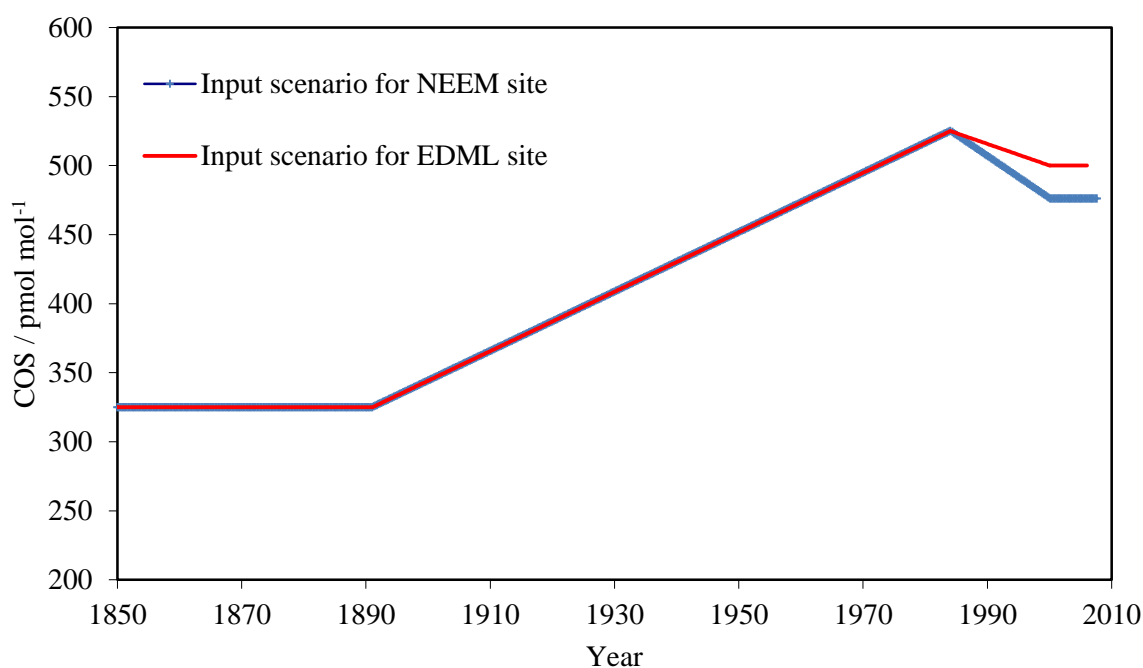


Figure 4.13. The initial input time series for the NEEM (blue line) and EDML (red line) sites. These scenarios were constructed using the constraints outlined in Table 4.12.

4.2.3 Results and discussion

Of the 25 samples that were reanalysed, 12 were found to have degraded slightly over their period of storage (Figure 4.14). A sample was judged to have degraded if there was either growth or loss of a compound beyond analytical uncertainties. CCl_4 and CH_3CCl_3 are typically the first species to exhibit growth or loss if the sample has degraded (assuming that the containers have not leaked, allowing the ingress of modern air). This effect is yet to be quantified and the reason for it is poorly understood, although a dependence on latitude and altitude has been noted (<http://www.esrl.noaa.gov/gmd/hats/combined/CCl4.html>). Where this effect was seen, the reanalysis was excluded and the original measurement is represented in subsequent figures using an open symbol (Figure 4.15). In the absence of sample degradation, good agreement is shown between the original measurements and those performed as part of this thesis (Figure 4.14). This suggests that both sets of measurements are consistent with the NOAA (2004) calibration scale and can be directly compared.

Laboratory air standards are measured relative to each other with respect to a range of compounds every few years. This process is a further test of measurement consistency because it tracks how the COS content of these standards changes with respect to each other. Figure 2.3 (Chapter 2) displays a long-term comparison between two standards (ALM-64957 and ALM-39753) and Table 4.7 (Section 4.1.3.2) shows the results of a recent comparison between three standards (AAL-071170, ALM-39753 and SX-0706077). All of the available standards are analysed during an inter-comparison, rather than just the working standard and one other. This is because including a larger number of standards reduces the chance of co-variation being mistaken for stability. Although concurrent drift is unlikely, it is possible since there are similarities in the filling procedure and storage environment of these standards. A variety of standards will introduce a range of container vessel types and mole fraction amounts, meaning that any drift is more likely to be identified. These tests show that the COS content of these standards has not drifted with respect to each other. This means that the two sets of analysis are quantitatively comparable and can be combined into a single data set.

Figure 4.14 displays the root firn air data used in this section. The initial best estimate atmospheric scenarios (Figure 4.13) were used as the input to the firn model. In this way, the previously published data can be compared to these new measured profiles (Figure 4.15).

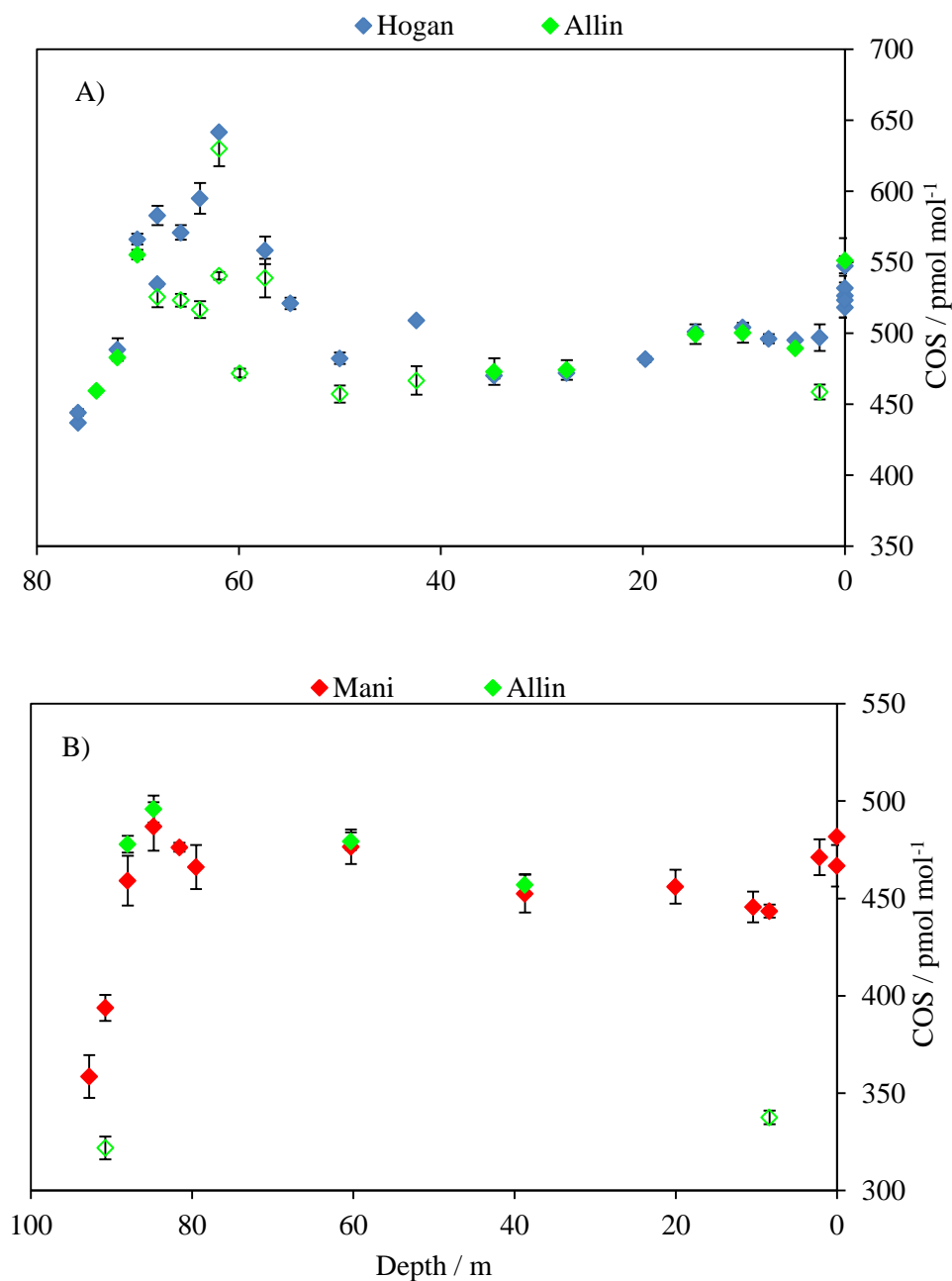


Figure 4.14. The results of the original firn air COS mole fraction measurements made by Dr. Chris Hogan (Hogan, 2013; blue diamonds) and Dr. Francis Mani (Mani, 2010; red diamonds), as well as the reanalyses conducted as part of this thesis (“Allin”; green diamonds). A) Samples from the NEEM site (Greenland), collected in 2008. B) Samples from the EDML site (Antarctica), collected in 2005/2006. 1 σ analytical uncertainties are included. Empty symbols indicate that there was evidence of degradation in the sample (as defined in the main text). The final data are displayed in Figure 4.15.

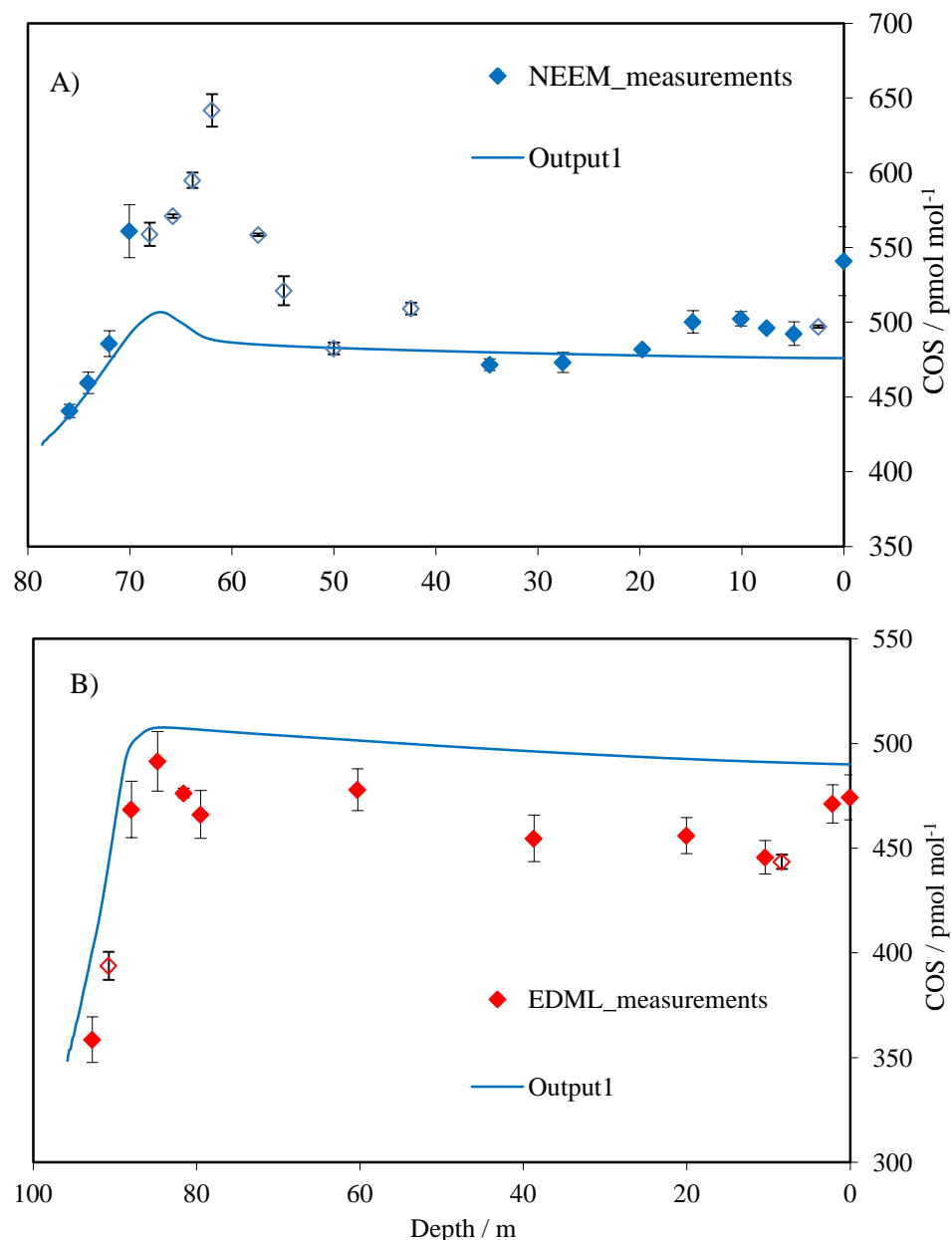


Figure 4.15. COS is modelled based on best estimate atmospheric scenarios (Figure 4.13). Using NEEM (A) and EDML (B) parameters, the model is run to produce site-specific output scenarios (blue lines). The firn measurements displayed in Figure 4.14 are combined to give these data. Where the original and new measurements at a given depth are both shown to be robust (as defined in the main text), the values were averaged. Where the reanalysis revealed slight degradation the original measurement was used and represented by an open symbol. A) Samples from the NEEM site (Greenland), collected in 2008 (blue diamonds). B) Samples from the EDML site (Antarctica), collected in 2005/2006 (red diamonds). 1σ analytical uncertainties are included. When multiple measurements are combined, the total uncertainty is calculated using equation 2.3 (Chapter 2).

The model output in Figure 4.15A shows good agreement with the deepest (72 – 76 m) and shallowest (0 – 50 m) NEEM measurements. The fit is less good near the surface where seasonal variability could be having an impact. Also, between approximately 55 and 70 m there is a large positive excursion in the firm measurements which is not replicated in the model output. Figure 4.15B shows that the Southern Hemisphere model output follows the shape of the EDML profile very well, although the firm measurements are consistently slightly lower than the model output. This offset is least significant as COS mole fractions reach their peak (85 – 88 m). The effect of seasonal variability on near-surface measurements is explored in Sections 4.2.3.1 and 4.2.3.2.

From this point, the input scenarios will be adjusted in atmospherically relevant ways (e.g. by including a seasonal cycle), to assess the potential reasons for the differences between measured and expected values (Figure 4.15).

4.2.3.1 Northern Hemisphere results

Figures 4.17A and 4.18A display NH input scenarios, to illustrate the adjustments that were made. These act as sensitivity tests, to determine the model output produced from various input scenarios.

Seasonality

Input 2 in Figure 4.17A includes seasonal variability into the original best estimate scenario (Figure 4.13). Seasonality data were taken from the ground-based NOAA site at Summit (Greenland) which covers the period from 2004 – 2014 (Table 4.12). The seasonal signal from the 12 months immediately preceding the drilling date at NEEM (Figure 4.16) was extrapolated to the whole record.

Surface variability is only transmitted to the highly diffusive upper part of the firm column, meaning that output 2 is very similar to output 1 at depths greater than approximately 20 m (Figure 4.17B). Closer to the surface, the model output tracks the firm profile very well, suggesting that these measurements have captured seasonal differences at NEEM.

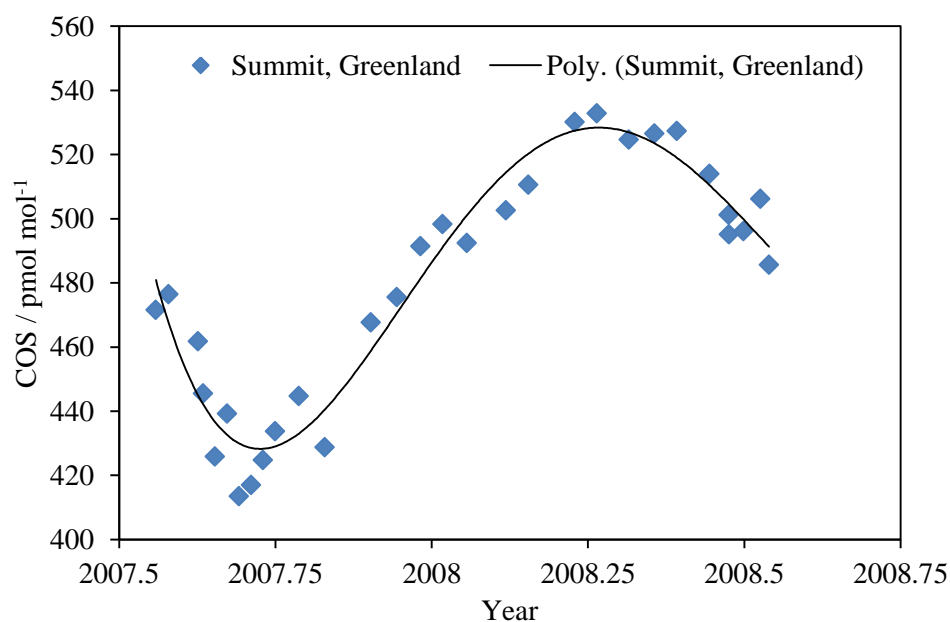


Figure 4.16. COS mole fraction measurements made at the NOAA ground-based station at Summit (Greenland). These measurements cover the 12 month period immediately preceding the firn air sampling at the nearby NEEM site. A polynomial trend line has been fitted to the data. The data were taken from ftp://ftp.cmdl.noaa.gov/hats/carbonyl%20sulfide/OCS_GCMS_flask.txt.

Regional anthropogenic emissions

The NH best estimate scenario (Figure 4.13) is constructed based on measurements from several sites. The NEEM site is closer to European anthropogenic emissions than the published 20th century constraints (Table 4.12). It could be that this proximity can explain the higher than expected COS values in the NEEM firn. The available data quantifying the hemispheric partitioning of anthropogenic emissions is limited. The most recent evaluations of the COS budget include large uncertainties (Kettle et al., 2002; Montzka et al., 2007). The size of these uncertainties precludes the possibility of quantifying the proposed proximity effect at NEEM. Instead, input scenario 3 (Figure 4.17A) was constructed based on the available data regarding the major anthropogenic source of COS (CS₂ released through viscose-rayon production). This production was constant between 1970 and 1990, before dropping by 24 % over the next 9 years (source: Acordis company). Sturges et al. (2001) calculated that this 24 % drop in global viscose-rayon production

would result in a 4 % drop in COS mole fractions. Regionally, this decrease is likely to have been larger due to changes in the location of CS₂ production over the same period. In the 1970s over a third was produced in Europe, compared to 7 % in the 1990s (Sturges et al., 2001). Linked to this, Asian synthetic fibre production made up 24 % of the global industry in 1977, rising to 65 % by 1997 (source: Fiber Economics Bureau, Ltd). Based on this, it is reasonable to assume that the change in COS mole fractions over Europe (and at NEEM) would have been larger than the global value calculated by Sturges et al. (2001). During the mid-1980s (as anthropogenic emissions peaked), COS mole fractions have been increased to 660 pmol mol⁻¹ for input scenario 3 (Figure 4.17A). The adjusted mole fractions decrease linearly before and after this point, reflecting the lower anthropogenic emissions away from this peak. This large change in COS mole fractions has been simulated because input scenario 3 is intended as a sensitivity test, comparing the potential effect of a large regional shift in CS₂ emissions on local COS mole fractions.

Figure 4.17B shows that the magnitude of some firm measurements is replicated more closely using this scenario (e.g. between 65 and 70 m). However, the fit is worse in the deepest (72 – 75 m) and shallowest (0 – 50 m) measurements. Also, the peak in the firm measurements comes at a shallower depth than in the model output. This suggests that although model output 3 is closer in magnitude to the measurements between 50 and 72 m, the shape (and therefore the timing) of the COS peak is not replicated. In contrast to the mid-1980s peak reported by previous studies (e.g. Montzka et al. 2004), it seems that a significantly enhanced COS flux into the atmosphere after this point is required to reconcile these NEEM data.

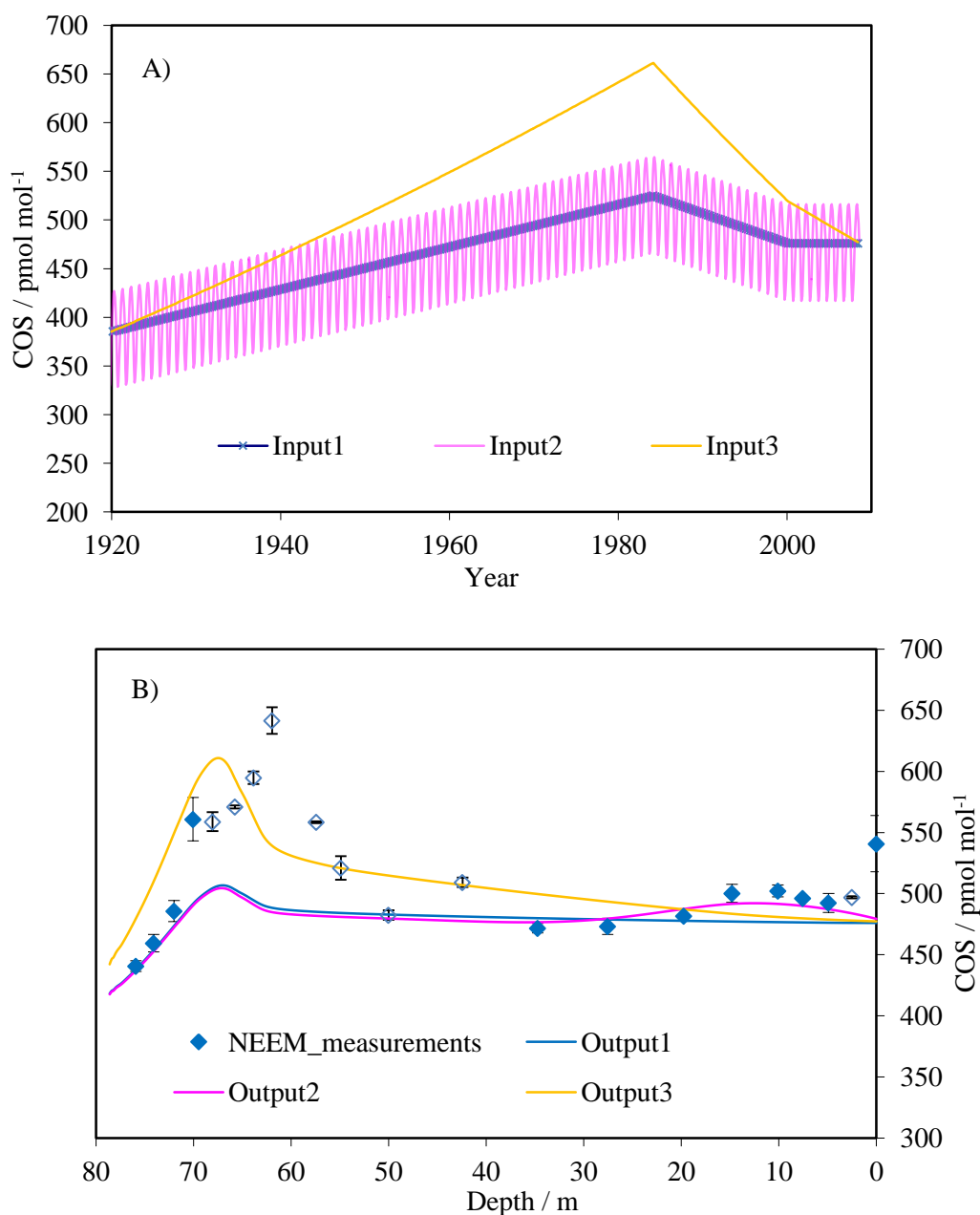


Figure 4.17. A) Northern Hemisphere model input scenarios for COS (a brief description is given here, with full details in the main text). Input 1: best estimate scenario from Figure 4.13. Input 2: as input 1, with the seasonal signal from Summit (Greenland) added (Table 4.9 and Figure 4.16). Input 3: as input 1, but assuming a greater proportion of anthropogenic COS emissions were recorded at NEEM, with minimal influence on other sites. B) COS mole fraction measurements made on NEEM firn air (as described in Figure 4.15). COS is modelled based on the input atmospheric scenarios shown in A. Specific output scenarios (solid lines) are numbered according to the input scenario that they result from.

Emission events

Localised emissions events and unusual meteorological activity are two possible explanations for the excess COS found in these firn samples. For example, a period of elevated emissions from a viscose-rayon factory, a biomass burning event or a volcanic plume coupled with meteorological conditions altering their distribution, could lead to unusually high levels of COS at a particular sampling site. Based on 15 years of measurements at ground-based NOAA stations, there is no direct evidence that these events occur, meaning that the scenarios presented in this section (Figure 4.18A, inputs 4 and 5) are unlikely to represent realistic atmospheric scenarios.

Input 4 (Figure 4.18A) takes the original best estimate scenario (Figure 4.13) and adds a COS level of 10,000 pmol mol⁻¹ for three months in 1999. An event of this magnitude and duration is unlikely to have remained localised, making this an extreme scenario. It was designed to determine whether this could replicate the size of the measured peak in firn air mole fractions.

Figure 4.18B shows that the magnitude of the positive excursion in the data has been replicated by this event and the fit between the model output and the firn measurements is good between 62 and 75 m. At shallower depths, the model output shows a gradual decrease from peak to surface levels, reflecting the more open porosity in this part of the firn. In contrast, the firn measurements show a sharp decline over the same period. This suggests that an emissions event and the model-constrained firn processes cannot fully explain the firn air measurements made at the NEEM site.

Input 5 is identical to input 4, except that the 3 months at 10,000 pmol mol⁻¹ are in 1965, to determine whether events of this nature would be detectable early in the firn record.

Figure 4.18B shows that the magnitude of this event is more significantly damped when it occurs earlier in the firn record. However, output 5 is still clearly visible above output 1, suggesting that this type of event should be detectable anywhere in the firn column (assuming a high enough sampling frequency). The measurement at 70 m could be due to a localised, short duration event characterised by very high COS. However, as stated previously, there is no evidence that the events described in inputs 4 and 5 occur. The section titled '*Other potential sources of elevated COS in firn*' explores this in more detail.

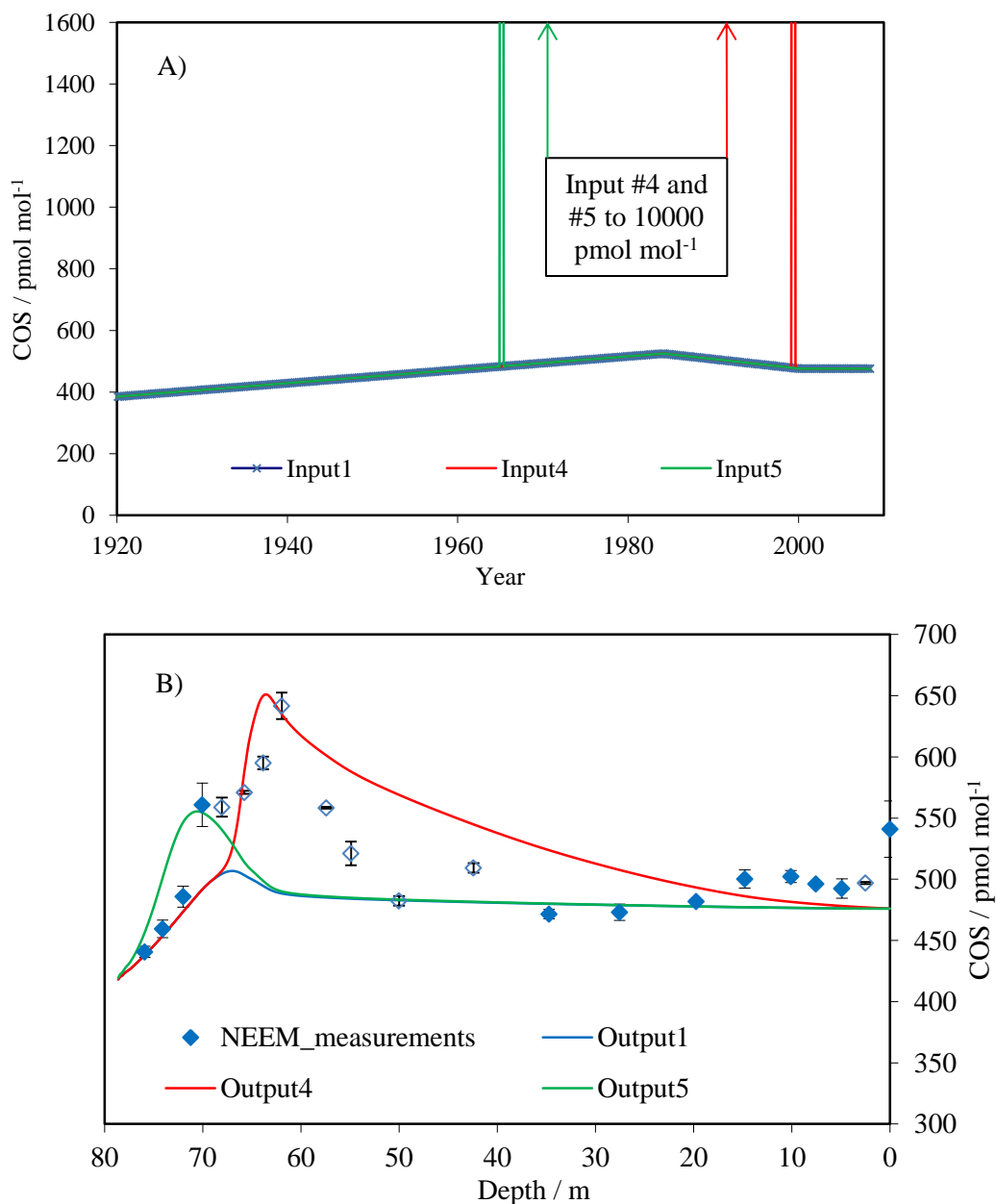


Figure 4.18. A) Northern Hemisphere model input scenarios for COS (a brief description is given here, with full details in the main text). Input 1: best estimate scenario from Figure 4.13. Input 4: as input 1, with a COS level of 10,000 pmol mol^{-1} for 3 months in 1999. Input 5: as input 1, with a COS level of 10,000 pmol mol^{-1} for 3 months in 1965. B) COS mole fraction measurements made on NEEM firn air (as described in Figure 4.15). COS is modelled based on the input atmospheric scenarios shown in A. Specific output scenarios (solid lines) are numbered according to the input scenario that they result from.

Model sensitivity to COS diffusivity

As described in Section 2.2 (Chapter 2), the movement of any gas in fire is constrained by its molecular mass and its diffusivity. In this study, the diffusivity of COS was calculated using the method outlined in Chen and Othmer (1962). As a final sensitivity test, the diffusivity constraint in the model was adjusted to be 25 % higher (Input 6) and 25 % lower (Input 7) than the calculated value. The original best estimate atmospheric scenario (Input 1, Figure 4.17A) was used without alteration.

Figure 4.19 shows that the large adjustments made to the diffusivity parameter have very little effect on the model output compared to the effect of potential atmospheric changes (Inputs 2 - 5). It is unlikely that an error in the diffusivity would have a significant effect on the model output.

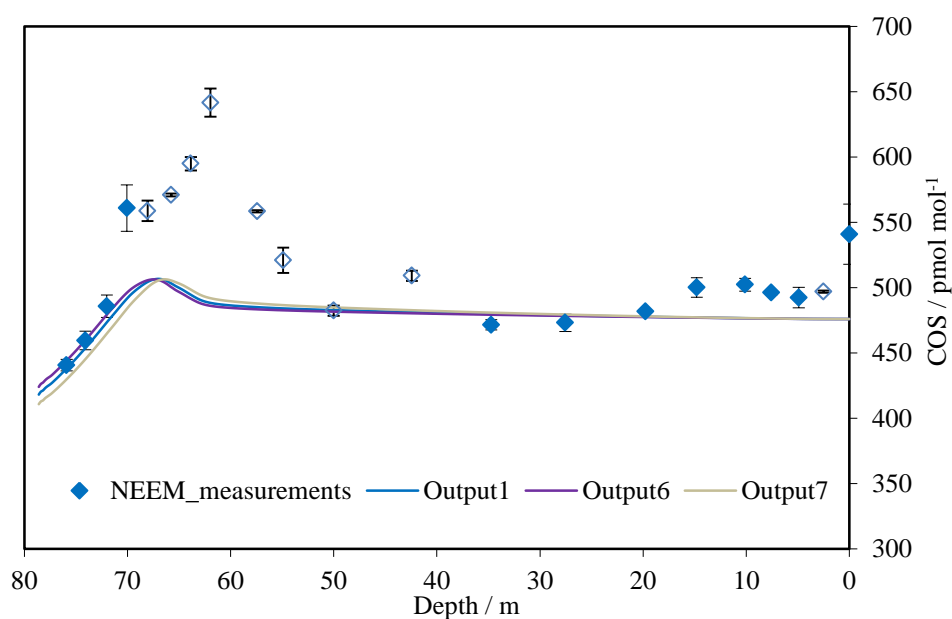


Figure 4.19. COS mole fraction measurements made on NEEM firn air (as described in Figure 4.15). COS is modelled based on input 1 (Figure 4.17A) and varying the COS diffusivity (as described in the main text). Specific output scenarios (solid lines) are numbered according to the input scenario that they result from.

Other potential sources of elevated COS in firn

In Section 4.2.3.1, atmospheric phenomena have been explored in an attempt to reconcile the NEEM firn air measurements with previously published COS atmospheric data. The magnitude of the large positive excursion between 50 and 72 m has been successfully replicated through a high intensity emissions event, although the rate of decline from 62 to 50 m cannot be reproduced. The emissions events discussed earlier in this section were designed to be unrealistic in order to show that the observed values can only be replicated with unrealistic atmospheric scenarios. This suggests that in-situ processes (which are confined to the section between 50 and 72 m) are likely to be producing the excess COS.

Several studies have presented trace gas measurements made on these NEEM samples (Hogan, 2013; Petrenko et al., 2013; Helmig et al., 2014). Hogan (2013) measured a wide range of trace gases using these samples. The mole fractions of several halogenated compounds (CH_3Cl , CHCl_3 , CH_2Cl_2 , CCl_2CCl_2 , $\text{CH}_2\text{ClCH}_2\text{Cl}$, $\text{C}_2\text{H}_5\text{Cl}$, $\text{CH}_2\text{BrCH}_2\text{Br}$, $\text{C}_2\text{H}_5\text{Br}$, CH_2BrCl , CHBrCl_2 and CF_3CHBrCl) were found to have increased and decreased in the atmosphere, in a similar way to COS. However, these halogenated species peak before COS and do not display the same rapid decline from a COS peak at 62 m to contemporary levels at 50 m. Helmig et al. (2014) reconstructed a 60 year NH atmospheric history of ethane, propane, *i*-butane, *n*-butane, *i*-pentane and *n*-pentane. In common with COS, all of these species were found to increase and decrease in abundance with a peak at approximately 1980. However, there is good agreement between the measurements and emissions inventories from Western Europe and North America. Petrenko et al. (2013) present a record of CO from these NEEM samples (Figure 4.20) which was shown to conflict with the predicted atmospheric history of CO over Greenland. A chemistry-climate model (CAM-Chem, (Lamarque et al., 2010)) was used to make these predictions, by setting emissions inventories as an input parameter. Petrenko et al. (2013) calculated that at 1950, measured CO is as much as a factor of 2 higher than expected. Also, emissions reductions were found to have occurred approximately 10 years earlier than reported (approximately 1980 compared to 1990) and the emissions reductions in the last 2 – 3 decades have been underestimated by as much as a factor of 2.5. Previous studies have found evidence of in-situ production of CO in NH firn and ice (Clarke et al., 2007; Haan and Raynaud, 1998). Figure 4.20 shows that peak CO and COS levels do not coincide, suggesting that if both peaks are caused by in-situ production, they are being produced through different mechanisms. The production mechanisms are not known, although it is assumed that the substrate in both cases is trace organic material. Petrenko et al. (2013)

reasoned that if an organic-rich layer at NEEM were the cause of the high CO levels at the lock-in depth, this layer would also be present in nearby drilling sites. Elevated CO levels were found at the neighbouring NGRIP site, but the mean ice-age of these layers was offset by 45 years from those at NEEM. Based on this finding, Petrenko et al. (2013) concluded that in-situ production was not the cause of the elevated CO mole fractions and that large errors in the emissions inventories were the most likely cause of the conflict between measured and predicted CO mole fractions.

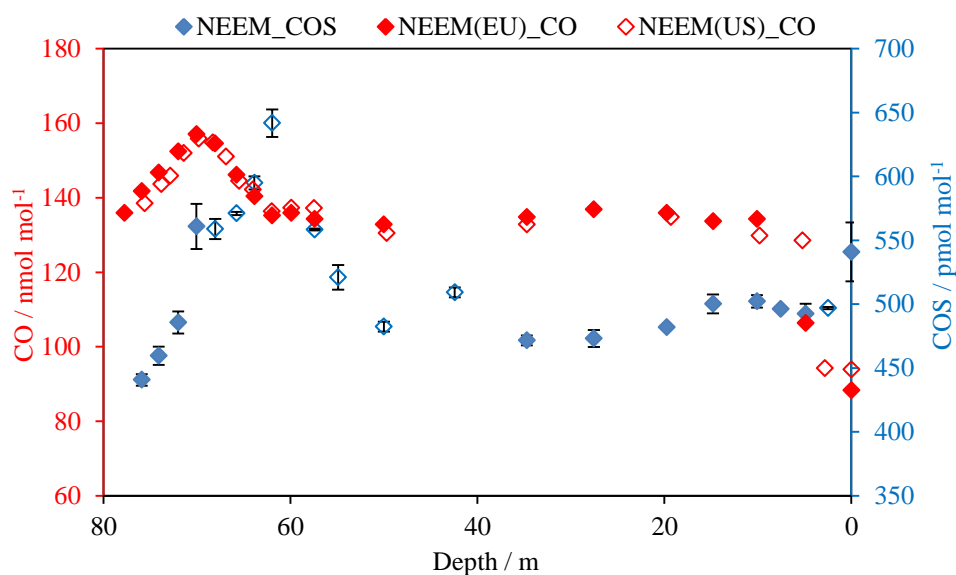


Figure 4.20. Measurements of CO (red diamonds) and COS (blue diamonds) mole fractions on NEEM 2008 firm air. The CO data were taken from Petrenko et al. (2013).

4.2.3.2 Southern Hemisphere results

Figures 4.21A and 4.23A display the SH input scenarios, to illustrate the adjustments that were made. These act as sensitivity tests, to investigate the discrepancies between measured and expected values (Figure 4.15) and to assess the effect of the NH scenarios discussed in Section 4.2.3.1.

Seasonality

Input 2 in Figure 4.21A includes seasonal variability into the original best estimate scenario (Figure 4.13). Seasonality data were taken from the ground-based NOAA site at the South Pole which covers the period from 2000 – 2014 (Table 4.12). The seasonal signal from the 12 months immediately preceding the drilling date at EDML (Figure 4.22) was extrapolated to the whole record.

Below the diffusive upper part of the firn column, surface processes (including seasonal changes) have no significant effect. This has resulted in outputs 1 and 2 being almost identical at depths greater than 20 m (Figure 4.21B). The predicted increase from 15 m to the surface (based on South Pole seasonality data, Figure 4.22) is reproduced in the EDML firn measurements. However, the model predicts an increase of 15 pmol mol^{-1} , compared to the 30 pmol mol^{-1} increase seen in the EDML measurements over the same period. This difference could reflect the greater distance between the South Pole and the oceanic COS flux, compared to EDML. Figure 4.21B also shows that there is an offset of $30 - 50 \text{ pmol mol}^{-1}$ between the measurements and the model output over the whole profile. The consistency of this offset suggests that the difference is significant and not due to measurement uncertainties. The likely cause of this difference is discussed later in this section, under “*Natural source variability*”.

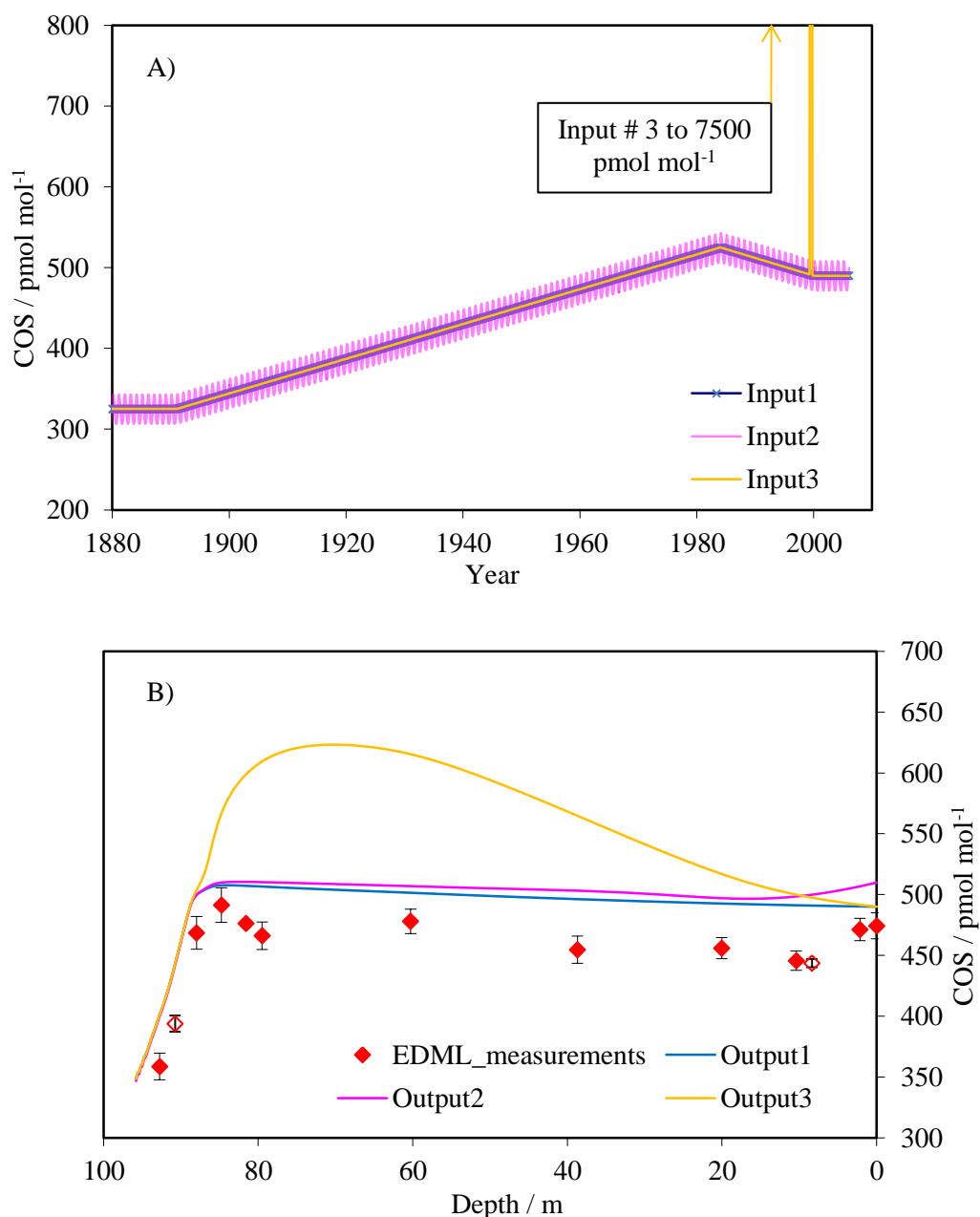


Figure 4.21. A) Southern Hemisphere model input scenarios for COS (full details in the main text). Input 1: best estimate scenario from Figure 4.13. Input 2: as input 1, with the seasonal signal from the South Pole added (Table 4.12 and Figure 4.22). Input 3: as input 1, with a COS level of $7500 \text{ pmol mol}^{-1}$ for 3 months in 1999. B) COS mole fraction measurements made on EDML firn air (as described in Figure 4.15). COS is modelled based on the input atmospheric scenarios shown in A. Specific output scenarios (solid lines) are numbered according to the input scenario that they result from.

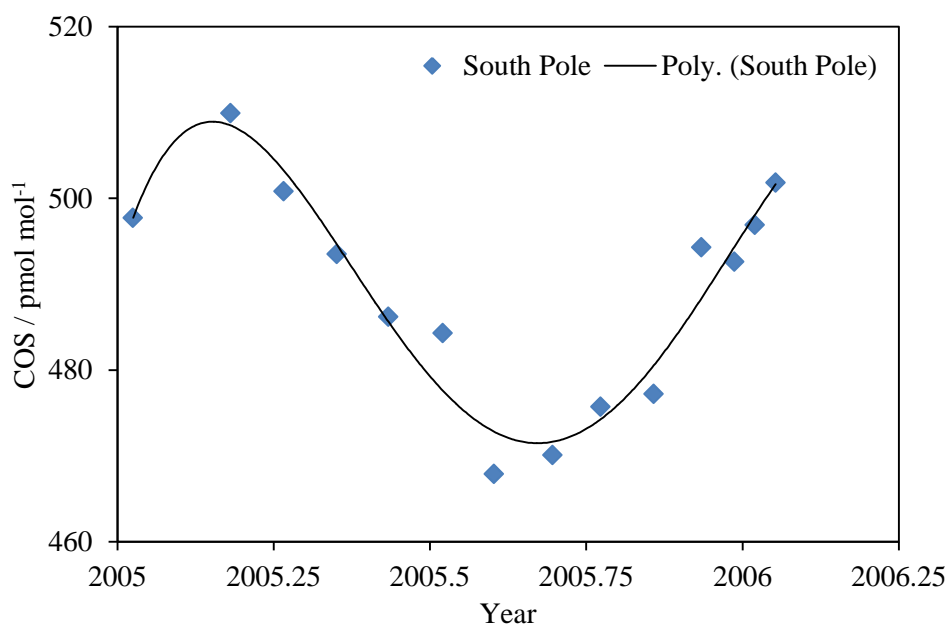


Figure 4.22. COS mole fraction measurements made at the NOAA ground-based station at the South Pole. These measurements cover the 12 month period immediately preceding the firn air sampling at the EDML site. A polynomial trend line has been fitted to the data. The data were taken from ftp://ftp.cmdl.noaa.gov/hats/carbonyl%20sulfide/OCS_GCMS_flask.txt.

Emission event

Short duration, intense emissions events in the NH have been suggested in Section 4.2.3.1 as a possible mechanism to explain some of the high COS measurements in NEEM firn air (Figure 4.18B). Input 3 in Figure 4.21 investigates the potential effect of one of these events on the record at EDML. Based on the 1999 NH emission event described in Section 4.2.3.1 (Figure 4.18A, Input 4) and assuming a 25 % loss during transport, this leaves a COS level of 7500 pmol mol⁻¹ for three months in the SH (Figure 4.21A, Input 3). The emissions are assumed to have originated in the NH because an anthropogenic source is more likely to produce a high intensity release like this and they are mostly located in the NH. Equation 4.1 describes how a loss rate of 25 % was calculated.

Figure 4.21B shows that this type of event would impact many of the measurements at EDML and would be clearly visible in the record. This scenario is not supported by the firn measurements which show no positive excursions above expected values. It is possible that

due to meteorological factors an emissions event in the NH was much more localised, although it seems unlikely that the effect of such a large event would be completely absent in the SH record. This supports the conclusion in Section 4.2.3.1 that the higher than expected mole fraction values measured on NEEM samples are not the result of atmospheric composition changes.

Natural source variability

The EDML measurements are generally slightly lower than expected (based on recent atmospheric measurements; Table 4.12), with the best agreement found as COS mole fractions reach their peak (88 – 85 m). An optimised SH input scenario has been produced to determine the atmospheric time series that provides the best fit to the measurements. Output 2 showed that the magnitude of the seasonal cycle at the South Pole was approximately half that of EDML (Figure 4.21B). The South Pole seasonal cycle (Figure 4.22) was doubled to produce the seasonality data for the optimised scenario (input 4, Figure 4.23A). To improve the fit over the whole firn profile, the original best estimate scenario (Figure 4.13) was lowered by 10 % at 1920, 2 % at 1984 and 8 % at 2006. The amount of lowering was changed linearly between these values and all points before 1920 were reduced by 10 % (Figure 4.23A).

Figure 4.23B shows that the atmospheric history of COS at EDML is different to previously published SH records (Table 4.12, Figure 4.13). Within the analytical uncertainties of the measurements and assuming a similar uncertainty in the output scenario (output 4, Figure 4.23B), all of the measurements agree with this optimised scenario. To achieve this fit, the relative adjustment required decreased to a minimum as COS peaked in the mid-1980s. This means that as anthropogenic emissions contribute more to COS sources, the difference between measurements from EDML and other SH sites reduces. Based on this, it seems likely that the natural COS budget is the main driver of this difference. It is unlikely that sink processes could produce this difference because the major sink (uptake by vegetation) is mostly located in the NH. The remote Antarctic sites used in this study (EDML and South Pole) are unlikely to be influenced differently by this distant sink. On the other hand, the oceans act as a significant net source of COS in the SH (Kettle et al., 2002). Regional variations in this source due to ocean dynamics and biological activity (e.g. the strength and location of phytoplankton blooms) provide the most viable cause of the difference between EDML and other SH sites. To investigate this further, these new EDML data should be incorporated into a chemical transport model (e.g.

GEOS-Chem, (Suntharalingam et al., 2008)) in order to better understand the temporal and spatial flux of COS from the oceans. In this case, the Southern Ocean would be of particular interest.

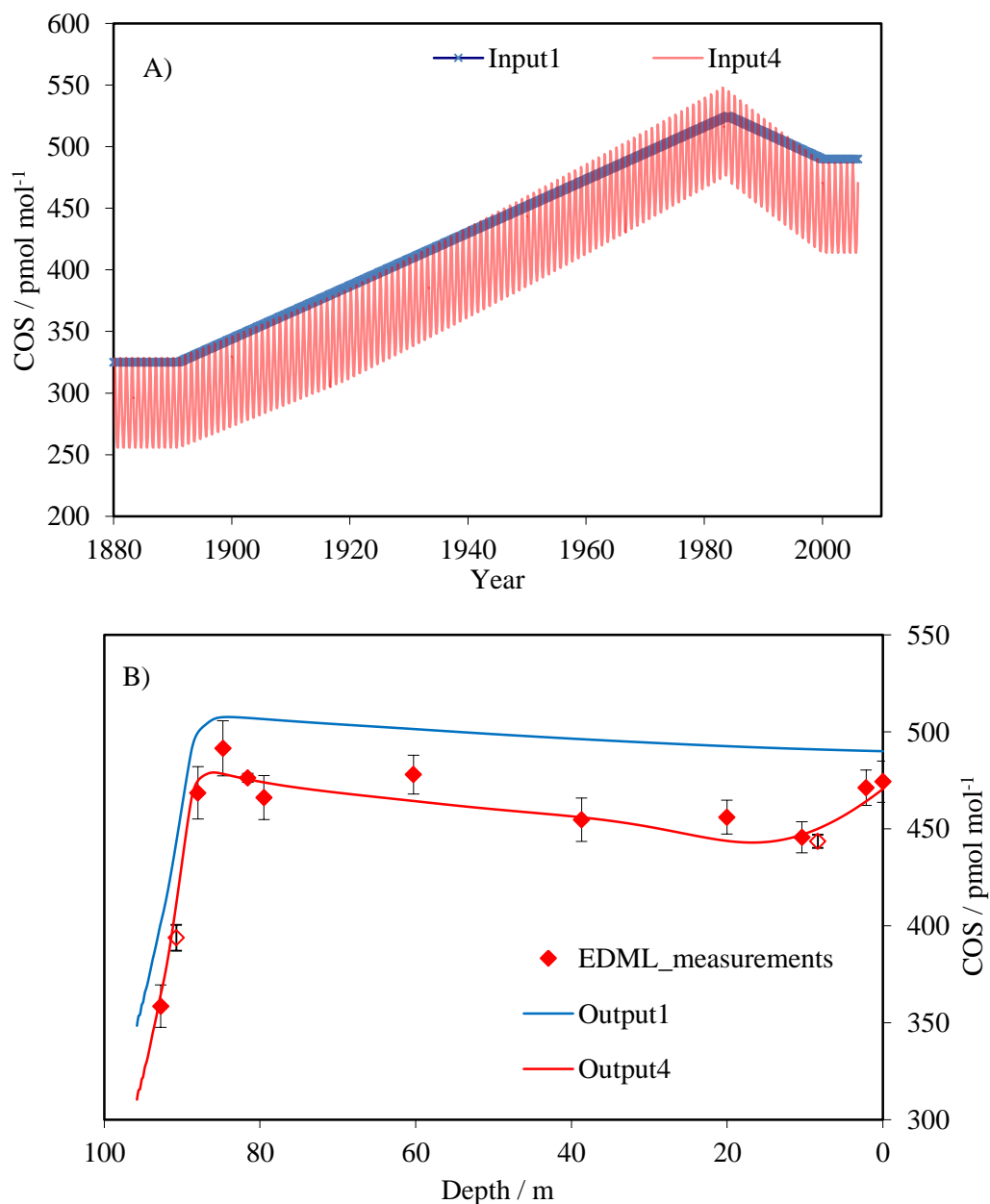


Figure 4.23. A) Southern Hemisphere model input scenarios for COS (full details in the main text). Input 1: as described in Figure 4.13. Input 4: peak COS levels are 2 % lower than input 1 and mole fractions decrease on either side of this peak to 10 % lower than input 1 at 1920 and 8 % lower at 2006. The seasonal signal from the South Pole (Figure 4.22) is doubled and added to input 4. B) COS mole fraction measurements made on EDML firn air (as described in Figure 4.15). COS is modelled based on the input atmospheric scenarios shown in A. Specific output scenarios (solid lines) are numbered according to the input scenario that they result from.

Model sensitivity to COS diffusivity

The diffusivity constraint in the model was adjusted to be 25 % higher (Input 5) and 25 % lower (Input 6) than the calculated value, as a final sensitivity test. The original best estimate atmospheric scenario (Input 1, Figure 4.21A) was used without alteration.

Figure 4.24 shows that these adjustments to the diffusivity parameter have a small effect on the model output, particularly at depths below the lock-in zone. Assuming an atmospheric input scenario uncertainty of 3 %, the changes shown in outputs 5 and 6 are not significant (Figure 4.24).

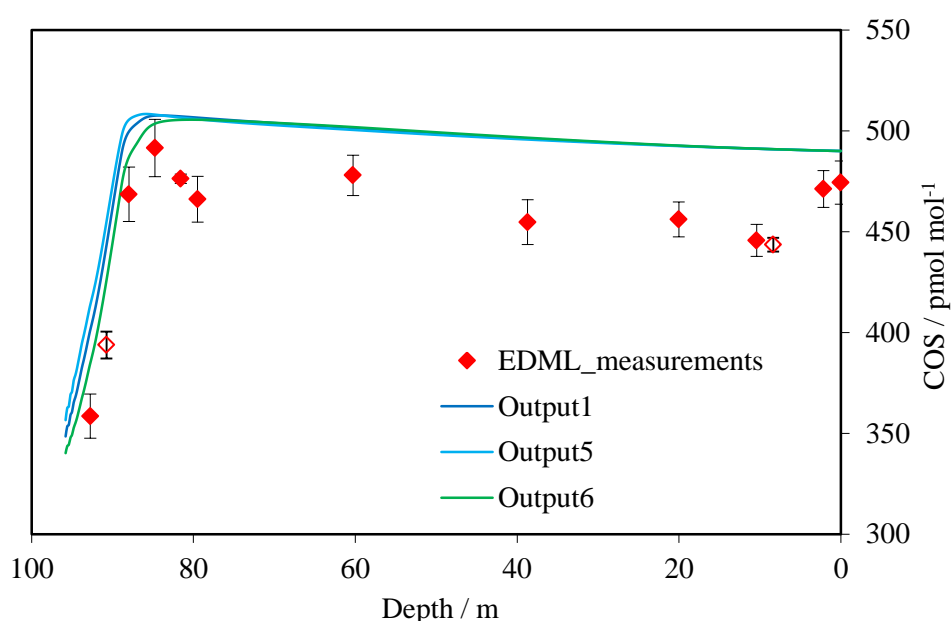


Figure 4.24. COS mole fraction measurements made on NEEM firn air (as described in Figure 4.15). COS is modelled based on input 1 (Figure 4.21A) and varying the COS diffusivity (as described in the main text). Specific output scenarios (solid lines) are numbered according to the input scenario that they result from.

4.2.4 Summary

- New Northern and Southern Hemisphere firn profiles of COS mole fractions have been presented.
- A firn diffusion model has been used to compare these profiles with previously published data.
- Using high temporal resolution data from ground-based stations as a comparison, the seasonal variability of COS mole fractions has been captured well at both sites. This suggests that the measurements in the diffusive part of the firn column are largely robust.
- The previously reported decline in the COS mole fractions since the 1980s is seen in both data sets.
- The Northern Hemisphere NEEM data show a significantly accelerated decline from very high levels between 50 and 65 m, compared to a previously reported Devon Island record. Although a causal mechanism has not been identified which can account for these elevated values, it has been shown that a high magnitude, short duration event at the turn of the century could account for the highest measurements, but not the observed rate of decline.
- In-situ production could have caused the high values at NEEM as well as the subsequent rapid decline, although there is no direct evidence to substantiate this. Evidence of in-situ production in the wide range of other trace species measured in these samples is also lacking.
- The Southern Hemisphere EDML measurements are slightly lower than predicted, based on previously published Antarctic data. It is likely that this discrepancy during the 20th and 21st centuries is due to regional changes in natural COS sources, although direct evidence has not been produced.

Chapter 5: Conclusions and recommendations

This chapter provides a summary of the main findings in this thesis and outlines how these results could be used to guide future inquiry.

5.1 An atmospheric history of the chlorine and carbon isotope composition in CFC-11, CFC-12 and CFC-113

CFCs are ozone depleting substances entirely of anthropogenic origin. It is important to understand how these gases interact with the environment to determine their likely impact on the climate system. Based on research directly linking CFCs to the destruction of stratospheric ozone (e.g. Molina and Rowland, 1974; Farman et al., 1985), the Montreal Protocol and its subsequent amendments were instigated. These agreements have been largely successful in phasing out the production and consumption of known ozone depleting substances. At this point, research into these gases should be directed at better understanding their behaviour, with a view to predicting and preparing for the atmospheric conditions of the future. In this study, significant progress has been made in the characterisation of the three most abundant CFCs (CFC-11, CFC-12 and CFC-113). Part of this work has been published (Allin et al., 2015), with a second publication in progress.

Previous studies have used IRMS techniques to measure isotope deltas in trace gases (e.g. Zuiderweg et al., 2013). Large samples of air, typically hundreds of litres, were needed to achieve measurable chromatograph peaks. Laube et al. (2010a) used a single-collector GC-MS instrument to analyse much smaller aliquots, to make the first stratospheric $\delta(^{37}\text{Cl}$, CFC-12) measurements. The measurements presented in this thesis also required small samples (200 - 600 ml) and were used to infer an atmospheric history of chlorine and carbon isotopes in CFC-11, CFC-12 and CFC-113. These measurements are the first to quantify the long-term changes of tropospheric $\delta(^{37}\text{Cl})$ and $\delta(^{13}\text{C})$ in CFC-11, CFC-12 and CFC-113.

Table 5.1. A summary of the $\delta(^{37}\text{Cl})$ measurement uncertainties achieved during this study. The ranges of mole fractions included are 7 - 258 pmol mol^{-1} (CFC-11), 22 - 544 pmol mol^{-1} (CFC-12) and 1 - 81 pmol mol^{-1} (CFC-113), corresponding to approximate air ages of 1946 - 2012 (CFC-11), 1955 - 2013 (CFC-12) and 1962 - 2012 (CFC-113). A sample volume of approximately 200 ml was used for these measurements.

Compound	Sample source	Number of samples	Overall mean values	
			$\delta(^{37}\text{Cl})$ uncertainty / ‰	Mole fraction / pmol mol^{-1}
CFC-11	Fletcher firn	20	3.2	221
	NEEM 2009 firn	12	1.9	197
	Cape Grim archive	12	2.6	222
CFC-12	Fletcher firn	20	3.2	471
	NEEM 2009 firn	12	2.3	421
	Cape Grim archive	42	2.5	493
CFC-113	Fletcher firn	20	4.6	63
	NEEM 2009 firn	11	2.6	58
	Cape Grim archive	17	3.5	61

Tables 5.1 – 5.3 provide a summary of the $\delta(^{37}\text{Cl})$ and $\delta(^{13}\text{C})$ measurements made on CFC-11, CFC-12 and CFC-113 in this study. This information can act as a starting point for future work investigating the $\delta(^{37}\text{Cl})$ and $\delta(^{13}\text{C})$ of these trace gases in the atmosphere. At present, a constant chlorine and carbon emissions isotope delta is compatible with the tropospheric measurements presented in Chapter 3. However, measurement uncertainty is too high to preclude the possibility of a change in the average emissions isotope delta. Measuring the isotope delta of CFCs at their point of release (e.g. old refrigeration units) would allow this to be constrained directly. The results of this study disagree with $\delta(^{13}\text{C})$, CFC-12) measurements made by Zuiderweg et al. (2013). It is likely that a chromatographic interference in the Zuiderweg et al. (2013) data can account for this difference at low mole fractions. In an attempt to add weight to this conclusion, the

samples measured for $\delta(^{13}\text{C})$ of CFC-11 and CFC-12 by Zuiderweg et al. (2012) will be reanalysed using the UEA system (as described in this thesis). This analysis is an important task because it will determine whether $\delta(^{13}\text{C})$ measurements made using the systems described in this thesis and in Zuiderweg et al. (2013) are entirely comparable.

Zuiderweg et al. (2012) found a significant relative $^{13}\text{C}/^{12}\text{C}$ enrichment of CFC-11 and CFC-12 during UV photolysis experiments. This suggests that the stratospheric breakdown of these species will show a similar fractionation. It would be informative to make $\delta(^{13}\text{C})$ measurements of CFCs in stratospheric samples to calculate apparent stratospheric isotope fraction (ϵ_{app}) values. This constraint is currently missing from the global isotope budget of these gases.

Table 5.2. A summary of the overall $\delta(^{13}\text{C})$ measurement uncertainties achieved during this study. A comparison is made to the equivalent uncertainties achieved before the methodological improvements were implemented (Section 3.2.2). The range of mole fractions included are 20 - 258 pmol mol⁻¹ (CFC-11), 54 - 544 pmol mol⁻¹ (CFC-12) and 23 - 81 pmol mol⁻¹ (CFC-113) corresponding to approximate air ages of 1953 - 2009 (CFC-11), 1955 - 2009 (CFC-12) and 1975 - 2009 (CFC-113). A sample volume of approximately 600 ml was used for these measurements.

Compound	Sample source	Number of samples	Overall mean values		
			$\delta(^{13}\text{C})$ uncertainty / ‰	$\delta(^{13}\text{C})$ uncertainty before methodological improvements / ‰	Mole fraction / pmol mol ⁻¹
CFC-11	NEEM 2009 firn	11	2.4	3.5	201
CFC-12	NEEM 2009 firn	12	3.7	11.2	436
CFC-113	NEEM 2009 firn	10	1.9	10.0	71

Table 5.3. A summary of the ‘modern’ $\delta(^{13}\text{C})$ measurement uncertainties achieved during this study. A comparison is made to the equivalent uncertainties achieved before the methodological improvements were implemented (Section 3.2.2). The range of mole fractions included are 231 - 258 pmol mol^{-1} (CFC-11), 527 - 544 pmol mol^{-1} (CFC-12) and 75 - 81 pmol mol^{-1} (CFC-113) corresponding to approximate air ages of 1991 - 2009 (CFC-11), 1999 - 2009 (CFC-12) and 1996 - 2009 (CFC-113). A sample volume of approximately 600 ml was used for these measurements.

Compound	Sample source	Number of samples	Modern mean values		
			$\delta(^{13}\text{C})$ uncertainty / ‰	$\delta(^{13}\text{C})$ uncertainty before methodological improvements / ‰	Mole fraction / pmol mol^{-1}
CFC-11	NEEM 2009 firn	7	1.7	2.7	251
CFC-12	NEEM 2009 firn	9	3.1	9.6	529
CFC-113	NEEM 2009 firn	8	1.7	9.6	78

The techniques described in this thesis could be extended to other trace gases. For example, investigating the atmospheric isotope history of CFC-114 and CFC-115 would provide constraints regarding their interaction with the atmosphere, just as the present study has for CFC-11, CFC-12 and CFC-113. The AutoSpec instrument at UEA is run at a mass resolution of 1000, meaning that it is simpler to measure isotope ratios in gases without interference ions (e.g. CFCs do not contain hydrogen which can cause interference). This makes CFC-114 and CFC-115 good candidates for isotopic analysis. Also, the high sensitivity of the AutoSpec instrument opens up the possibility of measuring the isotope delta of trace gases in the small air samples extracted from ice cores. This means that gases with both anthropogenic and natural sources could be investigated (e.g. COS, CH₃Cl and CH₃Br).

The link between COS and the terrestrial carbon cycle makes this a species that should be targeted for isotopic analysis in firn and ice core air samples. However, measuring isotope ratios in COS presents an analytical challenge because the mass resolution of the AutoSpec will limit which fragments can be robustly measured. The molecular ion of COS (m/z 60) is typically measured because it produces the largest chromatograph peak. However, the isotopologues of this molecular ion are subject to significant isotopic interferences. For example, the presence of ^{18}O precludes the possibility of making robust $\delta(^{34}\text{S})$ measurements. In this case, measuring individual fragment ions may be the only way to measure sulphur isotopes in COS (i.e. by measuring the S^+ ion at m/z 32, 33 and 34). It is likely that this approach will stretch the sensitivity of the instrument because in this case individual fragment ions produce smaller peaks than the corresponding molecular ions. To maximise the chance of success, potential methodological optimisations should be investigated (e.g. as described in Section 3.2.2).

Finally, although the methodology changes outlined in Section 3.2.2 produced a significant advance in the $\delta(^{13}\text{C})$ measurement precision, the current analytical uncertainties (Tables 5.2 and 5.3) can be improved further through additional adjustments. By increasing the size of chromatographic peaks, there was a risk that the detector would become saturated, preventing its use. To avoid this and to allow for the day-to-day variation in AutoSpec performance, peaks were kept well below the upper limit. This conservative approach limited the size of the peaks and therefore the precision achieved. By performing daily optimisations and approaching closer to the upper limit of detection, improvements in precision can be achieved.

5.2 Carbonyl sulphide (COS) in ice and firn

COS is the most abundant sulphur-containing trace gas in the atmosphere and has a wide range of natural and anthropogenic sources and sinks (Montzka et al., 2011). Since the 1970s, studies have focused on quantifying the atmospheric abundance of COS in an attempt to better understand its ozone depletion potential and the implications this has for the atmosphere (e.g. Hanst et al., 1975; Bandy et al., 1992; Sturges et al., 2001). Recently, COS has been investigated with a view to determining the nature of the link it shares with the carbon cycle through its uptake by terrestrial vegetation (e.g. Stimler et al., 2010; Blonquist et al., 2011; Berry et al., 2013).

The potential use of COS in global modelling makes a well constrained Northern and Southern Hemisphere atmospheric history over the last century highly valuable. In the same way, measuring the mole fractions of COS and CO₂, as well as $\delta(^{13}\text{C}, \text{CO}_2)$ (in the same air sample) will better constrain the link between COS and terrestrial Gross Primary Production (GPP) in the ice core record.

5.2.1 Antarctic and Greenland ice cores

Due to the small size of the samples and the highly dynamic nature of the polar environment, making robust measurements of trace gases in ice core air is very challenging. This study has presented the results of COS measurements made on 30 ice core samples from NEEM (Greenland) and DE08, DML (BAS) and DSS (Antarctica). The extractions were performed and CO₂ and $\delta(^{13}\text{C}, \text{CO}_2)$ measurements made at the CMAR laboratories in Australia, with the COS analysis performed at UEA. The ice core drilling and the air extraction procedure did not introduce any contamination into the samples, with excellent measurements made at CMAR (Rubino et al., in preparation). This shows that the extraction and analysis system was highly effective and produced robust data (the most notable exception to this is COS).

The COS mole fraction measurements presented in this thesis show no substantial trends over the last 1000 years, broadly in agreement with the record reported by Aydin et al. (2008). This work was a significant technical challenge because it involved quantifying a trace compound (at an abundance of a few hundred pmol mol⁻¹), in small air samples (approximately 30 ml). However, these measurements were compromised by a previously unknown effect, leading to higher than expected values. Due to this post-extraction growth of COS, the measurements presented in this study cannot be used to support or refute the previously reported increase of COS mole fractions during the 1600s (Aydin et al., 2008). This growth effect was qualitatively constrained, but the complexity of the contributory factors precluded a quantitative assessment. The presence of water (through sublimation from the ice surface) was shown to be the most significant factor in the COS growth rate. To reduce this effect, the surface area to volume ratio of the sample should be minimised. This can be achieved by maximising the size of the sample and minimising the number of ice pieces per sample. Finally, improving the sample drying procedure would reduce the amount of water vapour in the samples. For example, a magnesium perchlorate water trap could be included in the ice extraction system.

In stainless steel extraction systems, it is strongly recommended that all surfaces are electro-polished and Silco-treated, decreasing the overall reactivity of the surface. The firm air samples measured in Section 4.2 were treated in this way and show good stability over periods of 4 (NEEM) and 7 (EDML) years. At the very least, surfaces in prolonged contact with extracted air (e.g. the sample traps) should be treated in this way. If constructing a new extraction system, an inert material (e.g. glass) could be used. However, it would be very difficult to use only glass in an extraction system because certain components are subjected to significant stresses. For example, in the CMAR system very low temperatures, high pressures and vigorous shaking are essential for a successful extraction. It seems that electro-polishing and Silco-treating the existing stainless steel systems at UEA and CMAR gives the highest chance of success. Following this approach, individual components should be tested before the system is fully integrated.

The logistical challenges associated with a collaboration between research groups in the UK (UEA) and Australia (CMAR) introduced additional potential sources of error. For example, transporting the ice from the UK to Australia left the samples vulnerable to partial melting and the long transport time meant that the success of the COS measurements was dependent on the sample's stability within the traps. In future studies, if the COS growth cannot be eliminated entirely, the measurements should be made as soon after the extraction as possible to minimise the growth effect. In practice, this means that the analysis should take place as soon as the trapped sample has been allowed to equilibrate. Eliminating the transport time by performing the extraction and COS analysis at UEA would limit the output of the extractions because CMAR provided CO₂ and $\delta(^{13}\text{C}, \text{CO}_2)$ measurements which cannot be performed at UEA. However, in any future study, the priority must be to achieve robust COS measurements. The collaboration outlined in this thesis enabled the direct comparison of COS, CO₂ and $\delta(^{13}\text{C}, \text{CO}_2)$ measurements in a single air sample (due to the large volume of the CMAR extractor vessel). This capability would be lost if only one laboratory were to undertake these measurements, although compromises could be made to achieve a similar outcome. For example, if each ice core sample were split along its length, one half could be sent to CMAR for CO₂ and $\delta(^{13}\text{C}, \text{CO}_2)$ analysis and the other half could be analysed for COS at UEA.

5.2.2 Northern and Southern Hemisphere firm air

Two new firm profiles of COS mole fractions have been presented. The air samples were collected from the NEEM (Greenland) and EDML (Antarctica) drilling sites. A firm

diffusion model developed at the Laboratoire de Glaciologie et Géophysique de l'Environnement (LGGE) was used to compare these new data with previously published COS atmospheric histories.

COS mole fractions measured at EDML are slightly lower than previously reported measurements from the South Pole (Montzka et al., 2004). It is likely that this small difference is caused by regional differences in the oceanic COS flux, although direct evidence is currently lacking.

The new NEEM data exhibit a large positive excursion between 65 and 50 m which is a feature not previously seen in the Northern Hemisphere record. Potential atmospheric causes of these unexpectedly high measurements were included in the firm model input scenarios. For example, the impact of a short duration, high intensity emission event was tested. This was done to simulate the effect of these atmospheric phenomena on the firm profile, to determine whether the changes imposed could produce the measured values. These sensitivity tests showed that the large positive excursion can be partially explained by a localised short duration, high intensity emission event. However, it is unlikely that an event of this size would occur and if it did, it would be clearly visible in the Southern Hemisphere record, which it is not. Also, the effects of this type of event would reach the diffusive upper section of the firm column, significantly altering the most recent measurements. As stated previously, the fit in the upper part of the firm is very good and there is no evidence of a large emission event. It is likely that in-situ production of COS caused the high measurements which are confined to a small section of the firm column. However, there is no direct evidence to support this and previous studies which have measured a variety of trace gases in these NEEM samples have not found conclusive evidence of in-situ production (Hogan, 2013; Petrenko et al., 2013; Helmig et al., 2014).

It would be beneficial to make additional Northern Hemisphere measurements, particularly covering the period of peak COS mole fractions. Using the LGGE firm diffusion model, it was determined that atmospheric processes cannot fully account for the measurements in this period. Supplementary measurements would provide a reliable atmospheric history over this period.

The recent partial reanalysis of these firm air samples revealed some evidence of sample degradation. To determine the full extent of this effect, a complete reanalysis should be carried out. Once a complete and robust set of COS measurements from Northern and Southern Hemisphere firm air are available, further modelling studies can be used to infer changes in its atmospheric budget. A full inversion to atmospheric trends using the LGGE

firm diffusion model should be undertaken to obtain robust COS atmospheric time series. These should then be used as an input parameter in a chemical transport model, e.g. GEOS-Chem (Suntharalingam et al., 2008), to investigate the evolution of the carbon cycle and regional variations in COS mole fractions.

Finally, as demonstrated in Chapter 3 and discussed in Section 5.1, the AutoSpec instrument described in this thesis is able to measure isotope ratios in trace gases. Making $\delta(^{34}\text{S})$ and even $\delta(^{33}\text{S})$ and $\delta(^{13}\text{C})$ measurements in COS on firn and ice core air is a reasonable goal for the team at UEA over the next few years. These measurements could potentially provide information regarding COS sources and sinks, better constraining its atmospheric budget.

Abbreviations

BAS	British Antarctic Survey
BFI	Bubble-free ice
c.	Circa
CFC	Chlorofluorocarbon
CNRS	Centre National de la Recherche Scientifique
COD	Close-off depth
COS	Carbonyl sulphide
CS ₂	Carbon disulphide
CMAR	CSIRO Marine and Atmospheric Research
CMDL	Climate Monitoring and Diagnostics Laboratory
CSIRO	Commonwealth Scientific and Industrial Research Organisation
δ	The isotope ratio difference between a standard and a sample
δ_T and δ_S	Subscripts of “T” and “S” refer to the troposphere and stratosphere, respectively
DEP	Dielectric profiling
D _{gas}	Diffusion Coefficient
DML	Dronning Maud Land
DMS	Dimethyl sulphide
EI-SIR	Electron Impact-Selected Ion Recording
ESLR	Earth System Research Laboratory
GC-MS	Gas Chromatography-Mass Spectrometry
GHG	Greenhouse gas
GPP	Gross primary production
GWP	Global warming potential
ICELAB	Ice Core Extraction Laboratory
Input scenario	An atmospheric COS mole fraction time series used as the input

	for a firm diffusion model (Section 4.2)
IRMS	Isotope Ratio Mass Spectrometry
LGGE	Laboratoire de Glaciologie et Géophysique de l'Environnement
M_{gas}	Molecular mass of a gas
m/z	Mass to charge ratio
MSA ⁻	Methane sulphonate
NEEM	North Greenland Eemian Ice Drilling Project
NH/SH	Northern Hemisphere/Southern Hemisphere
NOAA	National Oceanic and Atmospheric Administration
Nss SO ₄ ²⁻	Non sea salt sulphate
Output scenario	A depth profile of COS mole fractions produced by a firm diffusion model (Section 4.2)
ppbv	Parts per billion by volume
ppmv	Parts per million by volume
pptv	Parts per trillion by volume
PSCs	Polar stratospheric clouds
τ	Atmospheric lifetime
UEA	University of East Anglia
UV	Ultra violet light
VPDB	Vienna Pee Dee Belemnite
‰	Per mill

References

- Ahn, J., Brook, E. J., Mitchell, L., Rosen, J., McConnell, J. R., Taylor, K., Etheridge, D., and Rubino, M.: Atmospheric CO₂ over the last 1000 years: A high-resolution record from the West Antarctic Ice Sheet (WAIS) Divide ice core, *Global Biogeochemical Cycles*, 26, GB2027, doi:10.1029/2011GB004247, 2012.
- Allin, S. J., Laube, J. C., Witrant, E., Kaiser, J., McKenna, E., Dennis, P., Mulvaney, R., Capron, E., Martinerie, P., Röckmann, T., Blunier, T., Schwander, J., Fraser, P. J., Langenfelds, R. L., and Sturges, W. T.: Chlorine isotope composition in chlorofluorocarbons CFC-11, CFC-12 and CFC-113 in firn, stratospheric and tropospheric air, *Atmospheric Chemistry and Physics*, 15, 6867-6877, doi:10.5194/acp-15-6867-2015, 2015.
- Andreae, M. O. and Crutzen, P. J.: Atmospheric aerosols: Biogeochemical sources and role in atmospheric chemistry, *Science*, 276, 5315, 1052-1058, doi:10.1126/science.276.5315.1052, 1997.
- Andreas, E. L.: New estimates for the sublimation rate for ice on the Moon, *ICARUS*, 186, 1, 24-30, doi:10.1016/j.icarus.2006.08.024, 2007.
- Appenzeller, C., Holton, J. R., and Rosenlof, K. H.: Seasonal variation of mass transport across the tropopause, *Journal of Geophysical Research*, 101, 15071-15078, doi:10.1029/96JD00821, 1996.
- Assonov, S. S., Brenninkmeijer, C. A. M., and Jöckel, P.: The ¹⁸O isotope exchange rate between firn air CO₂ and the firn matrix at three Antarctic sites, *Journal of Geophysical Research*, 110, D18310, doi:10.1029/2005JD005769, 2005.
- Aydin, M., De Bruyn, W. J., and Saltzman, E. S.: Preindustrial atmospheric carbonyl sulfide (OCS) from an Antarctic ice core, *Geophysical Research Letters*, 29, 9, 1359, doi:10.1029/2002GL014796, 2002.
- Aydin, M., Williams, M. B., and Saltzman, E. S.: Feasibility of reconstructing paleoatmospheric records of selected alkanes, methyl halides, and sulphur gases from Greenland ice cores, *Journal of Geophysical Research*, 112, D7, D07312, doi:10.1029/2006JD008027, 2007.
- Aydin, M., Williams, M. B., Tatum, C., and Saltzman, E. S.: Carbonyl sulfide in air extracted from a South Pole ice core: a 2000 year record, *Atmospheric Chemistry and Physics*, 8, 24, 7533-7542, 2008.

- Aydin, M., Montzka, S. A., Battle, M. O., Williams, M. B., De Bruyn, W. J., Butler, J. H., Verhulst, K. R., Tatum, C., Gun, B. K., Plotkin, D. A., Hall, B. D., and Saltzman, E. S.: Post-coring entrapment of modern air in some shallow ice cores collected near the firn-ice transition: evidence from CFC-12 measurements in Antarctic firn air and ice cores, *Atmospheric Chemistry and Physics*, 10, 11, 5135-5144, doi:10.5194/acp-10-5135-2010, 2010.
- Aydin, M., Fudge, T. J., Verhulst, K. R., Nicewonger, M. R., Waddington, E. D., and Saltzman, E. S.: Carbonyl sulfide hydrolysis in Antarctic ice cores and an atmospheric history for the last 8000 years, *Journal of Geophysical Research: Atmospheres*, 119, 13, doi:10.1002/2014JD021618, 2014.
- Bandy, A. R., Thornton, D.C., Scott, D. L., Lalevic, M., Lewin, E. E., and Driedger, A. R.: A time-series for carbonyl sulfide in the northern-hemisphere, *Journal of Atmospheric Chemistry*, 14, 1-4, 527-534, doi:10.1007/BF00115256, 1992.
- Barnes, I., Becker, K. H., and Patroescu, I.: The tropospheric oxidation of dimethyl sulfide – a new source of carbonyl sulfide, *Geophysical Research Letters*, 21, 22, 2389-2392, doi:10.1029/94GL02499, 1994.
- Bartoli, G., Sarnthein, M., Weinelt, M., Erlenkeuser, H., Garbe-Schönberg, D., and Lea, D. W.: Final closure of Panama and the onset of northern hemisphere glaciation, *Earth and Planetary Science Letters*, 237, 1-2, 33-44, doi:10.1016/j.epsl.2005.06.020, 2005.
- Batenburg, A. M., Schuck, T. J., Baker, A. K., Zahn, A., Brenninkmeijer, C. A. M., and Röckmann, T.: The stable isotopic composition of molecular hydrogen in the tropopause region probed by the CARIBIC aircraft, *Atmospheric Chemistry and Physics*, 12, 4633-4646, doi:10.5194/acp-12-4633-2012, 2012.
- Battle, M., Bender, M., Sowers, T., Tans, P. P., Butler, J. H., Elkins, J. T., Conway, T., Zhang, N., Lang, P., and Clarke, A. D.: Atmospheric gas concentrations over the past century measured in air from firn at the South Pole, *Nature*, 383, 6597, 231-235, doi:10.1038/383231a0, 1996.
- Bernard, S., Röckmann, T. R., Kaiser, J., Barnola, J. M., Fischer, H., Blunier, T., and Chappellaz, J.: Constraints on N₂O budget changes since pre-industrial time from new firn air and ice core isotope measurements, *Atmospheric Chemistry and Physics*, 6, 493-503, doi:10.5194/acp-6-493-2006, 2006.

References

- Berry, J., Wolf, A., Campbell, J. E., Baker, I., Blake, N., Blake, D., Denning, A. S., Kawa, S. R., Montzka, S. A., Seibt, U., Stimler, K., Yakir, D., and Zhu, Z.: A coupled model of the global cycles of carbonyl sulfide and CO₂: A possible new window on the carbon cycle, *Journal of Geophysical Research: Biogeosciences*, 118, 842-852, doi:10.1002/jgrg.20068, 2013.
- Bindoff, N.L., Stott, P. A., AchutaRao, K. M., Allen, M. R., Gillett, N., Gutzler, D., Hansingo, K., Hegerl, G., Hu, Y., Jain, S., Mokhov, I. I., Overland, J., Perlwitz, J., Sebbari, R., and Zhang, X.: Detection and Attribution of Climate Change: from Global to Regional. In: *Climate Change 2013: The Physical Science Basis*. Contribution of Working Group I to the Fifth Assessment Report of the Intergovernmental Panel on Climate Change [Stocker, T.F., Qin, D., Plattner, G. – K., Tignor, M., Allen, S. K., Boschung, J., Nauels, A., Xia, Y., Bex V., and Midgley, P. M. (eds.)]. *Cambridge University Press*, Cambridge, United Kingdom and New York, NY, USA, 2013.
- Bingemer, H. G., Bürgermeister, S., Zimmermann, R. L., and Georgii, H. –W.: Atmospheric OCS: Evidence for a Contribution of Anthropogenic Sources?, *Journal of Geophysical Research: Atmospheres*, 95, D12, 20617-20622, doi:10.1029/JD095iD12p20617, 1990.
- Blonquist Jr, J. M., Montzka, S. A., Munger, J. W., Yakir, D., Desai, A. R., Dragoni, D., Griffis, T. J., Monson, R. K., Scott, R. L., and Bowling, D. R.: The potential of carbonyl sulfide as a proxy for gross primary production at flux tower sites, *Journal of Geophysical Research*, 116, G04019, doi:10.1029/2011JG001723, 2011.
- Bo, S., Siebert, M. J., Mudd, S. M., Sugden, D., Fujita, S., Xiangbin, C., Yunyun, J., Xueyuan, T., and Yuansheng, L.: The Gamburtsev mountains and the origin and early evolution of the Antarctic Ice Sheet, *Nature*, 459, 690-693, doi:10.1038/nature08024, 2009.
- Brenninkmeijer, C. A. M., Janssen, C., Kaiser, J., Röckmann, T., Rhee, T. S., and Assonov, S. S.: Isotope effects in the chemistry of atmospheric trace gases, *Chemical Reviews*, 103, 12, 5125–5162, doi:10.1021/cr020644k, 2003.
- Brühl, C., Lelieveld, J., Crutzen, P. J., and Tost, H.: The role of carbonyl sulphide as a source of stratospheric sulphate aerosol and its impact on climate, *Atmospheric Chemistry and Physics*, 12, 3, 1239-1253, doi:10.5194/acp-12-1239-2012, 2012.

- Buizert, C., Martinerie, P., Petrenko, V. V., Severinghaus, J. P., Trudinger, C. M., Witrant, E., Rosen, J. L., Orsi, A. J., Rubino, M., Etheridge, D. M., Steele, L. P., Hogan, C., Laube, J. C., Sturges, W. T., Levchenko, V. A., Smith, A. M., Levin, I., Conway, T. J., Dlugokencky, E. J., Lang, P. M., Kawamura, K., Jenk, T. M., White, J.W. C., Sowers, T., Schwander, J., and Blunier, T.: Gas transport in firn: multiple-tracer characterisation and model intercomparison for NEEM, Northern Greenland, *Atmospheric Chemistry and Physics*, 12, 9, 4259–4277, doi:10.5194/acp-12-4259-2012, 2012.
- Butler, J. H., Battle, M., Bender, M. L., Monzka, S. A., Clarke, A. D., Saltzman, E. S., Sucher, C. M., Severinghaus, J. P., and Elkins, J. W.: A record of atmospheric halocarbons during the twentieth century from polar firn air, *Nature*, 399, 6738, 749–755, doi:10.1038/21586, 1999.
- Campbell, J. E., Carmichael, G. R., Chai, T., Mena-Carrasco, M., Tang, Y., Blake, D. R., Blake, N. J., Vay, S. A., Collatz, G. J., Baker, I., Berry, J. A., Montzka, S. A., Sweeney, C., Schnoor, J. L., and Stanier, C. O.: Photosynthetic control of atmospheric carbonyl sulfide during the growing season, *Science*, 322, 5904, 1085-1088, doi:10.1126/science.1164015, 2008.
- Carr, J. R., Vieli, A., and Stokes, C.: Influence of sea ice decline, atmospheric warming, and glacier width on marine-terminating outlet glacier behavior in northwest Greenland at seasonal to interannual timescales, *Journal of Geophysical Research – Earth Surface*, 118, 1210-1226, doi:10.1002/jgrf.20088, 2013.
- Chapman, S.: A theory of upper-atmospheric ozone, *Memoirs of the Royal Meteorological Society*, 3, 26, 103-125, 1930.
- Chen, N. H. and Othmer, D. F.: New Generalized Equation for Gas Diffusion Coefficient, *Journal of Chemical and Engineering Data*, 7, 1, 37-41, doi:10.1021/je60012a011, 1962.
- Chin, M. and Davis, D. D.: Global sources and sinks of OCS and CS₂ and their distributions, *Global Biogeochemical Cycles*, 7, 2, 321-337, doi:10.1029/93GB00568, 1993.
- Clark, I. D., Henderson, L., Chappellaz, J., Fisher, D., Koerner, R., Worthy, D. E. J., Kotzer, T., Norman, A. L., and Barnola, J. M.: CO₂ isotopes as tracers of firn air diffusion and age in an Arctic ice cap with summer melting, Devon Island,

References

- Canada, *Journal of Geophysical Research – Atmospheres*, 112, D01301, doi:10.1029/2006JD007471, 2007.
- Clerbaux, C. and Cunnold, D. M.: Long-lived compounds, in: *Scientific Assessment of Ozone Depletion*, Chapter 1, Global Ozone Research and Monitoring Project - Report No. 50, 572 pp., World Meteorological Organization, Geneva, Switzerland, 2007.
- Coffey, M. and Brasseur, G.: Middle Atmospheric Ozone in *Atmospheric Chemistry and Global Change*, Chapter 14, *Oxford University Press*, 1999.
- Colbeck, S. C.: Air movement in snow due to windpumping, *Journal of Glaciology*, 35, 120, 209-213, 1989.
- Craig, H., Horibe, Y., and Sowers, T.: Gravitational separation of gases and isotopes in polar ice caps, *Science*, 242, 1675-1678, 1988.
- CRC: CRC Handbook of Chemistry and Physics, 83rd Edition, *CRC Press*, Boca Raton, FL, USA, 2002.
- Daniel, J. S., Velders, G. J. M., Morgenstern, O., Toohey, D. W., Wallington, T. J., and Wuebbles, D. J.: A Focus on Information and Options for Policymakers, in: *Scientific Assessment of Ozone Depletion*, Chapter 5, World Meteorological Organization, Geneva, 2011.
- DeBruyn, W. J., Swartz, E., Hu, J. H., Shorter, J. A., Davidovits, P., Worsnop, D. R., Zahniser, M. S., and Kolb, C. E.: Henry's Law solubilities and setchenow coefficients for biogenic reduced sulphur species obtained from gas-liquid uptake measurements, *Journal of Geophysical Research – Atmospheres*, 100, D4, 7245-7251, doi:10.1029/95JD00217, 1995.
- Elliott, S., Lu, E., and Rowland, F. S.: Rates and mechanisms for the hydrolysis of carbonyl sulfide in natural waters, *Environmental Science and Technology*, 23(4), 458–461, 1989.
- EPICA Community Members: Eight glacial cycles from an Antarctic ice core, *Nature*, 429, 623-628, doi:10.1038/nature02599, 2004.
- Etheridge, D. M., Pearman, G. I., and de Silva, F.: Atmospheric trace-gas variations as revealed by air trapped in an ice core from Law Dome, Antarctica, *Annals of Glaciology*, 10, 28–33, 1988.

- Etheridge, D. M., Pearman, G. I., and Fraser, P. J.: Changes in tropospheric methane between 1841 and 1978 from a high accumulation-rate Antarctic ice core, *Tellus Series B-Chemical and Physical Meteorology*, 44, 4, 282-294, doi:10.1034/j.1600-0889.1992.t01-3-00006.x, 1992.
- Etheridge, D. M., Steele, L. P., Langenfelds, R. L., Francey, R. J., Barnola, J. M., and Morgan, V. I.: Natural and anthropogenic changes in atmospheric CO₂ over the last 1000 years from air in Antarctic ice and firn, *Journal of Geophysical Research - Atmospheres*, 101 (D2), 4115–4128, doi:10.1029/95JD03410, 1996.
- Etheridge, D. M., Steele, L. P., Francey, R. J., and Langenfelds, R. L.: Atmospheric methane between 1000 A.D. and present: Evidence of anthropogenic emissions and climatic variability, *Journal of Geophysical Research*, 103, D13, 15979–15993, doi:10.1029/98JD00923, 1998.
- Fahey, D. W., and Hegglin, M. I., et al.: Twenty questions and answers about the ozone layer: 2010 update in *Scientific Assessment of Ozone Depletion: 2010*, Report number 52, Global Ozone Research Monitoring Project, World Meteorological Organisation, Geneva, 2010.
- Fäin, X., Ferrari, C. P., Dommergue, A., Albert, M. C., Battle, M., Severinghaus, J., Arnaud, L., Barnola, J. -M., Cairns, W., Barbante, C., and Boutron, C.: Polar firn air reveals large-scale impact of anthropogenic mercury emissions during the 1970s, *Proceedings of the National Academy of Sciences of the United States of America*, 106, 16114–16119, doi:10.1073/pnas.0905117106, 2009.
- Farman, J. C., Gardiner, B. G., and Shanklin, J. D.: Large losses of total ozone in Antarctica reveal seasonal ClO_x/NO_x interaction, *Nature*, 315, 6016, 207-210, doi:10.1038/315207a0, 1985.
- Fihey, J. L. and Simoneau, R.: Weld penetration variation in GTA welding of some 304L stainless steels. Presented at the American Welding Society Conference, Kansas City, MO, May 16-19, 1982.
- Francey, R. J., Allison, C. E., Etheridge, D. M., Trudinger, C. M., Enting, I. G., Leuenberger, M., Langenfelds, R. L., Michel, E., and Steele, L. P.: A 1000-year high precision record of δ¹³C in atmospheric CO₂, *Tellus Series B-Chemical and Physical Meteorology*, 51, 2, 170–193, doi:10.1034/j.1600-0889.1999.t01-1-00005.x, 1999.

References

- Frank, D. C., Esper, J., Raible, C. C., Buntgen, U., Trouet, V., Stocker, B., and Joos, F.: Ensemble reconstruction constraints on the global carbon cycle sensitivity to climate, *Nature*, 463, 7280, 527-U143, doi:10.1038/nature08769, 2010.
- Fried, A. and Tyndall, G.: Sulfur Compounds in *Atmospheric Chemistry and Global Change*, Chapter 10, *Oxford University Press*, 1999.
- Gannes, L. Z., Del Rio, C. M., and Koch, P.: Natural Abundance Variations in Stable Isotopes and their Potential Uses in Animal Physiological Ecology, *Comparative Biochemistry and Physiology – A Molecular and Integrative Physiology*, 119, 3, 725-737, doi:10.1016/S1095-6433(98)01016-2, 1998.
- Goldan, P. D., Fall, R., Kuster, W. C., and Fehsenfeld, F. C.: Uptake of COS by Growing Vegetation: A Major Tropospheric Sink, *Journal of Geophysical Research*, 93, D11, 14186-14192, doi:10.1029/JD093iD11p14186, 1988.
- Goldstein, A. H. and Shaw, S. L.: Isotopes of volatile organic compounds: an emerging approach for studying atmospheric budgets and chemistry, *Chemical Reviews*, 103, 12, 5025–5048, doi:10.1021/cr0206566, 2003.
- Greve, R. and Blatter, H.: Dynamics of Ice Sheets and Glaciers, *Springer*, Berlin, ISBN 978-3-642-03414-5, 2009.
- Haan, D. and Raynaud, D.: Ice core record of CO variations during the last two millennia: atmospheric implications and chemical interactions within the Greenland ice, *Tellus Series B-Chemical and Physical Meteorology*, 50, 253–262, 1998.
- Hanst, P. L., Spiller, L. L., Watts, D. M., Spence, J. W., and Miller, M. F.: Infrared measurements of fluorocarbons, carbon-tetrachloride, carbonyl sulfide, and other atmospheric trace gases, *Journal of the Air Pollution Control Association*, 25, 12, 1220-1226, 1975.
- Hartmann, D. L., Klein Tank, A. M. G., Rusticucci, M., Alexander, L. V., Brönnimann, S., Charabi, Y., Dentener, F. J., Dlugokencky, E. J., Easterling, D. R., Kaplan, A., Soden, B. J., Thorne, P. W., Wild, M., and Zhai, P. M.: Observations: Atmosphere and Surface. In: *Climate Change 2013: The Physical Science Basis*. Contribution of Working Group I to the Fifth Assessment Report of the Intergovernmental Panel on Climate Change [Stocker, T.F., Qin, D., Plattner, G. –K., Tignor, M., Allen, S. K., Boschung, J., Nauels, A., Xia, Y., Bex V., and Midgley, P. M. (eds.)]. Cambridge University Press, Cambridge, United Kingdom and New York, NY, USA, 2013.

- Helmig, D., Petrenko, V., Martinerie, P., Witrant, E., Röckmann, T., Zuiderweg, A., Holzinger, R., Hueber, J., Thompson, C., White, J. W. C., Sturges, W., Baker, A., Blunier, T., Etheridge, D., Rubino, M. and Tans, P.: Reconstruction of Northern Hemisphere 1950-2010 atmospheric non-methane hydrocarbons, *Atmospheric Chemistry and Physics*, 14, 3, 1463-1483, doi:10.5194/acp-14-1463-2014, 2014.
- Hoefs, J.: *Stable Isotope Geochemistry*, Springer, Berlin, ISBN: 978-3-540-70703-5, 2009.
- Hofstede, C. M., van de Wal, R. S. W., Kaspers, K. A., van den Broeke, M. R., Karlöf, L., Winther, J. -G., Isaksson, E., Lappégard, G., Mulvaney, R., Oerther, H., and Wilhelms, F.: Firn accumulation records for the past 1000 years on the basis of dielectric profiling of six cores from Dronning Maud Land, Antarctica, *Journal of Glaciology*, 50, 169, 279-291, doi:10.3189/172756504781830169, 2004.
- Hogan, C.: Time series of atmospheric halogenated trace gases from Arctic and Antarctic firn air (<https://ueaeprints.uea.ac.uk/45657/1/2013HoganCJPhD.pdf>), Ph.D. thesis, University of East Anglia, Norwich, 2013.
- Holloway, A. M. and Wayne, R. P.: *Atmospheric Chemistry*, *The Royal Society of Chemistry*, 2010.
- Holton, J. R.: On the global exchange of mass between the stratosphere and troposphere, *Journal of Atmospheric Science*, 47, 392-395, doi:10.1175/1520-0469(1990)047<0392:OTGEOM>2.0.CO;2, 1990.
- Hurley, M. D., Wallington, T. J., Buchanan, G. A., Gohar, L. K., Marston, G., and Shine, K. P.: IR spectrum and radiative forcing of CF₄ revisited, *Journal of Geophysical Research D: Atmospheres*, 110, 2, 1-8, doi:10.1029/2004JD005201, 2005.
- Ishijima, K., Sugawara, S., Kawamura, K., Hashida, G., Morimoto, S., Murayama, S., Aoki, S., and Nakazawa, T.: Temporal variations of the atmospheric nitrous oxide concentration and its $\delta^{15}\text{N}$ and $\delta^{18}\text{O}$ for the latter half of the 20th century reconstructed from firn air analyses, *Journal of Geophysical Research - Atmospheres*, 112, D3, D03305, doi:10.1029/2006JD007208, 2007.
- Jouzel, J., Masson-Delmotte, V., Cattani, O., Dreyfus, G., Falourd, S., Hoffmann, G., Minster, B., Nouet, J., Barnola, J. -M., Chappellaz, J., Fischer, H., Gallet, J. C., Johnsen, S., Leuenberger, M., Loulergue, L., Luethi, D., Oerter, H., Parrenin, F., Raisbeck, G., Raynaud, D., Schilt, A., Schwander, J., Selmo, E., Souchez, R., Spahni, R., Stauffer, B., Steffensen, J. P., Stenni, B., Stocker, T. F., Tison, J. L., Werner, M., and Wolff, E. W.: Orbital and millennial Antarctic climate variability

References

- over the past 800,000 years. *Science*, 317, 5839, 793-796, doi:10.1126/science.1141038, 2007.
- Kaiser, J., Brenninkmeijer, C. A. M., and Röckmann, T.: Intramolecular ^{15}N and ^{18}O fractionation in the reaction of N_2O with $\text{O}(^1\text{D})$ and its implications for the stratospheric N_2O isotope signature, *Journal of Geophysical Research - Atmospheres*, 107, D14, 4214, doi:10.1029/2001JD001506, 2002.
- Kaiser, J.: Stable isotope investigations of atmospheric nitrous oxide (<http://archimed.uni-mainz.de/pub/2003/0004/>), Ph.D. thesis, Johannes Gutenberg-Universität, Mainz, 2002.
- Kaiser, J., Engel, A., Borchers, R., and Röckmann, T.: Probing stratospheric transport and chemistry with new balloon and aircraft observations of the meridional and vertical N_2O isotope distribution, *Atmospheric Chemistry and Physics*, 6, 3535–3556, doi:10.5194/acp-6-3535-2006, 2006.
- Kettle, A. J., Kuhn, U., von Hobe, M., Kesselmeier, J., and Andreae, M. O.: Global budget of atmospheric carbonyl sulfide: Temporal and spatial variations of the dominant sources and sinks, *Journal of Geophysical Research – Atmospheres*, 107, D22, 4658, doi:10.1029/2002JD002187, 2002.
- Khalil, M. A. K. and Rasmussen, R. A.: Global sources, lifetimes and mass balances of carbonyl sulfide (OCS) and carbon disulphide (CS_2) in the Earth's atmosphere, *Atmospheric Environment*, 18, 9, 1805-1813, doi:10.1016/0004-6981(84)90356-1, 1984.
- Kluczewski, S. M., Brown, K. A., and Bell, J. N. B.: Deposition of [^{35}S]-carbonyl sulfide to vegetable crops, *Radiation Protection Dosimetry*, 11, 3, 173-177, 1985.
- Kourtidis, K. A., Borchers, R., Fabian, P., and Harnisch, J.: Carbonyl sulfide (COS) measurements in the Arctic polar vortex, *Geophysical Research Letters*, 22, 4, 393-396, doi:10.1029/94GL03306, 1995.
- Lamarque, J.-F., Bond, T. C., Eyring, V., Granier, C., Heil, A., Klimont, Z., Lee, D., Liousse, C., Mieville, A., Owen, B., Schultz, M. G., Shindell, D., Smith, S. J., Stehfest, E., Van Aardenne, J., Cooper, O. R., Kainuma, M., Mahowald, N., McConnell, J. R., Naik, V., Riahi, K., and van Vuuren, D. P.: Historical (1850–2000) gridded anthropogenic and biomass burning emissions of reactive gases and aerosols: methodology and application, *Atmospheric Chemistry and Physics*, 10, 7017–7039, doi:10.5194/acp-10-7017-2010, 2010.

- Landais, A., Barnola, J. M., Kawamura, K., Caillon, N., Delmotte, M., Van Ommen, T., Dreyfus, G., Jouzel, J., Masson-Delmotte, V., Minster, B., Freitag, J., Leuenberger, M., Schwander, J., Huber, C., Etheridge, D., and Morgan, V.: Firn-air $\delta^{15}\text{N}$ in modern polar sites and glacial-interglacial ice: a model-data mismatch during glacial periods in Antarctica?, *Quaternary Science Reviews*, 25, 1-2, 49-62, doi:10.1016/j.quascirev.2005.06.007, 2006.
- Landsat Image Mosaic of Antarctica (LIMA) Project: <http://lima.usgs.gov/>
- Langenfelds, R. J., Fraser, P. J., Francey, R. J., Steele, L. P., Porter, L. W., and Allison, C. E.: The Cape Grim air archive: The first seventeen years, in *Baseline 94–95*, edited by: Francey, R. J., Dick, A. L., and Derek, N., 53–70, Bur. Meteorol. and CSIRO Atmos. Res., Melbourne, Victoria, Australia, 1996.
- Laube, J. C.: Determination of the distribution of halocarbons in the tropical upper troposphere and stratosphere (<http://publikationen.ub.uni-frankfurt.de/opus4/frontdoor/index/index/docId/5975>), Ph.D. thesis, Universität in Frankfurt, 2008.
- Laube, J. C., Kaiser, J., Sturges, W. T., Bönisch, H., and Engel, A.: Chlorine Isotope Fractionation in the Stratosphere, *Science*, 329, 5996, 1167, doi:10.1126/science.1191809, 2010a.
- Laube, J. C., Martinerie, P., Witrant, E., Blunier, T., Schwander, J., Brenninkmeijer, C. A. M., Schuck, T. J., Bolder, M., Röckmann, T., van der Veen, C., Bönisch, H., Engel, A., Mills, G. P., Newland, M. J., Oram, D. E., Reeves, C. E., and Sturges, W. T.: Accelerating growth of HFC-227ea (1,1,1,2,3,3,3-heptafluoropropane) in the atmosphere, *Atmospheric Chemistry and Physics*, 10, 13, 5903–5910, doi:10.5194/acp-10-5903-2010, 2010b.
- Laube, J. C., Hogan, C., Newland, M. J., Mani, F. S., Fraser, P. J., Brenninkmeijer, C. A. M., Martinerie, P., Oram, D. E., Röckmann, T., Schwander, J., Witrant, E., Mills, G. P., Reeves, C. E., and Sturges, W. T.: Distributions, long term trends and emissions of four perfluorocarbons in remote parts of the atmosphere and firn air, *Atmospheric Chemistry and Physics*, 12, 9, 4081-4090, doi:10.5194/acp-12-4081-2012, 2012.
- Laube, J. C., Keil, A., Bonisch, H., Engel, A., Röckmann, T., Volk, C. M., and Sturges, W. T.: Observation-based assessment of stratospheric fractional release, lifetimes,

References

- and ozone depletion potentials of ten important source gases, *Atmospheric Chemistry and Physics*, 13, 5, 2779-2791, doi:10.5194/acp-13-2779-2013, 2013.
- Laube, J. C., Newland, M. J., Hogan, C., Brenninkmeijer, C. A. M., Fraser, P. J., Martinerie, P., Oram, D. E., Reeves, C. E., Röckmann, T., Schwander, J., Witrant, E., and Sturges, W. T.: Newly detected ozone-depleting substances in the atmosphere, *Nature Geosciences*, 7, 4, 266-269, doi:10.1038/ngeo2109, 2014.
- Leuenberger, M. and Lang, C.: Thermal diffusion: An important aspect in studies of static air columns such as firn air, sand dunes, and soil air, in: Isotope aided studies of atmospheric carbon dioxide and other greenhouse gases – Phase II, IAEA, Vienna, 2002.
- Liu, S. and Ridley, B.: Tropospheric Ozone in *Atmospheric Chemistry and Global Change*, Chapter 13, *Oxford University Press*, 1999.
- Lüthi, D., LeFloch, M., Bereiter, B., Blunier, T., Barnola, J. –M., Siegenthaler, U., Raynaud, D., Jouzel, J., Fischer, H., Kawamura, K., and Stocker, T. F.: High-resolution carbon dioxide concentration record 650,000-800,000 years before present, *Nature*, 453, 7193, 379-382, doi:10.1038/nature06949, 2008.
- Loulergue, L., Schilt, A., Spahni, R., Masson-Delmotte, V., Blunier, T., Lemieux, B., Barnola, J.- M., Raynaud, D., Stocker, T. F., and Chappellaz, J.: Orbital and millennial-scale features of atmospheric CH₄ over the past 800,000 years, *Nature*, 453, 7193, 383-386, doi:10.1038/nature06950, 2008.
- Mani, F. S.: Measurements of $\delta^{15}\text{N}$ of nitrogen gas and composition of trace gases in air from firn and ice cores (https://ueaeprints.uea.ac.uk/10588/1/Thesis_mani_f_2010.pdf), Ph.D. thesis, University of East Anglia, Norwich, 2010.
- MacFarling Meure, C., Etheridge, D. E., Trudinger, C., Steele, P., Langenfelds, R., van Ommen, T., Smith, A., and Elkins, J.: Law Dome CO₂, CH₄ and N₂O ice core records extended to 2000 years BP, *Geophysical Research Letters*, 33, 14, L14810, doi:10.1029/2006GL026152, 2006.
- Martinerie, P., Nourtier-Mazaauric, E., Barnola, J.-M., Sturges, W. T., Worton, D. R., Atlas, E., Gohar, L. K., Shine, K. P., and Brasseur, G. P.: Long-lived halocarbon trends and budgets from atmospheric chemistry modelling constrained with measurements in polar firn, *Atmospheric Chemistry and Physics*, 9, 12, 3911–3934, doi:10.5194/acp-9-3911-2009, 2009.

- McCarthy, M. C., Connell, P., and Boering, K. A.: Isotopic fractionation of methane in the stratosphere and its effect on free tropospheric isotopic compositions, *Geophysical Research Letters*, 28, 3657-3660, doi:10.1029/2001GL013159, 2001.
- McKenna, E.: Investigation of the stratospheric isotope fractionation of chlorine and bromine in haloalkanes, Master's thesis, School of Environmental Sciences, University of East Anglia, UK, 2011.
- Mitchell, L. E., Brook, E. J., Sowers, T., McConnell, J. R., and Taylor, K.: Multidecadal variability of atmospheric methane, 1000–1800 C.E., *Journal of Geophysical Research-Biogeosciences*, 116, G02007, doi:10.1029/2010JG001441, 2011.
- Molina, M. J. and Rowland, F. S.: Stratospheric sink for chlorofluoromethanes – chlorine atomic-catalysed destruction of ozone, *Nature*, 249, 5460, 810-812, doi:10.1038/249810a0, 1974.
- Montzka, S. A., Aydin, M., Battle, M., Butler, J. H., Saltzman, E. S., Hall, B. D., Clarke, A. D., Mondeel, D., and Elkins, J. W.: A 350-year atmospheric history of carbonyl sulfide inferred from Antarctic firn air and air trapped in ice, *Journal of Geophysical Research – Atmospheres*, 109, D22, D22302, doi:10.1029/2004JD004686, 2004.
- Montzka, S. A., Calvert, P., Hall, B. D., Elkins, J. W., Conway, T. J., Tans, P. P., and Sweeney, C.: On the global distribution, seasonality, and budget of atmospheric carbonyl sulfide (COS) and some similarities to CO₂, *Journal of Geophysical Research – Atmospheres*, 112, D9, D09302, doi:10.1029/2006JD007665, 2007.
- Montzka, S. A., Reimann, S., Engel, A., Kruger, K., O'Doherty, S., Sturges, W. T., et al.: Ozone depleting substances (ODSs) and related chemicals. In: *Scientific Assessment of Ozone Depletion*, Report number 52, Chapter 1, Global Ozone Research Monitoring Project, World Meteorological Organisation, Geneva, 2011.
- Mu, Y. J., Wu, H., Zhang, X. S., and Jiang, G. B.: Impact of anthropogenic sources on carbonyl sulfide in Beijing City, *Journal of Geophysical Research – Atmospheres*, 107, D24, 4769, doi:10.1029/2002JD002245, 2002.
- Mu, Y. J., Wu, H., Wu, P. Z., and Wang, Y. S.: Vertical distributions of COS and CS₂ in Beijing City, *Journal of Environmental Sciences – China*, 16, 2, 226-229, 2004.
- Mulvaney, R., Oerther, H., Peel, D. A., Graf, W., Arrowsmith, C., Pasteur, E. C., Knight, B., Littot, G. C., and Miners, W. D.: 1000 year ice-core records from Berkner

References

- Island, Antarctica, *Annals of Glaciology*, 35, 45-51, doi:10.3189/172756402781817176, 2002.
- Mulvaney, R., Triest, J., and Alemany, O.: The James Ross Island and the Fletcher Promontory ice-core drilling projects, *Annals of Glaciology*, 55, 68, 179-188, doi:10.3189/2014AoG68A044, 2014.
- NEEM Community Members: Eemian interglacial reconstructed from a Greenland folded ice core, *Nature*, 493, 7433, 489-494, doi:10.1038/nature11789, 2013.
- NEEM ice core drilling project: <http://neem.dk/>
- Nevison, C. D., Keeling, R. F., Weiss, R. F., Popp, B. N., Fraser, P. J., Porter, L. W., and Hess, P. G.: Southern Ocean ventilation inferred from seasonal cycles of atmospheric N₂O and O₂/N₂ at Cape Grim, Tasmania, *Tellus Series B-Chemical and Physical Meteorology*, 57, 3, 218-229, doi:10.1111/j.1600-0889.2005.00143.x, 2005.
- Nevison, C. D., Dlugokencky, E., Dutton, G., Elkins, J. W., Fraser, P., Hall, B., Krummel, P. B., Langenfelds, R. L., O'Doherty, S., Prinn, R. G., Steele, L. P., and Weiss, R. F.: Exploring causes of interannual variability in the seasonal cycles of tropospheric nitrous oxide, *Atmospheric Chemistry and Physics*, 11, 8, 3713-3730, doi:10.5194/acp-11-3713-2011, 2011.
- NOAA global mean CO₂ level available at: <http://www.esrl.noaa.gov/gmd/ccgg/trends/global.html>
- NOAA ground-based CCl₄ data and brief description available at: <http://www.esrl.noaa.gov/gmd/hats/combined/CCl4.html>.
- NOAA ground-based COS data available at: <http://www.esrl.noaa.gov/gmd/hats/gases/OCS.html>.
- Notholt, J., Luo, B. P., Fueglistaler, S., Weisenstein, D., Rex, M., Lawrence, M. G., Bingemer, H., Wohltmann, I., Corti, T., Warneke, T., von Kuhlmann, R., and Peter, T.: Influence of tropospheric SO₂ emissions on particle formation and the stratospheric humidity, *Geophysical Research Letters*, 32, 7, 1-4, doi:10.1029/2004GL022159, 2005.
- Nye, J. F.: Correction factor for accumulation measured by the thickness of the annual layers in an ice sheet, *Journal of Glaciology*, 4, 785-788, 1963.

- Park, S., Croteau, P., Boering, K. A., Etheridge, D. M., Ferretti, D., Fraser, P. J., Kim, K. R., Krummel, P. B., Langenfelds, R. L., van Ommen, T. D., Steele, L. P., and Trudinger, C. M.: Trends and seasonal cycles in the isotopic composition of nitrous oxide since 1940, *Nature Geosciences*, 5, 4, 261-265, doi:10.1038/NGEO1421, 2012.
- Petrenko, V. V., Martinerie, P., Novelli, P., Etheridge, D. M., Levin, I., Wang, Z., Blunier, T., Chappellaz, J., Kaiser, J., Lang, P., Steele, L. P., Hammer, S., Mak, J., Langenfelds, R. L., Schwander, J., Severinghaus, J. P., Witrant, E., Petron. G., Battle, M. O., Forster, G., Sturges, W. T., Lamarque, J. -F., Steffen, K. and White, J. W. C.: A 60 yr record of atmospheric carbon monoxide reconstructed from Greenland firn air, *Atmospheric Chemistry and Physics*, 13, 15, 7567-7585, doi:10.5194/acp-13-7567-2013, 2013.
- Protoschill-Krebs, G. and Kesselmeier, J.: Enzymatic pathways for the consumption of carbonyl sulfide (COS) by higher-plants, *Botanica Acta*, 105, 3, 206-212, 1992.
- Protoschill-Krebs, G., Wilhelm, C., and Kesselmeier, J.: Consumption of carbonyl sulphide (COS) by higher plant carbonic anhydrase (CA), *Atmospheric Environment*, 30, 18, 3151-3156, doi:10.1016/1352-2310(96)00026-X, 1996.
- Ramaswamy, V., Boucher, O., Haigh, J., Hauglustaine, D., Haywood, J., Myhre, G., Nakajima, T., Shi, G. Y., and Solomon, S.: Radiative Forcing of Climate Change. In: *Climate Change 2001: The Physical Science Basis*. Contribution of Working Group I to the Third Assessment Report of the Intergovernmental Panel on Climate Change [Houghton, J. T., Ding, Y., Griggs, D. J., Noguer, M., van der Linden, P. J., Dai, X., Maskell, K., and Johnson, C. A. (eds.)]. *Cambridge University Press*, Cambridge, United Kingdom and New York, NY, USA, 2001.
- Rasmussen, S. O., Abbott, P. M., Blunier, T., Bourne, A. J., Brook, E., Buchardt, S. L., Buizert, C., Chappellaz, J., Clausen, H. B., Cook, E., Dahl-Jensen, D., Davies, S. M., Guillevic, M., Kipfstuhl, S., Laepple, T., Seierstad, I. K., Severinghaus, J. P., Steffensen, J. P., Stowasser, C., Svensson, A., Vallelonga, P., Vinther, B. M., Wilhelms, F., and Winstrup, M.: A first chronology for the North Greenland Eemian Ice Drilling (NEEM) ice core, *Climate of the Past*, 9, 6, 2713-2730, doi:10.5194/cp-9-2713-2013, 2013.
- Rinsland, C. P., Goldman, A., Mahieu, E., Zander, R., Notholt, J., Jones, N. B., Griffith, D. W. T., Stephen, T. M., and Chiou, L. S.: Ground-based infrared spectroscopic

References

- measurements of carbonyl sulfide: Free tropospheric trends from a 24-year time series of solar absorption measurements, *Journal of Geophysical Research*, 107, D22, 4657, doi:10.1029/2002JD002522, 2002.
- Rinsland, C. P., Chiou, L., Mahieu, E., Zander, R., Boone, C. D., and Bernath, P. F.: Measurements of long-term changes in atmospheric OCS (carbonyl sulfide) from infrared solar observations, *Journal of Quantitative Spectroscopy and Radiative Transfer*, 109, 2679-2686, doi:10.1016/j.jqsrt.2008.07.008, 2008.
- Redeker, K. R., Davis, S., and Kalin, R. M.: Isotope values of atmospheric halocarbons and hydrocarbons from Irish urban, rural, and marine locations, *Journal of Geophysical Research*, 112, D16, D16307, doi:10.1029/2006JD007784, 2007.
- Röckmann, T., Kaiser, J. and Brenninkmeijer, C. A. M.: The isotopic fingerprint of the pre-industrial and the anthropogenic N₂O source, *Atmospheric Chemistry and Physics*, 3, 315–323, doi:10.5194/acp-3-315-2003, 2003.
- Röckmann, T. and Levin, I.: High-precision determination of the changing isotopic composition of atmospheric N₂O from 1990-2002, *Journal of Geophysical Research - Atmospheres*, 110, D21, D21304, doi:10.1029/2005JD006066, 2005.
- Rommelaere, V., Arnaud, L., and Barnola, J. –M.: Reconstructing recent atmospheric trace gas concentrations from polar firm and bubbly ice data by inverse methods, *Journal of Geophysical Research: Atmospheres*, 102, 25, 30069-30083, 1997.
- Rossberg, M., Lendle, W., Pfleiderer, G., Tögel, A., Dreher, E., Langer, E., Rassaerts, H., Kleinschmidt, P., Strack, P., Cook, R., Beck, U., Lipper, K., Torkelson, T. R., Löser, E., Beutel, K. K. and Mann, T.: Chlorinated Hydrocarbons, Ullmann's Encyclopedia of Industrial Chemistry, 6th edition, Wiley-VCH, 2003.
- Rubino, M., Etheridge, D. M., Trudinger, C., Allison, C. E., Battle, M. O., Langenfelds, R. L., Steele, L. P., Curran, M., Bender, M., White, J. W. C., Jenk, T. M., Blunier, T., and Francey, R. J.: A revised 1000 year atmospheric d¹³C-CO₂ record from Law Dome and South Pole, Antarctica. *Journal of Geophysical Research - Atmospheres*, 118, 15, 8482–8499, doi:10.1002/jgrd.50668, 2013.
- Rubino, M. et al.: Atmospheric CO₂ and d¹³C-CO₂ reconstructions of the Little Ice Age from Antarctic ice cores, in preparation.

- Sandalls, F. J., and Penkett, S. A.: Measurements of carbonyl sulphide and carbon disulphide in the atmosphere, *Atmospheric Environment*, 11, 2, 197-199, doi:10.1016/0004-6981(77)90227-X, 1977.
- Sandoval-Soto, L., Stanimirov, M., von Hobe, M., Schmitt, V., Valdes, J., Wild, A., and Kesselmeier, J.: Global uptake of carbonyl sulfide (COS) by terrestrial vegetation: Estimates corrected by depositional velocities normalized to the uptake of carbon dioxide (CO₂), *Biogeosciences*, 2, 2, 125-132, 2005.
- Sarmiento, J. L. and Gruber, N.: Sinks for anthropogenic carbon, *Physics Today*, 55, 8, 30-36, doi:10.1063/1.1510279, 2002.
- Schilt, A., Baumgartner, M., Blunier, T., Schwander, J., Spahni, R., Fischer, H., and Stocker, T. F.: Glacial–interglacial and millennial-scale variations in the atmospheric nitrous oxide concentration during the last 800,000 years, *Quaternary Science Review*, 29, 182–192, doi:10.1016/j.quascirev.2009.03.011, 2010.
- Schmitt, J., Seth, B., Köhler, P., Willenbring, J. K., and Fischer, H.: A new ice core proxy of continental weathering and its feedback with atmospheric CO₂, *European Geosciences Union General Assembly*, EGU2012-7177, April 2012.
- Schmitt, J., Seth, B., Köhler, P., Willenbring, J., and Fischer, H.: Atmospheric CF₄ Trapped in Polar Ice – A New Proxy for Granite Weathering, *Mineralogical Magazine*, 77(5) 2160, 2013.
- Schwander, J.: The transformation of snow to ice and occlusion of gases, in: *The Environmental Record in Glaciers and Ice Sheets*, John Wiley & Sons, Inc., H. O. and C. C. Langway (Eds.), New York, 53-67, 1989.
- Schwander, J., Barnola, J. M., Andrie, C., Leuenberger, M., Ludin, A., Raynaud, D., and Stauffer, B.: The age of the air in the firn and the ice at Summit, Greenland, *Journal of Geophysical Research: Atmospheres*, 98, D2, 2831–2838, doi:10.1029/92JD02383, 1993.
- Schwander, J., Sowers, T., Barnola, J. –M., Blunier, T., Fuchs, A., and Malaizé, B.: Age scale of the air in the summit ice: Implications for glacial-interglacial temperature change, *Journal of Geophysical Research: Atmospheres*, 102, 16, 19483-19493, 1997.

References

- Seibt, U., Kesselmeier, J., Sandoval-Soto, L., Kuhn, U., and Berry, J. A.: A kinetic analysis of leaf uptake of COS and its relation to transpiration, photosynthesis and carbon isotope fractionation, *Biogosciences*, 7, 333-341, 2010.
- Severinghaus, J. P., Grachev, A., and Battle, M.: Thermal fractionation of air in polar firn by seasonal temperature gradients, *Geochemistry Geophysics Geosystems*, Volume 2, Paper number 2000GC000146, 2001.
- Severinghaus, J. P., Grachev, A., Luz, B., and Caillon, N.: A method for precise measurement of argon 40/36 and krypton/argon ratios in trapped air in polar ice with applications to past firn thickness and abrupt climate change in Greenland and at Siple Dome, Antarctica, *Geochimica et Cosmochimica Acta*, 67, 3, 325-343, doi:10.1016/S0016-7037(02)00965-1, 2003.
- Siegenthaler, U., Monnin, E., Kawamura, K., Spahni, R., Schwander, J., Stauffer, B., Stocker, T. F., Barnola, J. M., and Fischer, H.: Supporting evidence from the EPICA Dronning Maud Land ice core for atmospheric CO₂ changes during the past millennium, *Tellus Series B-Chemical and Physical Meteorology*, 57, 1, 51-57, doi:10.1111/j.1600-0889.2005.00131.x, 2005.
- Skoog, D. A., West, D. M., Holler, F. J., and Crouch, S. R.: Fundamentals of Analytical Chemistry, *Saunders College Publishing*, 2004.
- Sowers, T., Bender, M., Raynaud, D., and Korotkevich, Y. S.: $\delta^{15}\text{N}$ of N₂ in air trapped in polar ice: a tracer of gas transport in the firn and a possible constraint on ice age-gas age differences, *Journal of Geophysical Research*, 97, D14, 15683-15697, 1992.
- Sowers, T., Rodebaugh, A., Yoshida, N., and Toyoda, S.: Extending records of the isotopic composition of the atmospheric N₂O back to 1800 AD from air trapped in snow at the South Pole and the Greenland Ice Sheet Project II ice core, *Global Biogeochemical Cycles*, 16, 4, 1129, doi:10.1029/2002GB001911, 2002.
- Spahni, R., Chappellaz, J., Stocker, T. F., Loulergue, L., Hausammann, G., Kawamura, K., Flückiger, J., Schwander, J., Raynaud, D., Masson-Delmotte, V., and Jouzel, J.: Atmospheric methane and nitrous oxide of the late pleistocene from Antarctic ice cores, *Science*, 310, 1317–1321, doi:10.1126/science.1120132, 2005.
- SPARC: Report on the lifetimes of stratospheric ozone-depleting substances, their replacements, and related species, edited by: Ko, M., Newman, P., Reimann, S., Strahan, S., SPARC Report No. 6, WCRP-15, Zurich, Switzerland, 2013.

- Stedman, D. H., Creech, M. Z., Cloke, P. L., Kesler, S. E., and Gardner, M., D.: Formation of CS₂ and OCS from decomposition of metal sulfides, *Geophysical Research Letters*, 11, 9, 858-860, 1984.
- Stimler, K., Montzka, S. A., Berry, J. A., Rudich, Y., and Yakir, D.: Relationships between carbonyl sulfide (COS) and CO₂ during leaf gas exchange, *New Phytologist*, 186, 869-878, doi:10.1111/j.1469-8137.2010.03218.x, 2010.
- Sturges, W. T., Penkett, S. A., Barnola, J. M., Chappellaz, J., Atlas, E., and Stroud, V.: A long-term record of carbonyl sulfide (COS) in two hemispheres from firn air measurements, *Geophysical Research Letters*, 28, 21, 4095-4098, doi:10.1029/2001GL013958, 2001.
- Sturges, W. T., Oram, D. E., Laube, J. C., Reeves, C. E., Newland, M. J., Hogan, C., Martinerie, P., Witrant, E., Brenninkmeijer, C. A. M., Schuck, T. J., and Fraser, P. J.: Emissions halted of the potent greenhouse gas SF₅CF₃, *Atmospheric Chemistry and Physics*, 12, 8, 3653–3658, doi:10.5194/acp-12-3653-2012, 2012.
- Sturrock, G. A., Etheridge, D. M., Trudinger, C. M., Fraser, P. J., and Smith, A. M.: Atmospheric histories of halocarbons from analysis of Antarctic firn air: Major Montreal Protocol species, *Journal of Geophysical Research: Atmospheres*, 107, D24, 4765, doi:10.1029/2002JD002548, 2002.
- Sugawara, S., Nakazawa, T., Shirakawa, Y., Kawamura, K., Aoki, S., Machida, T., and Honda, H.: Vertical profile of the carbon isotopic ratio of stratospheric methane over Japan, *Geophysical Research Letters*, 24, 2989-2992, doi:10.1029/97GL03044, 1997.
- Suntharalingam, P., Kettle, A. J., Montzka, S. M., and Jacob, D. J.: Global 3-D model analysis of the seasonal cycle of atmospheric carbonyl sulfide: Implications for terrestrial vegetation uptake, *Geophysical Research Letters*, 35, 19, doi:10.1029/2008GL034332, 2008.
- Thompson, H. W., Kearton, L. F., and Lamb, S. A.: The Kinetics of the Reaction between Carbonyl Sulfide and Water, *Journal of the Chemical Society*, 238, 1033–1037, 1935.
- Thornton, D. C., Bandy, A. R., Blomquist, B. W., and Anderson, B. E.: Impact of anthropogenic and biogenic sources and sinks on carbonyl sulfide in the North Pacific troposphere, *Journal of Geophysical Research – Atmospheres*, 101, D1, 1873-1881, doi:10.1029/95JD00617, 1996.

References

- Trenberth, K. E. and Guillemot, C. J.: The total mass of the atmosphere, *Journal of Geophysical Research – Atmospheres*, 99, D11, 23079-23088, doi:10.1029/94JD02043, 1994.
- Trenberth, K. E., Fasullo, J. T., and Keihl, J.: Earth's global energy budget, *Bulletin of the American Meteorological Society*, 90, 3, 311-323, doi:10.1175/2008BAMS2634.1, 2009.
- Trudinger, C. M., Enting, I. G., Etheridge, D. M., Francey, R. J., Levchenko, V. A., Steele, L. P., Raynaud, D., and Arnaud, L.: Modeling air movement and bubble trapping in firn, *Journal of Geophysical Research: Atmospheres*, 102, D6, 6747-6763, 1997.
- Trudinger, C. M., Enting, I. G., Francey, R. J., Etheridge, D. M., and Rayner, P. J.: Long-term variability in the global cycle inferred from a high-precision CO₂ and δ¹³C ice-core record, *Tellus Series B-Chemical and Physical Meteorology*, 51, 2, 233-248, doi:10.1034/j.1600-0889.1999.t01-1-00009.x, 1999.
- Trudinger, C. M., Enting, I. G., and Rayner, P. J.: Kalman filter analysis of ice core data 1. Method development and testing the statistics, *Journal of Geophysical Research: Atmospheres*, 107, 20, 4-1-4-14, doi:10.1029/2001JD001111, 2002a.
- Trudinger, C. M., Enting, I. G., Rayner, P. J., and Francey, J. R.: Kalman filter analysis of ice core data 2. Double deconvolution of CO₂ and δ¹³C measurements, *Journal of Geophysical Research: Atmospheres*, 107, 20, 5-1-5-24, doi:10.1029/2001JD001112, 2002b.
- Trudinger, C. M., Enting, I., Etheridge, D., Francey, R., and Rayner, P. J.: The carbon cycle over the past 1000 years inferred from the inversion of ice core data, in *A History of Atmospheric CO₂ and its Effects on Plants, Animals and Ecosystems*, vol. 177, edited by J. R. Elheringer et al., pp. 329-349, Springer, New York, 2005.
- Ulshofer, V. S., Uher, G., and Andreae, M. O.: Evidence for a winter sink of atmospheric carbonyl sulfide in the north-east Atlantic Ocean, *Geophysical Research Letters*, 22, 19, 2601-2604, doi:10.1029/95GL02656, 1995.
- Ulshofer, V. S., Flock, O. R., Uher, G., and Andreae, M. O.: Photochemical production and air-sea exchange of carbonyl sulfide in the eastern Mediterranean Sea, *Marine Chemistry*, 53, 1-2, 25-39, doi:10.1016/0304-4203(96)00010-2, 1996.

- Velders, G. J. M. and Daniel, J. S.: Uncertainty analysis of projections of ozone-depleting substances: mixing ratios, EESC, ODPs, and GWPs, *Atmospheric Chemistry and Physics*, 14, 2757-2776, doi:10.5194/acp-14-2757-2014, 2014.
- Volk, C. M., Elkins, J. W., Fahey, D. W., Sutton, G. S., Gilligan, J. M., Loewenstein, M., Podolske, J. R., Chan, K. R., and Gunson, M. R.: Evaluation of source gas lifetimes from stratospheric observations, *Journal of Geophysical Research*, 102, 25543–25564, 1997.
- von Hobe, M., Bekki, S., Borrmann, S., Cairo, F., D'Amato, F., Di Donfrancesco, G., Dörnbrack, A., Ebersoldt, A., Ebert, M., Emde, C., Engel, I., Ern, M., Frey, W., Genco, S., Griessbach, S., Grooß, J.-U., Gulde, T., Günther, G., Hösen, E., Hoffmann, L., Homonnai, V., Hoyle, C. R., Isaksen, I. S. A., Jackson, D. R., Jánosi, I. M., Jones, R. L., Kandler, K., Kalicinsky, C., Keil, A., Khaykin, S. M., Khosrawi, F., Kivi, R., Kuttippurath, J., Laube, J. C., Lefèvre, F., Lehmann, R., Ludmann, S., Luo, B. P., Marchand, M., Meyer, J., Mitev, V., Molleker, S., Müller, R., Oelhaf, H., Olschewski, F., Orsolini, Y., Peter, T., Pfeilsticker, K., Piesch, C., Pitts, M. C., Poole, L. R., Pope, F. D., Ravegnani, F., Rex, M., Riese, M., Röckmann, T., Rognerud, B., Roiger, A., Rolf, C., Santee, M. L., Scheibe, M., Schiller, C., Schlager, H., Siciliani de Cumis, M., Sitnikov, N., Søvde, O. A., Spang, R., Spelten, N., Stordal, F., Sumińska-Ebersoldt, O., Ulanovski, A., Ungermann, J., Viciani, S., Volk, C. M., vom Scheidt, M., von der Gathen, P., Walker, K., Wegner, T., Weigel, R., Weinbruch, S., Wetzel, G., Wienhold, F. G., Wohltmann, I., Woiwode, W., Young, I. A. K., Yushkov, V., Zobrist, B., and Stroh, F.: Reconciliation of essential process parameters for an enhanced predictability of Arctic stratospheric ozone loss and its climate interactions (RECONCILE): activities and results, *Atmospheric Chemistry and Physics*, 13, 9233–9268, doi:10.5194/acp-13-9233-2013, 2013.
- Watts, S. F.: The mass budgets of carbonyl sulfide, dimethyl sulfide, carbon disulphide and hydrogen sulfide, *Atmospheric Environment*, 34, 5, 761-779, doi:10.1016/S1352-2310(99)00342-8, 2000.
- Weiss, P. S., Johnson, J. E., Gammon, R. H., and Bates, T. S.: Reevaluation of the open ocean source of carbonyl sulfide to the atmosphere, *Journal of Geophysical Research – Atmospheres*, 100, D10, 23083-23092, doi:10.1029/95JD01926, 1995.
- Wilhelm, E., Battino, R., and Wilcock, R. J.: Low-pressure solubility of gases in liquid water, *Chemical Reviews*, 77, 2, 219-262, doi:10.1021/cr60306a003, 1977.

References

- Williams, J.: Mass Spectrometric Methods for Atmospheric Trace Gases in *Analytical Techniques for Atmospheric Measurements*, Chapter 5, Wiley-Blackwell, 2006.
- Williams, R. G. and Follows, M. J.: Ocean Dynamics and the Carbon Cycle: Principles and Mechanisms, *Cambridge University Press*, 2011.
- Witrand, E., Martinerie, P., Hogan, C., Laube, J. C., Kawamura, K., Capron, E., Montzka, S. A., Dlugokencky, E. J., Etheridge, D., Blunier, T., and Sturges, W. T.: A new multi-gas constrained model of trace gas non-homogeneous transport in firn: evaluation and behaviour at eleven polar sites, *Atmospheric Chemistry and Physics*, 12, 23, 11465-11483, doi:10.5194/acp-12-11465-2012, 2012.
- Witrand, E. and Martinerie, P.: Input Estimation from Sparse Measurements in LPV Systems and Isotopic Ratios in Polar Firns, in: Proc. of the IFAC Joint Symposium on SSSC, TDS and FDA, pp. 659–664, The International Federation of Automatic Control, Grenoble, France, doi:10.3182/20130204-3-FR-2033.00201, 2013.
- Worton, D. R., Sturges, W. T., Gohar, L. K., Shine, K. P., Martinerie, P., Oram, D. E., Humphrey, S. P., Begley, P., Gunn, L., Barnola, J. –M., Schwander, J., and Mulvaney, R.: Atmospheric trends and radiative forcings of CF₄ and C₂F₆ inferred from firn air, *Environmental Science and Technology*, 41, 7, 2184-2189, doi:10.1021/es061710t, 2007.
- Xu, X., Bingemer, H. G., Georgii, H. W., Schmidt, U., and Bartell, T.: Measurements of carbonyl sulfide (COS) in surface seawater and marine air, and estimates of the air-sea flux of observations during two Atlantic cruises, *Journal of Geophysical Research – Atmospheres*, 106, D4, 3491-3502, doi:10.1029/2000JD900571, 2001.
- Xu, X., Bingemer, H. G., and Schmidt, U.: The flux of carbonyl sulfide and carbon disulphide between the atmosphere and a spruce forest, *Atmospheric Chemistry and Physics*, 2, 171-181, 2002.
- Yoshida, N. and Toyoda, S.: Constraining the atmospheric N₂O budget from intramolecular site preference in N₂O isotopomers, *Nature*, 405, 6784, 330-334, doi:10.1038/35012558, 2000.
- Zepp, R. G. and Andreae, M. O.: Factors affecting the photochemical production of carbonyl sulfide in seawater, *Geophysical Research Letters*, 21, 25, 2813-2816, doi:10.1029/94GL03083, 1994.

- Zuiderweg, A., Kaiser, J., Laube, J. C., Röckmann, T., and Holzinger, R.: Stable carbon isotope fractionation in the UV photolysis of CFC-11 and CFC-12, *Atmospheric Chemistry and Physics*, 12, 4379–4385, doi:10.5194/acp-12-4379-2012, 2012.
- Zuiderweg, A., Holzinger, R., Martinerie, P., Schneider, R., Kaiser, J., Witrant, E., Etheridge, D., Petrenko, V., Blunier, T., and Röckmann, T.: Extreme ¹³C depletion of CCl₂F₂ in firn air samples, *Atmospheric Chemistry and Physics*, 13, 2, 599-609, doi:10.5194/acp-13-599-2013, 2013.